

KINETICS OF IN SITU COMBUSTION

SUPRI TR 91

By
Daulat D. Mamora
Henry J. Ramey, Jr.
William E. Brigham
Louis M. Castanier

July 1993

Performed Under Contract No. FG22-90BC14600

Stanford University
Petroleum Research Institute
Stanford, California



Bartlesville Project Office
U. S. DEPARTMENT OF ENERGY
Bartlesville, Oklahoma

DISCLAIMER

This report was prepared as an account of work sponsored by an agency of the United States Government. Neither the United States Government nor any agency thereof, nor any of their employees, makes any warranty, express or implied, or assumes any legal liability or responsibility for the accuracy, completeness, or usefulness of any information, apparatus, product, or process disclosed, or represents that its use would not infringe privately owned rights. Reference herein to any specific commercial product, process, or service by trade name, trademark, manufacturer, or otherwise does not necessarily constitute or imply its endorsement, recommendation, or favoring by the United States Government or any agency thereof. The views and opinions of authors expressed herein do not necessarily state or reflect those of the United States Government or any agency thereof.

This report has been reproduced directly from the best available copy.

Available to DOE and DOE contractors from the Office of Scientific and Technical Information, P.O. Box 62, Oak Ridge, TN 37831; prices available from (615)576-8401, FTS 626-8401.

Available to the public from the National Technical Information Service, U.S. Department of Commerce, 5285 Port Royal Rd., Springfield, VA 22161.

Kinetics of In Situ Combustion

SUPRI TR 91

By
Daulat D. Mamora
Henry J. Ramey, Jr.
William E. Brigham
Louis M. Castanier

July 1993

Work Performed Under Contract No. DE-FG22-90BC14600

Prepared for
U.S. Department of Energy
Assistant Secretary for Fossil Energy

Thomas Reid, Project Manager
Bartlesville Project Office
P.O. Box 1398
Bartlesville, OK 74005

Prepared by
Stanford University
Petroleum Research Institute
Stanford, CA 94305-4042

Acknowledgements

The authors are grateful for the financial support from the Department of Petroleum Engineering of Stanford University, the SUPRI Industrial Associates and DOE through contract No. DE-FG22-90BC14600.

Abstract

Oxidation kinetic experiments with various crude oil types show two reaction peaks at about 250°C (482°F) and 400°C (725°F). These experiments lead to the conclusion that the fuel during high temperature oxidation is an oxygenated hydrocarbon.

A new oxidation reaction model has been developed which includes two partially-overlapping reactions: namely, low-temperature oxidation followed by high-temperature oxidation. For the fuel oxidation reaction, the new model includes the effects of sand grain size and the atomic hydrogen-carbon (H/C) and oxygen-carbon (O/C) ratios of the fuel. Results based on the new model are in good agreement with the experimental data.

Methods have been developed to calculate the atomic H/C and O/C ratios. These methods consider the oxygen in the oxygenated fuel, and enable a direct comparison of the atomic H/C ratios obtained from kinetic and combustion tube experiments.

The finding that the fuel in kinetic tube experiments is an oxygenated hydrocarbon indicates that oxidation reactions are different in kinetic and combustion tube experiments. A new experimental technique or method of analysis will be required to obtain kinetic parameters for oxidation reactions encountered in combustion tube experiments and field operations.

Contents

Acknowledgements	iii
Abstract	v
List of Tables	xi
List of Figures	xiii
1 Introduction	1
2 Literature Review	9
2.1 Methods of Analysis	9
2.1.1 Qualitative Analysis	9
2.1.2 Quantitative Analysis	11
2.1.3 Compositional Analysis	13
2.2 In-Situ Combustion Reactions	15
2.2.1 Fuel Deposition	15
2.2.2 Fuel Combustion	16
2.2.3 Low-Temperature Oxidation	19
3 Experimental Apparatus	23
3.1 Apparatus Common to Kinetic and Combustion Tube Experiments .	23
3.2 Kinetic Tube Experimental Apparatus	27
3.3 Combustion Tube Experimental Apparatus	29
3.4 Other Apparatus	34

3.4.1	Weight Versus Temperature Apparatus	34
3.4.2	Apparatus for Analysis of Produced Liquids	36
3.4.3	Fuel Extraction Apparatus	38
3.5	Calibration of Instruments	38
3.5.1	Gas Analyzer Calibration	41
3.5.2	Gas Chromatograph Calibration	43
3.5.3	Flow Meter Calibration	46
3.5.4	Pressure Transducer Calibration	47
4	Ancillary Experimental Results	48
4.1	Elemental Analysis Results	48
4.2	Weight Versus Temperature Results	50
4.3	DSC and TGA Results	56
4.4	Grain Sieve Analysis Results	61
4.5	X-Ray Diffraction Results	61
5	Combustion Tube Experimental Results	64
5.1	Cold Lake Bitumen Run CL13	65
5.2	Hamaca Crude Oil Run VEN5	74
5.3	Hamaca Crude Oil Run VEN14	80
5.4	Hamaca Crude Oil Run VEN21	87
6	Kinetic Experimental Results	94
6.1	Kinetic Tube Experimental Results	99
6.2	An Oxygenated Fuel for HTO	118
6.3	Apparent O/C Ratio From Gas Analysis	142
6.4	Heat of Combustion of Oxygenated Fuel	154
6.5	Error Analysis	156

6.6	Previous Oxidation Reaction Model	159
6.7	Summary of Kinetic Experimental Results	167
7	New Oxidation Reaction Model	169
7.1	Spherical-Fuel-Geometry Model	173
7.2	Varying-Fuel-Geometry Model	177
7.2.1	Fuel in the Toroid ($t \geq t_c$)	177
7.2.2	Fuel in Non-Toroidal Part ($t < t_c$)	179
7.2.3	Calculation of Oxygen Consumption	180
7.3	LTO Reaction Model	183
7.4	Verification of Oxidation Reaction Model	186
7.4.1	Verification with Carbon Runs	187
7.4.2	Verification with Crude Oil Runs	187
8	Summary, Conclusions and Recommendations	219
8.1	Summary and Conclusions	219
8.2	Recommendations	221
	Nomenclature	223
	Bibliography	226
	Appendix: Computer Programs	236

List of Tables

2.1	Fuel Deposition Rates (<i>After Fassih, 1981</i>)	17
2.2	Combustion Reaction Rates (<i>After Fassih, 1981</i>)	20
2.3	LTO Reaction Rates (<i>After Fassih, 1981</i>)	22
3.1	Equipment Common to Kinetic and Combustion Tube Experiments .	26
3.2	Equipment Solely for Kinetic Tube Experiments	30
3.3	Equipment Solely for Combustion Tube Experiments	35
3.4	Equipment for Produced Liquid Analysis	37
3.5	Equipment for Fuel Extraction	40
4.1	Results of Elemental Analysis	49
4.2	Experimental Conditions for Sample Weight Versus Temperature Runs	51
4.3	Sieve Analysis of 20–30 Mesh Ottawa Sand	62
4.4	Sieve Analysis of 170–270 Mesh Sand	62
5.1	Properties of Sand Packs for Combustion Tube Runs	65
5.2	Summary of Combustion Tube Experimental Results	73
6.1	Atomic H/C Ratios From Hougen and Watson Correlation	97
6.2	Experimental Conditions for Kinetic Runs	100
6.3	Oxygen Consumption Peaks at LTO and HTO	109
6.4	Average Apparent H/C and <i>m</i> -Ratios at HTO Temperature Range .	110
6.5	Kinetic and Combustion Tube Experimental Sets	119
6.6	Apparent H/C Ratios for Kinetic and Combustion Tube Experiments	130

6.7	Averaged Apparent H/C, O/C and <i>m</i> -Ratios	143
6.8	Estimated Errors in Apparent H/C and <i>m</i> -Ratios	159
7.1	Estimated Grain Sizes and Fuel Densities	172
7.2	Kinetic Parameters Obtained From Experiments	197

List of Figures

1.1	Main Heavy Oil and Oil Sands Deposits: Initial-in-Place Volumes (After AOSTRA, 1990)	1
1.2	In-Situ Combustion: Schematic Diagram of Temperature and Saturation Profiles and Zones (After Wu and Fulton, 1971)	4
2.1	Differential Thermal Analysis of an Oil Sand (Tadema, 1959)	10
3.1	Schematic Diagram of Kinetic and Combustion Tube Apparatus	25
3.2	Schematic Diagram of Kinetic Tube	28
3.3	Schematic Diagram of Combustion Tube	31
3.4	Schematic Diagram of Fuel Extraction Apparatus	39
3.5	Calibration of Carbon Dioxide and Carbon Monoxide Analyzers	44
3.6	Calibration of Oxygen Analyzer and Gas Chromatograph	45
4.1	Cold Lake Bitumen - Sample Weight Versus Temperature (Runs CL6 and CL7)	52
4.2	Huntington Beach Oil - Sample Weight Versus Temperature (Runs HBO3 and HBO4)	53
4.3	Hamaca Crude Oil - Sample Weight Versus Temperature (Runs VEN12 and VEN13)	54
4.4	Hamaca Crude Oil - Sample Weight Versus Temperature (Runs VEN17 and VEN18)	55
4.5	TGA Thermogram - Huntington Beach Oil and Sand Mixture	57

4.6	DSC Thermogram - Huntington Beach Oil and Sand Mixture	58
4.7	TGA Thermogram - Hamaca Crude Oil and Sand Mixture	59
4.8	DSC Thermogram - Hamaca Crude Oil and Sand Mixture	60
4.9	X-Ray Diffraction Pattern of Mortar Clay	63
5.1	Produced Gas Composition Versus Time (Run CL13)	67
5.2	Apparent H/C and <i>m</i> -Ratios Versus Time (Run CL13)	69
5.3	Temperature Profiles (Run CL13)	70
5.4	Production, Oil gravity and Combustion Front Location Versus Time (Run CL13)	71
5.5	Oil Viscosity Versus Temperature (Run CL13)	72
5.6	Produced Gas Composition Versus Time (Run VEN5)	75
5.7	Apparent H/C and <i>m</i> -Ratios Versus Time (Run VEN5)	76
5.8	Temperature Profiles (Run VEN5)	77
5.9	Production, Oil Gravity and Combustion Front Location Versus Time (Run VEN5)	78
5.10	Oil Viscosity Versus Temperature (Run VEN5)	79
5.11	Produced Gas Composition Versus Time (Run VEN14)	81
5.12	Apparent H/C and <i>m</i> -Ratios Versus Time (Run VEN14)	82
5.13	Temperature Profiles (Run VEN14)	83
5.14	Production, Oil Gravity and Combustion Front Location Versus Time (Run VEN14)	84
5.15	Oil Viscosity Versus Temperature (Run VEN14)	85
5.16	Produced Gas Composition Versus Time (Run VEN21)	89
5.17	Apparent H/C and <i>m</i> -Ratios Versus Time (Run VEN21)	90
5.18	Temperature Profiles (Run VEN21)	91
5.19	Production, Oil Gravity and Combustion Front Location Versus Time (Run VEN21)	92

5.20	Oil Viscosity Versus Temperature (Run VEN21)	93
6.1	Atomic H/C Ratio Versus Oil Gravity and UOP K-Factor (<i>After Lim, 1991</i>)	95
6.2	Measured Atomic H/C Ratios Versus Values Derived From Hougen and Watson Correlation	98
6.3	Produced Gas Composition and Temperature Versus Time (Run CL2)	102
6.4	Produced Gas Composition and Temperature Versus Time (Run CL5)	103
6.5	Produced Gas Composition and Temperature Versus Time (Run CL14)	104
6.6	Produced Gas Composition and Temperature Versus Time (Run HBO2)	105
6.7	Produced Gas Composition and Temperature Versus Time (Run VEN6)	106
6.8	Produced Gas Composition and Temperature Versus Time (Run VEN15)	107
6.9	Produced Gas Composition and Temperature Versus Time (Run VEN23)	108
6.10	Apparent H/C and m-Ratios Versus Time (Run CL2)	111
6.11	Apparent H/C and m-Ratios Versus Time (Run CL5)	112
6.12	Apparent H/C and m-Ratios Versus Time (Run CL14)	113
6.13	Apparent H/C and m-Ratios Versus Time (Run HBO2)	114
6.14	Apparent H/C and m-Ratios Versus Time (Run VEN6)	115
6.15	Apparent H/C and m-Ratios Versus Time (Run VEN15)	116
6.16	Apparent H/C and m-Ratios Versus Time (Run VEN23)	117

6.17 Produced Gas Composition and Temperature Versus Time (Run VEN19)	120
6.18 Apparent H/C and m-Ratios Versus Time (Run VEN19)	121
6.19 Cumulative H/C Ratio Versus Time (Run CL2)	122
6.20 Cumulative H/C Ratio Versus Time (Run CL5)	123
6.21 Cumulative H/C Ratio Versus Time (Run CL14)	124
6.22 Cumulative H/C Ratio Versus Time (Run HBO2)	125
6.23 Cumulative H/C Ratio Versus Time (Run VEN6)	126
6.24 Cumulative H/C Ratio Versus Time (Run VEN15)	127
6.25 Cumulative H/C Ratio Versus Time (Run VEN19)	128
6.26 Cumulative H/C Ratio Versus Time (Run VEN23)	129
6.27 Oxygen Consumed Versus Time (Run CL2)	132
6.28 Oxygen Consumed Versus Time (Run CL5)	133
6.29 Oxygen Consumed Versus Time (Run CL14)	134
6.30 Oxygen Consumed Versus Time (Run HBO2)	135
6.31 Oxygen Consumed Versus Time (Run VEN6)	136
6.32 Oxygen Consumed Versus Time (Run VEN15)	137
6.33 Oxygen Consumed Versus Time (Run VEN19)	138
6.34 Oxygen Consumed Versus Time (Run VEN23)	139
6.35 Produced Gas Composition and Temperature Versus Time (Run VEN7)	140
6.36 Oxygen Consumed Versus Time (Run VEN7)	141
6.37 Apparent O/C Ratio Versus Time (Run CL2)	144
6.38 Apparent O/C Ratio Versus Time (Run CL5)	145
6.39 Apparent O/C Ratio Versus Time (Run CL14)	146
6.40 Apparent O/C Ratio Versus Time (Run HBO2)	147
6.41 Apparent O/C Ratio Versus Time (Run VEN6)	148

6.42	Apparent O/C Ratio Versus Time (Run VEN15)	149
6.43	Apparent O/C Ratio Versus Time (Run VEN23)	150
6.44	Produced Gas Composition and Temperature Versus Time (Run CL10)	151
6.45	Apparent H/C and <i>m</i> -Ratios Versus Time (Run CL10)	152
6.46	Produced Gas Composition and Temperature Versus Time (Run VEN10)	153
6.47	Fuel Oxidation Paths	154
6.48	Heat of Combustion Versus Atomic H/C, O/C and <i>m</i> -Ratios	157
6.49	Huntington Beach Oil - Analysis Based on Previous Model (<i>After Shallcross, 1989</i>)	161
6.50	Huntington Beach Oil - Analysis Based on Previous Model (<i>After Shallcross, 1989</i>)	162
6.51	Cold Lake Bitumen (Run CL14) - Arrhenius Graph for HTO Data Based on Previous Model	164
6.52	Carbon (Run C3) - Arrhenius Graph Based on Previous Model	165
6.53	Produced Gas Composition and Temperature Versus Time (Run CLC1)	166
7.1	Schematic Diagram of Spherical-Fuel-Geometry Model	170
7.2	Schematic Diagram of Varying-Fuel-Geometry Model	170
7.3	Arrhenius Graphs Based on Spherical-Fuel-Geometry and Previous Models (Carbon Run C3)	175
7.4	Arrhenius Graphs Based on Spherical-Fuel-Geometry and Previous Models (Cold Lake Bitumen Run CL14)	176
7.5	Produced Gas Composition and Temperature Versus Time (Run C3)	188
7.6	Apparent H/C and <i>m</i> -Ratios Versus Time (Run C3)	189
7.7	Arrhenius Graph (Run C3)	190

7.8	Fuel Height Versus Time (Run C3)	191
7.9	Oxygen Consumption – Model Results and Data (Run C3)	192
7.10	Produced Gas Composition and Temperature Versus Time (Run C4)	193
7.11	Arrhenius Graph (Run C4)	194
7.12	Oxygen Consumption – Model Results and Data (Run C4)	195
7.13	Arrhenius Graph for HTO Data (Run CL5)	198
7.14	Fuel Height Versus Time (Run CL5)	199
7.15	Oxygen Consumption at HTO – Model Results and Data (Run CL5)	200
7.16	Arrhenius Graph for LTO Data (Run CL5)	201
7.17	Oxygen Consumption at LTO – Model Results and Data (Run CL5)	202
7.18	Oxygen Consumption – Model Results and Data (Run CL5)	203
7.19	Arrhenius Graph for HTO Data (Run CL2)	204
7.20	Arrhenius Graph for LTO Data (Run CL2)	205
7.21	Oxygen Consumption – Model Results and Data (Run CL2)	206
7.22	Arrhenius Graph for HTO Data (Run CL14)	207
7.23	Arrhenius Graph for LTO Data (Run CL14)	208
7.24	Oxygen Consumption – Model Results and Data (Run CL14)	209
7.25	Arrhenius Graph for HTO Data (Run HBO2)	210
7.26	Arrhenius Graph for LTO Data (Run HBO2)	211
7.27	Oxygen Consumption – Model Results and Data (Run HBO2)	212
7.28	Arrhenius Graph for HTO Data (Run VEN6)	213
7.29	Arrhenius Graph for LTO Data (Run VEN6)	214
7.30	Oxygen Consumption – Model Results and Data (Run VEN6)	215
7.31	Arrhenius Graph for HTO Data (Run VEN23)	216
7.32	Arrhenius Graph for LTO Data (Run VEN23)	217
7.33	Oxygen Consumption – Model Results and Data (Run VEN23)	218

1. Introduction

Crude oils are often grouped into three categories based on specific gravity range: heavy oil (10° – 20° API), intermediate oil (20° – 30° API), and light oil (greater than 30° API). Heavy oils consist mainly of high density naphthenes, aromatics and heteroatoms that are poor in alkanes, while light oils consist mainly of alkanes (Boduszynski 1987, 1988). Bitumen or tar are extremely dense hydrocarbons (about 10° API or less), and are non-volatile liquids, semi-solids or solids. The deposits are often referred to as oil sands or tar sands. The main accumulations of heavy oil and oil sands worldwide (AOSTRA 1990) are shown in Fig. 1.1.

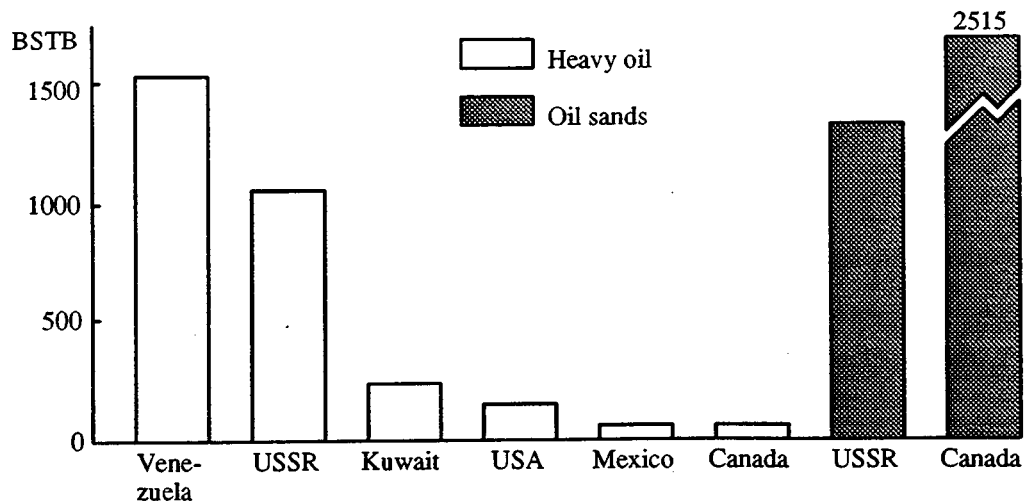


Figure 1.1: Main Heavy Oil and Oil Sands Deposits: Initial-in-Place Volumes (After AOSTRA, 1990)

1. INTRODUCTION

Figure 1.1 indicates the large potential target for thermal recovery. The National Petroleum Council has estimated that the reserves for enhanced oil recovery in the U.S. is about 14.5 BSTB oil, of which 45% or 6.5 BSTB are expected to be developed by thermal recovery methods (Broome *et al.* 1984). For brevity, the term, heavy oil, will subsequently be used to refer to both heavy crude oil and the oil sands.

Heavy oil reservoirs contain highly viscous crudes which have little or practically no mobility. For such reservoirs to attain practical flowrates, the oil viscosity must be reduced significantly. This may be achieved by introducing heat to the reservoir. This is usually done by injecting hot water or steam from the surface or by generating the heat in the reservoir through a process called *in-situ combustion*.

The most common form of in-situ combustion is *dry, forward combustion*. In this process, air is injected into a heavy oil reservoir, the crude is ignited in-situ, and the resulting combustion front moves away from the injection well. The heat generated at the combustion front propagates through the reservoir, reduces the oil viscosity and thereby increases the oil production rate and recovery. Studies have shown that the propagation of a combustion front in a reservoir is the most rapid method of thermal recovery. The combustion front can move more rapidly than heat can be moved by conduction and convection in a reservoir. Martin *et al.* (1958) and Ramey (1971) showed that the convective heat wave velocity for the case of air injection is about one-quarter that of the combustion front. The research reported in this thesis is primarily related to the dry, forward in-situ combustion process.

Another form of in-situ combustion is the *wet combustion* method in which air and water are injected concurrently or alternately. The purpose of injecting water is to recuperate and transport heat from the burned zone to the colder regions downstream of the combustion front. This method may be considered for thin reservoirs, where heat loss to adjacent formations is significant (Dietz and Weijdema 1963, Parrish and Craig 1969, Dietz 1970, Beckers and Harmsen 1970, Burger and Sahuquet 1973).

1. INTRODUCTION

A third variation of the in-situ combustion process is the *reverse combustion* method. In this technique, the combustion zone is initiated at a production well. The reverse combustion front travels countercurrent to the air towards the injection well where air is injected. The oil flows towards the production well, through the combustion zone. Since no oil bank is formed, the total flow resistance decreases with time, and thus this method is particularly suitable for reservoirs containing very viscous crudes. One disadvantage of this method is the likelihood of spontaneous ignition. Spontaneous ignition would result in oxygen being consumed near the injector, and the process would change to forward combustion (Dietz and Weijdemans 1968). Another disadvantage of reverse combustion is the inherent instability of the process, resulting in narrow combustion channels being formed and therefore an inefficient burn (Gunn and Krantz 1980, Johnson *et al.* 1980).

Patents for the in-situ combustion process were first awarded in the U.S. in 1923 to Wolcott (1923) and Howard (1923). Sheinman *et al.* (1969) reported that the process was first applied to an oil reservoir in the Soviet Union in 1934. Intentional field tests were conducted in the U.S. in 1952 in Oklahoma (Kuhn and Koch 1953, Grant and Szasz 1954). Since then, in-situ combustion has been applied in over a hundred fields. Reviews of many of these fields have been made and reported in the literature (Farouq Ali 1972; Chu 1977, 1982; Brigham *et al.* 1980). The South Belridge project which began commercial operations in 1964 is of special significance. This project was a commercial success and analyses of the field data yielded a number of useful, new concepts and correlations. Certain ideas carried over from water flooding were found to be inappropriate to the in-situ combustion process (Gates and Ramey 1958, 1980; Ramey *et al.* 1992).

Figure 1.2 is a schematic representation of the temperature and saturation profiles and the various zones that are formed during a dry, forward in-situ combustion process. As the combustion front approaches a volume element in the reservoir, the

1. INTRODUCTION

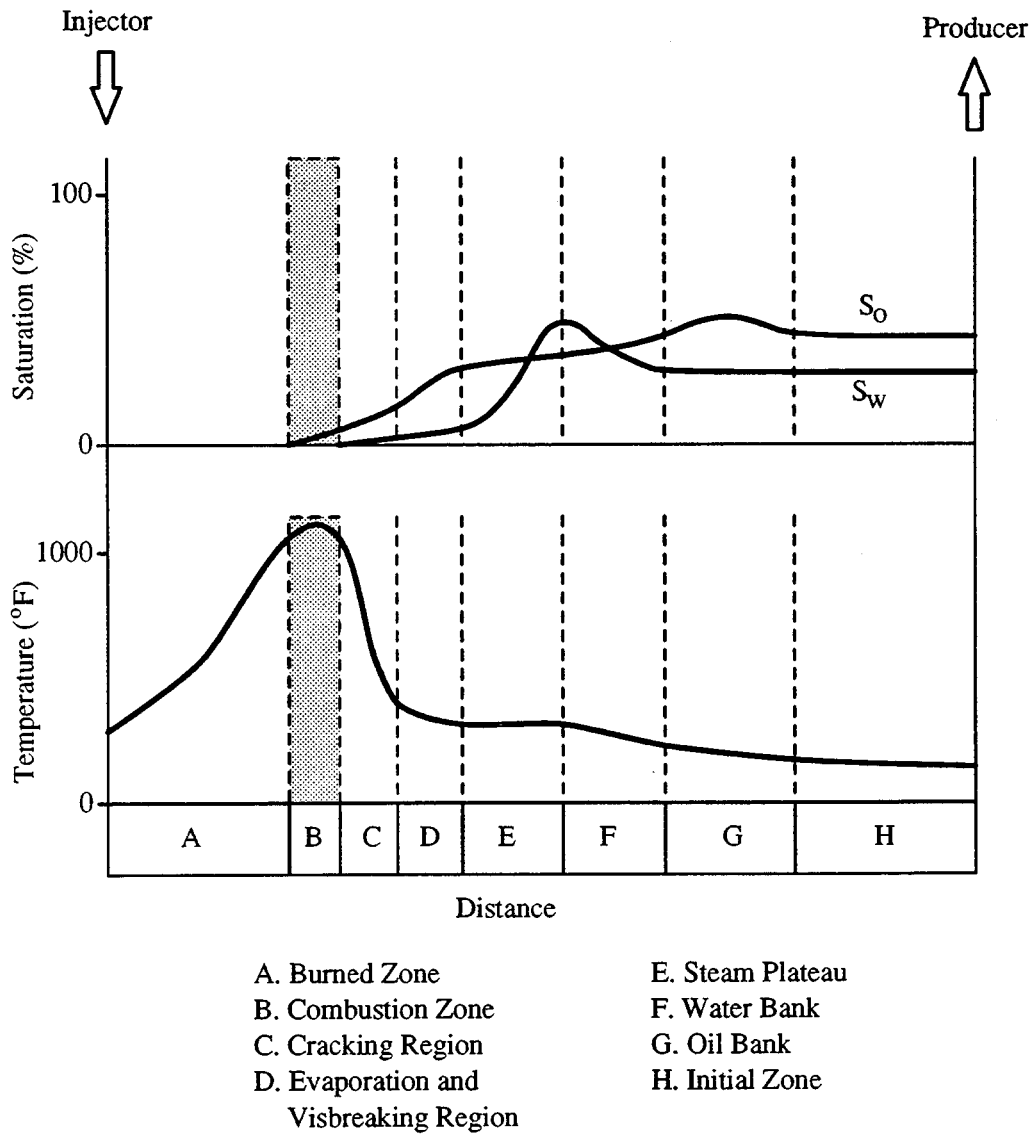


Figure 1.2: In-Situ Combustion: Schematic Diagram of Temperature and Saturation Profiles and Zones (After Wu and Fulton, 1971)

1. INTRODUCTION

changes to the fluids in a volume element can be visualized in the following manner (Martin *et al.* 1958, Wilson *et al.* 1958, Tadema 1959, Ramey 1971, Wu and Fulton 1971). As the temperature of the volume element rises, the first liquids to be vaporized are water and light hydrocarbons. The vapors are carried in the gas stream and condense in the colder regions ahead of the combustion zone. The water vapors condense first to form a water bank (F), followed by the light hydrocarbons (G). The steam plateau (E) is the steam-liquid, two-phase region. Figure 1.2 represents a linear system like a combustion tube experiment. Field operations are three dimensional and the steam plateau and other regions ahead of the combustion front are compressed. Figure 1.2 exaggerates the length of the steam plateau and represents a linear system with little pressure drop.

As the various zones pass through the volume element, the oil is subjected to a combination of miscible displacement by the condensed light hydrocarbons, hot water drive, vaporization and steam and gas drive. As the temperature in the volume element exceeds about 650°F (345°C), the oil may undergo a process called thermal cracking to form a volatile fraction and a low-volatility, heavy residue (C and D). The former is carried in the gas stream, while the latter constitutes the fuel which is burned in the combustion zone. The heat generated at the combustion zone (B) is transported ahead of the front by conduction through the formation matrix and by convection of the vapors and liquids.

The combustion zone is only a few inches thick and has a temperature in the range 650°–1200°F (345°–650°C). For a given oxygen flux, the velocity of the combustion front is dependent on the amount of fuel burned. As the combustion front moves past the volume element, a zone of clean sand (A) is left behind where only air flows. As a result of distillation and thermal cracking, the produced oil gravity increases. In South Belridge, for example, the produced oil gravity was as high as 18°API, compared to 12.9°API for the original oil.

1. INTRODUCTION

The main parameters required in the design of an in-situ combustion project are (Alexander *et al.* 1962): (1) the fuel concentration per unit reservoir volume burned, (2) the composition of the fuel, (3) the amount of air required to burn the fuel, (4) the volume of reservoir swept by the combustion zone, (5) the required air-injection rates and pressures, (6) the oil production rate and recovery, and (7) the operating costs.

Data from combustion tube experiments form the main basis for determining these design parameters. Nelson and McNiel (1961) have described a method for calculating some of these parameters. Gates and Ramey (1980) have incorporated the effect of initial gas saturation on an oil recovery versus volume burned correlation for South Belridge which includes gravity drainage in this field operation.

Initial models to describe the in-situ combustion process were analytical heat transfer models (Vogel and Krueger 1955, Ramey 1959, Bailey and Larkin 1960, Chu 1963, Thomas 1963, Penberthy and Ramey 1966, Godfried 1966, Penberthy 1967). Subsequent models have included the kinetics of lumped reactions: a steady-state model by Agca and Yortsos (1985), and a model for simulation of combustion tube experiments which incorporates thermal cracking and low-temperature oxidation (Millour *et al.* 1985, Belgrave *et al.* 1990). Numerical simulation models have been presented in which the physical and chemical reactions are described by basic kinetic relationships (Crookston *et al.* 1979, Youngren 1980, Coats 1980).

The rate of propagation of the combustion front, and therefore, the overall in-situ combustion process can be described by a simple chain reaction consisting of two competitive steps: fuel deposition and fuel combustion (Bousaid and Ramey 1968, Dabbous and Fulton 1974, Thomas *et al.* 1979). Fuel deposition is the process of leaving fuel on the reservoir matrix. Fuel concentration is a key parameter in the design and operation of an in-situ combustion project. The maximum oil recovery is equal to the difference between the initial oil-in-place and the amount of fuel consumed.

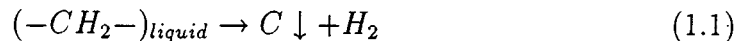
1. INTRODUCTION

Hence, if the fuel concentration is excessively large, the combustion front will advance slowly and the amount of air per unit oil displaced will be larger, resulting in high air compression costs. If the fuel concentration is too low, however, the heat generated at the combustion front will be insufficient to propagate self-sustaining combustion.

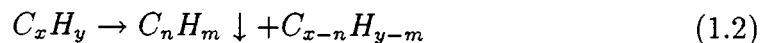
In the ideal situation, oxygen reaching the combustion front is totally consumed for fuel oxidation. However, some oxygen may move through the combustion front resulting in low-temperature oxidation (LTO) of the crude oil (Ramey 1959, Moss *et al.* 1959, Tadema 1959, Tadema and Weijdema 1970, Burger 1976). This condition may be caused by incomplete oxygen consumption in the combustion zone, air channeling through or around the combustion zone, or a tilted combustion front surface (Dabbous and Fulton 1974). Of course low-temperature oxidation occurs during air injection prior to ignition and may lead to spontaneous ignition.

There is, however, some uncertainty with regard to the nature of the fuel and the mechanism for fuel deposition, as evident from the following reports in the literature.

- Burger and Sahuquet (1972) envisaged the fuel to consist of a mixture of liquid hydrocarbons and solid carbon. The carbon, deposited on the reservoir matrix, was thought to be formed by the pyrolysis of crude oil:



- Other researchers believed that thermal cracking was the main mechanism for fuel deposition. In this case, hydrocarbon molecules were “cracked” by the high temperature just ahead of the combustion zone. A heavy residue called “coke” was deposited on the reservoir matrix:



- Experiments carried out on core samples of fuel deposits from the South Belridge field indicated that the fuel had an atomic hydrogen-carbon ratio of 1.67 and

1. INTRODUCTION

a specific gravity of 1.38 (Gates and Ramey 1958). The original crude had an atomic hydrogen-carbon ratio of 1.67 and a specific gravity of 0.98 (12.9° API). These results indicated that the fuel consisted of heavy, low-volatility hydrocarbon fractions which were left behind by distillation. Gates and Ramey believed “coke” was a misnomer for the fuel burned in in-situ combustion. The H/C ratio was too high to be coke.

- Wilson *et al.* (1963) and Bae (1977) deduced from their experiments that steam distillation is the main mechanism for fuel deposition.
- In modeling the high-temperature oxidation (HTO) reaction in kinetic experiments, Fassihi (1981) assumed the fuel during HTO to be carbon.

Two questions will be addressed in this thesis:

1. What constitutes the fuel at the combustion zone?
2. What are the main parameters that affect fuel deposition?

A literature survey of experimental studies on crude oil oxidation reactions, including the various types of analysis and equations used, is given in Chapter 2. A description of the experimental apparatus and procedure used in this study is given in Chapter 3. The results of experiments are presented in Chapters 4–6. Chapter 4 presents ancillary experiments and Chapter 5 presents combustion tube experiments. Chapter 6 presents kinetic tube experiments which lead to the finding that fuel during HTO in kinetic tube experiments is an oxygenated hydrocarbon. A mathematical model to describe oxidation reactions in kinetic tube experiments is given in Chapter 7.

2. Literature Review

There is an extensive literature on oxidation of hydrocarbons. Many articles concern manufacture of various oxygenated products. This review will concern oxidation reactions in porous media, and particularly articles relating to in-situ combustion oil recovery.

2.1 Methods of Analysis

Experimental studies of oxidation of crude oil in porous media have been carried out using three different types of analysis: qualitative, quantitative and compositional. A review of results of each method follows.

2.1.1 Qualitative Analysis

Differential thermal analysis (DTA) and thermogravimetric analysis (TGA) were used during early studies of crude oil oxidation. Results of these experiments, which are qualitative in nature, have provided clues to the broad nature of oxidation reactions in in-situ combustion oil recovery.

In DTA experiments, a crude oil and sand mixture is heated at a uniform rate while air is passed through the mixture. The amount of heat released affects temperature which is recorded on a thermogram. DTA thermograms obtained by Tadema (1959)

2. LITERATURE REVIEW

indicated two exothermic reaction peaks, one at about 270°C (520°F) and the other at about 400°C (750°F) (Fig. 2.1). Similar results were obtained by Berry (1968).

Thermogravimetric experiments also involve heating a crude oil and sand sample at a constant rate in the presence of flowing air. However, the change in weight of the sample is recorded against temperature. Based on TGA and DTA thermograms, Bae (1977) concluded that at least two reactions occur at different temperatures during the oxidation of crude oil.

Figure 2.1: Differential Thermal Analysis of an Oil Sand (*Tadema, 1959*)

2. LITERATURE REVIEW

2.1.2 Quantitative Analysis

Qualitative techniques have largely been superseded by the effluent gas analysis (EGA) technique and combustion tube experiments. The former is performed to determine reaction kinetic parameters, while the latter yields data required for the design of an in-situ combustion project. Henceforth, an EGA experiment will simply be called a kinetic tube experiment.

Some of the early reaction kinetic studies were carried out by Bousaid and Ramey (1968), Weijdemer (1968), Dabbous and Fulton (1974), and Thomas *et al.* (1979). In these experiments, the temperature of a sample of crude oil and sand mixture was increased at a constant rate, or kept constant at the temperature of interest. Depending on whether pyrolysis or oxidation was being studied, nitrogen or an oxygen-containing gas was continuously flowed through the sample. The produced gas was analyzed to determine the concentrations of carbon dioxide, carbon monoxide, oxygen and nitrogen.

The rate of oxidation of crude oil in a porous medium, R_c , can be described as follows (Wilson *et al.* 1963, Bousaid and Ramey 1968, Burger and Sahuquet 1972):

$$R_c = -\frac{dC_f}{dt} = kP_{O_2}^a C_f^b \quad (2.1)$$

where:

- C_f = fuel concentration
- k = rate constant
- P_{O_2} = partial pressure of oxygen
- a, b = reaction orders

The reaction constant, k , is usually a function of temperature and follows the Arrhenius Law (Smith 1970, Carberry 1976):

$$k = A_r \exp(-E/RT) \quad (2.2)$$

2. LITERATURE REVIEW

where:

$$\begin{aligned}A_r &= \text{Arrhenius constant} \\E &= \text{activation energy} \\R &= \text{universal gas constant}\end{aligned}$$

Substituting Eq. 2.2 into Eq. 2.1 yields:

$$R_c = A_r P_{O_2}^a C_f^b \exp(-E/RT) \quad (2.3)$$

Using Eq. 2.3, the kinetic parameters, A_r , E , a and b can be obtained from experimental data. In heterogeneous reactions, the Arrhenius constant, A_r , is a function of the rock surface area (Smith 1970, Burger and Sahuquet 1972, Dabbous and Fulton 1974).

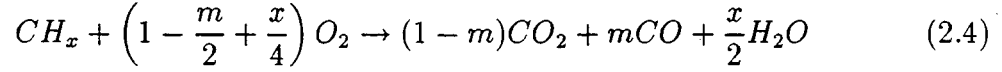
Studies of crude oil oxidation in a porous medium under a programmed linear temperature rise with time indicate two successive oxidation reactions (Burger and Sahuquet 1972, Fassihi 1981, De los Rios 1987, Shallcross 1989). The first reaction has a reaction peak at about 250°C (482°F), and is termed low-temperature oxidation (LTO). The second reaction, called high-temperature oxidation (HTO), has a reaction peak at about 400°C (725°F). An oxidation reaction model was presented by Fassihi (1981). Fassihi's model required a third reaction, medium-temperature oxidation (MTO), to fit the data.

In combustion tube experiments, the crude oil and sand mixture is placed in a steel tube and ignited at one end. Air is passed continuously through the sand pack as the combustion front advances towards the other end of the tube. The produced gas is analyzed as in kinetic tube experiments. Produced oil, water and gas are collected for volume determination and analysis. Gas analysis readings may be used to calculate the apparent atomic hydrogen-carbon ratio of the fuel, x , and the m -ratio (fraction of carbon oxidized to carbon monoxide).

Following Benham and Poettmann (1958), fuel combustion can be described by

2. LITERATURE REVIEW

the stoichiometric equation:



If O_{2p} and N_2 denote the mole percent of oxygen and nitrogen in the produced gas respectively, from a nitrogen material balance, the mole percent of oxygen consumed, O_{2c} , is:

$$O_{2c} = 0.2682N_2 - O_{2p} \quad (2.5)$$

If CO_2 and CO are the mole percent of carbon dioxide and carbon monoxide respectively in the produced gas, the m -ratio is defined as:

$$m = \frac{CO}{(CO_2 + CO)} \quad (2.6)$$

From an oxygen material balance, the apparent atomic hydrogen-carbon ratio can be calculated:

$$x = 4 \frac{[0.2682N_2 - (O_{2p} + CO_2 + CO/2)]}{(CO_2 + CO)} \quad (2.7)$$

Equation 2.7 assumes air injection and that all oxygen not produced as free oxygen or carbon oxides is used to oxidize hydrogen in the fuel. Combustion tube experiments yield other extremely useful data, such as fuel concentration, oil recovery, air-fuel ratio, and the API gravity and viscosity of the produced oil.

2.1.3 Compositional Analysis

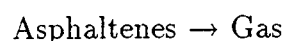
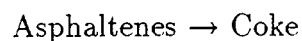
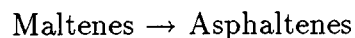
The objective of this type of analysis is to determine the concentration by weight of the pseudo-components of a crude oil sample as oil is subjected to oxidation or thermal cracking. The definition of pseudo-components may vary with the technique of analysis used. Typically, the pseudo-components are defined as maltenes, asphaltenes, coke and gas. Maltenes are crude oil fractions which are insoluble in n-pentane and may be further separated into saturates, aromatics and resins using

2. LITERATURE REVIEW

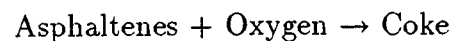
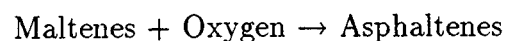
liquid chromatography. Adegbesan (1982), for example, carried out LTO experiments of Athabasca bitumen in which the LTO products were first separated by filtration into maltenes and a residue of asphaltenes and coke, using n-pentane as the solvent. The asphaltenes were separated from the coke by using toluene. Coke was defined as the fraction insoluble in toluene. The experimental results were analyzed by using an Arrhenius-type equation for each of the pseudo-component reactions.

This type of analysis involves an elaborate sequence of time-consuming experiments and relation of the results from different experiments may not be satisfactory. Nevertheless, the results provide insight into compositional changes during crude oil reactions. The main results of a number of experiments in the literature are as follows.

- Hayashitani (1978) deduced from experimental studies that thermal cracking of Athabasca bitumen consists of the following first order reactions.



- Boduszynski (1981) studied the reactions resulting from blowing asphalt with air, and deduced that the amount of asphaltenes increased while the aromatics decreased during the reaction.
- LTO experiments with Athabasca bitumen indicated the oxidation process consisted of the following reactions (Adegbesan 1982).



- Babu and Cormack (1984) also studied the LTO of Athabasca bitumen and deduced that the LTO reaction involves the following steps.

2. LITERATURE REVIEW

Aromatics → Resins → Asphaltenes

- Fassihi *et al.* (1990) studied the LTO of crude oils ranging from 10.1° to 31.1° API. Their results confirm the reactions deduced by Babu and Cormack (1984).

Two important conclusions can be reached from the results of these compositional studies. First, the product left after thermal cracking or LTO is hydrocarbon and not carbon. Second, one of the main effects of LTO on crude oil is to transform the aromatic compounds to asphaltenes.

2.2 In-Situ Combustion Reactions

The in-situ combustion process can be described by a chain reaction consisting of two steps: fuel deposition and fuel combustion. A third reaction, LTO, may be involved if oxygen is present downstream of the combustion front. The results of experimental studies of the oxidation reactions of crude oil are summarized in the following subsections. Most of these studies were based on kinetic and combustion tube experiments.

2.2.1 Fuel Deposition

Studies of core samples from South Belridge indicate that the reservoir lithology is an important parameter in fuel deposition (Gates and Ramey 1958). Kinetic experiments carried out by Bousaid and Ramey (1968) show that the amount of fuel deposited increases with the addition of clay to the sample of oil and sand.

Alexander *et al.* (1962) carried out effluent gas analysis experiments using flood-pot apparatus to investigate the factors that affect fuel deposition. In their studies, the following factors were considered: API gravity of the oil, original and residual oil saturations, atomic hydrogen-carbon ratio, oil viscosity, and the ASTM Conradson

2. LITERATURE REVIEW

carbon residue. The results indicated that the amount of fuel deposited increased with increasing initial oil saturation, oil viscosity and the Conradson carbon residue, and decreased with increasing atomic hydrogen-carbon ratio and API gravity of the oil.

Based on combustion tube experimental results, Showalter (1963) concluded that the amount of fuel deposited and air required increase with decreasing API gravity of the oil. Other results obtained are similar to those of Alexander *et al.* (1962).

Bae (1977) carried out thermogravimetric studies for a wide range of crude oil gravities (6°–38° API) in which both nitrogen and air were flowed through the sample. The results showed that crude oil oxidation generally starts at a higher temperature with less heat being evolved as the pressure is decreased. The weight loss at 50 psig and 500°F (260°C) and in the presence of air or nitrogen averaged 60%. From these results, it was concluded that the dominant mechanism for fuel deposition is distillation. This conclusion is also evident from the observation that at high pressure more fuel was deposited because less distillation occurred.

Poettmann *et al.* (1967) deduced from their studies that the specific surface area of the porous medium is an important parameter for fuel deposition, particularly for high-gravity, paraffin base crude oils. Results of combustion tube experiments carried out by Vossoughi *et al.* (1982) show that clay particles increase the amount of fuel deposited. Results of some studies on fuel deposition rate are shown in Table 2.1.

2.2.2 Fuel Combustion

Experimental studies by Martin *et al.* (1958) for a wide range of oil gravities (10.9°–34.2° API) indicate that the combustion front velocity is nearly proportional to the air flux and directly proportional to the rate of oxygen consumed. These results are supported by similar studies made by Benham and Poettmann (1958),

2. LITERATURE REVIEW

Table 2.1: Fuel Deposition Rates (*After Fassih, 1981*)

	Crude Type	Reactor Bed	$A_r(10^6 s^{-1})$	E (KJ/mol)	a	b
1.	Hydrocarbon vapor	Synthetic catalyst	n.a.	70.3	n.a.	n.a.
	Hydrocarbon vapor	Natural clay	n.a.	63.3	n.a.	n.a.
2.	12.4°API	Silica sand (100-200 mesh)	n.a.	69.3	n.a.	n.a.
3.	n.a.	Sand	n.a.	46.0	n.a.	n.a.
4a.	27°API	Sand quarry	3.88	65.1	0	1
4b.	27°API	and kaolinite	3.66	65.1	0	1
4c.	27°API	clay	8.33	69.1	n.a.	n.a.

1. Crawford and Cunningham (1956)

2. Madgwick *et al.* (1959)

3. Weijdema (1968); $P = 4 \times 10^4$ kPa

4. Crawford and Cunningham (1956); P (kPa) = 1×10^4 (a), 2.7×10^4 (b), 4.8×10^4 (c); if $a = 1$, $A_r = 0.6-1.8$

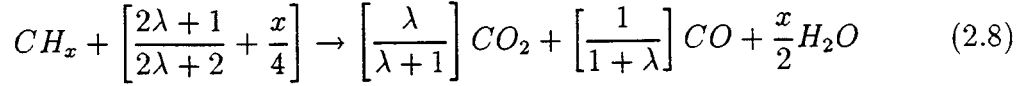
$$R_c = A_r \exp(-E/RT) P_{O_2}^a C_f^b$$

R_c = g fuel deposited on 100 g sand per sec.

n.a.=not available

2. LITERATURE REVIEW

who described the stoichiometry of fuel combustion as follows.



where λ is the mole percent ratio of carbon dioxide to carbon monoxide produced. Equation 2.8 is a version of Eq. 2.4, of course. Assuming all the fuel deposited to be consumed, Benham and Poettmann used Eq. 2.8 to derive the combustion front velocity.

$$V_F = \frac{1.109 \times 10^{-3}(12 + x)}{\left[\frac{2\lambda + 1}{\lambda + 1} + \frac{x}{2} \right] C_f} YU \quad (2.9)$$

where:

- V_F = combustion front velocity, ft/hr
- U = air flux at combustion front, scf/hr-ft²
- Y = fraction of oxygen consumed
- C_f = fuel concentration, lb/ft³ of reservoir bulk volume

Equation 2.9 can be expressed in a more general form (Penberthy and Ramey 1966):

$$V_F = \frac{U}{C_f R_{af}} \quad (2.10)$$

where R_{af} is the air-fuel ratio (scf/lb_m).

Moss *et al.* (1959), Showalter (1963) and Wilson *et al.* (1963) deduced similar relationships from their studies. Wilson *et al.* (1963) found that the combustion front temperature increased with air flux but was independent of the air flux at sufficiently high pressures. At high air flux, pressure had little effect on the combustion front temperature and velocity. At low air flux, an increase in pressure increased the combustion front temperature and decreased the combustion front velocity (Martin *et al.* 1958, Wilson *et al.* 1963). The effect of pressure was minor, however.

Berry and Parrish (1960) presented a theoretical study of reverse combustion to investigate the effect of pressure and air flux on the combustion front temperature.

2. LITERATURE REVIEW

The results agree with the experimental data of Wilson *et al.* (1963). Barry and Parish also found that heat loss reduced the combustion front velocity without changing combustion temperature. The results of some combustion rate studies are shown in Table 2.2.

2.2.3 Low-Temperature Oxidation

Low-temperature oxidation of crude oil is characterized by either little or no carbon oxides being produced by the reaction. LTO occurs at temperatures less than about 650°F (345°C) and is an exothermic reaction. The main products of LTO are oxygenated compounds such as carboxylic acids, aldehydes, ketones, alcohols and hyperoxides (Burger and Sahuquet 1972).

Dabbous and Fulton (1974) showed that during LTO diffusion of oxygen into the oil phase is faster than the oxidation reaction. Thus, LTO occurs with the oxygen dissolved throughout the oil phase.

Crawford (1968) found that aldehydes promote LTO reactions. The LTO reaction rate was found to be proportional to the specific surface area of the matrix raised to a power between 0 and 1 (Dabbous and Fulton 1974, Burger and Sahuquet 1977). Certain soils and metallic derivatives have a catalytic effect on LTO (Boussaid and Ramey 1968, Johnson and Burwell 1968, Crawford 1968, Vossoughi *et al.* 1982).

Alexander *et al.* (1962) studied the effect of LTO on fuel formation by subjecting a sample of oil and sand to a heating schedule in the presence of air. They found that over an extended period of time, LTO reactions result in the formation of a coke-like residue on the sand matrix. For a 21.8°API crude oil, the amount of this residue increased to a maximum at 425°F (218°C) and decreased sharply to zero at about 650°F (345°C). The apparent atomic hydrogen-carbon ratio decreased from a high value of about 50 at 250°F (121°C) to about 1 at 650°F (345°C). The large apparent

2. LITERATURE REVIEW

Table 2.2: Combustion Reaction Rates (*After Fassihi, 1981*)

	Crude Type	Reactor Bed	$A_r(1/\text{Pa}\cdot\text{s})$	E (KJ/mol)	a	b
1a.	Metallurgical coke	Fluidized	7.4×10^{-2}	121.4	1	1
1b.	Hardwood charcoal	Fluidized	2.0×10^{-3}	66.5	1	1
1c.	Graphite	Fluidized	1.3×10^3	205.8	1	1
2.	Coke	Sand pack	6.67×10^5	157.3	0	1
3.	n.a.	Sand pack	n.a.	125.5	n.a.	n.a.
4a.	13.9°API	Berea sand (170-230 mesh)	2.37×10^{-3}	61.9	1	1
4b.	13.9°API	80% Beria 20% clay	2.43×10^{-4}	48.4	1	1
4c.	22.1°API	Berea sand	1.38×10^{-3}	59.8	1	2
5.	19.9°API precoked	Berea sand (60 mesh)	1.38×10^{-3}	58.9	1	2
6a.	27°API	Sand quarry,	30.0	58.8	1	1
6b.	27°API	5% kaolinite	18.0	58.8	1	1
6c.	27°API		48.4	58.8	1	1

- Lewis *et al.* (1954); $P=100$ kPa
 - Weisz and Goodwin (1966); $P=100$ kPa; if $a=1$, $A_r=31.3$
 - Weijdema (1968); $P=4 \times 10^3$ kPa
 - Bousaid and Ramey (1968); $P(\text{kPa})=300$ (a), 500 (b), 200 (c)
 - Dabbous and Fulton (1974); $P=300$ kPa
 - Thomas *et al.* (1979); $P(\text{kPa})=1 \times 10^4$ (a), 2.8×10^4 (b), 4.8×10^4 (c)
- Here a is exponent of fuel deposited less fuel burned.

$$R_c = A_r \exp(-E/RT) P_{\text{O}_2}^a C_c^b$$

R_c = g carbon per 100 g sand per sec.

n.a.=not available

2. LITERATURE REVIEW

hydrogen-carbon ratio at low temperatures is due to the fact that oxygen is consumed in reactions which do not produce carbon oxides. Decreasing the heating schedule rate increased the amount of fuel deposited due to increased LTO reactions. Alexander *et al.* (1962) also found that LTO reactions increase the viscosity and boiling range of the oil. Bae (1977) found that crude oils generally increase in total weight as a result of LTO.

The heat released during LTO has been used by several investigators to estimate the spontaneous ignition time for an in-situ combustion project (Gates and Ramey 1958, Tadema and Weijdema 1970, Burger 1976). Light crude oils have been found to be more susceptible to LTO than heavy oils (Dabbous and Fulton 1974). Alexander *et al.* (1962) concluded that LTO reactions have a dominant effect on fuel deposition and composition. The results of some LTO investigations are shown in Table 2.3.

Having completed the literature survey of fuel oxidation, we turn now to consideration of experimental apparatus used in this study.

2. LITERATURE REVIEW

Table 2.3: LTO Reaction Rates (*After Fassih, 1981*)

	Crude Type	Reactor Bed	A_r (gmole/Pa ^m cc-s)	E (KJ/mol)	a
1.	n.a.	Sand pack	n.a.	44.2	n.a.
2a.	14.4°API	Sand pack	9.2×10^2	73.7	0.46
2b.	12.8°API	Sand pack	4.0×10^2	48.4	0.45
2c.	n.a.	Sand pack	7.78×10^1	71.9	0.57
2d.	n.a.	Sand pack	3.31	73.9	0.79
2e.	n.a.	Sand pack	2.01×10^4	85.5	0.48
2f.	n.a.	Sand pack	1.24×10^4	78.9	0.31
3.	13.9°API	Pressure bomb	5.1×10^{-2}	53.3	1
4a.	19.9°API	Sand pack	3.51	70.5	0.5
4b.	27.1°API	Sand pack	1.6	73.3	0.75
4c.	27.1°API	Sand pack	1.25	73.5	0.75
5.	27.0°API	Sand pack	9.4×10^{-2}	70.7	0.7

1. Weijdema (1968); P= n.a.

2. Tadema and Weijdema (1970); P= n.a.

3. Bousaid and Ramey (1968); P= 1.3×10^3 kPa

4. Dabbous and Fulton (1974); P=100 kPa

5. Bardon and Gadelle (1977); P= 9.1×10^3 kPa

$$R_{O_2} = A_r \exp(-E/RT) P_{O_2}^a$$

$$R_{O_2} = \text{g-mole oxygen/s-cc}$$

n.a.=not available

3. Experimental Apparatus

Two main types of experiments were performed in this study: kinetic tube experiments and combustion tube experiments. In addition, ancillary experiments were conducted on samples of oil, sand, clay and mixtures of these constituents. A description of the experimental apparatus and procedures follows.

3.1 Apparatus Common to Kinetic and Combustion Tube Experiments

Previous studies at Stanford have produced apparatus for carrying out both kinetic and combustion tube experiments. This apparatus was modified for improved accuracy of measurements and ease of operation. The main modifications were as follows.

1. Equipment, including fittings and lines common to both types of experiments, was integrated (e.g. a common ice-cooled condenser), minimizing redundancy and dead volumes.
2. All instruments, gages and control valves were mounted on panels for ease of operation and monitoring.

3. EXPERIMENTAL APPARATUS

3. A gas chromatograph (GC) with an automatic gas sampler was installed for measuring nitrogen concentration in the produced gas.
4. A new computer program was written to control the recording of data on a personal computer (PC) and to graph critical results for ease of monitoring of the experiments.
5. A new dual-thermowell system was fabricated for the combustion tube, enabling measurements to be made on one moveable and nine, stationary thermocouples. This system enabled rapid temperature measurements for high resolution temperature profiles at the combustion zone and ease of operation.

Figure 3.1 is a schematic diagram of the apparatus. Table 3.1 lists the equipment used. Operation of the apparatus is as follows. Air or the oxidant gas was supplied from pressurized gas cylinders and injected into either the combustion tube or the kinetic tube, depending on the experiment being conducted. Injected gas rate and pressure were maintained constant by means of the mass flow controller and the back-pressure regulator. Produced fluid passed through a condenser coil in an ice-cooled water bath to cool and remove liquids from the produced stream. Further liquid removal was achieved in the separator system. Produced gas passed through a trap containing Drierite (anhydrous calcium sulfate) to remove water. A tube containing Purafil II Chemisorbant was placed at the inlet end of the oxygen analyzer to remove acid in the gas stream. Dry, produced gas passed through the three analyzers and gas chromatograph where the carbon dioxide, carbon monoxide, oxygen and nitrogen concentrations were measured.

The PC was programmed to: (1) record, at 30-sec intervals, the gas analyzer readings, pressure, injected gas rate, produced gas rate and temperature (for kinetic tube experiments only); and (2) compute and record nitrogen concentration data at six minute intervals.

3. EXPERIMENTAL APPARATUS

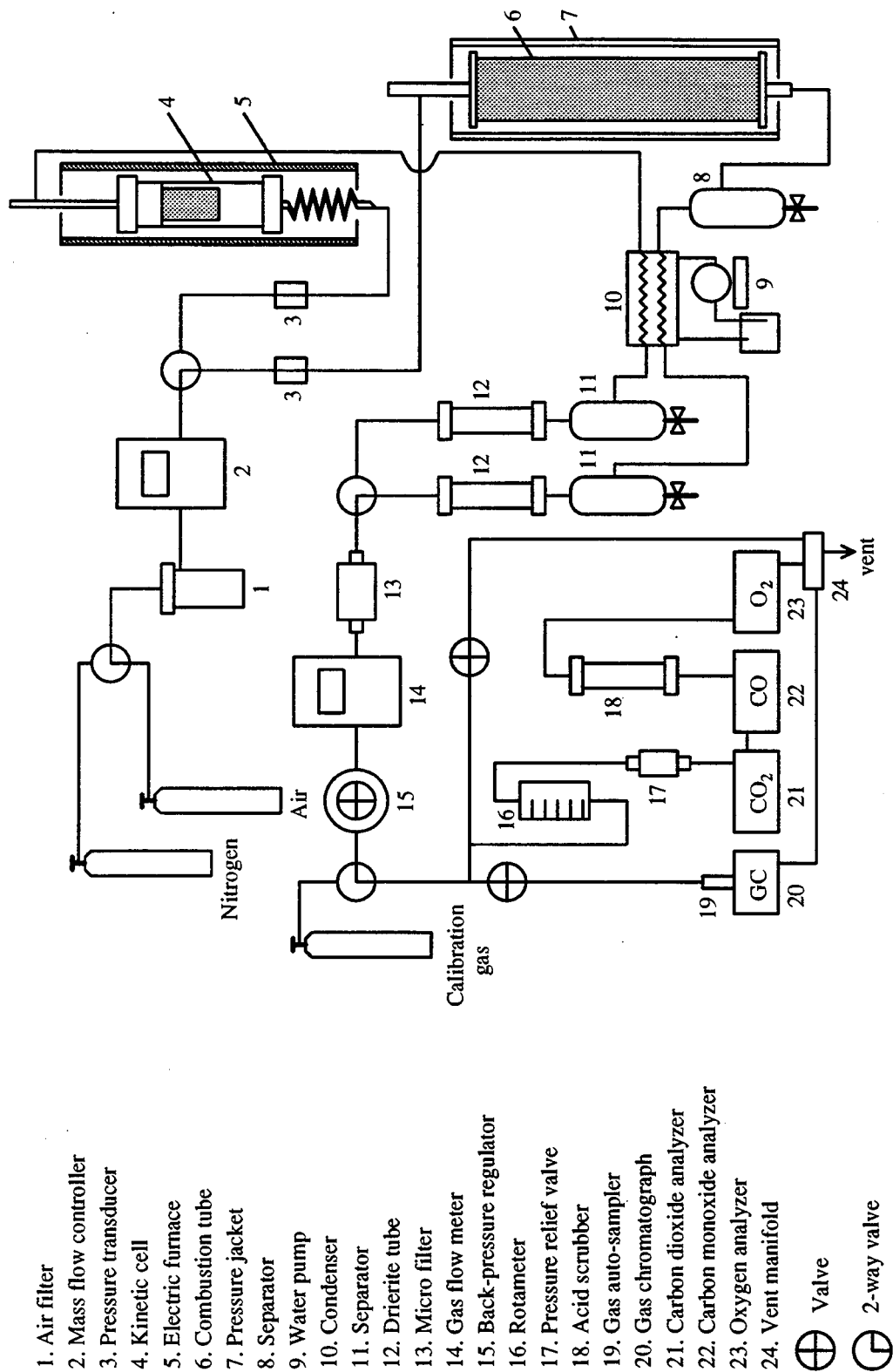


Figure 3.1: Schematic Diagram of Kinetic and Combustion Tube Apparatus

3. EXPERIMENTAL APPARATUS

Table 3.1: Equipment Common to Kinetic and Combustion Tube Experiments

Mass flow controller	Matheson electronic mass flow controller, model 8240, range 0.1–5 SLPM air, with model 8142 flow transducer.
Gas flow meter	Matheson electronic mass flow indicator, model 8160, range 0.1–5 SLPM air, with model 8141 flow transducer.
CO ₂ analyzer	Beckman infrared analyzer with linearizer, model 864 for carbon dioxide, two ranges: 0–5%, 0–20%.
CO analyzer	Beckman infrared analyzer with linearizer, model 864 for carbon monoxide, two ranges: 0–2%, 0–10%.
Oxygen analyzer	Teledyne Analytical Instruments oxygen analyzer, model 326, fuel cell, ranges: 0–5%, 0–25%, 0–100%.
Gas chromatograph	Hewlett-Packard gas chromatograph, model 5700A, thermal conductivity detector, 1mV FS sensitivity.
GC columns (two)	Alltech molecular sieve 4A, 80/100 mesh, custom packed in 6 ft.×1/8 in. stainless steel tubing.
Auto gas sampler	VICI 8-port 2-position switching valve, with electric actuator, model EC8UWP, 1/16 in. fittings.
Data logger	Hewlett-Packard data acquisition/control unit, model 3497A, with types 44421A guarded acquisition, 44428A actuator, 44422A T-couple acquisition assy.
Digital thermometer	Omega digital thermometer, model 2176A, 10 channels, °F or °C option.
Back-press. regulator	Tescom back-pressure regulator, model 26-1700.
Analyzer flow meter	Matheson tube-cube flowmeter, model J212, range: 0.2–4.2 SCFH air, 250 psig max.
Recorders (two)	Soltec 3-pen precision recorder, connected to GC and gas analyzers.

3. EXPERIMENTAL APPARATUS

3.2 Kinetic Tube Experimental Apparatus

The kinetic tube (Fig. 3.2) consisted of a thick-walled stainless steel cylinder measuring 5-1/4 in. (12.3 cm) long with an O.D. of 1.9 in. (4.8 cm). The ends of the cylinder were sealed by a system of stainless steel plugs and copper gaskets. End caps were screwed over the plugs and a high temperature and pressure seal was obtained by tightening the four bolts on the end caps. The thermowell consisted of a 14 in. long \times 1/16 in. O.D. stainless steel tubing in which a thermocouple was inserted. A long coil of 1/8 in. tubing was connected to the bottom of the lower plug to preheat the air entering the kinetic tube. Two thin-walled stainless steel cups were placed in the kinetic tube. The upper cup was 2.8 in. (7.1 cm) long with an I.D. of 1.049 in. (2.66 cm) and contained the sample. The lower cup was filled with dry sand and acted as a preheater. The bottom of both cups was perforated to allow flow of air. 200-mesh screens were placed at the bottom of the cups to help retain sand.

Alexander et al. (1962) concluded that the initial water saturation had little effect on the reaction kinetics. In kinetic experiments by Fassihi (1981), the samples were dry. However, to simulate initial field saturations closely, water was included in the samples. For maximum instrument sensitivity, the highest CO₂ and CO readings should be close to the scale maximum of the analyzers. Thus, the concentration of oil in a sample may vary, depending on the oil reactivity. Trial-and-error runs may be necessary to obtain the desirable oil concentration.

A typical kinetic experiment was carried out as follows. About 50 g sand and 2 g water were placed in a round bottomed dish and mixed using a spatula until the mixture was evenly moist. To this mixture, 2 g crude oil was added and mixing continued until a homogeneous mixture was obtained. This usually required about one hour. The resulting oil and water saturations were about 0.20. The sand mixture was tamped (about 10 ml each time) into the sample cup using a wooden plunger.

3. EXPERIMENTAL APPARATUS

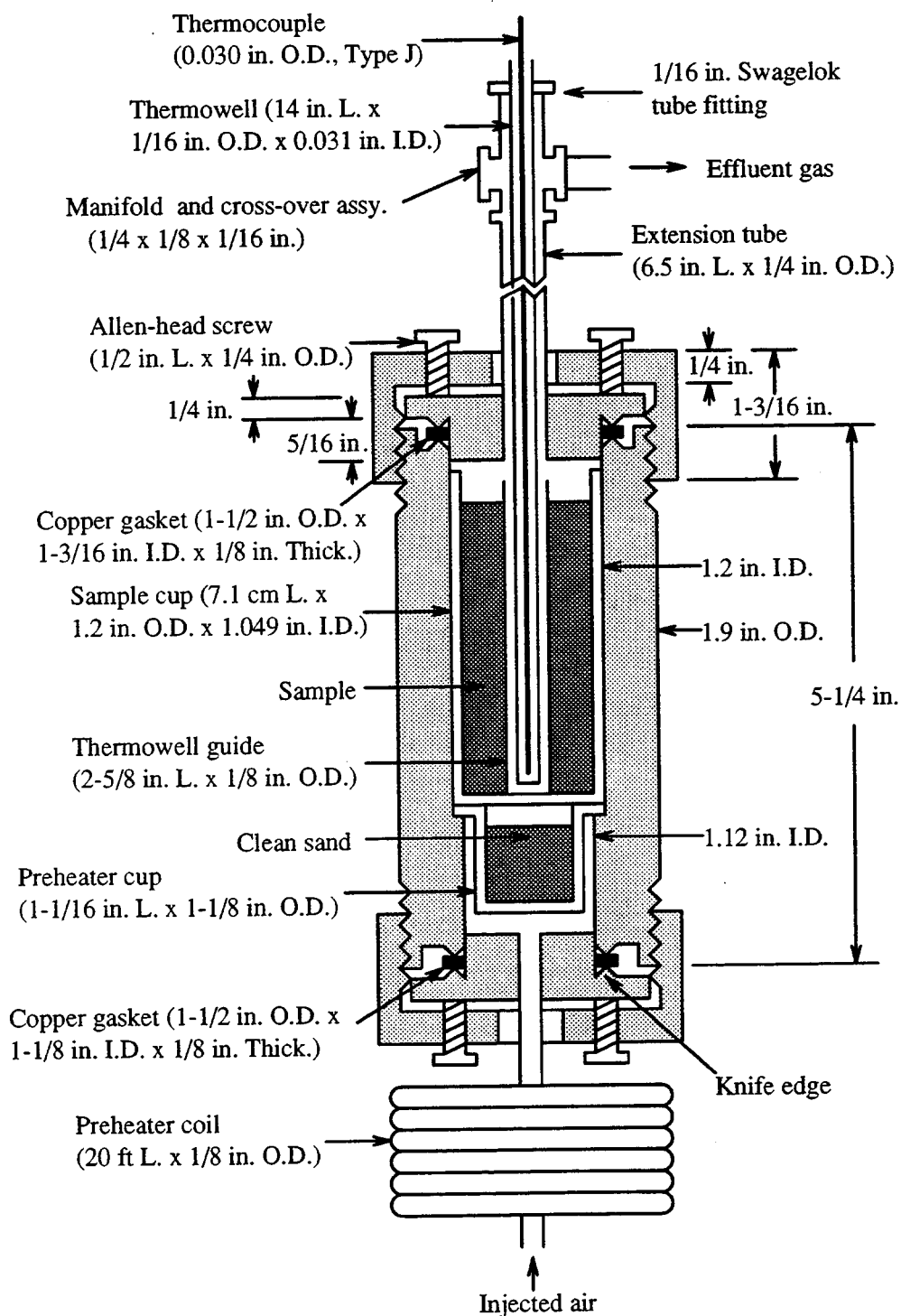


Figure 3.2: Schematic Diagram of Kinetic Tube

3. EXPERIMENTAL APPARATUS

The weight and length of the sample was measured before a run. With the sample in the kinetic tube, the end plugs were tightened. The kinetic tube was flushed with nitrogen, the pressure gradually increased to about 200 psig, and the kinetic tube was immersed in a large container of water to check for leaks. The kinetic tube was placed in the electric furnace and the temperature set at about 70°C. The kinetic tube was left in the furnace for about one hour to attain the starting temperature. After that, the furnace temperature was programmed to increase at about 50 °C/hr until a final temperature of about 500°C was reached. Air was injected at a constant rate of 0.7 L/min. Back-pressure was applied to maintain the kinetic tube pressure at 100 psig. The kinetic experimental run was fully automated.

A listing of the PC program for kinetic experiments is given in the Appendix. A list of the equipment used solely for kinetic experiments is given in Table 3.2.

3.3 Combustion Tube Experimental Apparatus

The combustion tube consisted of a thin-walled stainless steel tube measuring 39 in. long \times 3 in. O.D. \times 0.016 in. wall thickness (Fig. 3.3). Bored, knife-edge flanges were silver soldered to both ends of the tube. On the inside of the bottom (cap) flange, interconnected, concentric grooves were machined to allow uniform flow at the bottom end of the tube. A 9 in. long \times 1 in. I.D. brass tube was silver soldered to the top (cap) flange. A 1/4 in. Swagelok tube fitting was silver soldered to the side of the brass tube, through which air was injected into the tube. A pair of 1/8 in. and 1/16 in. Swagelok tube fittings was silver soldered to the top of the brass tube, through which two thermowells passed and were secured.

The thermowells consisted of 1/8 in. and 1/16 in. O.D. stainless steel tubes about 94 cm long which were silver soldered together at several places along the length. A bundle of nine thermocouples (each of 0.020 in. O.D.) were silver soldered

3. EXPERIMENTAL APPARATUS

Table 3.2: Equipment Solely for Kinetic Tube Experiments

Kinetic tube	Type 316 seamless, stainless steel, 5-1/4 in. long \times 1.9 in. O.D., custom-machined copper gaskets (2 sizes): 1/8 in. thick \times 1-1/2 in. O.D. \times (1-1/8 and 1-3/16 in. I.D.).
Sample cups	(1) Type 316 stainless steel, 2.8 in. long \times 1.185 in. O.D. \times 1.049 in. I.D. (2) Titanium, 2-3/4 in. long \times 1.185 in. O.D. \times 1.122 in. I.D.
Thermocouple	Omega type J iron-constantan, 50 in. long \times 0.030 in. O.D., 2100°F max.
Temperature programmer	TECO thermocouple temperature programmer, model TP-2000, 0–200°C/hr, 0–1000°C range, type K thermocouple, 3000 watts max.
Electric furnace	Marshall electric furnace, model 1046, 20 in. long \times 3 in. I.D., 2000°F max, 1.9KVA.
Pressure transducer and indicator	Celesco pressure transducer and indicator, model CD10B, 0–200 psi pressure plate.
Moisture trap	Tandem stainless steel tubes, 1 ft long \times 3/8 in. I.D. containing Drierite.
Balance	Torbil electronic balance, model EA-1, 0–160 g, 0.0001 g per division.

3. EXPERIMENTAL APPARATUS

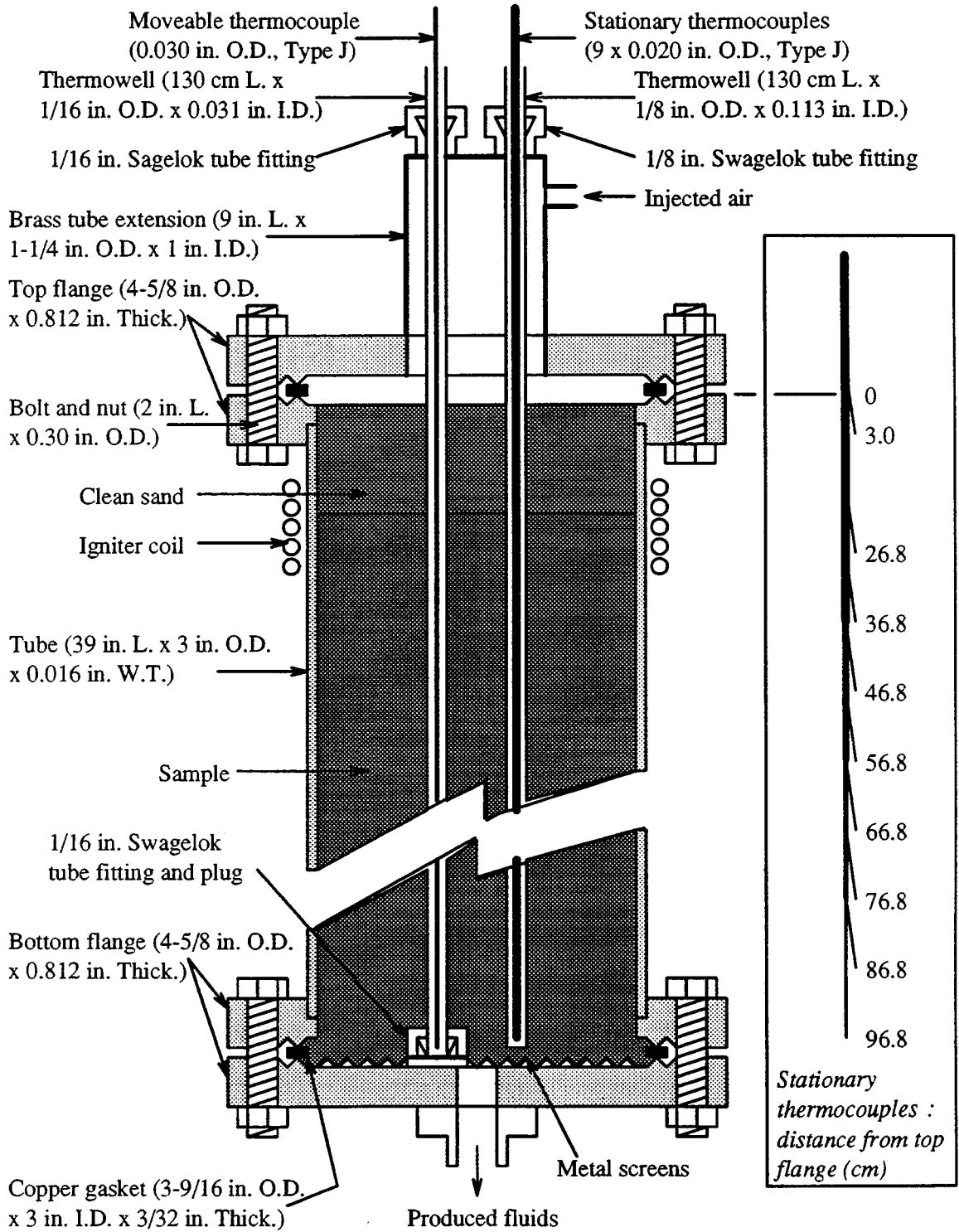


Figure 3.3: Schematic Diagram of Combustion Tube

3. EXPERIMENTAL APPARATUS

together with the tips spaced at 10 cm intervals. The thermocouple bundle was inserted into the larger thermowell, and temperatures recorded at known positions in the tube. A thermocouple (0.030 in. O.D.) was placed inside the smaller thermowell. This thermocouple could be moved freely to measure temperatures in small traverse increments. A pair of 40- and 60- mesh metal screens were secured at the tube fitting-plug assembly that sealed the bottom end of the larger thermowell. The bottom end of the smaller thermowell was capped with silver solder. The combustion tube was sealed by a system of copper gaskets between the flanges, and Teflon twin ferrules at the thermowell-tube fitting connections. An electric igniter coil was wound around the tube, some 10 cm below the top flange.

A typical combustion experiment was carried out as follows. About 8500 g sand and 450 g mortar clay were placed in a large pail and mixed thoroughly using a small shovel. About 400 g water was added to the sand-clay mixture. The mixture was thoroughly mixed until evenly moist. The mixture was placed in two separate pails to allow easy mixing with oil. About 450 g crude oil was added, about half this amount to each pail. The mixture in each pail was thoroughly stirred. The contents of each pail were intermixed a few times to obtain a homogeneous mixture. The mixture was then placed in one pail and weighed.

The thermowells were anchored at the bottom flange and the flange bolts were tightened. With the combustion tube securely fastened in a vertical position, portions (totaling about 200 ml) of the sample were introduced into the tube. Using a heavy, metal plunger that passed over the thermowells, the sample was tamped into the tube. This process of adding about 200 ml of the sample followed by tamping was continued until the tube was filled to about 10 cm from the top. About 5 ml linseed oil was placed on the sample to accelerate ignition. Linseed oil is more reactive to oxidation than crude oil. The tube was filled to the top with clean sand to help achieve a uniform air flow. The thermowells were carefully guided through the tube

3. EXPERIMENTAL APPARATUS

fittings on top of the brass tube. The top flange was bolted and Teflon ferrules passed over the thermowells and tightened.

Nitrogen was introduced at the injection inlet at the top of the combustion tube to flush the sand pack. With the outlet of the combustion tube plugged, the tube was pressure tested to about 150 psig for 15 minutes. A thermocouple was secured to the igniter coil to monitor the temperature of the coil during ignition. The combustion tube was placed in the pressure jacket and the annulus filled with an insulating material, Vermiculite. The inlet and outlet connections to the tube were tightened. The thermocouples were inserted into the thermowells. The jacket heaters were set at about 120°F and left on overnight to allow the temperature to stabilize throughout the sand pack.

Electric current was introduced into the igniter coil in gradual steps using the variable power transformer (variac). When the temperature in the combustion tube at the igniter level reached about 650°F (345°C), air injection was initiated. The air injection rate was set on the mass flow controller at about 3 L/min. The back-pressure regulator was adjusted to obtain an injection pressure of about 100 psig. The computer program on the PC was activated to commence data recording.

Usually, after about two hours, a stable combustion was reached, as evident from stable gas composition readings. Temperature profiles were taken every 20-30 min. An accurate temperature profile of the combustion zone was obtained by shifting the moveable thermocouple in steps of about 5 mm in the vicinity of the combustion zone. Recordings of the temperature measurements were made by pressing specific keys on the PC as explained in the Appendix.

Almost from the start, water was produced. However, oil was produced after about 4 hours, depending on the oil type. All produced liquids were collected in graduated sample bottles which were tightly capped for subsequent analysis. The sand pack was burned to the bottom flange so that the amount of fuel burned could

3. EXPERIMENTAL APPARATUS

be determined accurately. A run usually required about 8-10 hours. At the end of a run, the combustion tube was flushed with nitrogen.

A listing of the PC program for combustion tube experiments is given in the Appendix. Equipment used solely for combustion experiments is shown in Table 3.3.

3.4 Other Apparatus

Special equipment was required for kinetic tube weight experiments, produced liquid and fuel analyses and other special purposes. These are discussed next.

3.4.1 Weight Versus Temperature Apparatus

The kinetic tube experimental apparatus was used to measure the change in weight of a sample with temperature in the presence of an oxidant gas or nitrogen. For this purpose, the stainless steel sample cup was replaced by a cup made of titanium. This reduced the weight (about 26 g versus 93 g) so that the Torbal electronic balance (160 g maximum weight) could be used.

The experimental procedure was the same as that for standard kinetic tube runs as described in Section 3.2. The injection rate and pressure were set at 0.7 L/min and 100 psig. The temperature was increased at 50°C/hr, until the final temperature for a schedule was reached. The electric furnace was turned off and the kinetic tube was flushed with nitrogen if air was used in the run. The kinetic tube was allowed to cool to room temperature, keeping the pressure in the kinetic tube constant at about 120 psig to avoid further vaporization. The sample cup was removed and weighed on the Torbal balance. The sample and the kinetic tube were replaced in the furnace. This process was repeated for a number of temperature schedules. The final temperature of each schedule was increased by about 50°C, until a final temperature of about 550°C was reached.

3. EXPERIMENTAL APPARATUS

Table 3.3: Equipment Solely for Combustion Tube Experiments

Combustion tube	Type 321 seamless, stainless steel, 39 in. long \times 3 in. O.D. \times 0.016 in. W.T.
Pressure jacket	Type 304 stainless steel , 44 in. long \times 6-5/8 in. O.D. \times 0.28 in. W.T.
Flanges	Kurt J. Lesher Co. F-style, knife-edge, 4-5/8 in. O.D. \times 0.812 in. thick, 3.010 in. bored I.D., 10 bolt holes.
Gaskets	Kurt J. Lesher Co. copper gaskets, 3-9/16 in. O.D. \times 3 in. O.D. \times 3/32 in. thick.
Thermowells	Stainless steel tubings, silver soldered together. (1) 130 cm long \times 1/16 in. O.D. \times 0.031 in. I.D. (2) 130 cm long \times 1/8 in. O.D. \times 0.113 in. I.D.
Thermocouples	(1) Moveable: Omega type J iron-constantan, 0.030 in. O.D., 2100°F max. (2) Stationary: Omega type J iron-constantan, 0.020 in. O.D., 2100°F max.
Jacket heater control	Love Controls Corp. temperature controller, 0-800°F, type J thermocouple.
Igniter control	Powerstat variable power transformer, 240/120 ACV, 25 A max.
Moisture trap	18 in. long \times 1-1/2 in. I.D. plexiglass tube containing Drierite.
Balance	OHAUS heavy duty solution balance, 20 kg capacity, 1 g/division.

3. EXPERIMENTAL APPARATUS

3.4.2 Apparatus for Analysis of Produced Liquids

The liquids produced during a combustion tube experiment were analyzed to determine the volumes of water and oil, the oil API gravity, and the oil viscosity at various temperatures. The equipment used are listed in Table 3.4.

About two drops of Petrolite RP-890 demulsifier were added to the sample. The samples were placed in a Damon/IEC centrifuge and spun at 3000 rpm for about 20 minutes. The volumes of water and oil in the graduated sample bottles were measured.

The viscometer was calibrated as follows: 40 ml of each of the Brookfield viscosity standard liquids was placed in clean, graduated sample bottles. Using Brookfield spindle No. 4, viscometer readings based on the highest rpm were obtained for each viscosity standard. A straight line relationship for viscosity versus viscometer-reading was obtained.

The oil sample bottles were drained of water through a small hole made at the bottom of each bottle, which was then capped by a small metal plug. The sample bottles were filled with oil to the 40 ml mark. A sample bottle was placed in a water bath which was set at a particular temperature. After about one hour, when the temperature in the sample bottle had equilibrated with that of the bath, viscometer measurements were made. Oil viscosity was obtained using the viscometer calibration curves. The temperature of the bath was increased in steps of about 20°C, and the procedure was repeated to obtain oil viscosities at various temperatures.

The sample was allowed to cool to room temperature. The contents were poured into a specific gravity bottle, and in the standard manner, the specific gravity and API gravity were determined.

3. EXPERIMENTAL APPARATUS

Table 3.4: Equipment for Produced Liquid Analysis

Centrifuge	Damon/IEC centrifuge, model PR-6000, 6000 rpm max., 12 × 50 ml samples maximum.
Demulsifier	Petrolite demulsifier RP-890.
Sample bottles	Corning graduated sample bottles, 50 ml, conical bottom.
Viscometer	Brookfield synchro-lectric viscometer, model LVT, 8 speeds (0.3 to 60 rpm).
Viscosity standards	Brookfield viscosity standards, viscosities (cP) at 20°C: 490, 950, 4775, 11360, 30800, 60000.
S.G. bottle	Kimax specific gravity bottle for viscous liquids, approx. 24 ml, stopper with 1.6 mm hole.

3. EXPERIMENTAL APPARATUS

3.4.3 Fuel Extraction Apparatus

The fuel at the combustion zone was extracted for elemental analysis to determine the composition by weight of hydrogen, carbon, oxygen and nitrogen. The apparatus used for extracting the fuel from the sand mixture is shown in Fig. 3.4. The equipment used is listed in Table 3.5.

After a combustion tube run, the contents of the tube were carefully removed with the aid of a scraper. The burned sands were loose and light gray in color. The combustion zone, about one inch thick, was usually consolidated and dark gray in color. The unburned sand mixture ahead of the combustion zone was dark brown-to-black in color, very moist and exuded a strong smell of crude oil. The combustion zone was scraped clean of crude oil and burned sands and was crushed into small pieces.

The crushed combustion zone sample was placed in a cellulose thimble which was inserted in a Soxhlet extraction tube. Toluene was allowed to boil, condense at the condenser, drip through the sample, and dissolve the fuel. Both toluene and the dissolved fuel were collected in a flat-bottom flask. The contents of the flask and distilling receiver were emptied into a beaker, capped with perforated aluminium foil, and placed in the vacuum oven. The oven was set at about 20 in. Hg vacuum and the temperature was gradually increased to distill off the toluene. The fuel was left as residue and was subsequently sent to Corelab for elemental analysis.

3.5 Calibration of Instruments

The gas analyzers and gas chromatograph were calibrated at the beginning and end of every experiment, as they were subject to instrument drift. The pressure transducers, mass flow controller and gas flow indicator were calibrated only before

3. EXPERIMENTAL APPARATUS

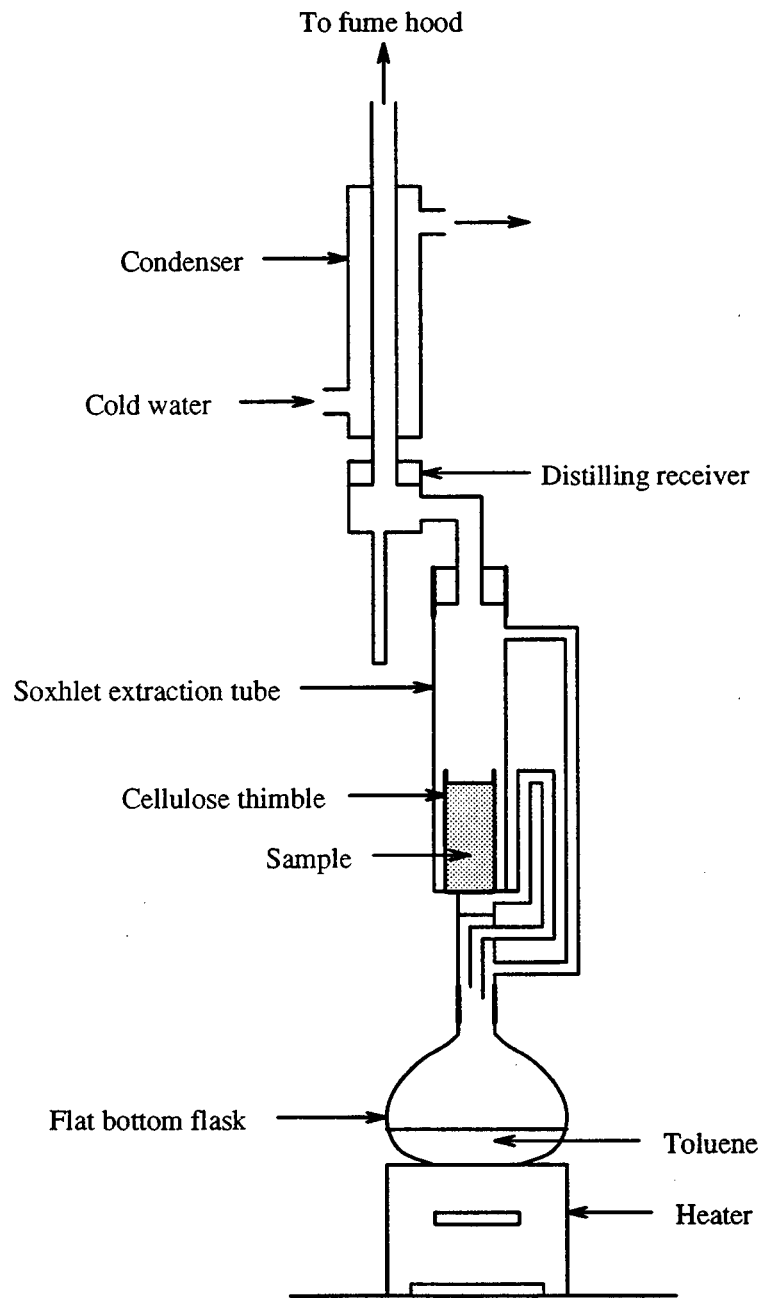


Figure 3.4: Schematic Diagram of Fuel Extraction Apparatus

3. EXPERIMENTAL APPARATUS

Table 3.5: Equipment for Fuel Extraction

Heater	Precision Scientific Co. rheostat controlled heater, 550 watts maximum.
Flask	Pyrex flat bottom flask, 300 ml, top joint no. 24/40.
Soxhlet tube	ACE Glass Inc. Soxhlet extraction tube, bottom jt. no. 24/40, top jt. no. 45/50, 85 ml capacity.
Distilling receiver	ACE Glass Inc. distilling receiver, bottom jt. no. 45/50, top jt. no. 24/40.
Condenser	Pyrex condenser, 30 cm long, top joint no. 24/40.
Thimble	Whatman cellulose extraction thimble, 8 cm long \times 3.5 cm O.D.
Oven	Precision Scientific Co. vacuum oven, model 10, 150°C max., atmos. to 30 in. Hg.
Vacuum pump	Sargent-Welch vacuum pump, model 8804.

3. EXPERIMENTAL APPARATUS

each experimental run. During calibration of the gas chromatograph, the program on the PC was run to enable automatic gas injection and backflushing and computation of the nitrogen concentration.

3.5.1 Gas Analyzer Calibration

The analyzers were switched on at least one day before an experiment to allow the instruments to stabilize at the operating temperatures. The gas analyzers were calibrated using standard gases. Depending on the analyzer range being used, the standard gases were as follows.

1. Kinetic tube experiments

Carbon dioxide analyzer (range 3: 0-5%)

Carbon monoxide analyzer (range 3: 0-2%)

Oxygen analyzer (medium range: 0-25%)

Standard gas	CO ₂ (%)	CO (%)	O ₂ (%)
Zero gas (N ₂)	0	0	0
Span gas*	4.46	1.84	2.57
	2.53	1.04	0.99
	17.30 [†]	7.37 [†]	10.50
	1.11	0.50	18.29
Span gas**	0.03	0	20.95

* For CO₂ and CO analyzers. ** For O₂ analyzer. [†] Switch to range 1.

3. EXPERIMENTAL APPARATUS

2. Combustion tube experiments

Carbon dioxide analyzer (range 1: 0–10%)

Carbon monoxide analyzer (range 1: 0–5%)

Oxygen analyzer (medium range: 0–25%)

Standard gas	CO ₂ (%)	CO (%)	O ₂ (%)
Zero gas (N ₂)	0	0	0
Span gas*	17.30	7.37	10.5
	2.53	1.04	0.99
	6.98	3.98	4.52
	1.11	0.50	18.29
Span gas**	0.03	0	20.95

* For CO₂ and CO analyzers. ** For O₂ analyzer.

The voltage of each analyzer reading was read off the corresponding channel on the Hewlett-Packard data acquisition and control unit. The voltmeter on this unit is accurate to 1 micro-volt. In addition, the Soltec plotter connected to the analyzers was used to monitor the stability of the analyzer readings. The inlet pressure and gas flow rotameter rate were set as close as possible to the values expected in the experiment to obtain maximum accuracy. Typically, these were 1.3 SCFH and 1.2 psig. The linearizers on the CO₂ and CO analyzers were not used because of the tedious calibration process needed to obtain a linear response.

The CO₂ and CO analyzers were first zeroed using nitrogen. The O₂ analyzer need not be zeroed. Span gas was flowed and the "Gain" potentiometers on the analyzers were adjusted to give the corresponding maximum readings. This process of zeroing and spanning the analyzers was repeated until the readings were constant.

3. EXPERIMENTAL APPARATUS

The intermediate calibration gases were flowed through the analyzers in increasing oxygen concentration so that at the end of calibration, the analyzers were set to measure air with minimum stabilisation time required. Each calibration gas was flowed for about 15 minutes, depending on stability of gas readings on the Soltec plotter. Voltage of stable readings could usually be read to 0.1 milli-volt. At the end of each experiment, the same calibration procedure was carried out, except no adjustment was made to the analyzer potentiometers.

Both sets of calibration data were input to the calibration program, GASCAL.F (Appendix). The program calculates a 5th order polynomial that best fits the CO₂ and CO calibration data. In view of the specified linear response of the O₂ analyzer, a least-squares straight line fit was calculated for the O₂ calibration data. Examples of these calibration fits are shown in Figs. 3.5a, 3.5b, and 3.6a.

3.5.2 Gas Chromatograph Calibration

At least one day before an experiment, the GC was switched on with the temperature of the thermal conductivity detector set at 100°C. During this period, the carrier gas, helium ("Zero" grade, 99.995% pure) was flowed through the columns at a low rate of less than 0.01 SCFH. About two hours before the calibration, the GC oven was turned on and set at 35°C; helium was flowed at the rate used in the experiments, 0.09 SCFH; "Detector Power" switch was set at Dial Position 3; and "Attenuation" control switch was set at Dial Position 1. The Soltec plotter was switched on to monitor the onset of a stabilized baseline. The GC columns were injected and backflushed a few times using the Hewlett-Packard data acquisition and control unit.

Calibration runs with a wide range of nitrogen concentrations confirmed the linear response of the Alltech molecular sieve columns (Fig. 3.6b). Thus, calibration with

3. EXPERIMENTAL APPARATUS

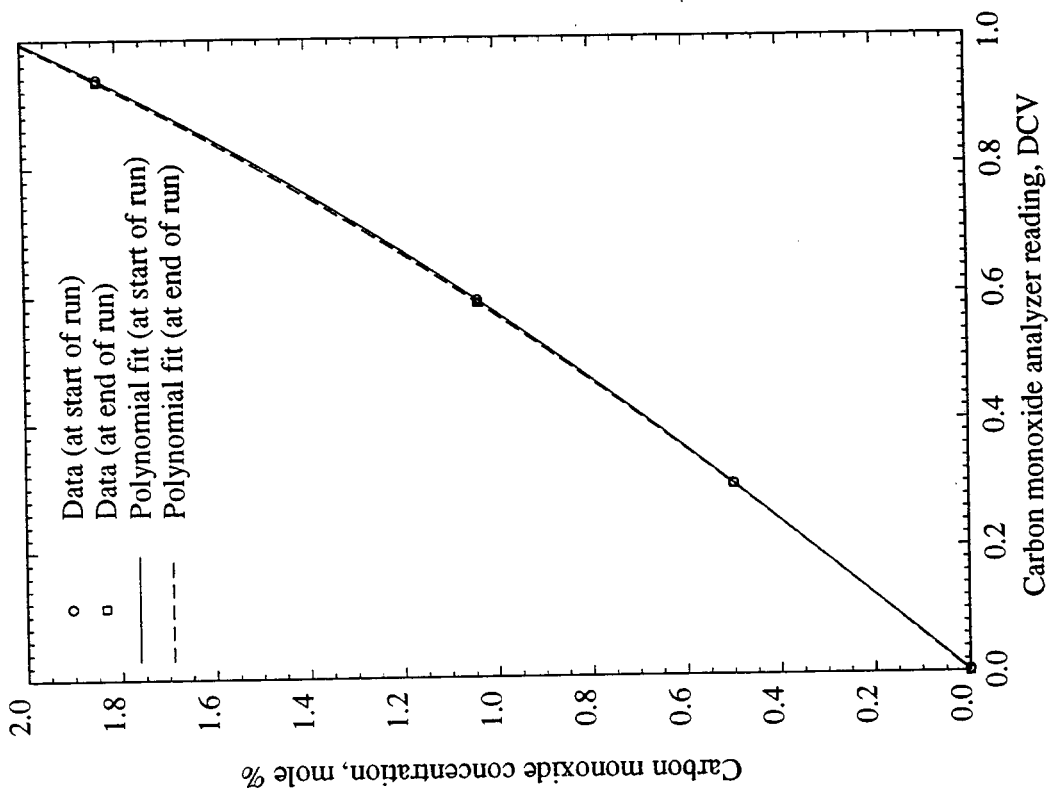


Figure 3.5a: Carbon Dioxide Analyzer Calibration

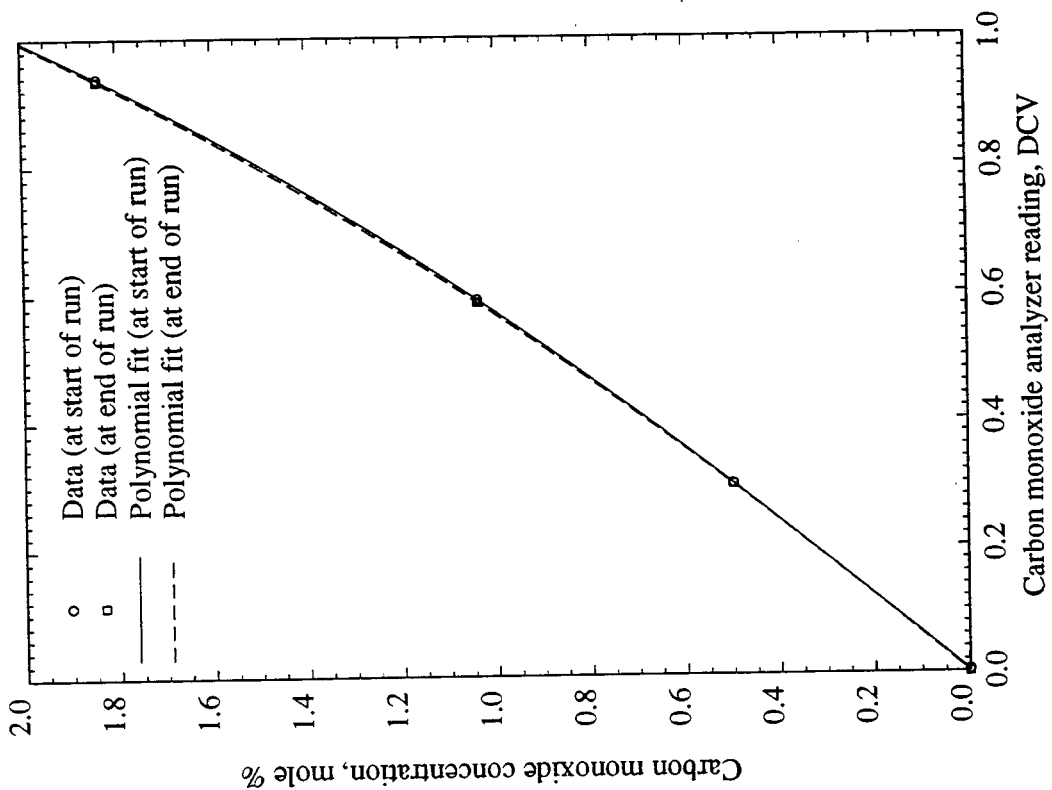


Figure 3.5b: Carbon Monoxide Analyzer Calibration

3. EXPERIMENTAL APPARATUS

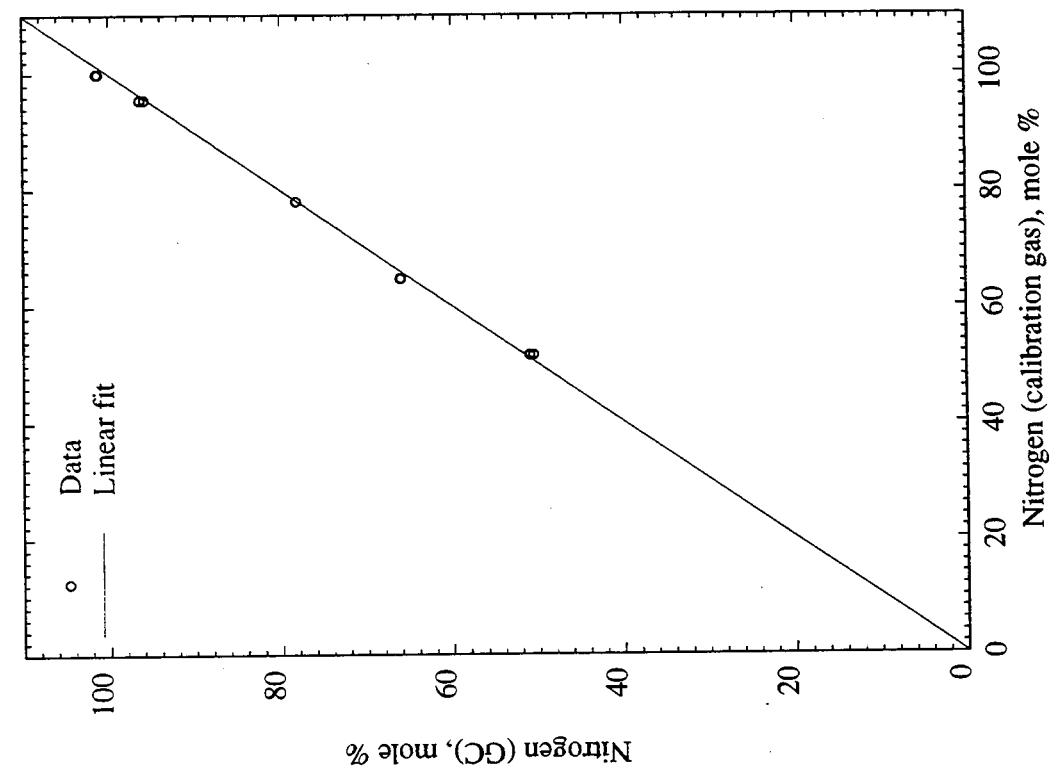


Figure 3.6a: Oxygen Analyzer Calibration

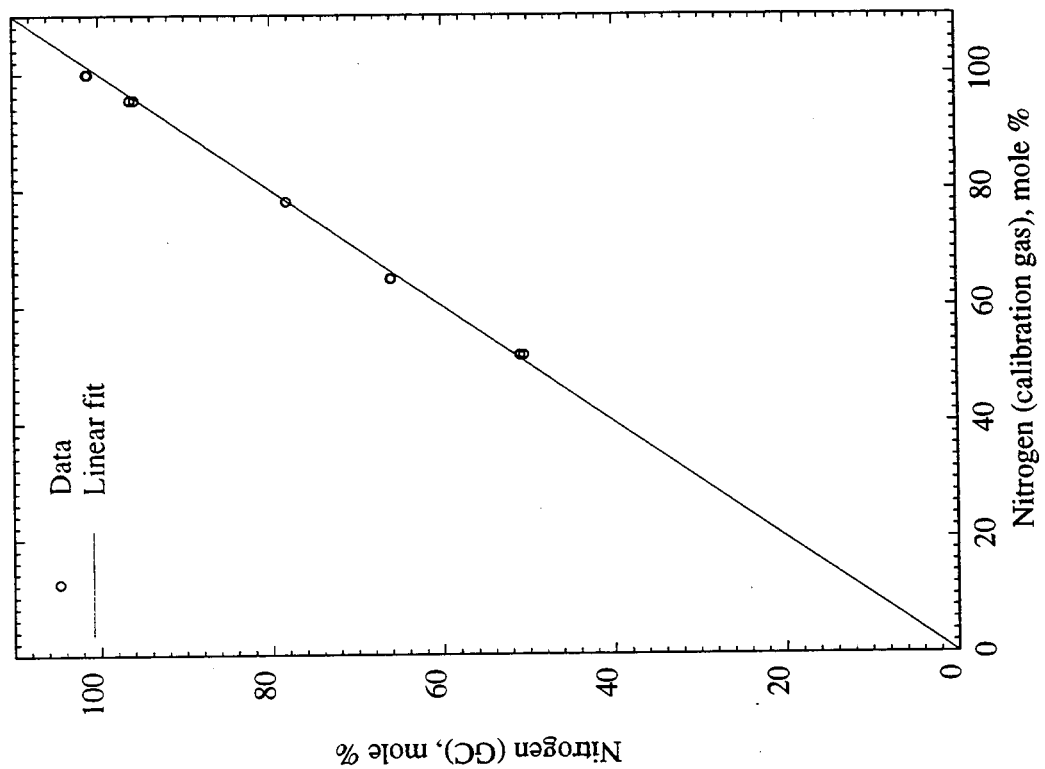


Figure 3.6b: Gas Chromatograph Calibration

3. EXPERIMENTAL APPARATUS

air only was carried out before and after an experimental run. The nitrogen reading computed by the PC program was adjusted by correcting the variable, FACGC (Appendix), to yield a value close to 78%. For example, if the computed nitrogen value is 80%, then $FACGC(\text{new}) = FACGC(\text{old}) \times 78.084/80$. Three sets of constant nitrogen readings were sufficient to confirm the validity of the calibration.

3.5.3 Flow Meter Calibration

The equipment required to calibrate the Matheson mass flow controller (Model 8240) and mass flow meter (Model 8160) were as follows.

1. Precision Scientific Co. wet-test meter, 3L/rotation, 0.01L/div.
2. Hewlett-Packard digital multimeter, model 3465A.
3. Fluke digital multimeter, model 8050A.

The outlet of the transducer on the mass flow controller was connected directly to the inlet of the transducer on the gas flow meter by a 1/8 in. plastic tubing. The wet-test meter was connected to the outlet of the transducer on the gas flow meter with an in-line needle valve for fine flow rate control. The multimeters were connected to the flow controller and flow meter, and set to read 20 DCV maximum.

The instruments were allowed to warm up for about one hour. Three flow rate calibrations were made: zero, mid-range and span. The "Zero" potentiometers were adjusted to give a positive reading close to zero in value, about 0.01 DCV. Air was flowed through the instruments. The flow rate was adjusted using the needle valve to give approximately 5 DCV on the multimeters. Once these readings were stable, a stop-watch (accurate to 0.01 sec.) was used to record the time of flow of 6 L of air through the wet-test meter. The flow rate was thus calculated. With air still flowing, any necessary adjustments to the "Span" potentiometers were made so that

3. EXPERIMENTAL APPARATUS

the voltages on the multimeters corresponded to the gas flow rate measured by the wet-test meter.

A similar calibration procedure was used at mid-range at a reduced flow rate, corresponding to 2.5 DCV on the multimeters. The suite of zero, mid-range and span calibration steps were repeated until the readings were constant.

3.5.4 Pressure Transducer Calibration

The pressure transducers were calibrated using a dead-weight tester (Barnet Instruments Ltd., 500 psig maximum). Nitrogen was used to pressurize the transducers. The voltmeter on the Hewlett-Packard data acquisition and control unit was used to measure the transducer output voltage.

The pressure transducer was turned on about an hour before calibration. With no weight on the dead-weight tester, the "Zero" potentiometer was adjusted to read a value close to zero. A weight of 200 lb. was placed on the dead-weight tester, corresponding to the range on the pressure transducer. With the weights spinning steadily, the "Span" potentiometer was adjusted to give a 10 DCV reading. The zero and span calibrations were repeated until constant readings were obtained.

In addition to standard measurements, special analyses of oil and sand are required. The results of these special analyses are reported in Chapter 4.

4. Ancillary Experimental Results

In addition to kinetic and combustion tube experiments, six other types of analyses were carried out: elemental analysis, weight versus temperature, differential scanning calorimetry, thermogravimetric analysis, grain sieve analysis and X-ray diffraction. The results of these analyses are presented in this chapter.

4.1 Elemental Analysis Results

Elemental analyses were made on samples of Cold Lake bitumen, Huntington Beach and Hamaca crude oils, and samples of fuel extracted from the combustion zone in tube experiments. The main objectives of these analyses were to determine the atomic hydrogen-carbon ratios of the original crude oils and fuel, and the atomic oxygen-carbon ratios of the fuels. These analyses were carried out by *Corelab* in Houston, Texas. The results are summarized in Table 4.1.

The results indicate the atomic H/C ratio of the crude oil increases with increasing oil gravity. Oil from the last sample in Run VEN14 yields an atomic oxygen-carbon (O/C) ratio of 0.25, compared to 0.01 for the original crude oil. This indicates that the oil just ahead of the combustion zone has undergone low temperature oxidation. This result is in line with the observation that Run VEN14 is a low temperature oxidation experiment. This is evident from the low combustion temperature (about 350°C) and the high apparent H/C ratio, about 4.4, obtained from gas analysis.

4. ANCILLARY EXPERIMENTAL RESULTS

Table 4.1: Results of Elemental Analysis

Crude oil*	Sample [†]	Weight %				Atomic H/C ratio	Atomic O/C ratio
		C	H	N	O		
CLB	Original crude	82.98	10.62	0.37	1.29	1.53	0.01
HBO	Original crude	84.89	11.72	0.84	0.88	1.65	0.01
HCO	Original crude	83.97	10.55	0.60	1.36	1.50	0.01
HCO	Last sample from tube Run VEN14	63.40	10.56	0.42	20.69	1.99	0.25
HCO	Combustion zone extract (Run VEN14)	84.48	12.02	0.18	2.08	1.70	0.02
HCO	Combustion zone extract (Run VEN21)	82.55	10.36	0.39	2.51	1.50	0.02

* CLB = Cold Lake bitumen, HBO = Huntington Beach oil, HCO = Hamaca crude oil.

[†] VEN14: crude and 20–30 mesh sand mixture.

VEN21: crude and 170–270 mesh sand mixture.

4. ANCILLARY EXPERIMENTAL RESULTS

The atomic O/C ratio is 0.02 for the fuel extracted from the combustion zone in Run VEN14. This is significantly lower than the value of 0.25 for the oil from the last sample. One possible explanation for this difference is that most of the oxygen in the fuel sample has been used in oxidation reactions at the elevated temperatures of the combustion zone. Another possible explanation is that the oxygenated hydrocarbons may have reacted with toluene, and are distilled off during the separation process in the vacuum oven.

The atomic H/C and O/C ratios of the original crude oils are similar to those of the combustion zone sample in Run VEN21. These results agree with the observation that low temperature oxidation is absent in this run, as inferred from the high combustion temperature (about 500°C) and the apparent H/C ratio of 1.77 calculated from gas analysis.

Discussion of the atomic H/C ratios obtained by the various methods is presented in Chapter 6.

4.2 Weight Versus Temperature Results

The experimental conditions are summarized in Table 4.2. The results are plotted in Figs. 4.1–4.4. Two runs are shown in each figure: one run with air injected, and one with nitrogen. These pairs of runs have been normalized by matching them at the boiling point of water at the pressure used in the runs. The match points are 162°C at 80 psig for Run Pair CL6 and CL7 and Run Pair HBO3 and HBO4; and 170°C at 100 psig for Run Pair VEN12 and VEN13 and Run Pair VEN17 and VEN18.

A large decrease in weight is observed in the approximate range 20°–100°C. This is due to vaporization of water and light hydrocarbons. From about 100°C to 350°C, a lower rate of decrease is seen in weight versus temperature. Above 350°C, the weight decreases more sharply again due to rapid oxidation of the hydrocarbons.

4. ANCILLARY EXPERIMENTAL RESULTS

Table 4.2: Experimental Conditions for Sample Weight Versus Temperature Runs

Run No.	Crude oil*	Inj. gas	Flow-rate, L/min	Pressure, psig	Temp. rate, °C/hr	Sample weight, g	Weight %			
							Sand	Clay	Oil	Water
CL6	CLB	Air	0.94	80	50	53.4521	92.1	0	4.2	3.7
CL7	CLB	N ₂	0.94	80	50	53.0489	92.6	0	3.7	3.7
HBO3	HBO	Air	0.94	80	50	53.6376	92.0	0	3.8	4.2
HBO4	HBO	N ₂	0.94	80	50	53.3844	92.4	0	3.9	3.7
VEN12	HCO	N ₂	0.70	100	50	63.1281	86.8	4.6	4.6	4.1
VEN13	HCO	Air	0.70	100	50	60.9649	86.8	4.6	4.6	4.1
VEN17	HCO	N ₂	0.70	100	50	50.5697	90.8	0	4.9	4.3
VEN18	HCO	Air	0.70	100	50	53.3284	90.8	0	4.9	4.3

* CLB = Cold Lake bitumen, HBO = Huntington Beach oil, HCO = Hamaca crude oil.

The samples in these runs contain crude oil and 20–30 mesh sand, except for Run Pair VEN12 and VEN13 which also contain clay. The results indicate that for mixtures containing no clay, the decrease in weight with temperature in the approximate range 100°–350°C is slightly less for the case where air is injected than that where nitrogen is injected. This is probably due to low temperature oxidation, in which oxygen is added to the hydrocarbons.

For samples containing clay, however, the decrease in weight with temperature is similar for both air and nitrogen injection. This appears to indicate that with clay present the weight reduction due to vaporization and oxidation is approximately offset by the increase due to low temperature oxidation.

The main characteristics of the weight versus temperature trends are similar to those observed on TGA thermograms (Section 4.3).

4. ANCILLARY EXPERIMENTAL RESULTS

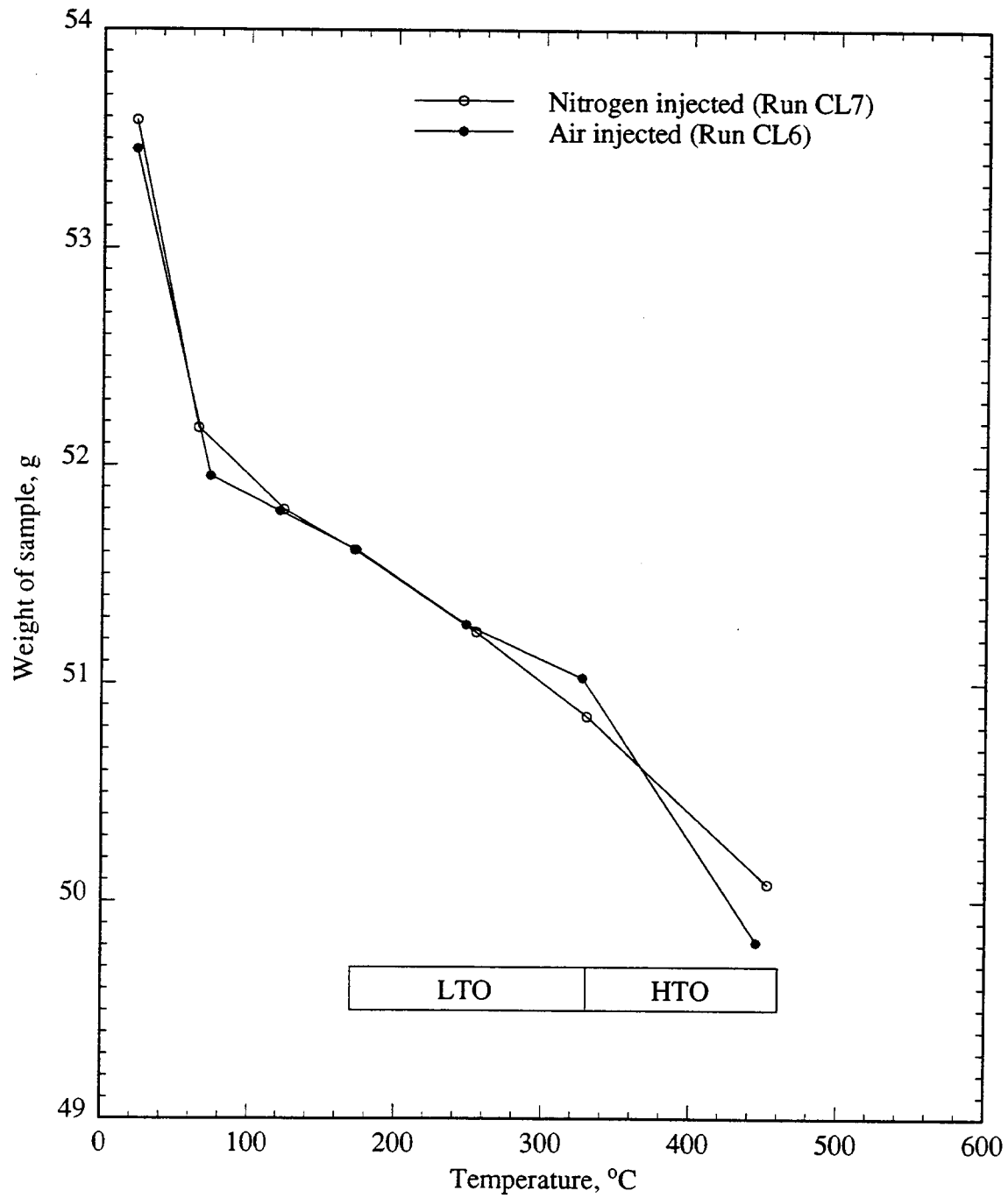


Figure 4.1: Cold Lake Bitumen – Sample Weight Versus Temperature (Runs CL6 and CL7)

4. ANCILLARY EXPERIMENTAL RESULTS

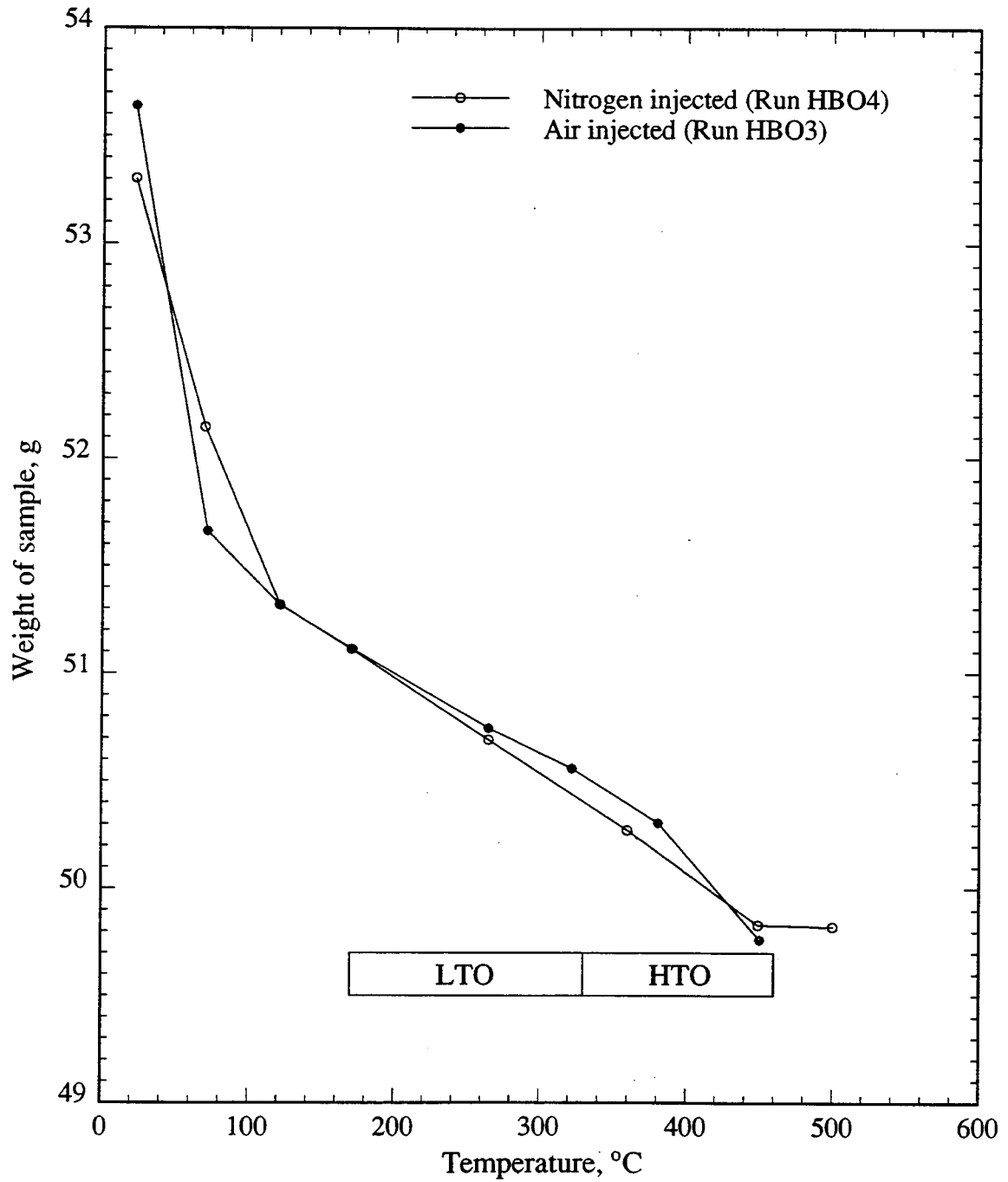


Figure 4.2: Huntington Beach Oil – Sample Weight Versus Temperature (Runs HBO3 and HBO4)

4. ANCILLARY EXPERIMENTAL RESULTS

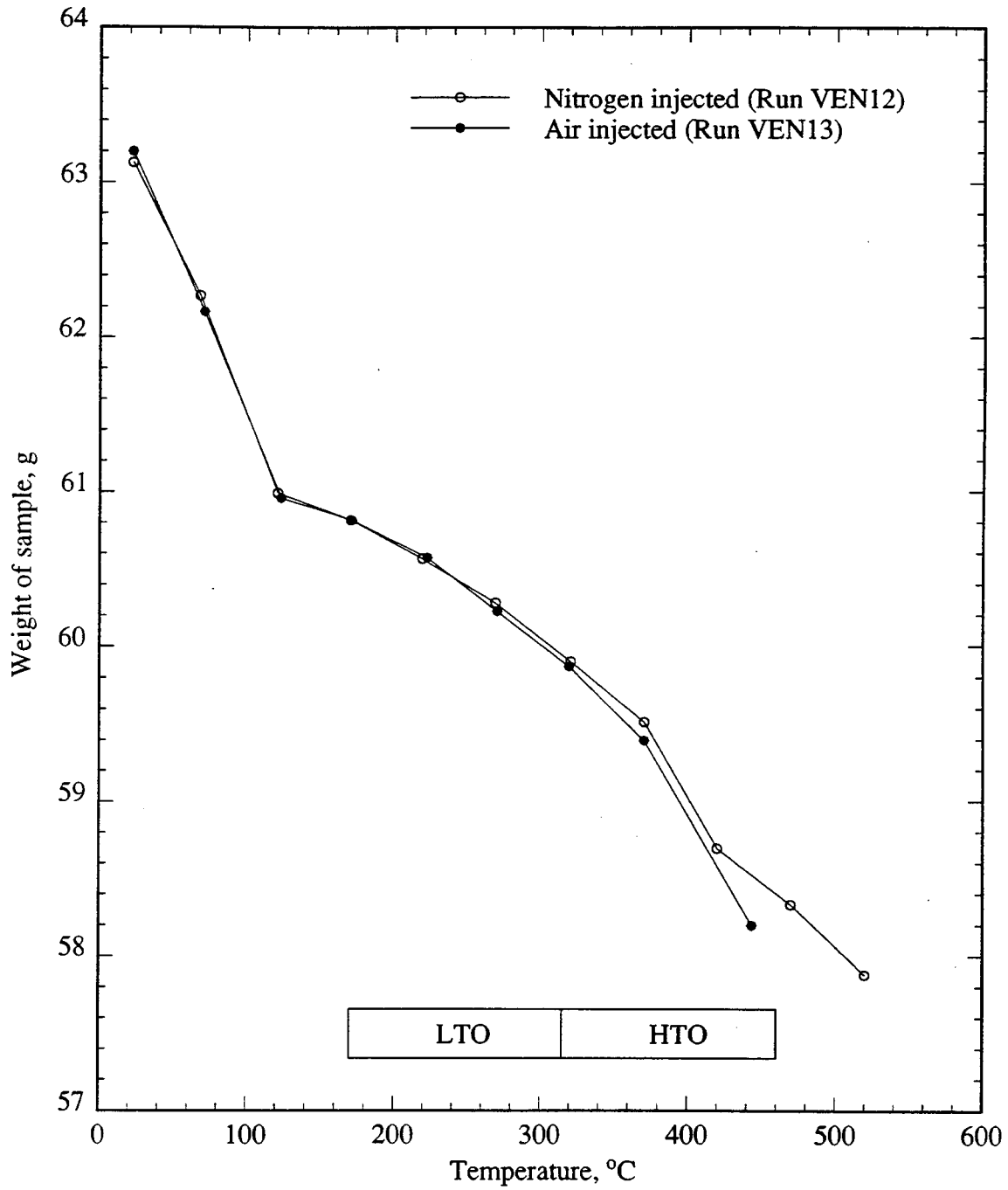


Figure 4.3: Hamaca Crude Oil – Sample Weight Versus Temperature (Runs VEN12 and VEN13)

4. ANCILLARY EXPERIMENTAL RESULTS

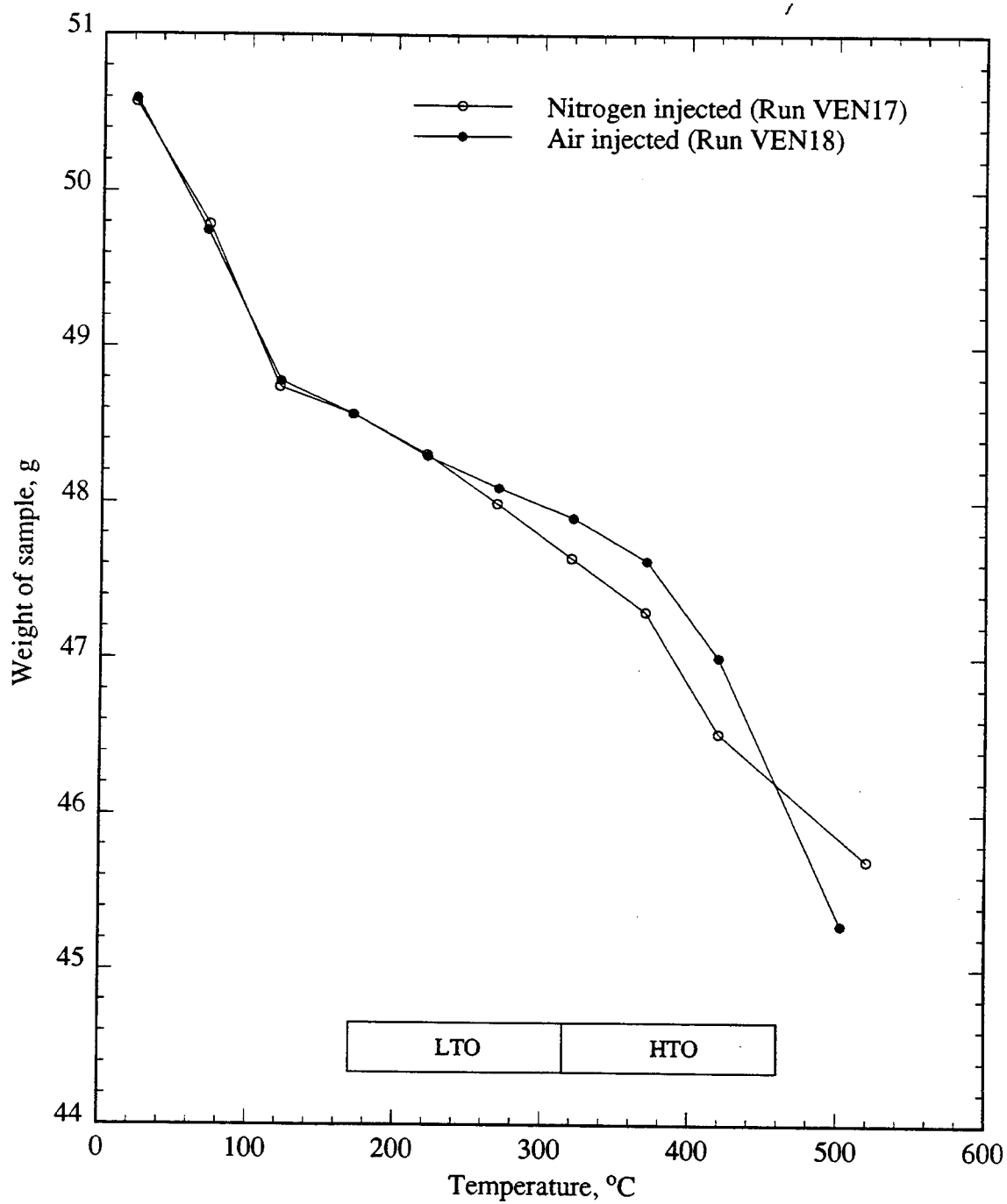


Figure 4.4: Hamaca Crude Oil - Sample Weight Versus Temperature (Runs VEN17 and VEN18)

4. ANCILLARY EXPERIMENTAL RESULTS

4.3 DSC and TGA Results

Differential scanning calorimetry (DSC) and thermogravimetric analysis (TGA) were performed on samples of Huntington Beach and Hamaca crude oils. These analyses were made at The Middle East Technical University in Ankara, Turkey. In addition, analyses were conducted on mixtures of crude oil and sand, and mixtures of crude oil, sand and clay. In these analyses, the sample mixture size was about 9 mg. Air was injected at a constant rate of 53 ml/min, while the temperature was increased at a fixed rate of 2°C/min. The results indicate that inclusion of sand or clay in the crude oil samples had little effect on the main characteristics of the thermograms. Consequently, only DSC and TGA thermograms for samples containing crude oil and sand are presented in Figs. 4.5 - 4.8.

The rate of decrease in weight with temperature on the TGA thermogram indicate three main temperature regions. In the range, 27°-280°C, a steep rate of decrease in weight was observed. This is mainly due to vaporization of the light hydrocarbon fractions, as evident from the slightly endothermic reaction observed on the DSC thermograms. A gentle rate of decrease in weight was measured in the temperature range, 280°-400°C, corresponding to the first exothermic reaction on the DSC thermogram. In the range, 400°-500°C, the weight decreases greatly due to rapid oxidation of the hydrocarbons. This corresponds to the second, highly-exothermic reaction seen on the DSC thermograms, which have peaks at about 450°C. The two temperature peaks on the DSC thermograms are in line with the LTO and HTO peaks observed in kinetic experiments on these crude oils (Chapter 6).

The DTA thermogram obtained by Tadema (1959), for a typical crude oil with air flow (Fig. 2.1), also shows two main oxidation reaction peaks at about 270°C and 400°C.

4. ANCILLARY EXPERIMENTAL RESULTS

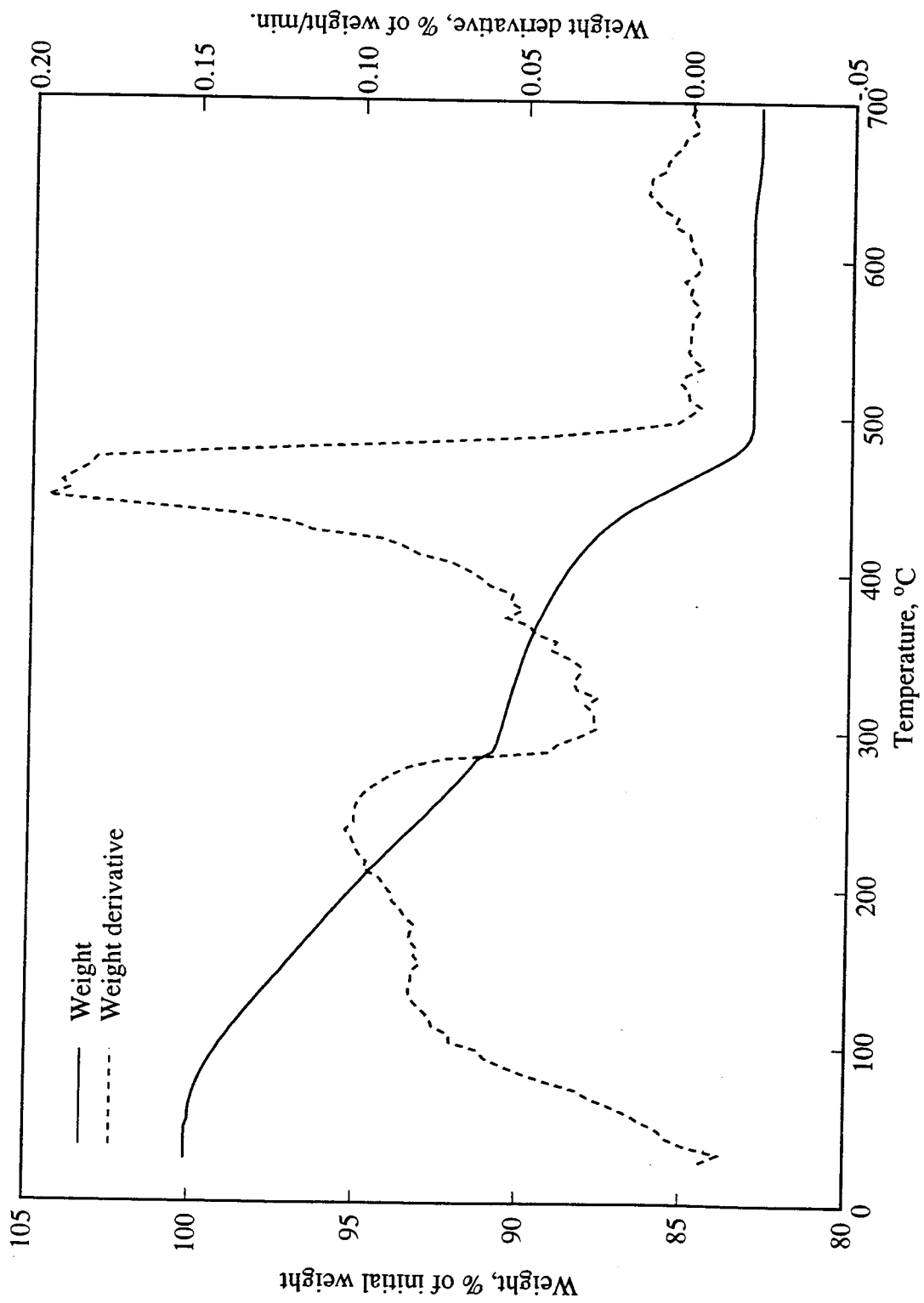


Figure 4.5: TGA thermogram - Huntingon Beach Oil and Sand Mixture

4. ANCILLARY EXPERIMENTAL RESULTS

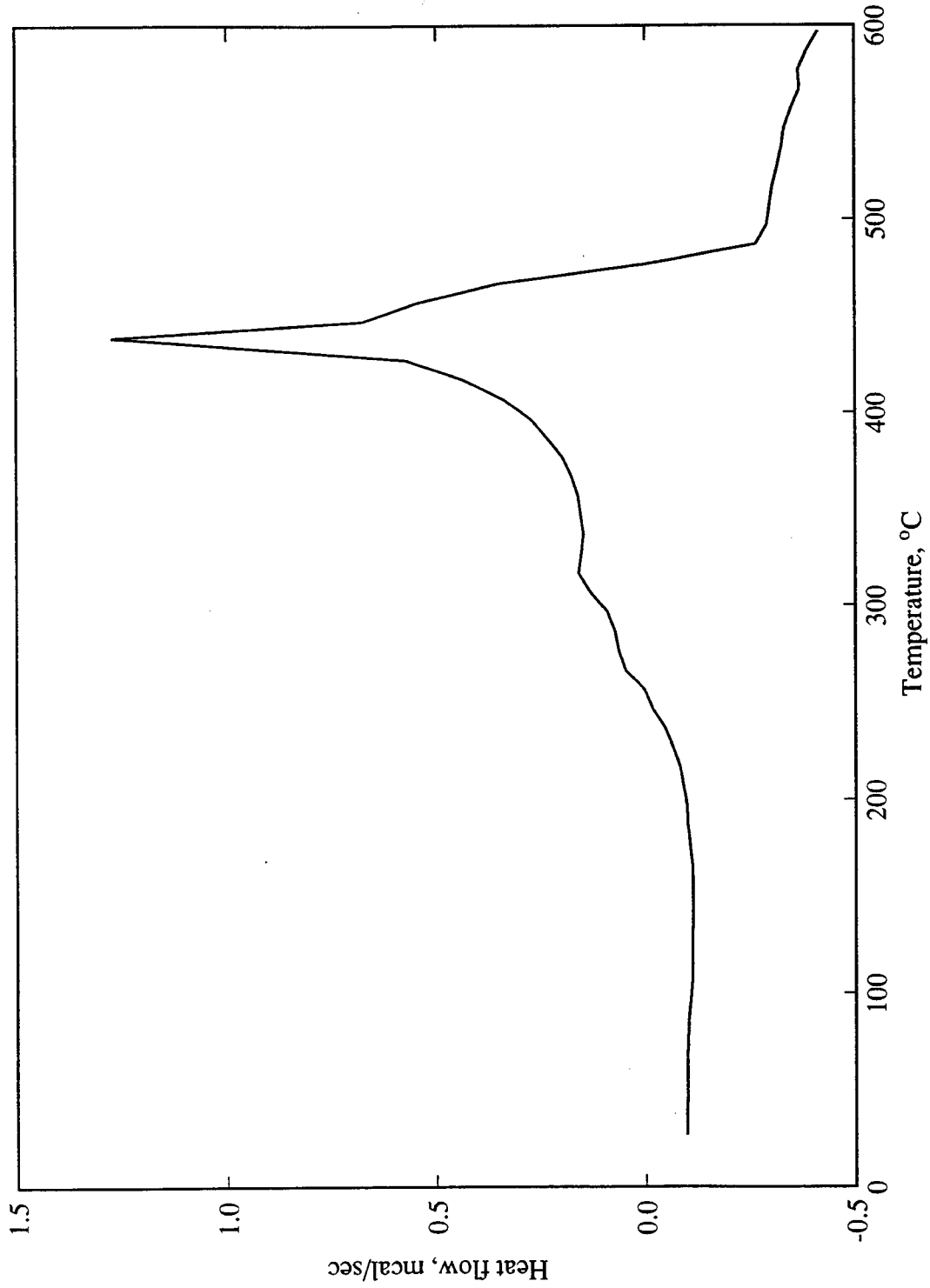


Figure 4.6: DSC Thermogram - Huntington Beach Oil and Sand Mixture

4. ANCILLARY EXPERIMENTAL RESULTS

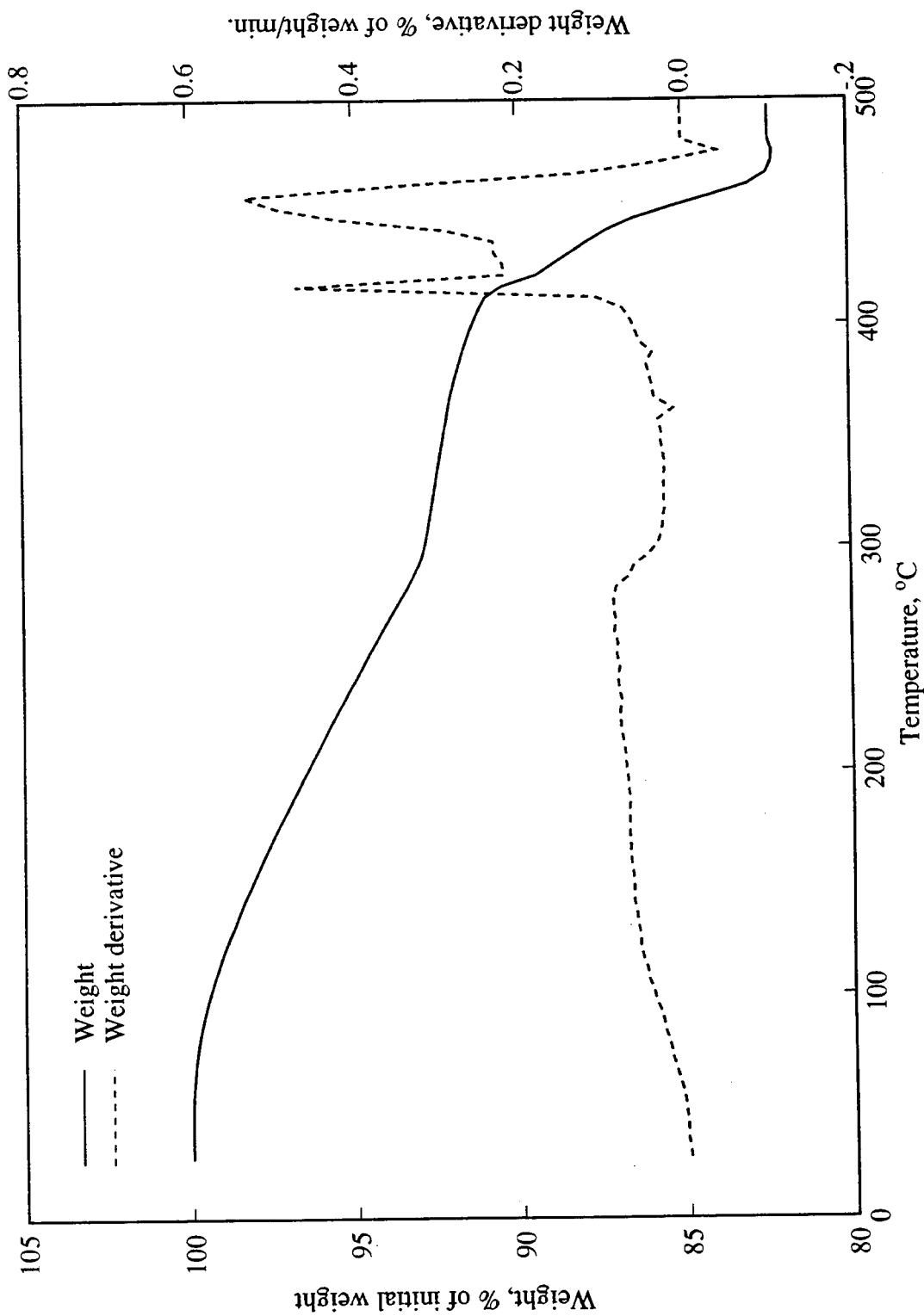


Figure 4.7: TGA Thermogram - Hamaca Crude Oil and Sand Mixture

4. ANCILLARY EXPERIMENTAL RESULTS

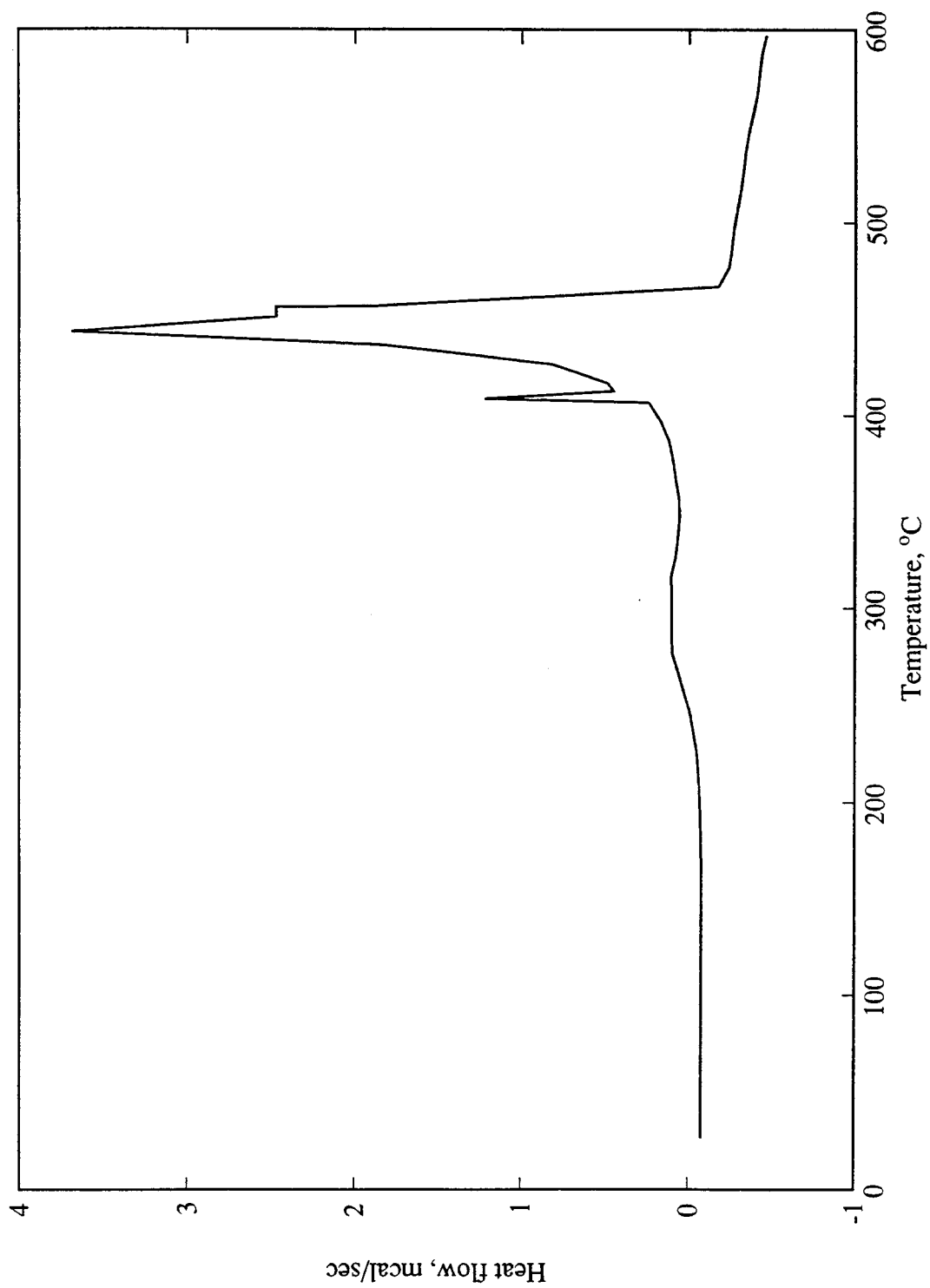


Figure 4.8: DSC Thermogram - Hamaca Crude Oil and Sand Mixture

4. ANCILLARY EXPERIMENTAL RESULTS

4.4 Grain Sieve Analysis Results

In the main, 20–30 mesh Ottawa sand was used in the experiments. However, to investigate the effect of surface area on oxidation reactions, 45–75 mesh and 170–270 mesh sands were also used.

A 45–75 mesh sand was used only in Run C4 (kinetic tube run with carbon). This sand, retained on sieve No. 75 after passing through sieve No. 45, has a mean grain size diameter of 0.0284 cm. Results of sieve analysis of 20–30 mesh and 170–270 mesh sands are shown in Table 4.3 and Table 4.4 respectively.

4.5 X-Ray Diffraction Results

A sample of mortar clay used in the experiments was subjected to X-ray diffraction analysis to determine the main types of clay present. The analysis was carried out at the Geology Department, Stanford University. The results (Fig. 4.9) indicate mortar clay to consist of kaolinite, quartz and some illite.

4. ANCILLARY EXPERIMENTAL RESULTS

Table 4.3: Sieve Analysis of 20–30 Mesh Ottawa Sand

U.S. Standard sieve No.	Weight %	Sieve size, cm	Grain size, cm
16	0.002	0.1180	–
20	3.381	0.0850	0.1015
25	68.897	0.0710	0.0780
30	25.207	0.0600	0.0655
35	1.791	0.0495	0.0548
40	0.278	0.0425	0.0460
45	0.186	0.0355	0.0390
50	0.122	0.0295	0.0325
60	0.051	0.0250	0.0273
>60	0.085	–	–

Average grain radius, $r_s = 0.0375$ cm.

Table 4.4: Sieve Analysis of 170–270 Mesh Sand

U.S. Standard sieve No.	Weight %	Sieve size, cm	Grain size, cm
170	0.000	0.0090	–
200	67.846	0.0075	0.00825
270	12.423	0.0053	0.00640
>270	19.730	–	0.00265

Average grain radius, $r_s = 0.00346$ cm.

4. ANCILLARY EXPERIMENTAL RESULTS

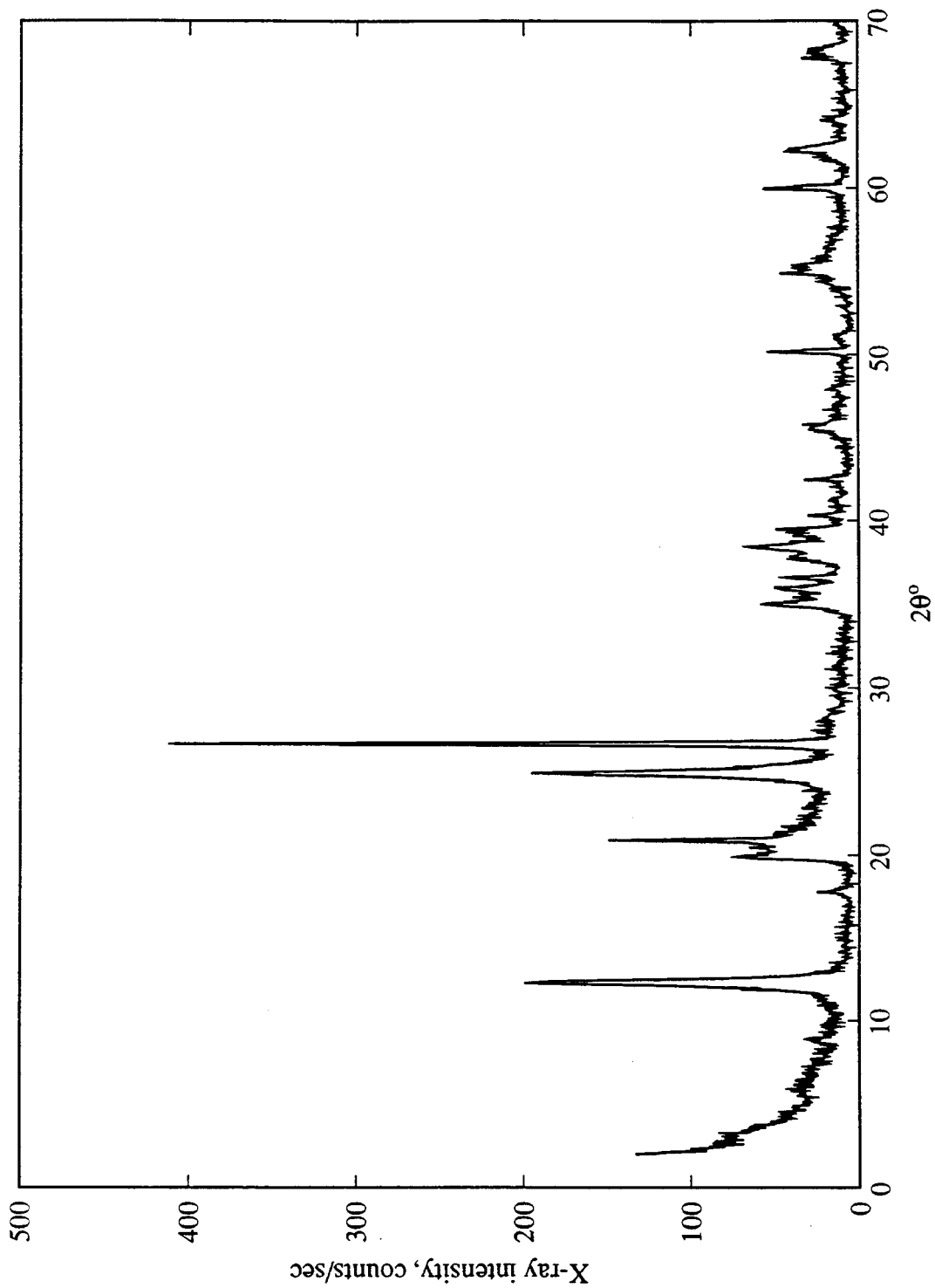


Figure 4.9: X-Ray Diffraction Pattern of Mortar Clay

5. Combustion Tube Experimental Results

The main objective of conducting combustion tube experiments in this study is to compare the H/C ratios from combustion tube experiments with those obtained from kinetic experiments. Nonetheless, a complete analysis of combustion tube data has been made and the results are presented in this chapter.

Six combustion tube runs were performed. The crude oils used were Cold Lake bitumen (11.5°API), Huntington Beach oil (20.8°API) and Hamaca (Venezuela) crude oil (10.2°API). Properties of the sand packs for the tube runs are shown in Table 5.1. To allow direct comparison of results from different runs, the following conditions were kept constant: air injection rate and pressure were 3 L/min and 100 psig respectively; concentration by weight of oil and water in a sample were 4.5–4.9% and 4.1–4.3% respectively, and for sand was 86.8–91.0%; and for runs using clay, the concentration by weight was 4.6%.

Runs HBO5 and CL15 were aborted because combustion could not be sustained after obtaining initial ignition. The probable causes for this are as follows. In Run CL15, clay was not included in the sample. It appeared the fuel concentration was insufficient to sustain combustion. The sample in Run HBO5 contained clay. However, since the crude gravity was 20.8°API, the amount of fuel deposited was probably insufficient for a self-sustaining combustion.

5. COMBUSTION TUBE EXPERIMENTAL RESULTS

Table 5.1: Properties of Sand Packs for Combustion Tube Runs

	Run No.					
	CL13	CL15	HBO5	VEN5	VEN14	VEN21
Crude	Cold Lake bitumen	Cold Lake bitumen	Huntington Beach oil	Hamaca crude oil	Hamaca crude oil	Hamaca crude oil
Oil gravity ($^{\circ}$ API)	11.5	11.5	20.8	10.2	10.2	10.2
Length (cm)	86.5	86.8	86.8	85.4	87.1	85.4
Weight (g)	7795	7579	7810	7739	7461	7447
Oil (wt. %)	4.6	4.8	4.5	4.6	4.9	4.6
Water (wt. %)	4.1	4.3	4.1	4.1	4.3	4.1
Sand (wt. %)	86.8	91.0	86.8	86.8	90.8	86.8
Clay (wt. %)	4.6	0	4.6	4.6	0	0
Sand fines (wt. %) [†]	0	0	0	0	0	4.6
S_o (frac. pore vol.)	0.29	0.27	0.29	0.29	0.26	0.26
S_w (frac. pore vol.)	0.26	0.24	0.26	0.27	0.23	0.24
S_g (frac. pore vol.)	0.45	0.49	0.45	0.44	0.51	0.50
ϕ (frac. bulk vol.)	0.31	0.34	0.31	0.31	0.35	0.33

[†] 170–270 mesh sand.

Data for the four successful runs are stored in a computer diskette and is available on request from SUPRI-A. Results of the combustion tube runs are discussed in the following sections.

5.1 Cold Lake Bitumen Run CL13

The sample consisted of a mixture of Cold Lake bitumen, water, 20-30 mesh sand and clay. When the sand pack temperature across the electric igniter reached 330°C, air injection was initiated. The electric igniter was turned off 25 minutes after commencing air injection.

A fairly stable burn was obtained within an hour of ignition as evident from the

5. COMBUSTION TUBE EXPERIMENTAL RESULTS

fairly stable produced gas readings (Fig. 5.1). In the period 1–7 hours, the average molar concentrations of the produced gases were: CO₂, 11.1%; CO, 5.0%; O₂, 1.8% and N₂, 81.1%.

Produced gas readings (except for nitrogen) were oscillatory. Produced oxygen readings varied between 1 to 5% during the period 1–4.5 hours, but thereafter oscillations diminished to within 1 to 2%. Carbon dioxide and carbon monoxide readings varied in step, mirror imaging those of oxygen. Combustion tube experiments using identical apparatus with 11.2°API San Ardo crude oil (Fassihi 1991) also yielded unsteady produced gas readings. Using the same apparatus, Holt (1992) also obtained oscillatory produced gas readings for 12°API Cymric heavy oil. Produced oxygen readings varied between 1 to 5%. However, in runs where iron nitrate was added to the sample, produced gas readings were steady, and the produced oxygen readings varied only slightly in the range 1 to 2%. Kinetic tube experiments performed on 18.5°API Huntington Beach oil (De los Rios 1987) showed a significant reduction in the activation energy for high-temperature oxidation (HTO) from 128 KJ/mol for runs with no metallic additives to 109 KJ/mol for samples containing zinc or chromium. The results of De los Rios and Holt indicate that certain metals increase fuel reactivity and thus combustion stability.

In comparison, produced gas readings were less oscillatory for Run VEN5 (Hamaca crude oil with clay) as described in the next section. Based on kinetic experiments (Table 7.2), HTO activation energy for samples identical to those in Runs CL13 and VEN5 are 219 KJ/mol and 150 KJ/mol respectively. The results indicate that combustion is more stable for a crude with a higher fuel reactivity. The decrease in gas reading oscillations in the later half of the experiment was probably due to increase in temperature of the insulation jacket thereby permitting increased fuel oxidation.

Apparent H/C and *m*-ratios based on produced gas analysis data are presented in Fig. 5.2. In the period 1–7 hours, the average apparent H/C and *m*-ratios are 1.60

5. COMBUSTION TUBE EXPERIMENTAL RESULTS

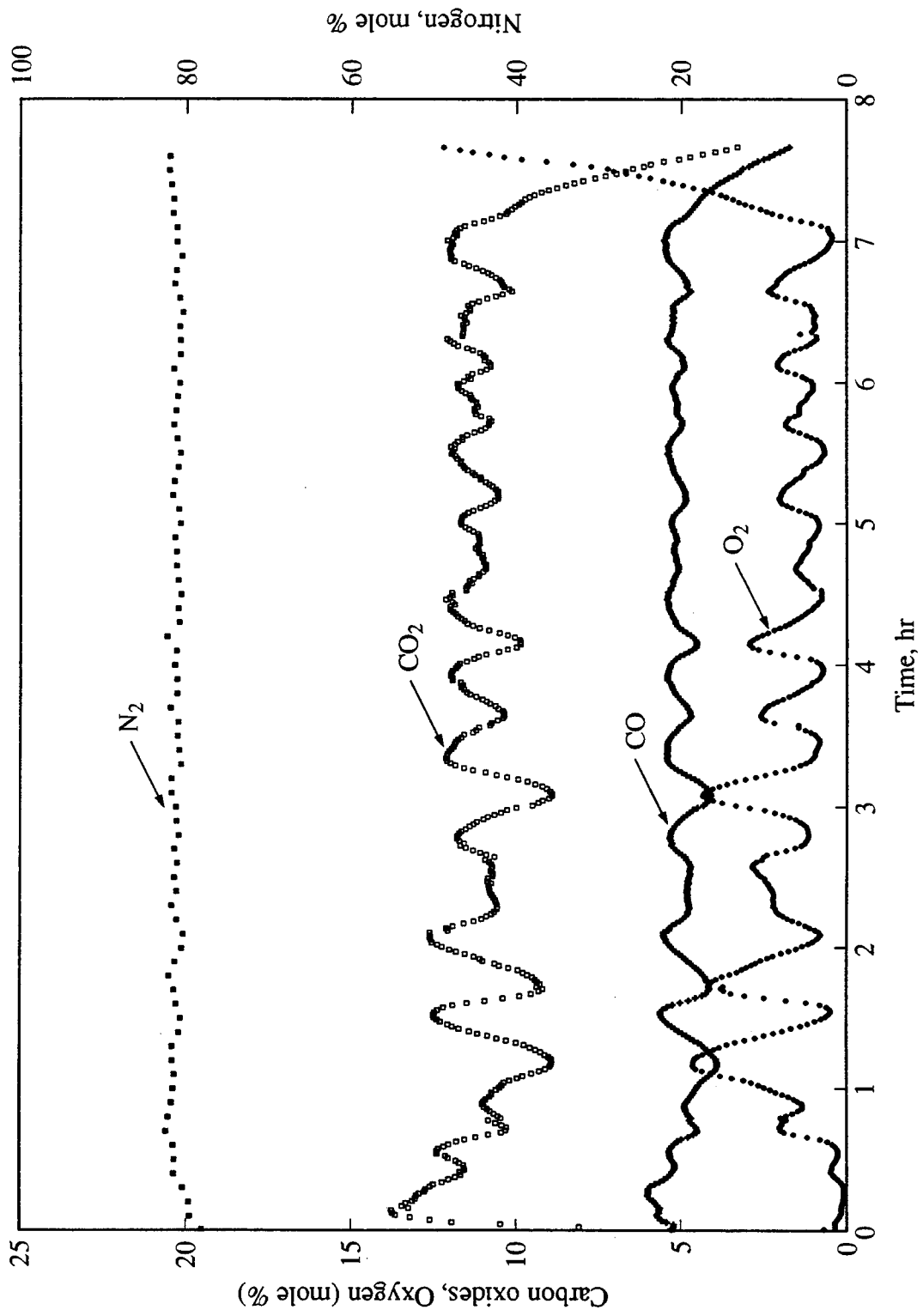


Figure 5.1: Produced Gas Composition Versus Time (Run CL13)

5. COMBUSTION TUBE EXPERIMENTAL RESULTS

and 0.311 respectively. By comparison, the atomic H/C ratio for the original crude is 1.53 based on elemental analysis (Chapter 4). The similarity in H/C ratios of the fuel and original crude oil indicates that there was practically no low-temperature oxidation in Run CL13, and that distillation is chiefly responsible for fuel deposition.

Temperature profiles are presented in Fig. 5.3. The average combustion zone temperature was 500 °C. This relatively high combustion zone temperature is also indicative of the absence of low-temperature oxidation. Visual inspection of the sand pack at the end of the run indicated a combustion zone thickness of 1.5 cm. Penberthy and Ramey (1966) inferred from their experiments a combustion zone thickness of about 2 cm. From the slope of the straight line drawn through the combustion front location data (Fig. 5.4), the combustion front velocity is calculated to be 11.2 cm/hr (0.37 ft/hr). From Eq. 2.10, the combustion front velocity is directly proportional to the air flux and inversely proportional to the product of fuel concentration and air-fuel ratio. Since air flux was constant, the constant combustion front velocity obtained implies a constant fuel concentration-air/fuel ratio product.

Cumulative oil and water volumes and produced oil gravity versus time are presented in Fig. 5.4. Produced oil gravity increased to as high as 16.6°API compared to 11.5°API for the original crude. Similar increases in produced oil gravity were observed in the South Belridge in-situ combustion project: 18°API compared to 12.9°API for the original crude. Produced oil gravity increases due to increasing light hydrocarbon content of the crude as a result of distillation ahead of the combustion zone. The heavy fractions left as residue constitute the fuel burned at the combustion zone.

Viscosity of the produced oil decreased significantly with time as a result of the increasing light hydrocarbon content of the oil (Fig. 5.5). At the end of the run, the produced oil viscosity was 70 cP at 35°C compared to 10,000 cP for the original crude. Results of this tube run and those of Hamaca oil are summarized in Table 5.2.

5. COMBUSTION TUBE EXPERIMENTAL RESULTS

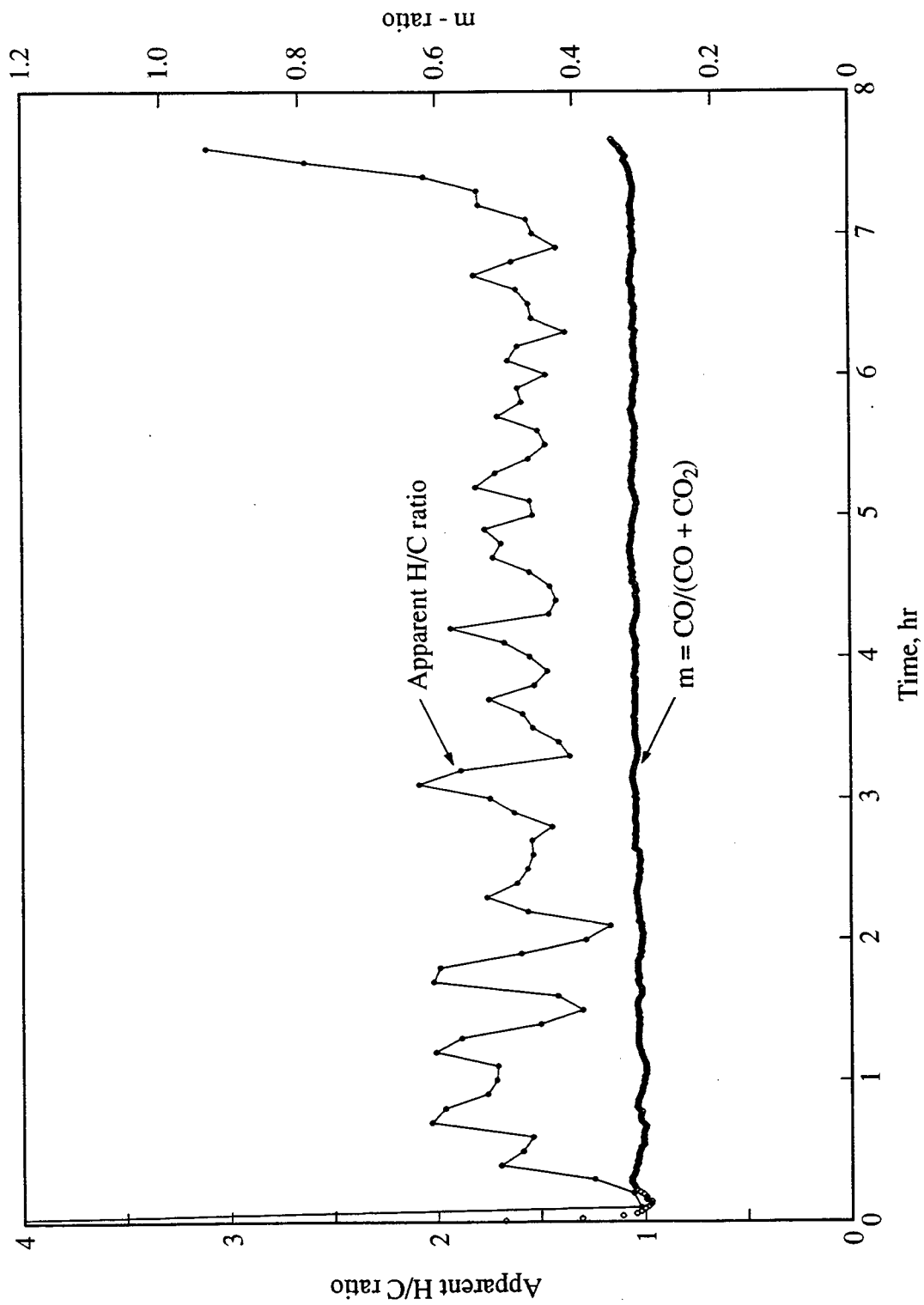


Figure 5.2: Apparent H/C and m-Ratios Versus Time (Run CL13)

5. COMBUSTION TUBE EXPERIMENTAL RESULTS

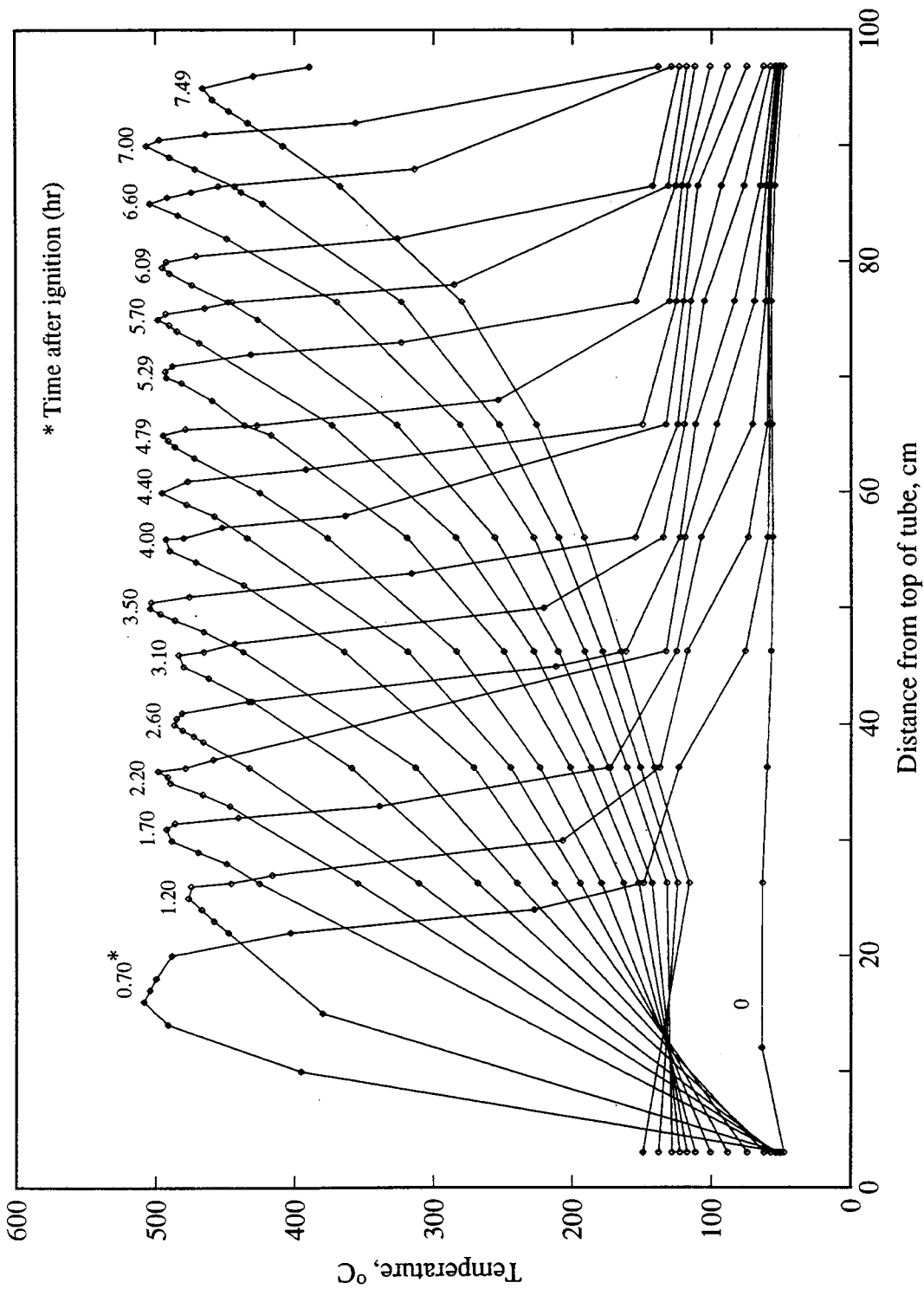


Figure 5.3: Temperature Profiles (Run CL13)

5. COMBUSTION TUBE EXPERIMENTAL RESULTS

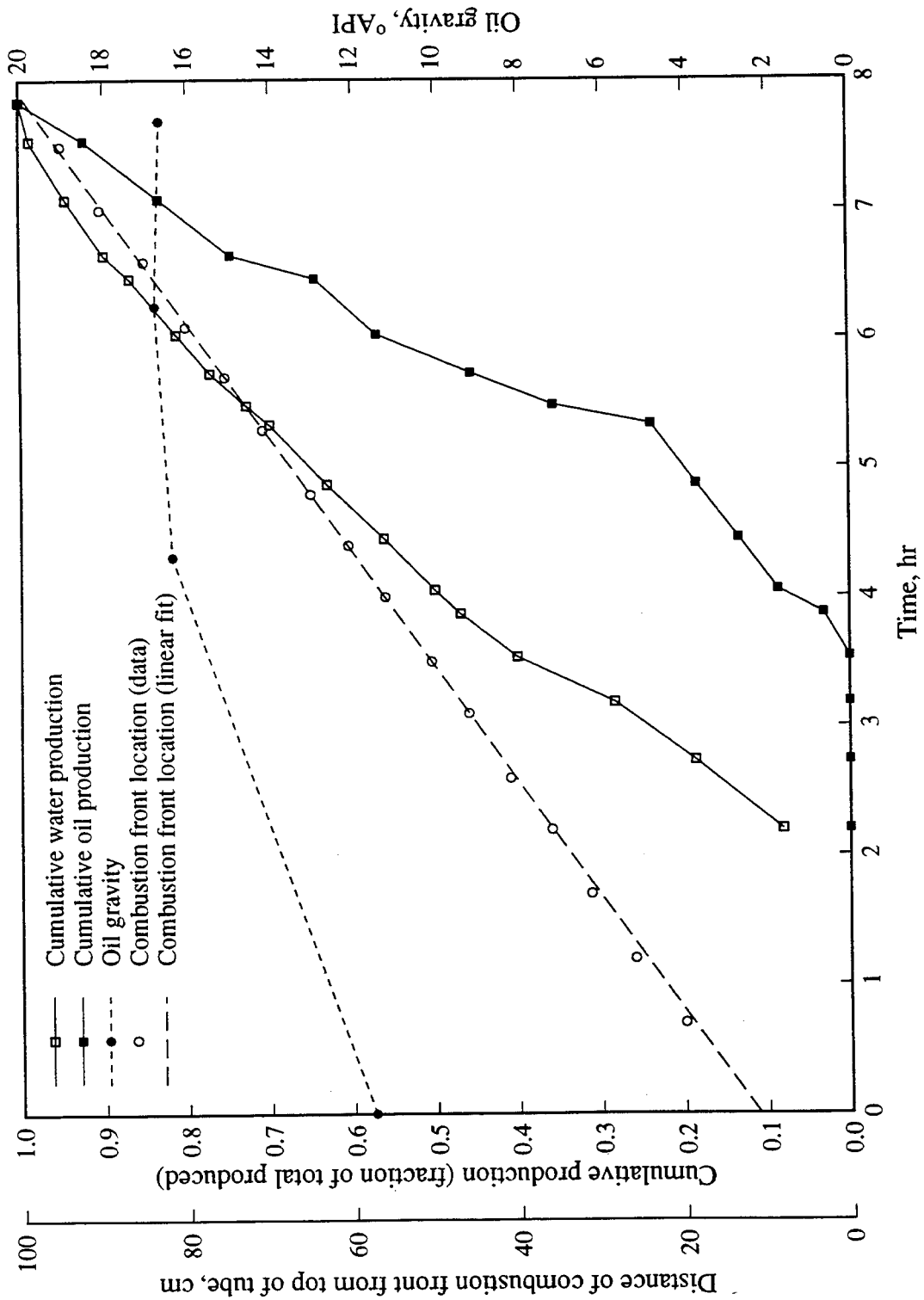


Figure 5.4: Production, Oil Gravity and Combustion Front Location Versus Time (Run CL13)

5. COMBUSTION TUBE EXPERIMENTAL RESULTS

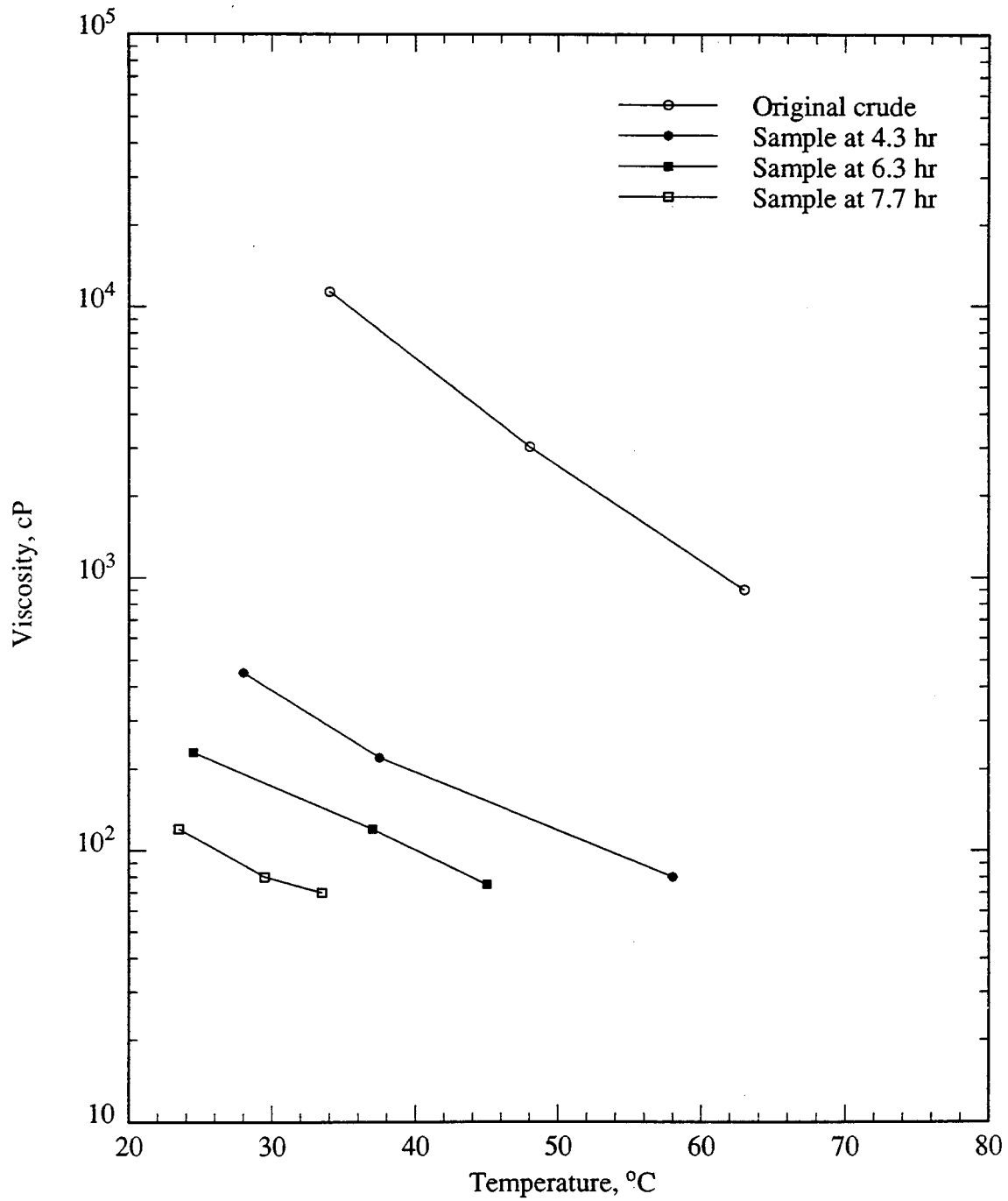


Figure 5.5: Oil Viscosity Versus Temperature (Run CL13)

5. COMBUSTION TUBE EXPERIMENTAL RESULTS

Table 5.2: Summary of Combustion Tube Experimental Results

	Run No.			
	CL13	VEN5	VEN14	VEN21
Initial oil gravity (°API)	11.5	10.2	10.2	10.2
Initial oil viscosity (cP)	10,000	14,000	14,000	14,000
	at 35°C	at 50°C	at 50°C	at 50°C
Injection pressure (psig)	100	100	100	100
Air injection rate (L/min)	3.00	3.00	3.00	3.00
Air flux (scf/hr-ft ²)	130.9	130.9	130.9	130.9
Comb. front temp. (°C)	500	500	350	500
Comb. front velocity (cm/hr)	11.2	10.5	7.7	11.1
Produced liquids:				
Oil gravity (°API)	16.6	14.0	9.8	11.2
Oil viscosity (cP)	70	260	17,000	2600
	at 35°C	at 50°C	at 50°C	at 50°C
Produced water vol. (ml)	392	353	285	271
Produced oil vol. (ml)	263	287	346	298
Oil recovery (wt. %)	71	78	94	88
Produced gas:				
Ave. prod. rate (L/min)	3.09	2.80	2.55	3.05
CO ₂ (mole %)	11.1	11.6	4.3	9.7
CO (mole %)	5.0	4.9	2.0	4.3
O ₂ (mole %)	1.8	1.1	10.1	3.8
N ₂ (mole %)	81.1	81.4	82.8	81.2
<i>m</i> -ratio	0.311	0.298	0.312	0.308
Apparent H/C ratio	1.60	1.63	4.35	1.77
Residue after burn (g)	33.0	28.7	143.9	8.6
Fuel conc. (lb/ft ³ bulk vol.)	1.149	0.784	-	0.539
O ₂ utilization efficiency (%)	91.7	95.0	54.5	82.6
Air-fuel ratio (scf/lb _{fuel})	165	167	-	169
Air requirements (scf/ft ³ bulk vol.)	208	139	-	112
Heat of combustion (Btu/lb _{fuel})	16,253	16,458	-	16,773

5. COMBUSTION TUBE EXPERIMENTAL RESULTS

5.2 Hamaca Crude Oil Run VEN5

The sample consisted of a mixture of Hamaca crude oil, water, 20-30 mesh sand and clay. Air injection was initiated when the temperature of the sand pack across the electric igniter reached 330°C. The electric igniter was switched off 30 minutes after air injection started.

Stable combustion was observed almost from the start of the run as indicated by the stable produced gas composition readings (Fig. 5.6). In the period 1-7.5 hours, the average concentrations of the produced gases were: CO₂, 11.6%; CO, 4.9%; O₂, 1.1% and N₂, 81.4 %. Oscillatory produced gas readings observed in Run CL13 were absent in this run. As explained in Section 5.1, this result is probably due to Hamaca crude oil being more reactive than Cold Lake bitumen.

Apparent H/C and *m*-ratios based on gas analysis are presented in Fig. 5.7. The average apparent H/C and *m*-ratios in the period 1-7.5 hours are 1.63 and 0.298 respectively. Based on elemental analysis (Chapter 4), the atomic H/C ratio of the original Hamaca crude is 1.65. The fact that H/C ratios of the fuel and original crude are almost the same in this run indicates the absence of low-temperature oxidation and the predominance of distillation as the fuel deposition mechanism.

The average combustion temperature was 500°C (Fig. 5.8). From combustion front versus time data (Fig. 5.8), combustion front velocity was 10.5 cm/hr (0.35 ft/hr).

Figure 5.9 shows cumulative volumes of produced water and oil and oil gravity versus time. Produced oil gravity at the end of the run was 3.8°API higher than that of the original crude. Viscosity of the produced oil dropped to 260 cP at 50°C from its original value of 14,000 cP (Fig. 5.10).

5. COMBUSTION TUBE EXPERIMENTAL RESULTS

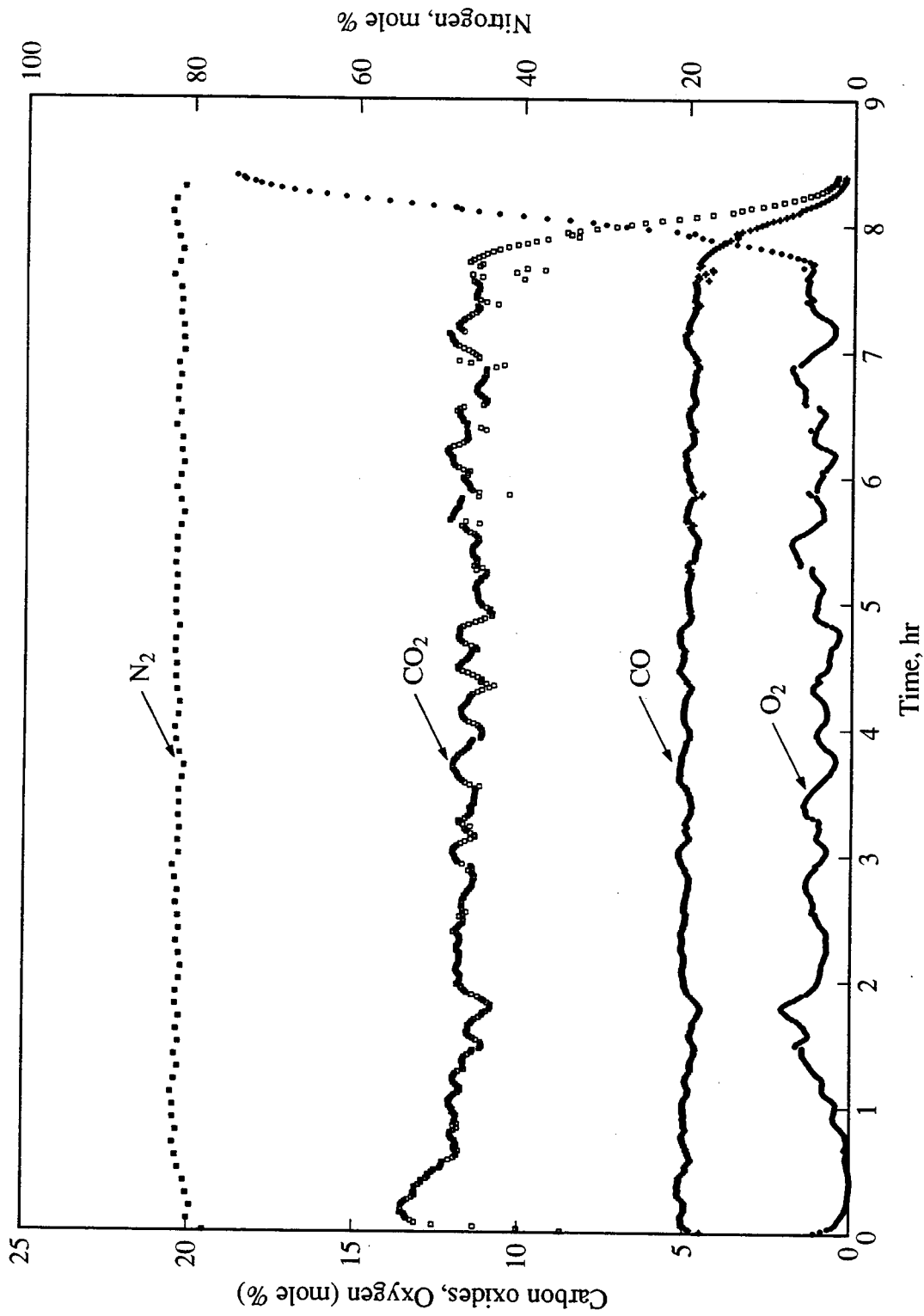


Figure 5.6: Produced Gas Composition Versus Time (Run VEN5)

5. COMBUSTION TUBE EXPERIMENTAL RESULTS

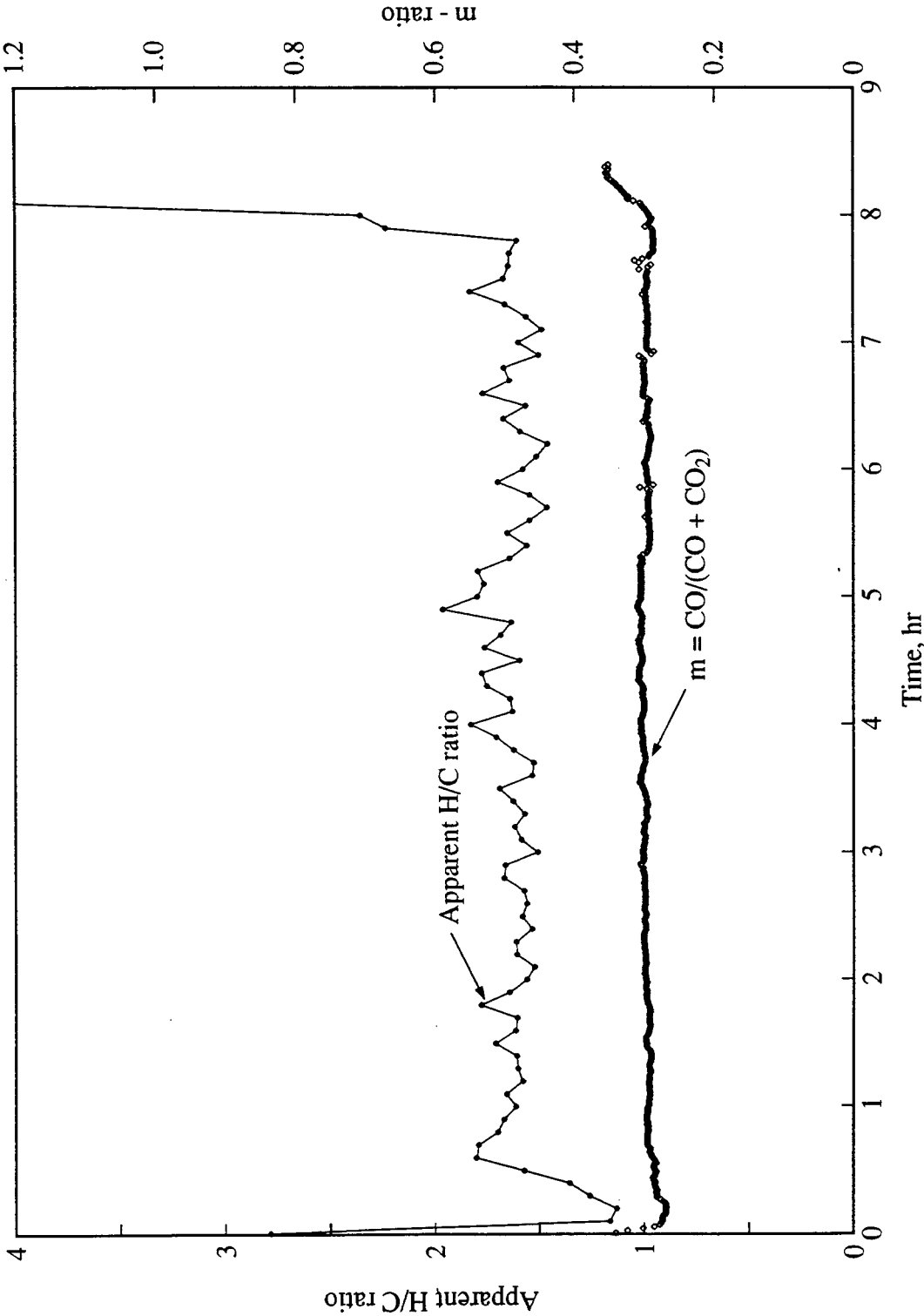


Figure 5.7: Apparent H/C and m-Ratios Versus Time (Run VEN5)

5. COMBUSTION TUBE EXPERIMENTAL RESULTS

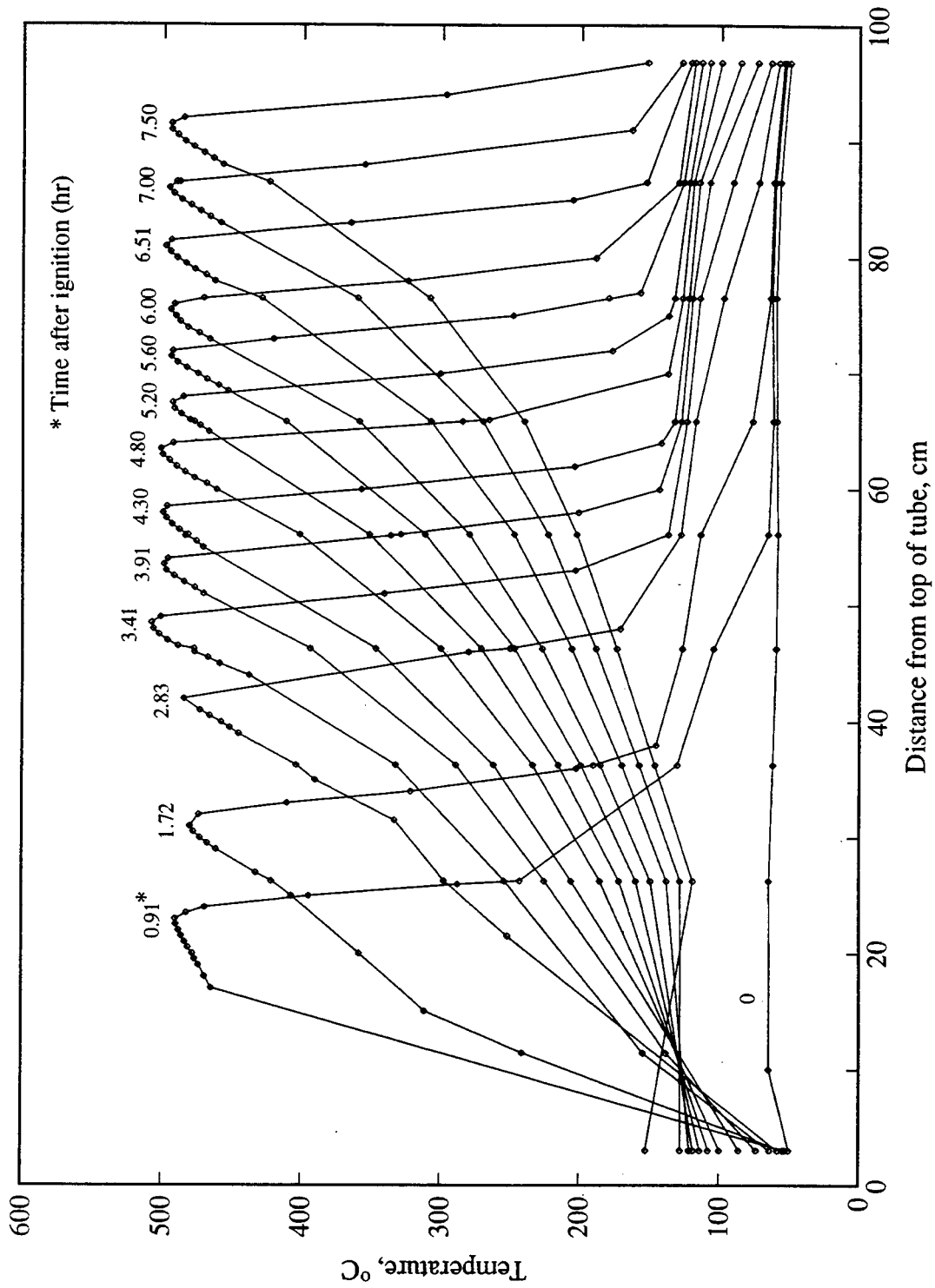


Figure 5.8: Temperature Profiles (Run VEN5)

5. COMBUSTION TUBE EXPERIMENTAL RESULTS

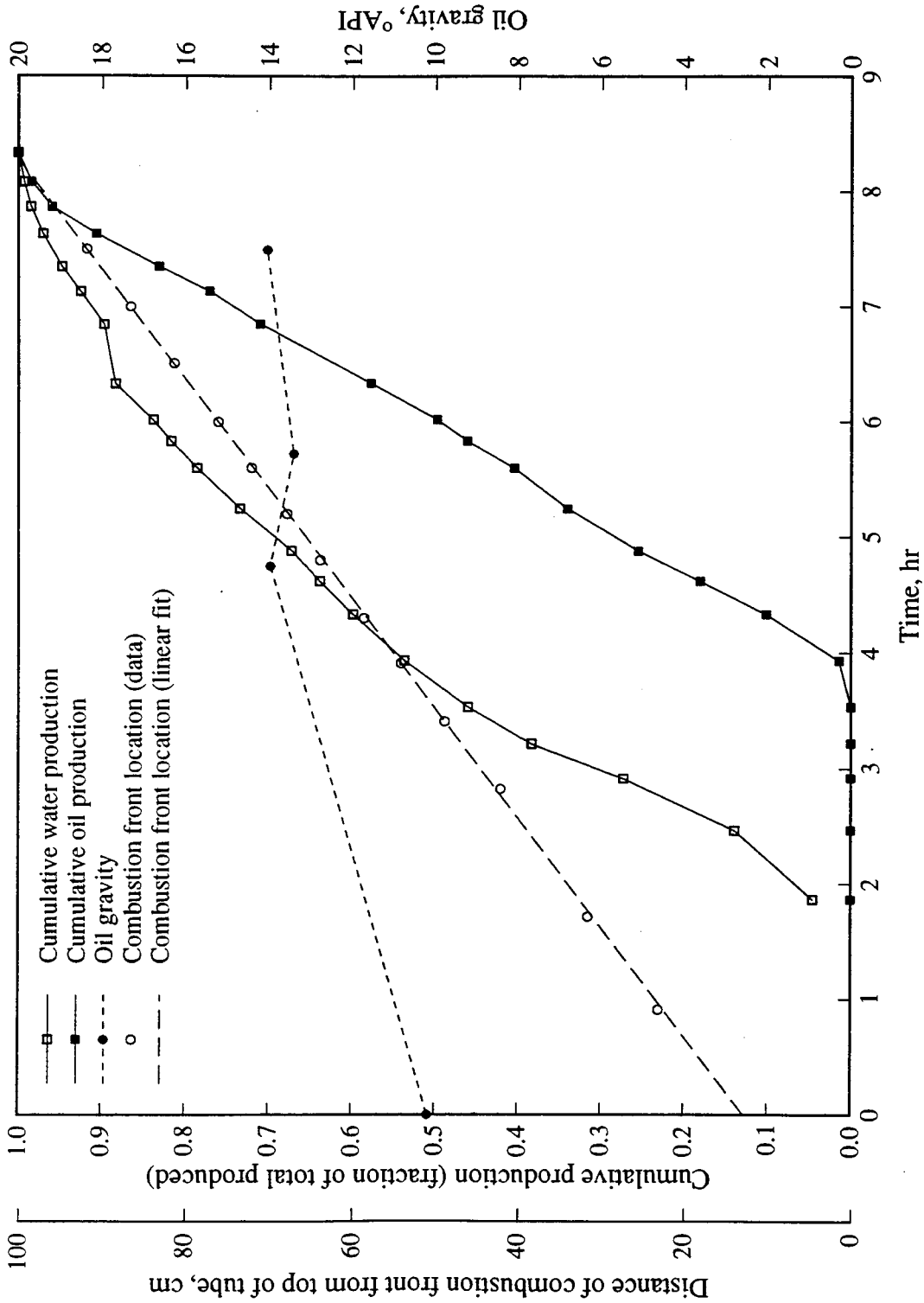


Figure 5.9: Production, Oil Gravity and Combustion Front Location Versus Time (Run VEN5)

5. COMBUSTION TUBE EXPERIMENTAL RESULTS

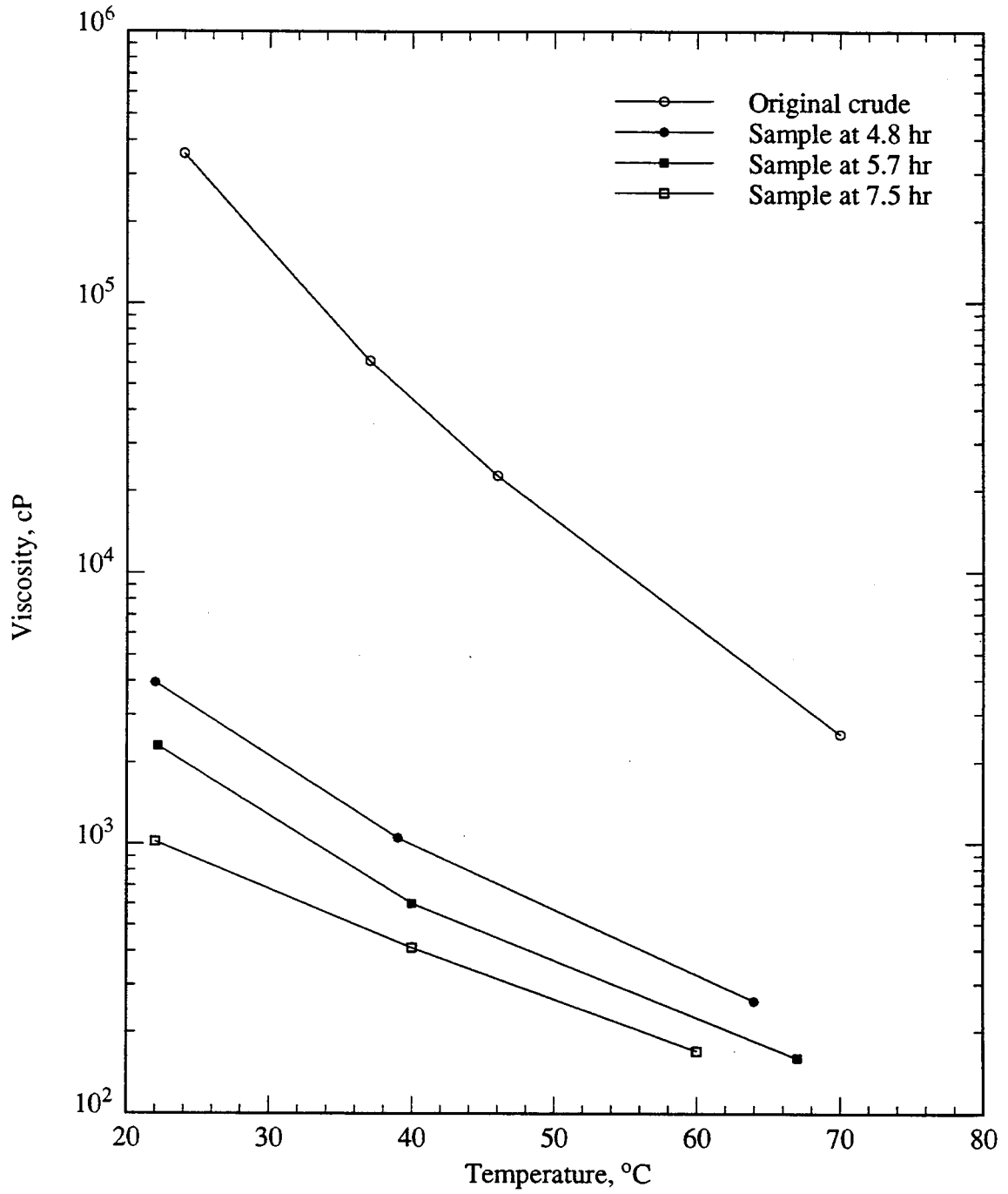


Figure 5.10: Oil Viscosity Versus Temperature (Run VEN5)

5. COMBUSTION TUBE EXPERIMENTAL RESULTS

5.3 Hamaca Crude Oil Run VEN14

In this run no clay was added to the sample. During the first two hours of the run, produced oxygen concentration varied, increasing to as high as 13%. The electric igniter was left on for two hours into the run to aid ignition. However no ignition was achieved. This run was a low-temperature burn as indicated by the temperature and gas analysis data.

Produced gas composition readings stabilized after about three hours (Fig. 5.11). In the period 3–9 hours, produced gas molar concentrations were: CO₂, 4.3%; CO, 2.0%; O₂, 10.1% and N₂, 82.8%. The average apparent H/C and *m*-ratios were 4.35 and 0.312 (Fig. 5.12). Given the atomic H/C ratio of 1.65 for the original crude, the high apparent H/C ratio observed during the run indicates that low-temperature oxidation was the main oxidation reaction.

Temperature profiles are shown in Fig. 5.13. The average combustion zone temperature was 350°C. A kinetic tube experiment (Run VEN15, described in Chapter 6) was performed on a sample identical to that used in this tube run: 350°C corresponded to the temperature at the saddle between low- and high-temperature oxidation peaks. Therefore it is concluded that only low-temperature oxidation occurred during this tube run. Combustion front location data are shown in Fig. 5.14 and indicate a low burning front velocity of 7.7 cm/hr (0.25 ft/hr) compared to about 11 cm/hr for Runs CL13 and VEN5.

Produced oil gravity and viscosity data are presented in Figs. 5.14 and 5.15 respectively. Produced oil gravity (9.8° API) was slightly lower than that of the original crude (10.2° API). Produced oil viscosity was 17,000 cP at 50°C compared to 14,000 cP for the original crude. The decrease in oil gravity and increase in oil viscosity were due to low-temperature oxidation. Alexander *et al.* (1962) also observed an increase in viscosity of oil subjected to low-temperature oxidation. Bae (1977)

5. COMBUSTION TUBE EXPERIMENTAL RESULTS

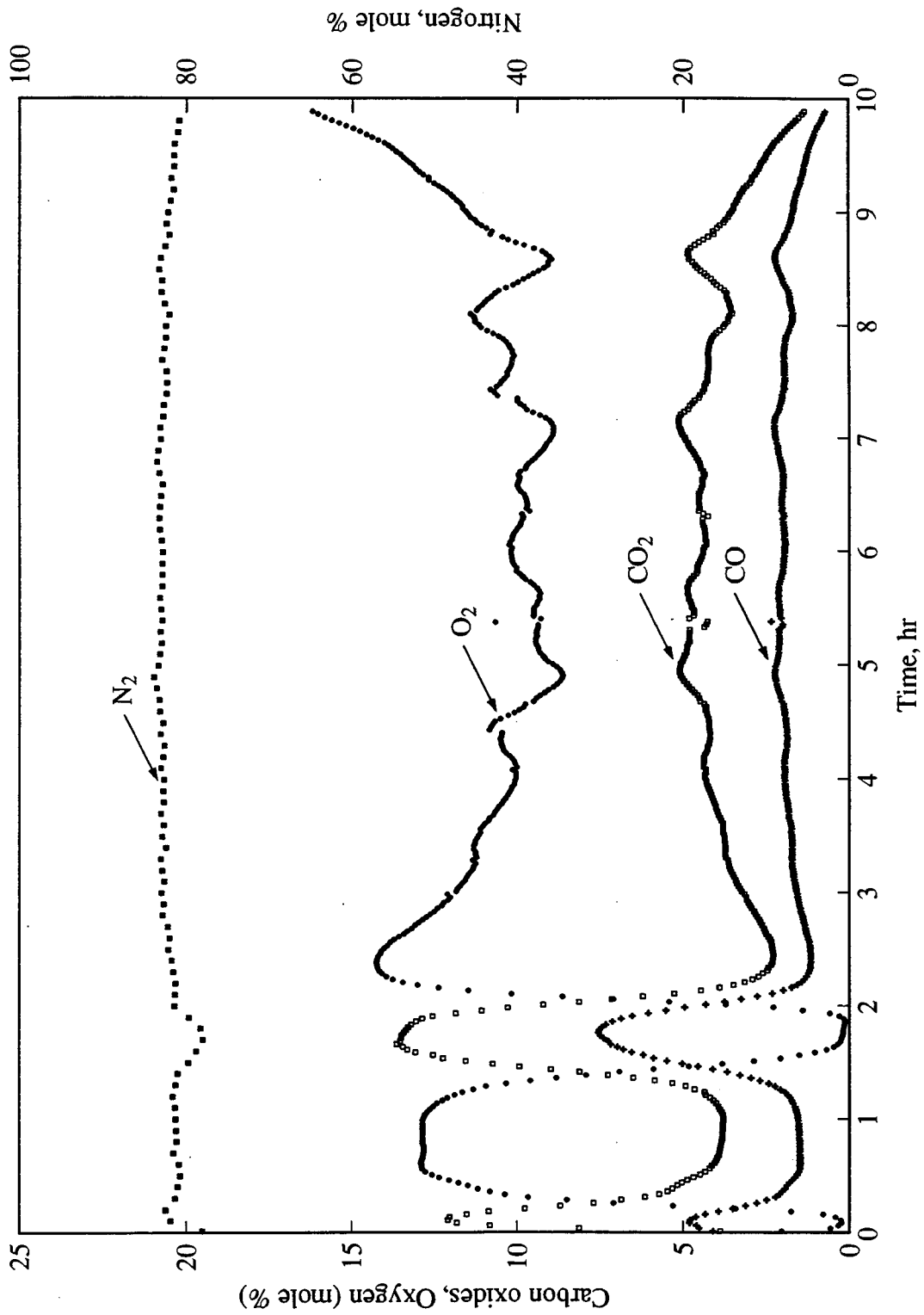


Figure 5.11: Produced Gas Composition Versus Time (Run VEN14)

5. COMBUSTION TUBE EXPERIMENTAL RESULTS

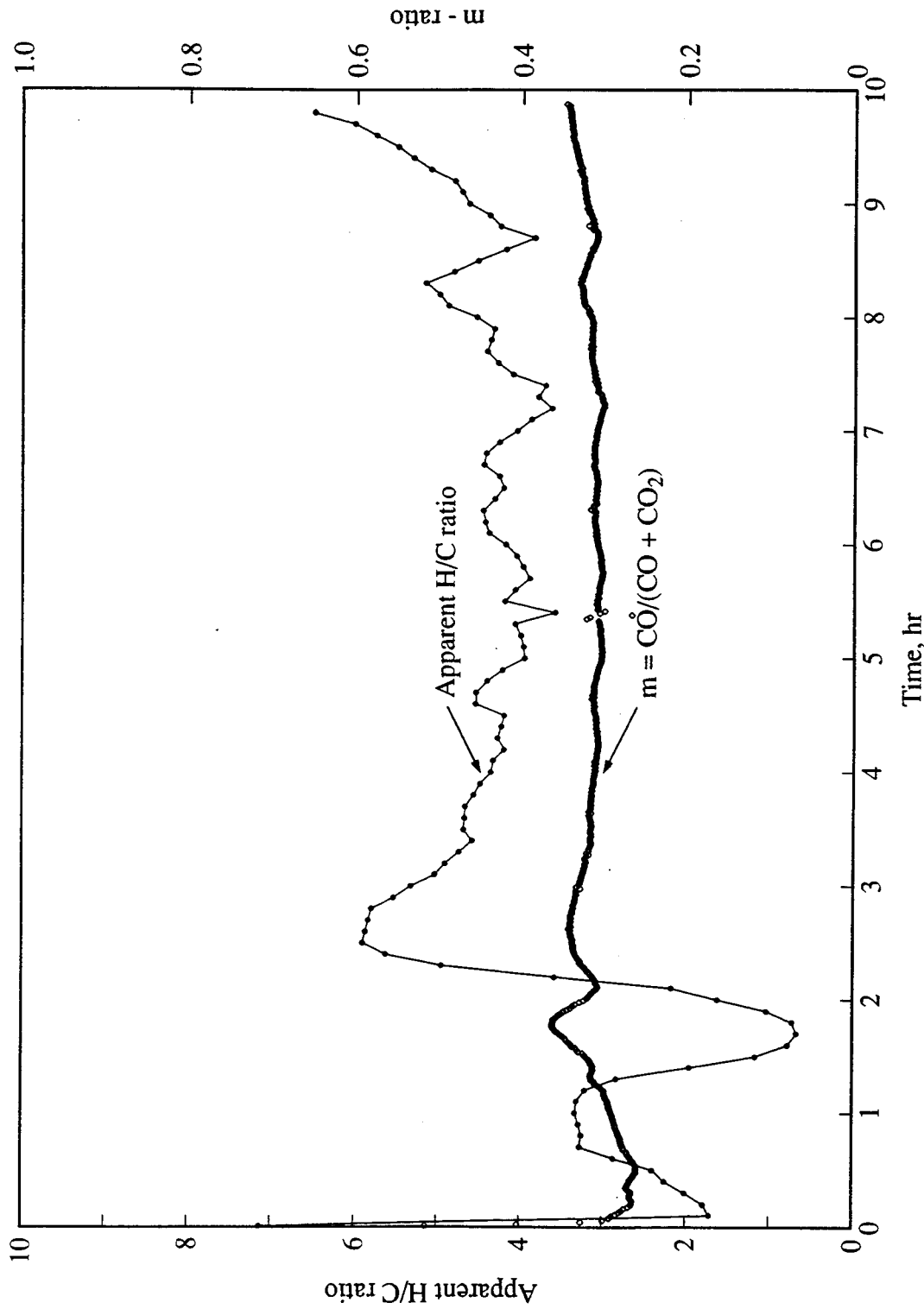


Figure 5.12: Apparent H/C and m-Ratios Versus Time (Run VEN14)

5. COMBUSTION TUBE EXPERIMENTAL RESULTS

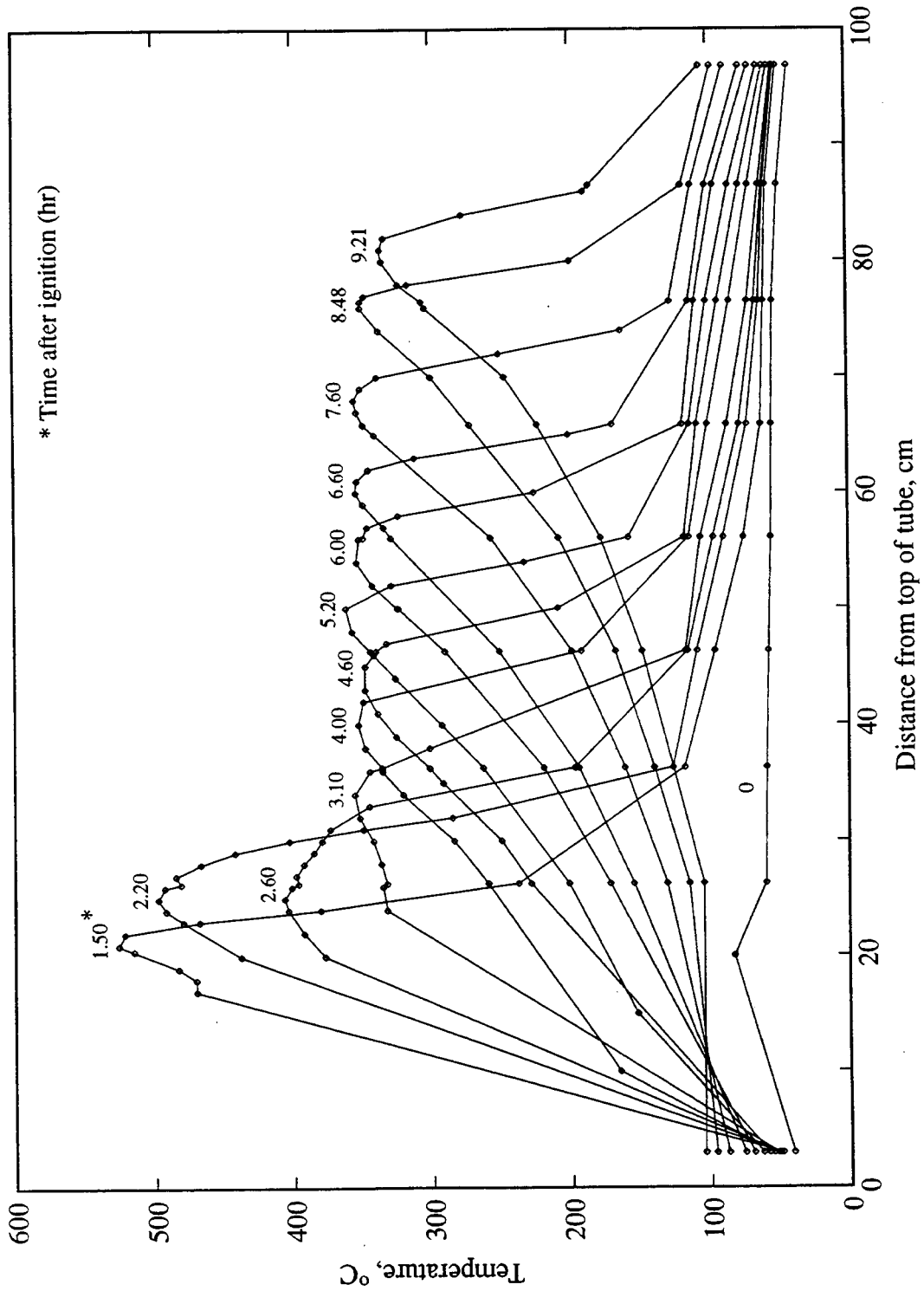


Figure 5.13: Temperature Profiles (Run VEN14)

5. COMBUSTION TUBE EXPERIMENTAL RESULTS

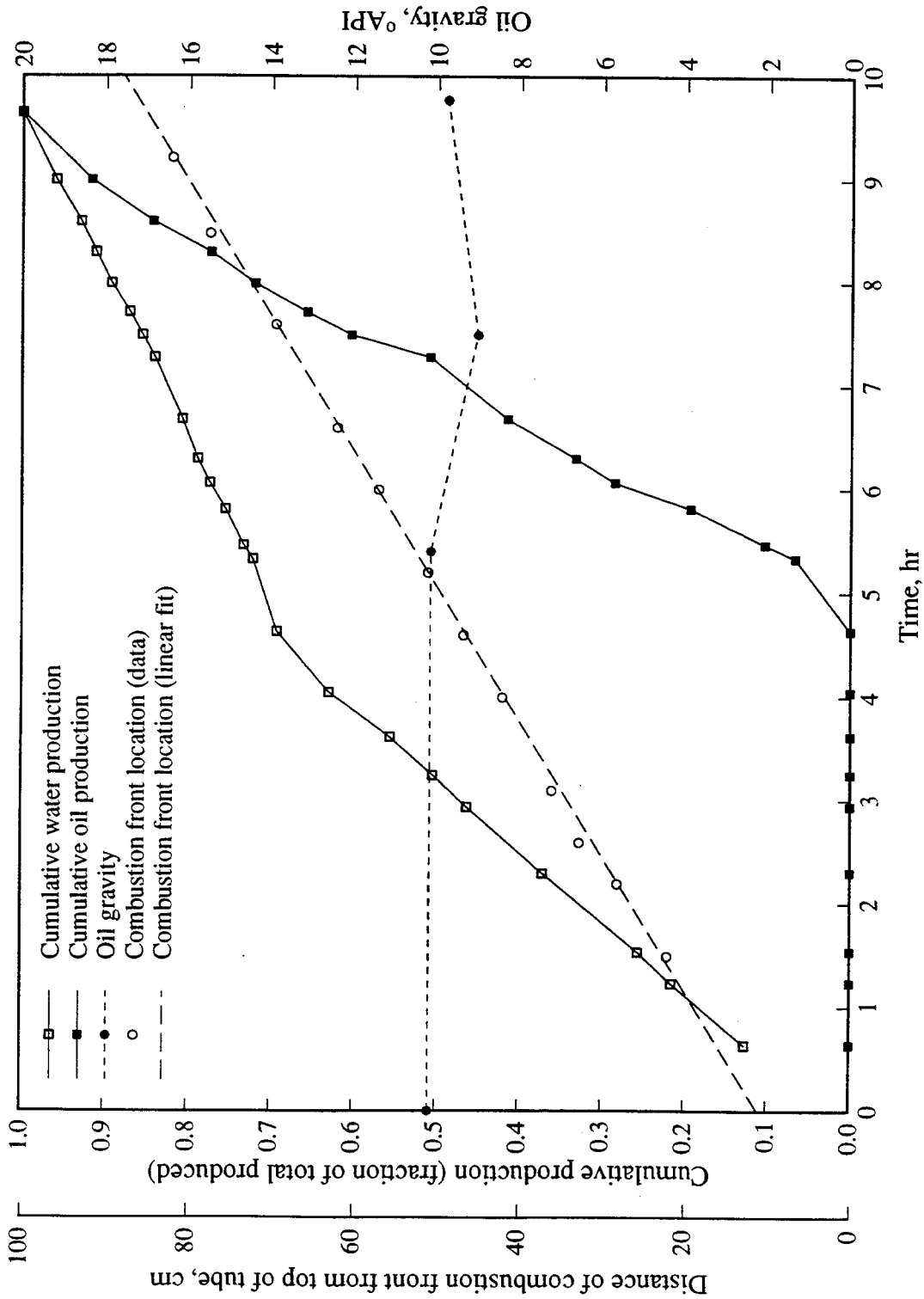


Figure 5.14: Production, Oil Gravity and Combustion Front Location Versus Time (Run VEN14)

5. COMBUSTION TUBE EXPERIMENTAL RESULTS

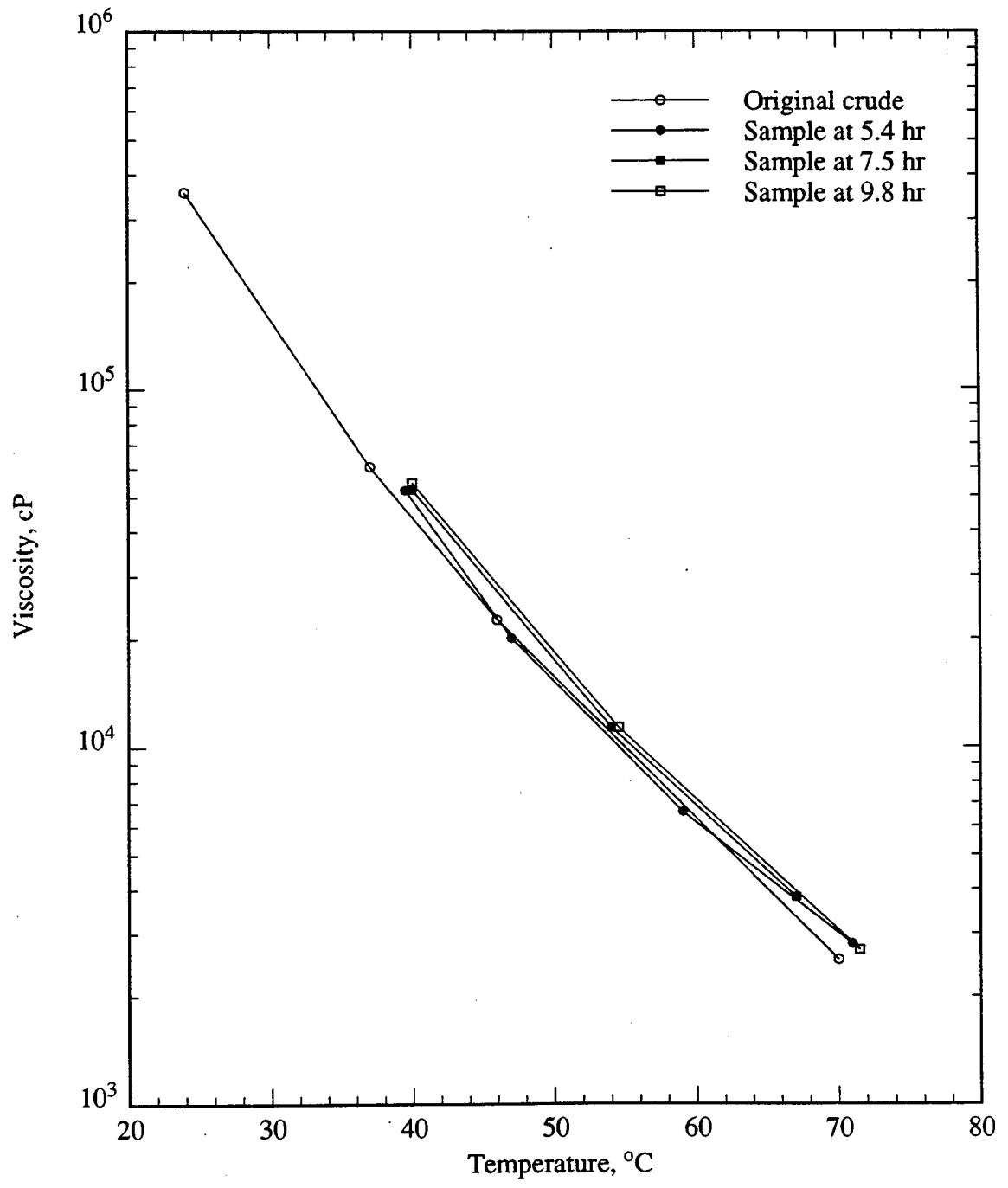


Figure 5.15: Oil Viscosity Versus Temperature (Run VEN14)

5. COMBUSTION TUBE EXPERIMENTAL RESULTS

also found a decrease in API gravity of oil which had undergone low-temperature oxidation. Combustion did not occur in this tube run because fuel concentration was low, for reasons described in Section 5.4.

After the tube run, the sand pack was examined. The “burned” zone was black in color as opposed to dark grey in the other three runs. Samples of this “burned” zone were fired in an oven. An average sample weight loss of 2.1% was observed compared to 0.1–0.5% for the other three tube runs (Table 5.2). These results indicate that some heavy hydrocarbon residue was left unburned in this run.

The percentage of oxygen used in LTO is given by Eq. 5.1 (Ramey *et al.* 1992).

$$\text{Percent oxygen in LTO} = \frac{100(x_{\text{apparent}} - x_{\text{true}})(CO_2 + CO)}{4(0.2682N_2 - O_{2p})} \quad (5.1)$$

Based on Eq. 5.1, 35% of oxygen injected went into LTO and 46% of oxygen injected was produced and did not generate heat. Thus only 19% went into HTO reactions. The result of this operation was a slight decrease in API oil gravity and a large increase in viscosity of the produced oil. A material balance on oil indicated 43% was deposited as an immobile residue and 57% was displaced with no or little improvement in quality.

The oxygen-carbon ratio, y , has been estimated, assuming all produced carbon oxides are the products of HTO reactions. The mass of fuel consumed per second in HTO reactions is $q_o(CO + CO_2)(12 + x)/(60 \times 22.4138)$, as derived for Eq. 7.2 in Chapter 7. The duration of the tube run was 593 minutes. Thus:

$$\begin{aligned} \text{Mass of fuel in HTO reactions} &= \frac{q_o(CO + CO_2)(12 + x) \times 593 \times 60}{60 \times 22.4138} \\ &= 57.8 \text{ g} \end{aligned}$$

using data on Table 5.2 and $x = 1.6$. Based on mass conservation of the hydrocarbon fuel, the initial mass of oil in the sand pack is equal to the sum of the mass of oil

5. COMBUSTION TUBE EXPERIMENTAL RESULTS

recovered plus the unburned hydrocarbon residue plus the fuel in HTO reactions, as follows:

$$367.7 = (346.9 + 143.9)y + 57.8$$

That is:

$$y = 0.63$$

This estimated value of y , 0.63, is considerably larger than that obtained by elemental analysis, 0.25, of a produced oil sample from this tube run (Section 4.1). However, based on gas analysis in kinetic tube Run VEN15 (Table 6.7), the oxygen-carbon ratio is 0.5; a closer match.

Elemental analysis of a produced oil sample from Run VEN14 confirmed the oxygenation of oil as a result of LTO. Clearly LTO should be avoided in field operations by regular monitoring of the apparent H/C ratio. Combustion tube Run VEN14 is one of the most important results of this study.

5.4 Hamaca Crude Oil Run VEN21

The sample consisted of oil, water, 20-30 mesh sand and 4.6% by weight of 170-270 mesh sand. One hour after commencing air injection, the igniter was turned off.

A fairly stable burn was observed. The produced gas composition readings were however oscillatory (Fig. 5.16). In the period 1-7 hours, the average values were: CO₂, 9.7%; CO, 4.3%; O₂, 3.8% and N₂, 81.2%. Apparent H/C and m -ratios averaged 1.77 and 0.308 respectively (Fig. 5.17). The average combustion zone temperature was 500°C (Fig. 5.18). The combustion front velocity averaged 11.1 cm/hr (0.36 ft/hr). Produced oil gravity increased by 1° API while oil viscosity decreased to 2,600 cP at 50°C from 14,000 cP for the original crude (Figs. 5.19 and 5.20).

5. COMBUSTION TUBE EXPERIMENTAL RESULTS

Except for the oscillatory gas composition readings, results of this tube run were similar to that of Run VEN5 in which clay was included in the sample. Voussoughi *et al.* (1982) inferred from combustion tube experiments that clay did not have a catalytic effect on combustion. A possible effect of clay and fine sand on combustion is as follows. Both clay and 170-270 mesh sand particles are smaller than those of 20-30 mesh sand. It is conceivable therefore that these smaller particles increase oil entrapment and thereby increase fuel concentration. Oil entrapment may be the result of permeability reduction and the greater surface area by these smaller particles. Similarly, with no clay or sand fines, fuel concentration is decreased. This may lead to low-temperature burns as observed in Run VEN14. Future research is suggested to investigate the relative effect of clay and sand grain size on fuel concentration.

Typical products of thermal cracking of crude oil are hydrogen and short chain paraffins, e.g. methane (Burger *et al.* 1985). In all tube runs, hydrogen and methane were not present in the produced gas, based on gas chromatograph measurements. The absence of these gases, and thus thermal cracking, indicate that distillation is the main mechanism for fuel deposition.

In the next chapter, results of kinetic experiments will be presented. In particular we will see whether a comparison can be made between kinetic and combustion tube experiments for identical samples.

5. COMBUSTION TUBE EXPERIMENTAL RESULTS

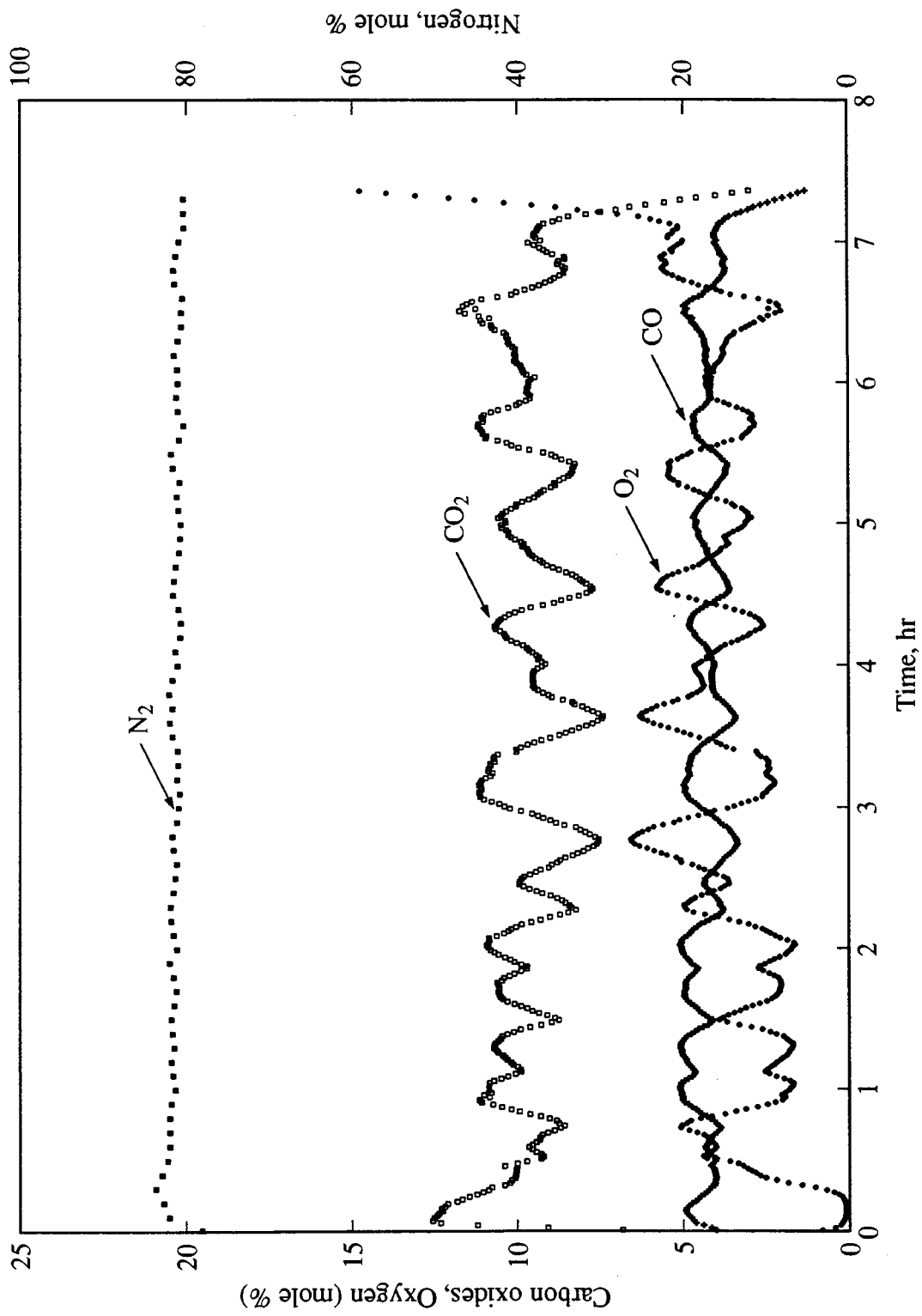


Figure 5.16: Produced Gas Composition Versus Time (Run VEN21)

5. COMBUSTION TUBE EXPERIMENTAL RESULTS

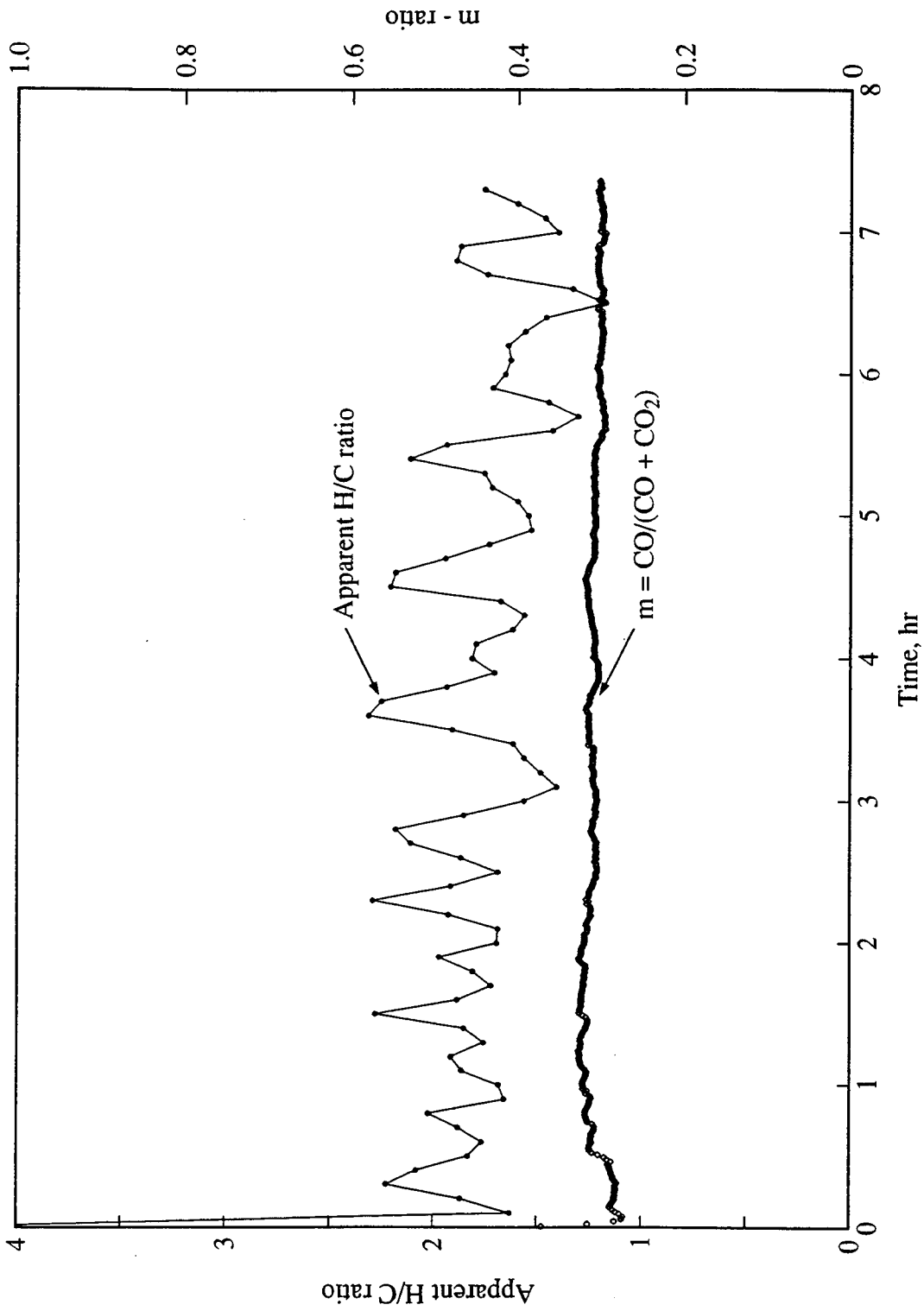


Figure 5.17: Apparent H/C and m-Ratios Versus Time (Run VEN21)

5. COMBUSTION TUBE EXPERIMENTAL RESULTS

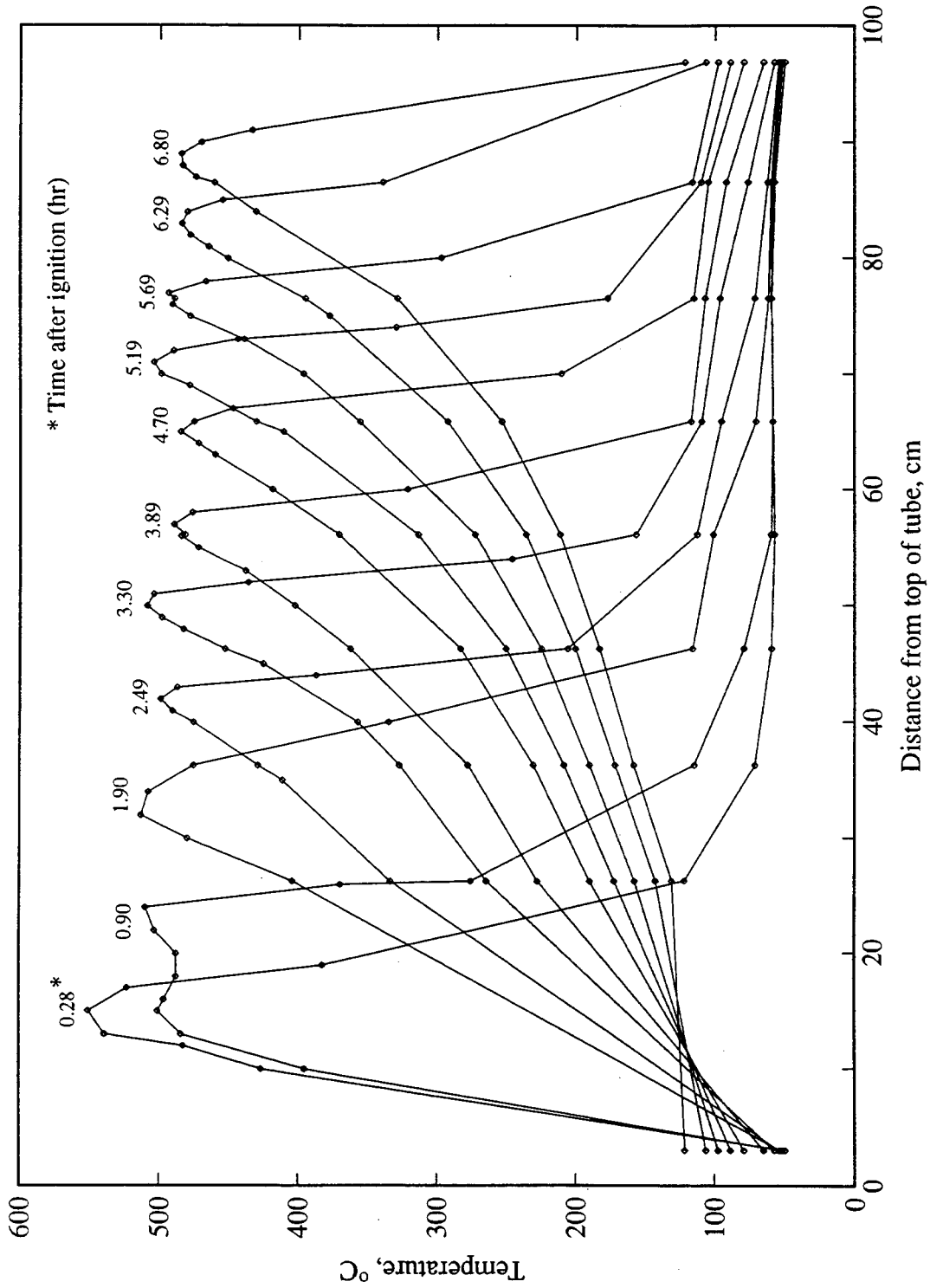


Figure 5.18: Temperature Profiles (Run VEN21)

5. COMBUSTION TUBE EXPERIMENTAL RESULTS

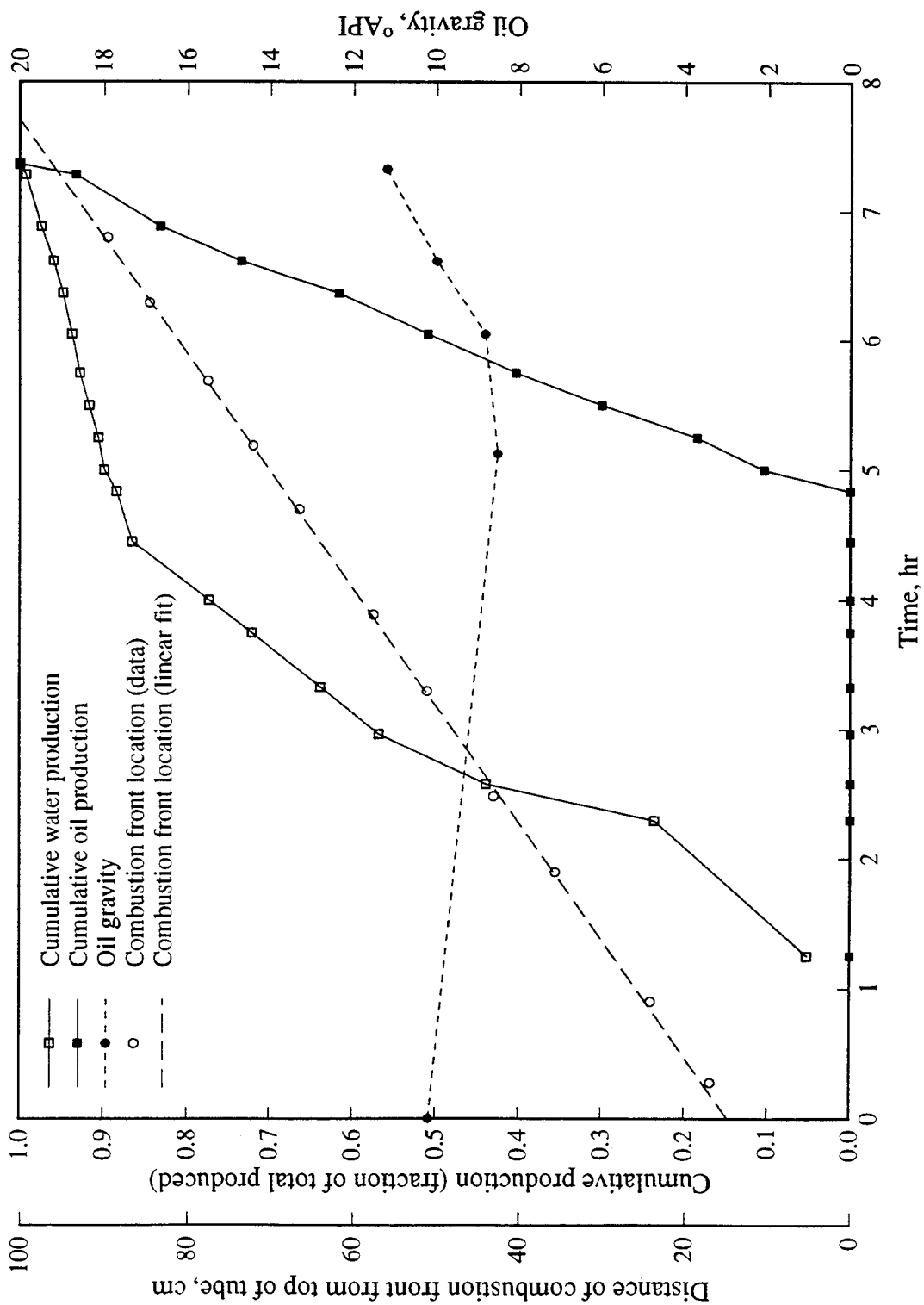


Figure 5.19: Production, Oil Gravity and Combustion Front Location Versus Time (Run VEN21)

5. COMBUSTION TUBE EXPERIMENTAL RESULTS

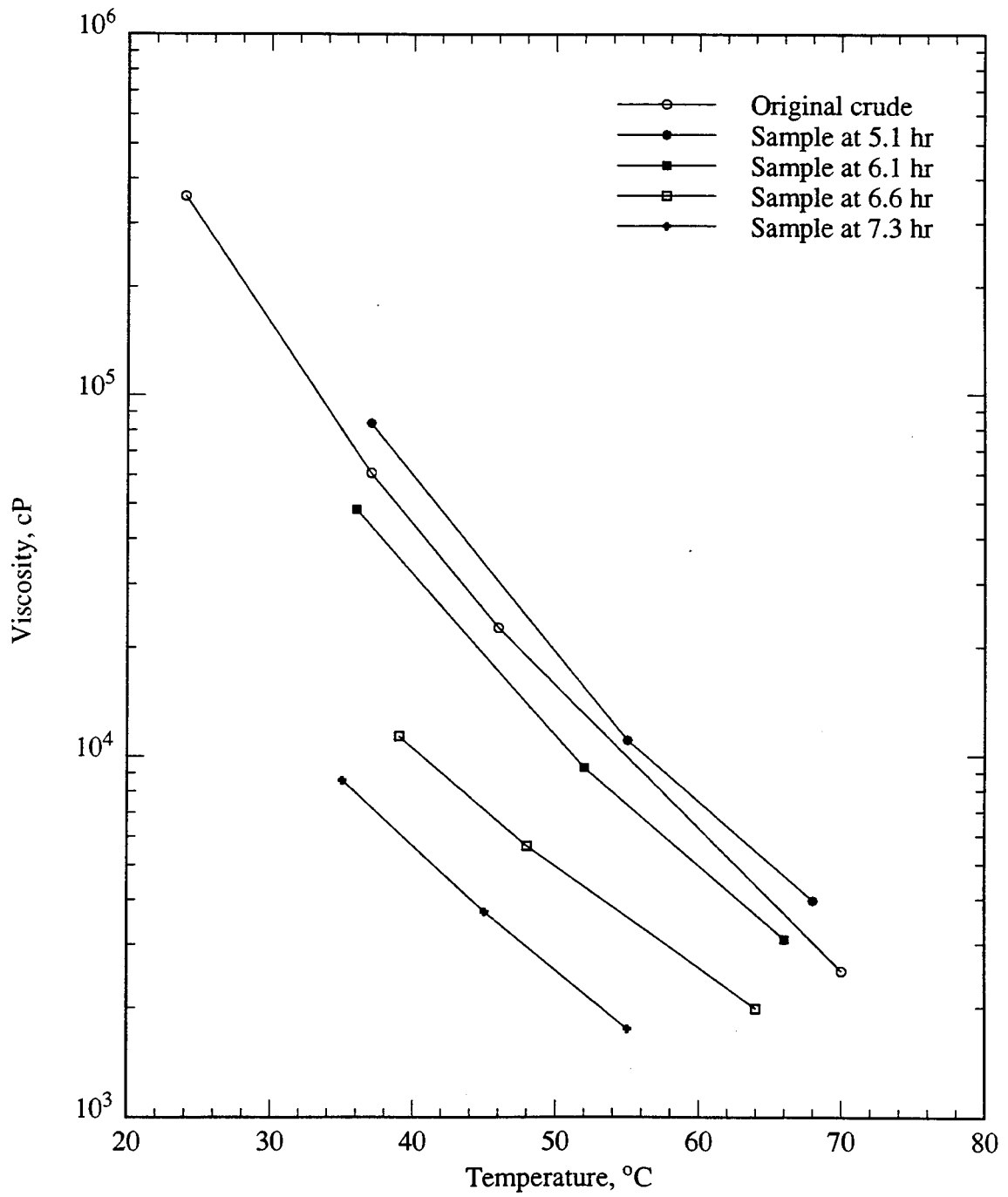


Figure 5.20: Oil Viscosity Versus Temperature (Run VEN21)

6. Kinetic Experimental Results

The original objective of performing kinetic tube experiments was to study the rate, order and mechanisms of reactions during combustion of crude oil. However based on data from initial kinetic tube runs, two puzzling results were obtained.

1. During high-temperature oxidation (HTO), apparent H/C ratios were typically in the range 0 to 1 compared to values of 1 to 2 based on combustion tube experiments (Chapter 5).
2. An Arrhenius graph of HTO data did not yield a straight line as predicted by a previous oxidation reaction model (Fassihi 1981).

Using the same experimental technique, Burger *et al.* (1985) and Fassihi (1981) also found apparent H/C ratios between 0 and 1 for crude oil in the HTO range. Fassihi (1981) obtained the following apparent H/C ratios at the HTO peaks: 0.3 (Huntington Beach oil), 0.2 (Venezuela Jobo crude oil) and 0.1 (San Ardo crude oil). Burger *et al.* (1985) attributed the low apparent H/C ratios to the fuel being made up of heavy oil fractions. Since heavy crude oil is a mixture of aromatic and saturated hydrocarbons, whose limiting atomic H/C ratios are between 1 and 2, a different explanation must be sought.

Figure 6.1 presents a correlation of atomic H/C ratio as a function of oil gravity and Universal Oil Products (UOP) K-factor. This graph is based on the Hougen and Watson correlation charts for petroleum hydrocarbon properties (Hougen *et al.*

6. KINETIC EXPERIMENTAL RESULTS

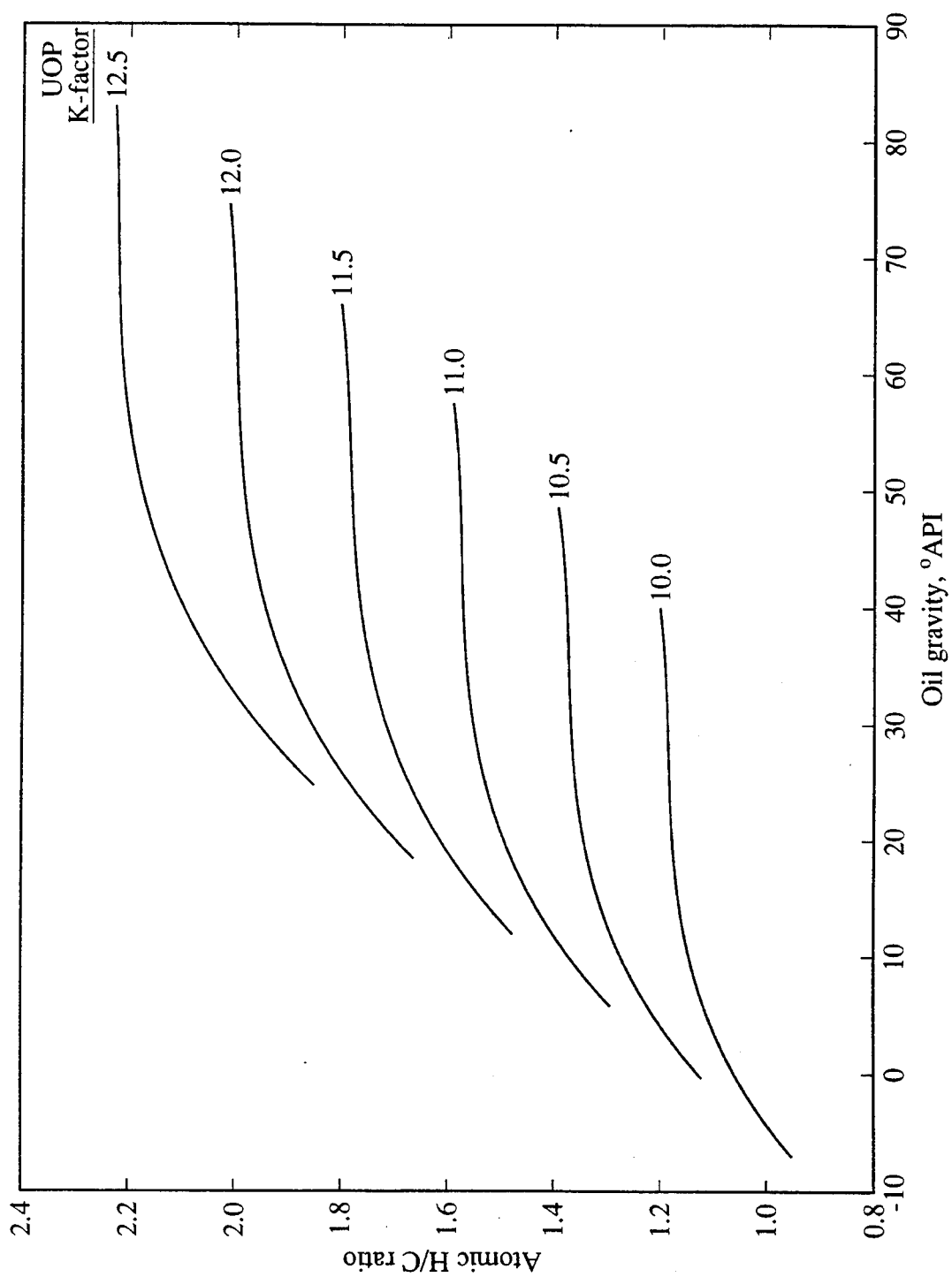


Figure 6.1: Atomic H/C Ratio Versus Oil Gravity and UOP K-Factor (After Lim, 1991)

6. KINETIC EXPERIMENTAL RESULTS

1954). The Hougen and Watson correlation charts represent a wide range of petroleum hydrocarbon types including crude oil distillation fractions with atmospheric boiling points of 1000°F. Figure 6.1 is a variation of a correlation presented by Lim (1991).

The UOP K-factor characterizes a crude oil based on the cube root of the mean boiling point. A curve fit of UOP K-factor was produced as a function of specific gravity and kinematic viscosity:

$$\text{UOP K-factor} = \frac{(2.87A - SG)}{(2.87A - 1)SG} \left[12.75B - \frac{7.78}{(2.17 + \log(\mu/\rho))} - 8.24 \right] + \frac{8.24}{SG} \quad (6.1)$$

where:

$$\begin{aligned} SG &= \text{oil specific gravity (60°F/60°F),} \\ A &= 1 + 8.69 \log [(T + 460)/560], \\ B &= 1 + 0.554 \log [(T + 460)/560], \\ \rho &= \text{density (g/cc) at } T = SG / \left[1 + 0.000321(T - 60) \times 10^{0.00462API} \right], \\ \mu &= \text{viscosity (cP) at } T, \\ T &= \text{temperature, °F.} \end{aligned}$$

Equation 6.1 was then used to produce the atomic H/C ratio from a Hougen and Watson correlation of weight fraction of hydrogen. The Hougen and Watson correlation was tested against measured atomic H/C ratios for 23 crude oils whose oil gravities ranged between 10° and 36°API. The results are presented in Table 6.1. Measured atomic H/C ratios and those obtained from the UOP K-factor correlation are plotted on Fig. 6.2 for comparison. The straight line in Fig. 6.2 represents a perfect match between the measured data and H/C ratios from the correlation. Atomic H/C ratio data for crude oils agree reasonably well with H/C ratios obtained from the Hougen and Watson correlation.

Based on correlation of residuum at equivalent normal boiling point of 335°C (635°F) versus original oil gravity (Lim 1991), residuum gravity is 5°API for an

6. KINETIC EXPERIMENTAL RESULTS

Table 6.1: Atomic H/C Ratios From Hougen and Watson Correlation

Source	Oil gravity (°API)	Viscosity (cP)	Temp. (°F)	UOP K-factor	Atomic H/C (correlation)	Atomic H/C (measured)
Alexander <i>et al.</i> (1962)	10.3	5,129	130	11.62	1.46	1.52
	12.6	625	130	11.58	1.50	1.57
	16.3	358	130	11.83	1.60	1.66
	17.0	406	130	11.91	1.62	1.55
	21.3	12	130	11.46	1.62	1.64
	21.8	43	130	11.89	1.72	1.63
	24.0	27	130	11.95	1.76	1.70
	24.4	94	130	12.30	1.81	1.62
	25.8	16	130	11.93	1.79	1.66
	29.5	7	130	11.95	1.84	1.76
	35.6	3	130	12.04	1.92	1.87
	36.0	3	130	12.09	1.94	1.79
Wilson <i>et al.</i> (1962)	12.9	1,922	100	11.59	1.50	1.57
	22.0	251	100	12.13	1.75	1.68
	24.0	34	100	11.86	1.74	1.65
	28.7	127	100	12.59	1.94	1.87
	30.6	9	100	11.97	1.85	1.73
Bousaid and and Ramey (1968)	13.9	3,480	77	11.63	1.53	1.56
	22.1	158	77	11.94	1.73	1.65
Hvizdos <i>et al.</i> (1982)	10.0	1,002	185	11.68	1.46	1.48
Greaves <i>et al.</i> (1989)	22.8	40	100	11.80	1.71	1.54
This study	10.2	14,000	122	11.66	1.46	1.65
	11.5	10,000	95	11.75	1.48	1.53

6. KINETIC EXPERIMENTAL RESULTS

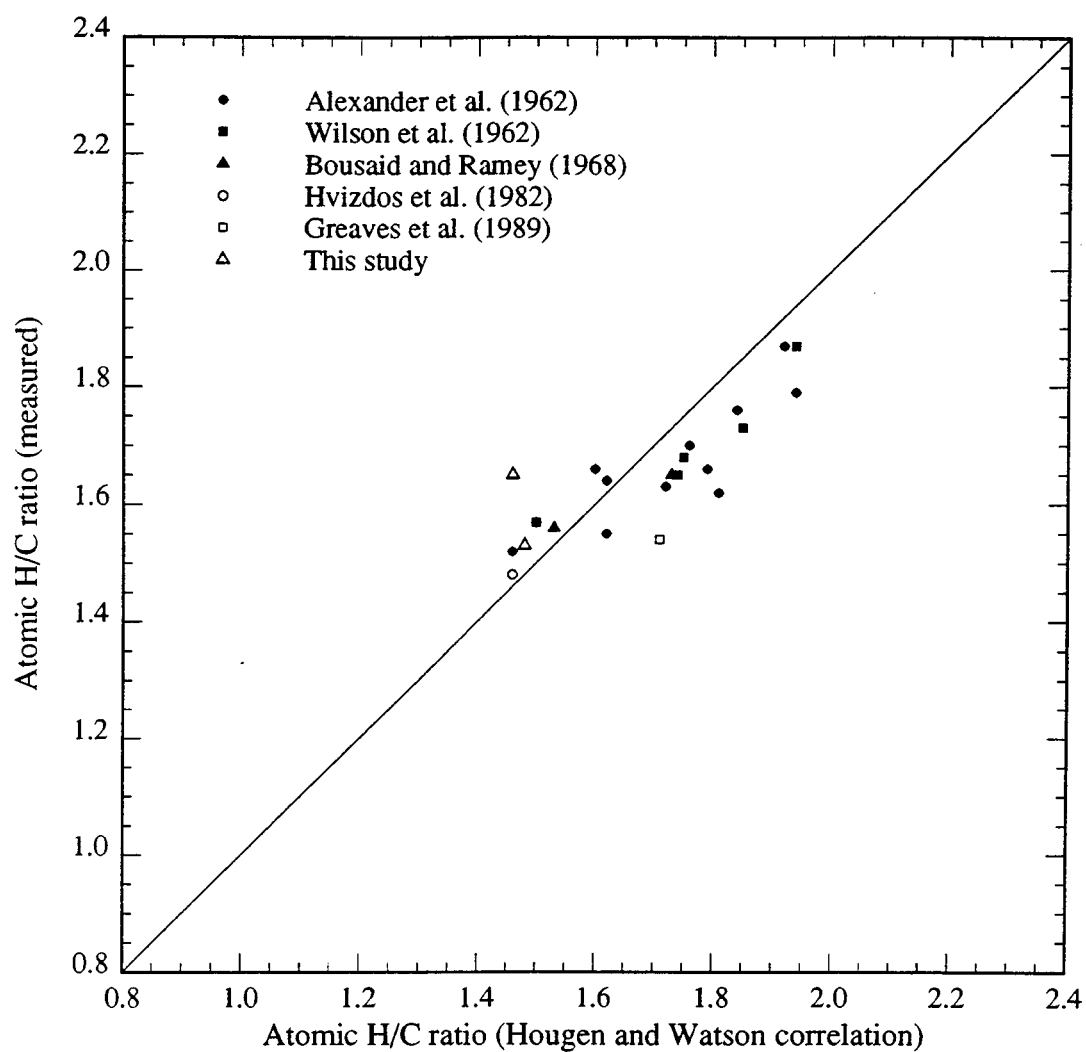


Figure 6.2: Measured Atomic H/C Ratios Versus Values Derived From Hougen and Watson Correlation

6. KINETIC EXPERIMENTAL RESULTS

original oil gravity of 10°API. Figure 6.1 indicates H/C ratios greater than 1 even for an unrealistically low fuel gravity of 0°API.

Fassihi (1981) obtained the atomic H/C ratios of distillation cuts of Huntington Beach oil based on elemental analysis. The atomic H/C ratio decreased from 1.95 for a distillation cut at 150°C (80 psig) to 1.5 for a distillation cut at 550°C, compared to 1.64 for the original oil. Fassihi's results indicate that fuel burned during combustion would have atomic H/C ratios slightly lower than those of the original crude, as typically observed in combustion tube experiments.

The apparent H/C ratios observed during HTO from kinetic tube experiments are much lower than the lowest H/C ratios on Fig. 6.1. This fact constituted a main reason for performing kinetic tube experiments in this study. If atomic H/C ratios and thus fuels oxidized in kinetic and combustion tube experiments are different, then kinetic experimental results do not reflect oxidation reactions in the combustion zone.

To resolve this puzzle and other problems related to the previous kinetic oxidation experiments, eleven kinetic experiments were carried out using three crude oils: Cold Lake bitumen, Huntington Beach oil and Hamaca crude oil. In addition, three runs were made using carbon (Reagent grade, 60-mesh) and a mixture of carbon and Cold Lake bitumen. The conditions for these runs are listed in Table 6.2. Unless stated otherwise, the samples consisted of crude oil and 20–30 mesh Ottawa sand. For some runs (as indicated) the sample matrix contained clay or 170–270 mesh sand. Air was the usual injection medium. However, in three kinetic runs, nitrogen was followed by air, or vice versa, as indicated on the table.

6.1 Kinetic Tube Experimental Results

Seven kinetic tube experiments were conducted in which air was flowed through an oil-sand mixture. Composition of the produced gas and temperature data are

6. KINETIC EXPERIMENTAL RESULTS

Table 6.2: Experimental Conditions for Kinetic Runs

Run No.	Crude oil or fuel*	Gas flow-rate, L/min	Pressure, psig	Temp. rate, °C/hr	Sample length, cm	Sample weight, g	Initial weight %			
							Sand	Clay	Oil/Fuel	Water
C3**	C	0.70	100	50	5.6	52.3635	94.3	0	1.9	3.8
C4***	C	0.70	100	50	6.0	52.3505	93.9	0	1.9	4.3
CLC1	CLB+C	1.08	85	50	6.2	53.8340	91.6	0	2.9	4.0
CL2	CLB	1.10	80	50	5.3	53.2740	92.9	0	3.0	4.1
CL5	CLB	0.95	85	50	5.5	52.8474	92.3	0	3.8	3.9
CL10†	CLB	0.30	95	150	5.4	53.0834	91.6	0	4.1	4.3
CL14	CLB	0.70	100	50	5.0	52.6357	86.8	4.6	4.6	4.1
HBO2	HBO	1.09	85	50	5.4	53.6500	92.3	0	4.1	3.7
VEN6	HCO	0.70	100	50	5.5	57.7968	86.8	4.6	4.6	4.1
VEN7‡	HCO	0.70	100	50	5.5	57.5726	86.8	4.6	4.6	4.1
VEN10†	HCO	0.70	100	50	1.8	17.2630	86.8	4.6	4.6	4.1
VEN15	HCO	0.70	100	50	4.9	49.8876	90.8	0	4.9	4.3
VEN19††	HCO	0.70	100	50	4.3	44.4586	90.8	0	4.9	4.3
VEN23	HCO	0.70	100	50	4.3	35.4507	86.8	0°	4.6	4.1

* C = Carbon, CLB = Cold Lake bitumen, HBO = Huntington Beach oil, HCO = Hamaca crude oil.

** 20-25 mesh sand.

*** 45-70 mesh sand.

† Nitrogen injected until end of LTO, then air injected.

†† Temperature decreased on reaching 350°C.

‡ Air injected until end of LTO, then nitrogen injected.

° Includes 4.6% by weight of 170-270 mesh sand.

6. KINETIC EXPERIMENTAL RESULTS

shown in Figs. 6.3 - 6.9. The following observations were made.

- The oxygen consumption data indicates two oxidation reactions. The first reaction (LTO) starts at about 170°C and has a peak at about 250°C. This is followed by a second oxidation reaction (HTO) which has a peak at about 400°C.
- Temperature of the kinetic tube was programmed to increase at 50°C/hr. However, temperatures at the LTO and HTO peaks were higher than programmed temperatures, indicating both oxidation reactions to be exothermic.
- Oxygen consumption during LTO increased significantly if the sample matrix contained clay (Table 6.3, page 109). For example, consider Hamaca oil Runs VEN6 (Fig. 6.7), VEN15 (Fig. 6.8) and VEN23 (Fig. 6.9). In Run VEN15 (no clay), the ratio of the oxygen consumption peak during LTO to that during HTO was 0.11. However in Run VEN6 (with clay), the ratio increased to 0.90, while in Run VEN23 (with 170-270 mesh sand), the ratio was 0.18. Clay increased oxygen consumption during LTO.
- The initial amounts of oil in the samples were: 2.66 g (Run VEN6), 2.44 g (Run VEN15) and 1.63 g (Run VEN23). Given the same air injection rate, 0.7 L/min, the oxygen consumption peak during HTO was higher in Run VEN15 (14.0 %) - with less oil - than in Run VEN23 (6.8 %). The sample in Run VEN15 had 50 % more oil than in Run VEN6. However, the HTO peak in Run VEN15 was about three times higher than that in Run VEN6 (4.6 %). An increase in oxygen consumption during LTO resulted in a decrease in oxygen consumption during HTO.

These perplexing observations appear to be a result of changes in the fuel during LTO, and are explained in Section 6.7.

6. KINETIC EXPERIMENTAL RESULTS

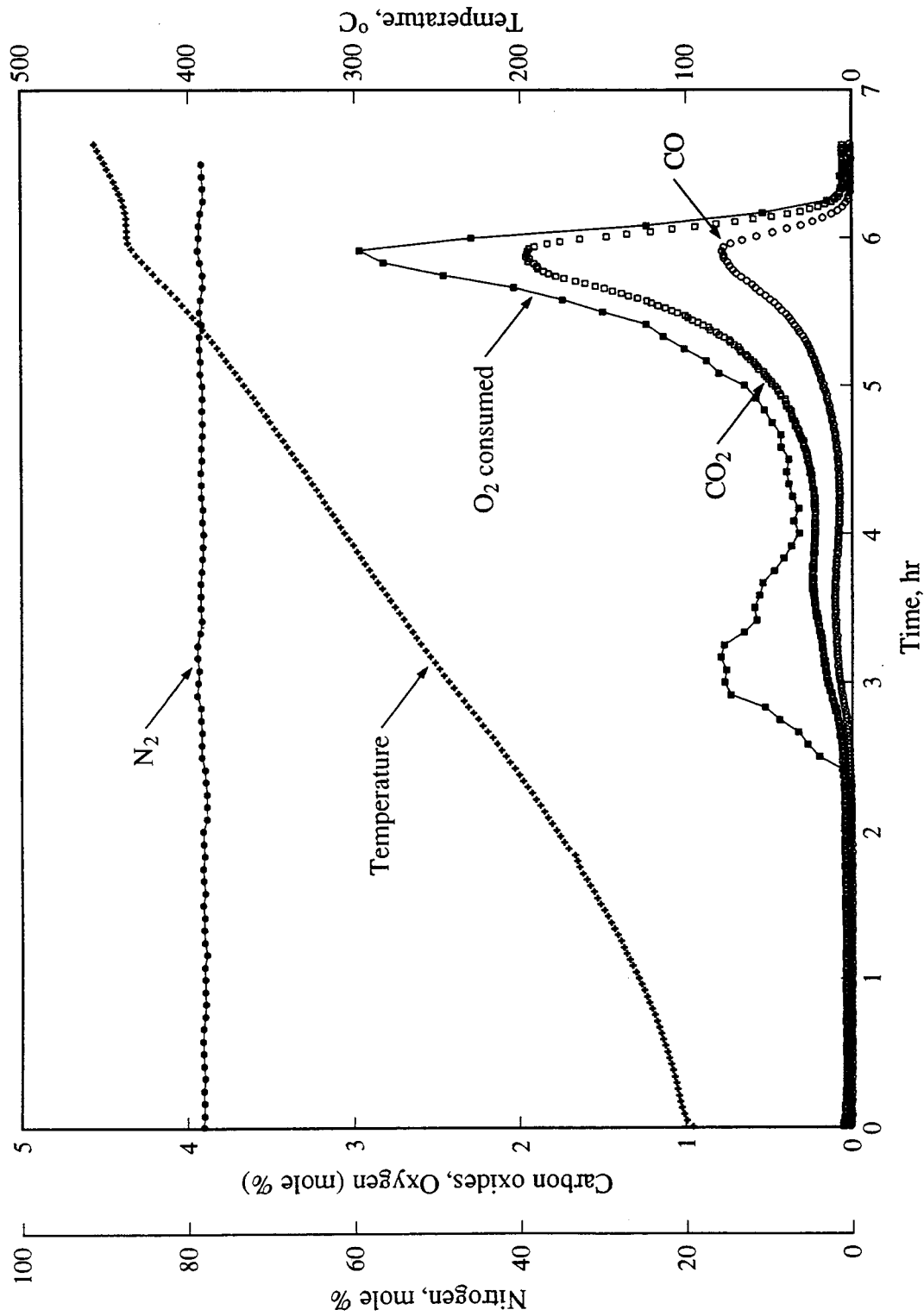


Figure 6.3: Produced Gas Composition and Temperature Versus Time (Run CL2)

6. KINETIC EXPERIMENTAL RESULTS

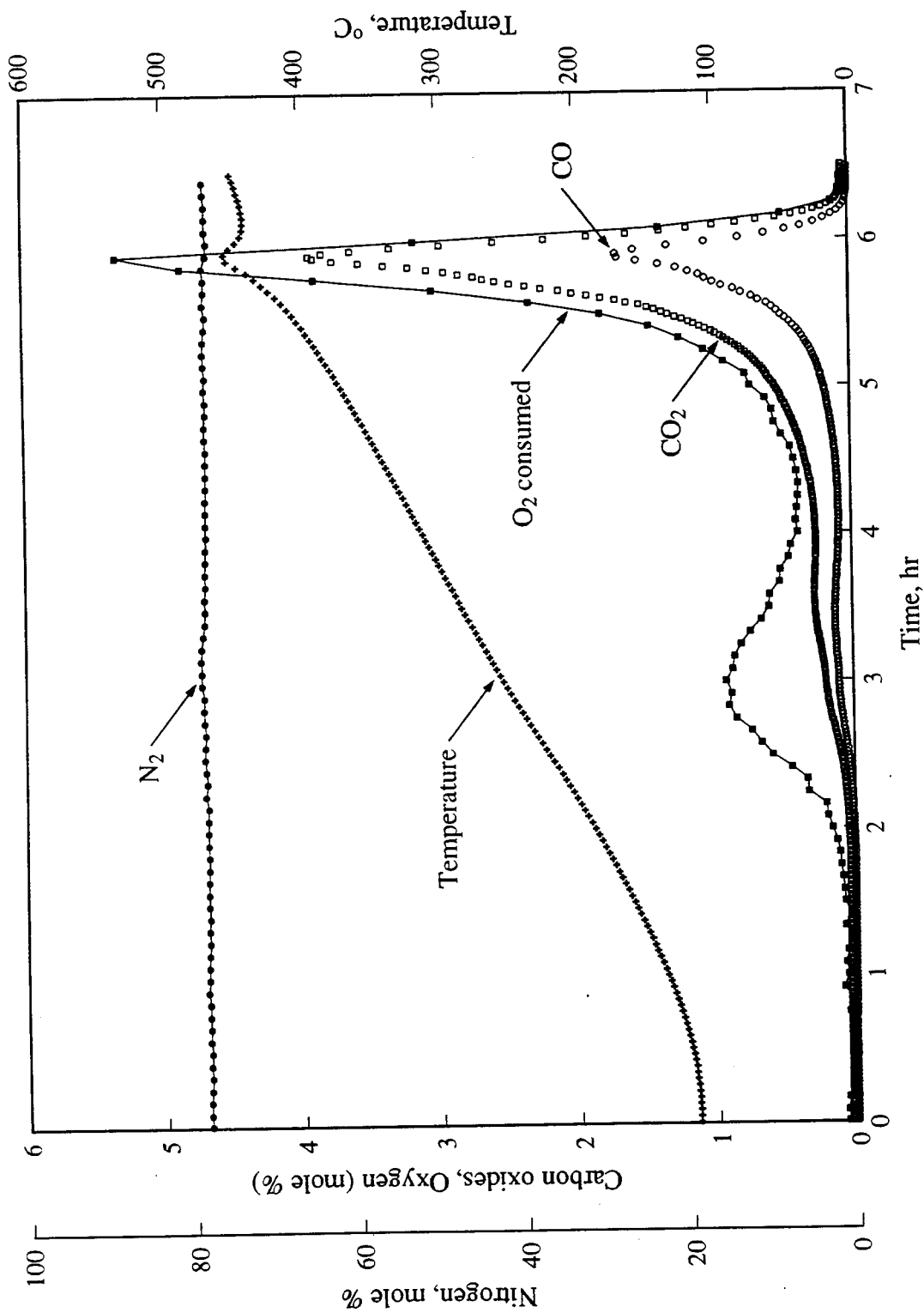


Figure 6.4: Produced Gas Composition and Temperature Versus Time (Run CL5)

6. KINETIC EXPERIMENTAL RESULTS

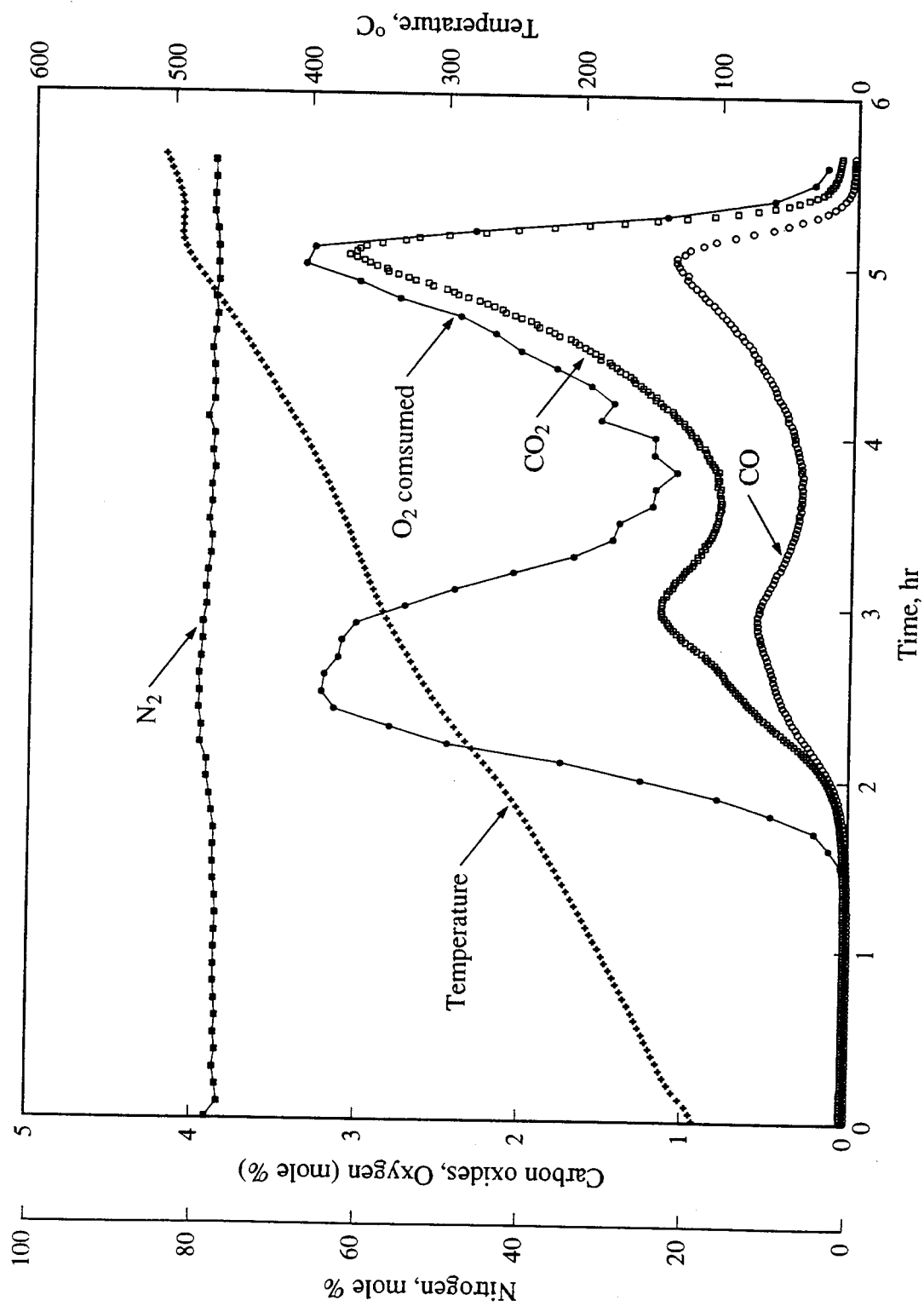


Figure 6.5: Produced Gas Composition and Temperature Versus Time (Run CL14)

6. KINETIC EXPERIMENTAL RESULTS

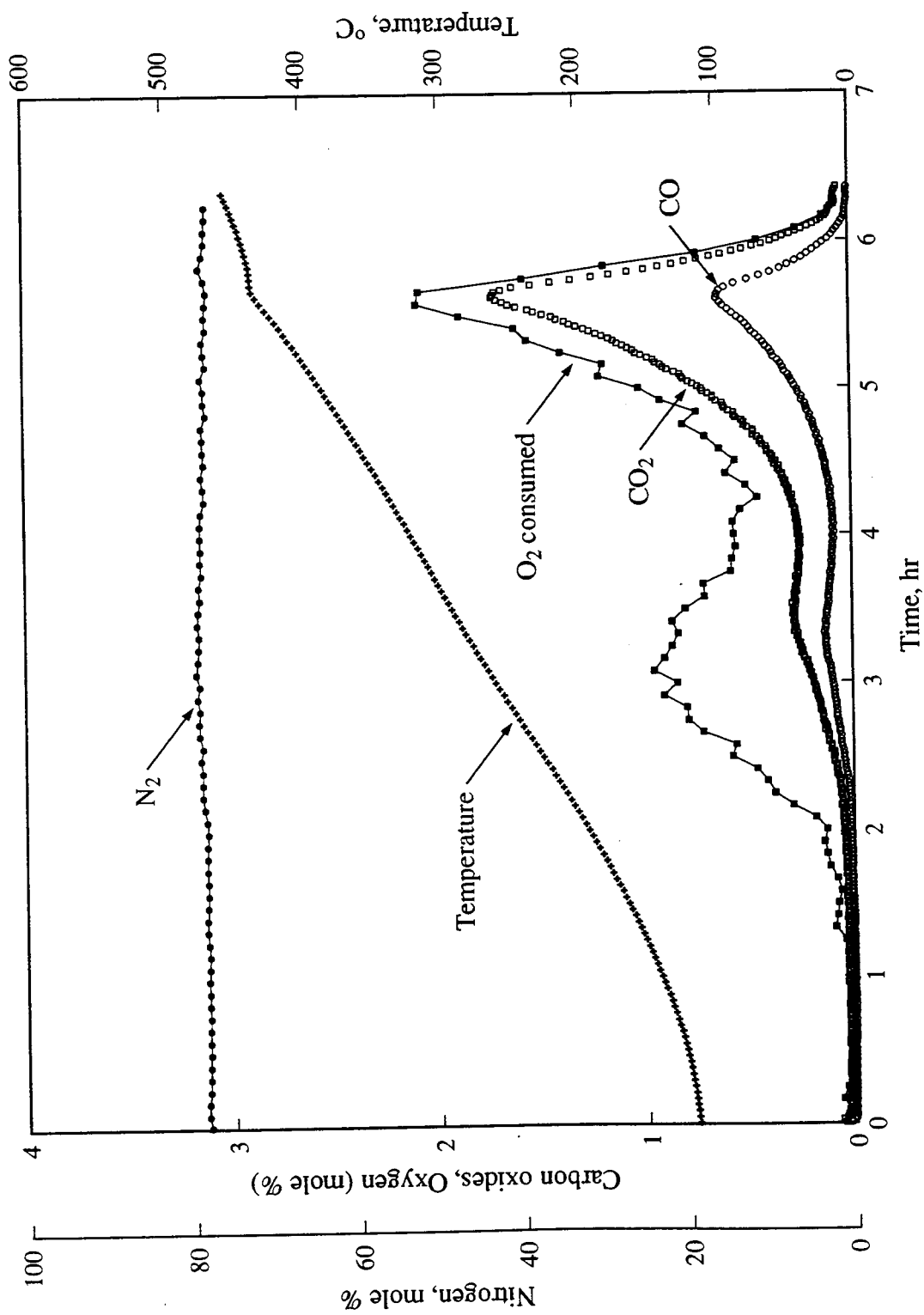


Figure 6.6: Produced Gas Composition and Temperature Versus Time (Run HBO2)

6. KINETIC EXPERIMENTAL RESULTS

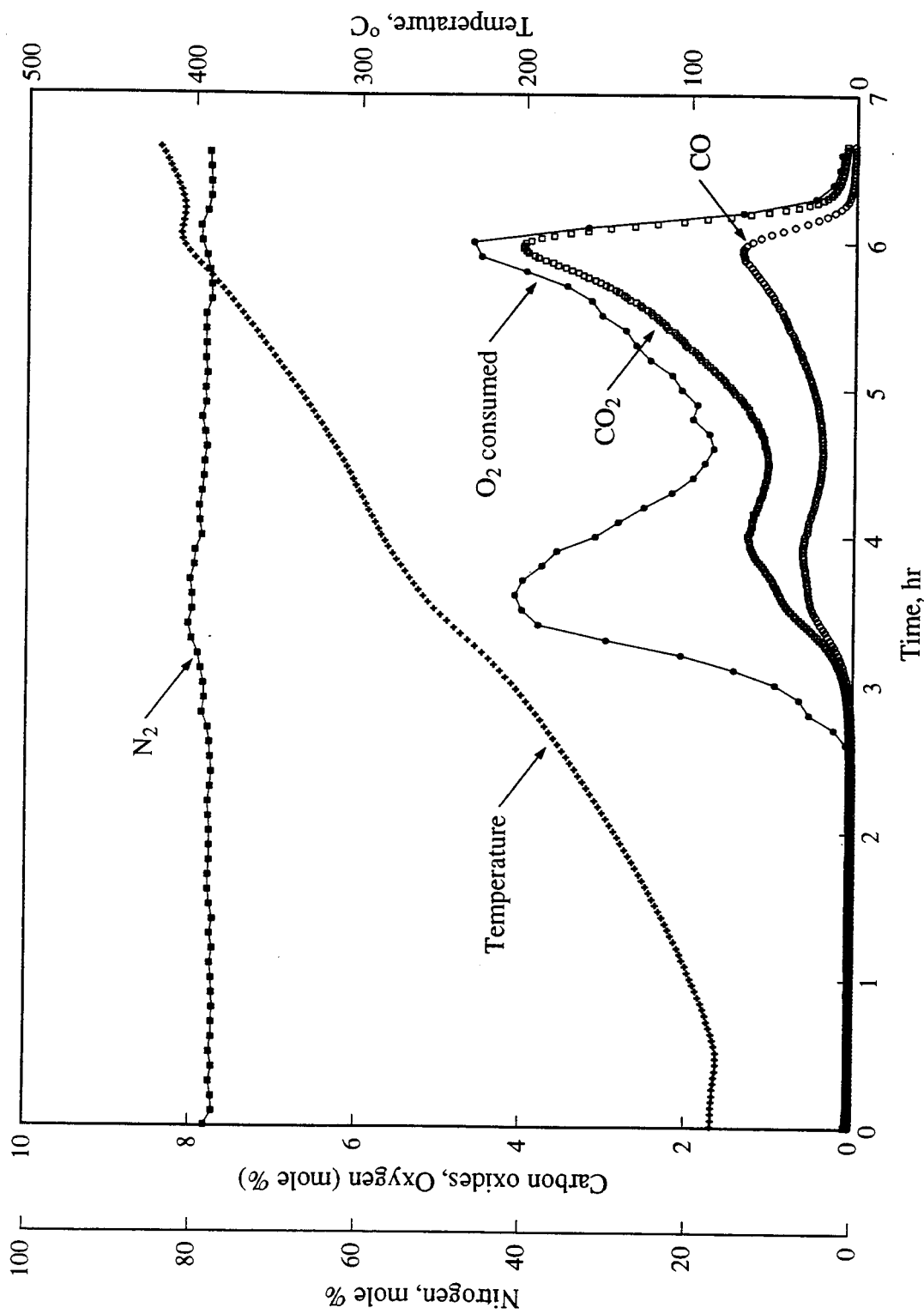


Figure 6.7: Produced Gas Composition and Temperature Versus Time (Run VEN6)

6. KINETIC EXPERIMENTAL RESULTS

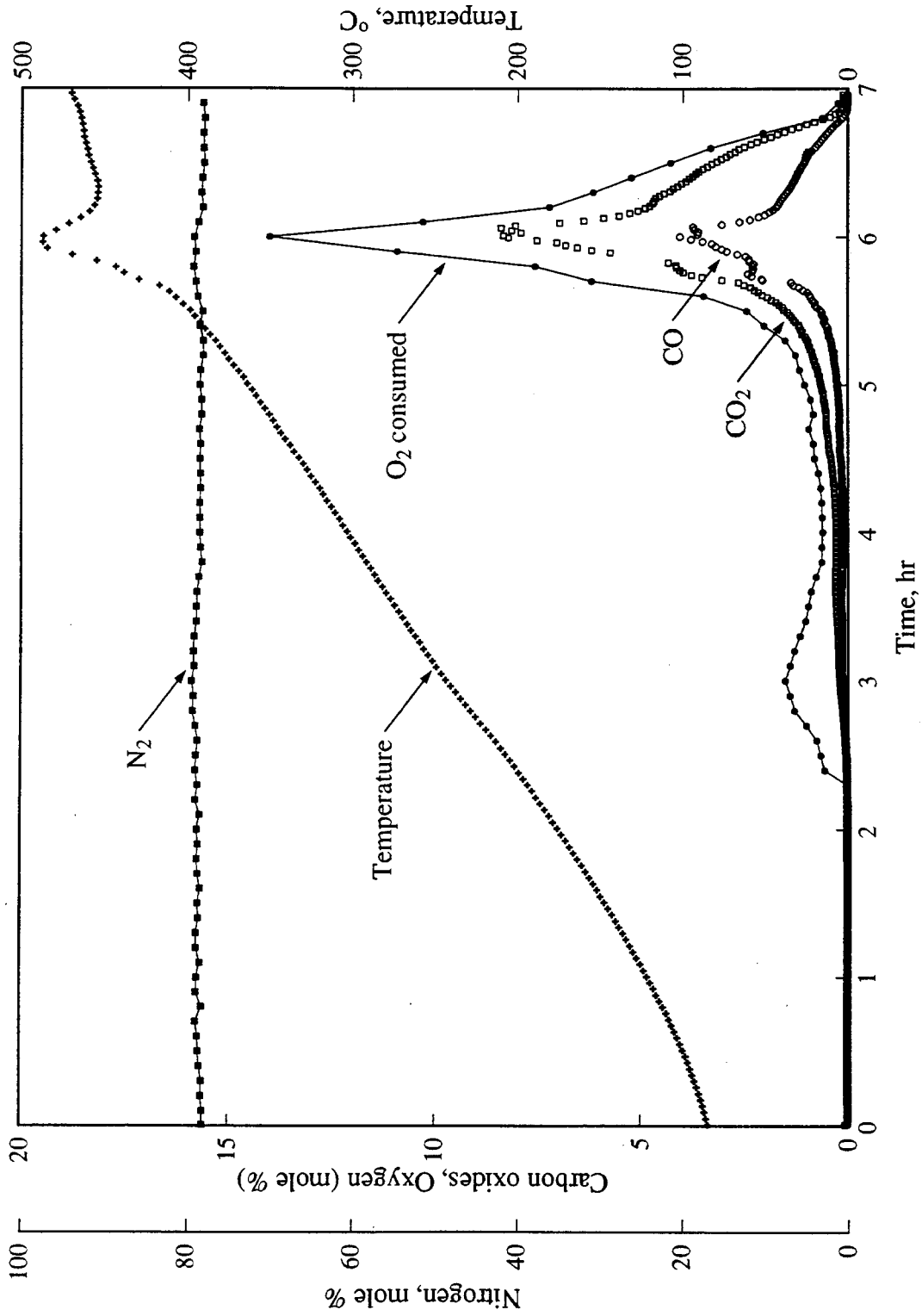


Figure 6.8: Produced Gas Composition and Temperature Versus Time (Run VEN15)

6. KINETIC EXPERIMENTAL RESULTS

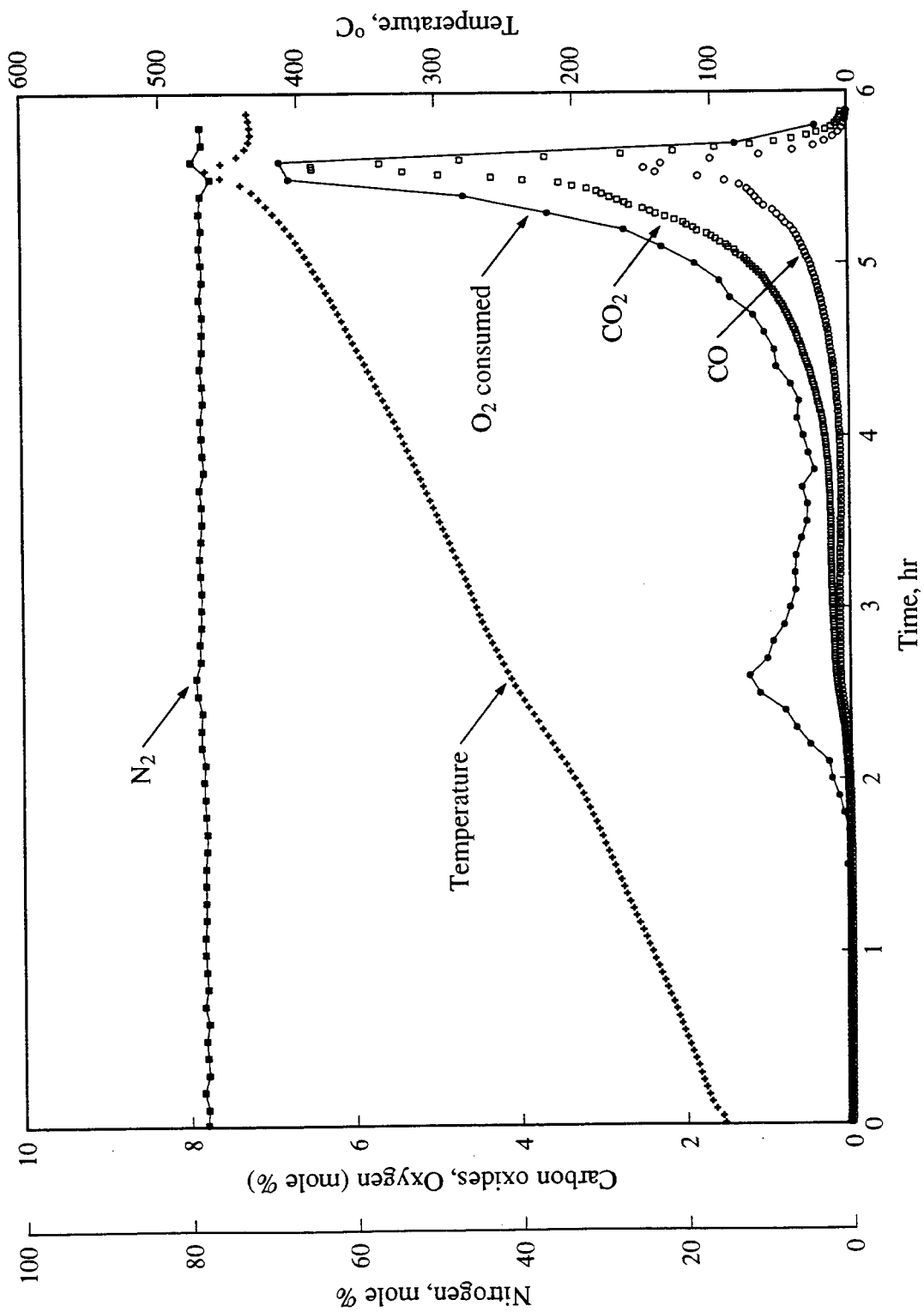


Figure 6.9: Produced Gas Composition and Temperature Versus Time (Run VEN23)

6. KINETIC EXPERIMENTAL RESULTS

Table 6.3: Oxygen Consumption Peaks at LTO and HTO

Run No.	Sample matrix (in addition to 20-30 mesh sand)	Oxygen consumption peak (mole %)		
		LTO (a)	HTO (b)	(a) ÷ (b)
CL2	-	0.79	2.95	0.27
CL5	-	0.91	5.32	0.17
CL14	clay	3.23	3.35	0.96
HBO2	-	0.94	2.09	0.45
VEN6	clay	4.09	4.57	0.90
VEN15	-	1.50	14.02	0.11
VEN23	170-270 mesh sand	1.22	6.81	0.18

The apparent atomic H/C and m -ratios were calculated from gas composition data using Eqs. 2.7 and 2.6. The results are presented in Figs. 6.10 – 6.16. Based on the apparent atomic H/C and m -ratio graphs, the following observations were made.

- The apparent H/C ratio increased to values ranging from about 15 to 40 at the LTO peak temperature, indicating that a large amount of oxygen entered into LTO reactions which did not produce carbon oxides.
- Fairly constant apparent H/C ratios were observed following the first oxygen consumption peak. The HTO reaction may be considered to be the oxidation of a fuel consisting of a hydrocarbon with a particular H/C ratio.
- The apparent H/C trends of these runs support the conclusion that there are two main oxidation reaction mechanisms: oxygen addition to the hydrocarbon with little carbon oxide generation at low temperatures, followed by high temperature oxidation of this fuel.

6. KINETIC EXPERIMENTAL RESULTS

- The m -ratio, fraction of carbon converted to carbon monoxide, decreased from about 0.4 for the LTO temperature range to about 0.3 for HTO. The m -ratio was fairly constant throughout the temperature range of these experiments. This observation also indicated the existence of two oxidation reactions.
- Apparent H/C ratios in the HTO temperature range were typically between 0 and 1 (Table 6.4). As discussed at the beginning of this chapter, this observation posed a major problem because fuel atomic H/C ratios of 1 to 2 were indicated by combustion tube results, elemental analysis and the Hougen and Watson correlation.

Table 6.4: Average Apparent H/C and m -Ratios at HTO Temperature Range

Run No.	Period (hrs)	m -ratio	Apparent H/C ratio
CL2	5.33 – 6.33	0.260	0.71
CL5	5.25 – 6.25	0.268	0.49
CL14	4.20 – 5.30	0.266	0.00
HBO2	4.83 – 6.25	0.247	0.37
VEN6	5.10 – 6.30	0.246	0.21
VEN15	5.30 – 6.80	0.288	1.02
VEN23	4.80 – 5.70	0.276	1.04

6. KINETIC EXPERIMENTAL RESULTS

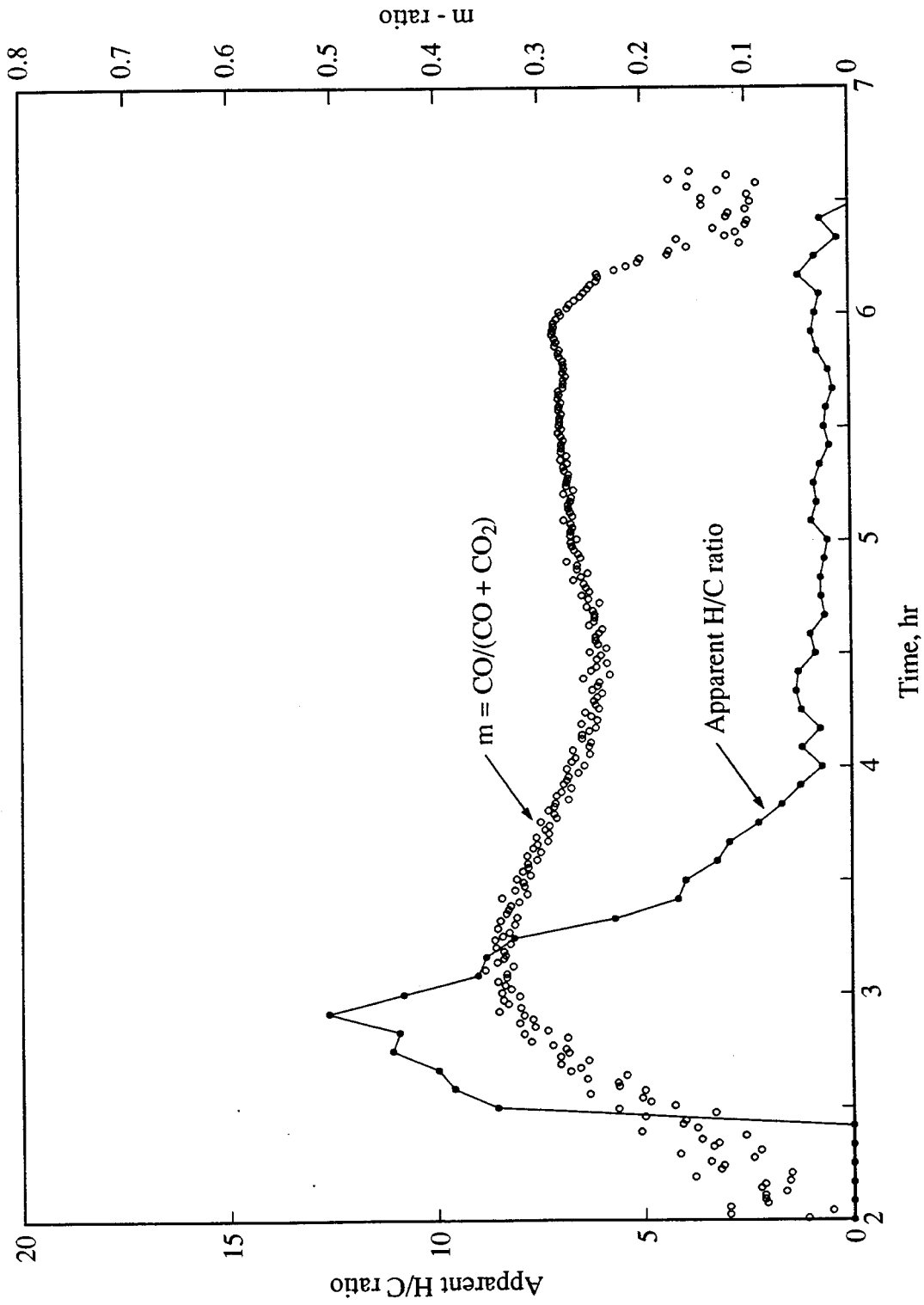


Figure 6.10: Apparent H/C and m-Ratios Versus Time (Run CL2)

6. KINETIC EXPERIMENTAL RESULTS

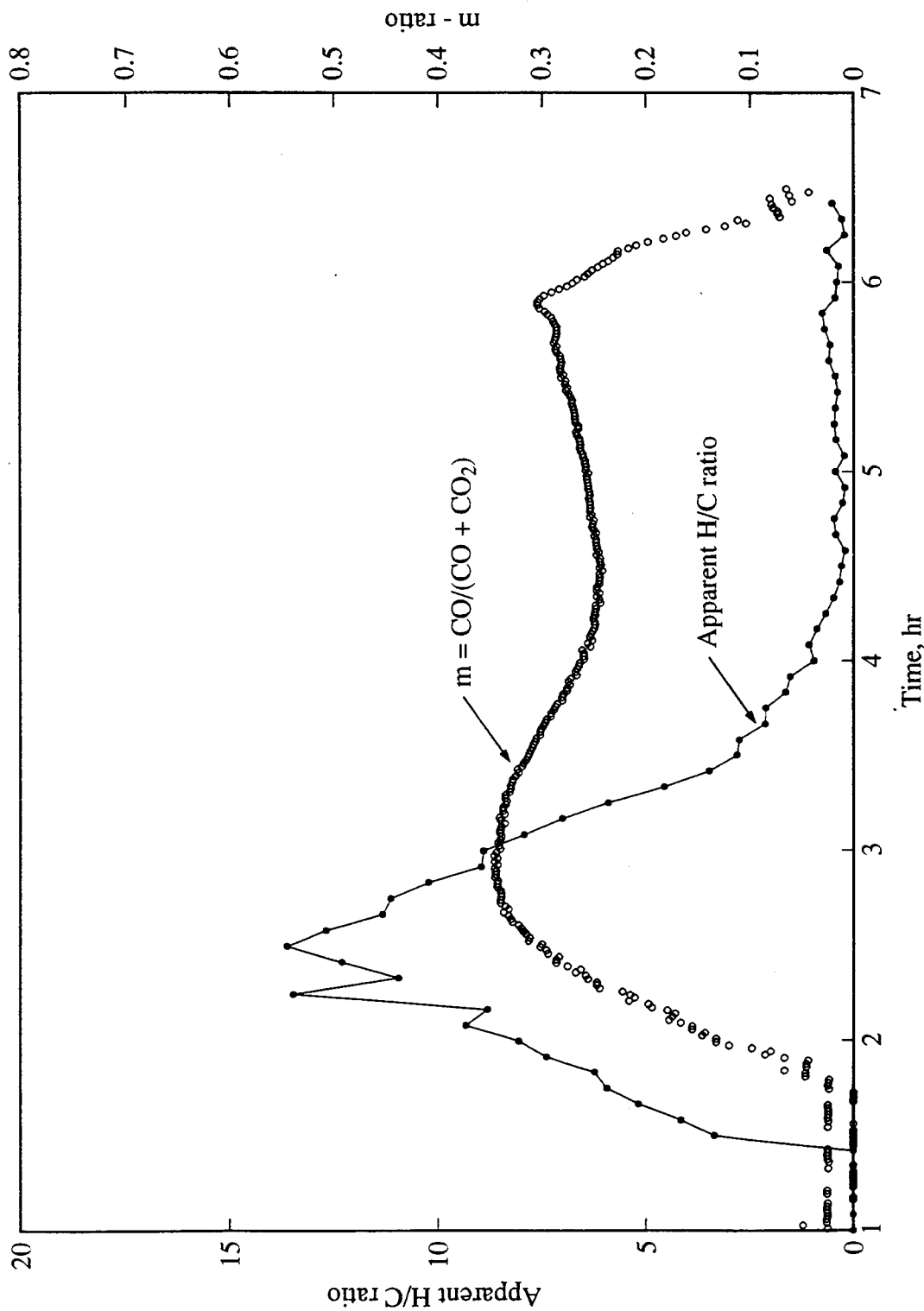


Figure 6.11: Apparent H/C and m-Ratios Versus Time (Run CL5)

6. KINETIC EXPERIMENTAL RESULTS

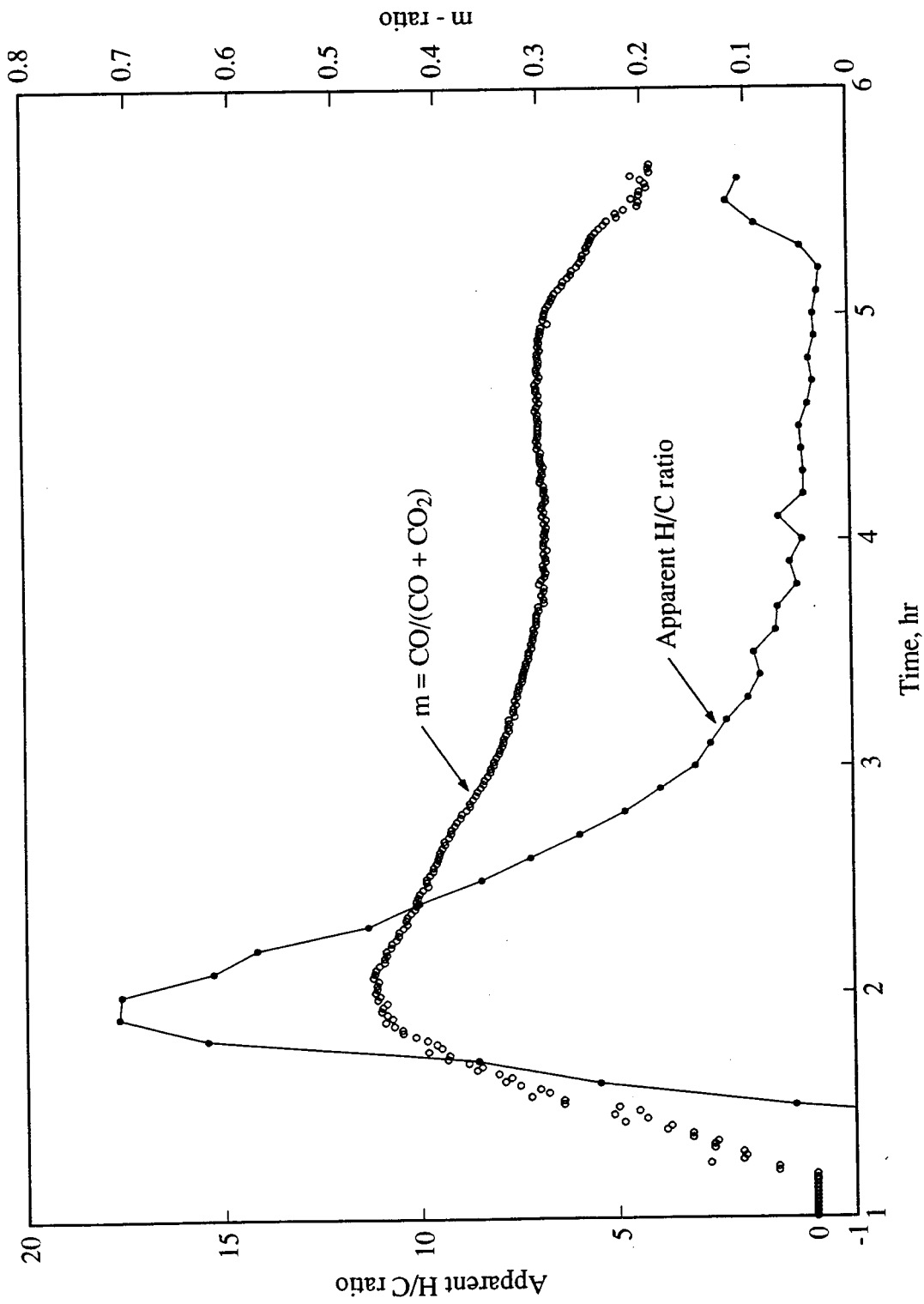


Figure 6.12: Apparent H/C and m-Ratios Versus Time (Run CL14)

6. KINETIC EXPERIMENTAL RESULTS

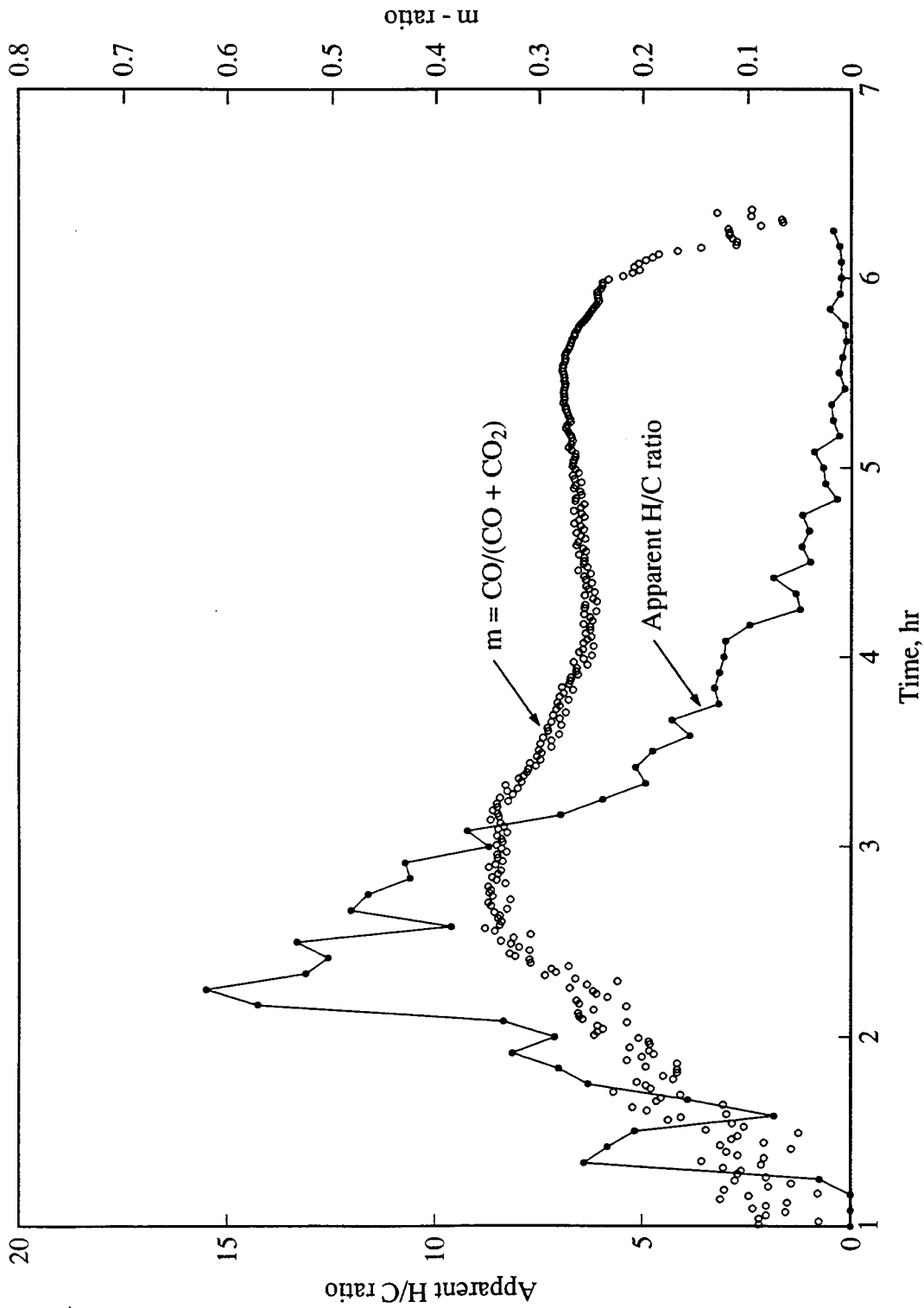


Figure 6.13: Apparent H/C and m-Ratios Versus Time (Run HBO2)

6. KINETIC EXPERIMENTAL RESULTS

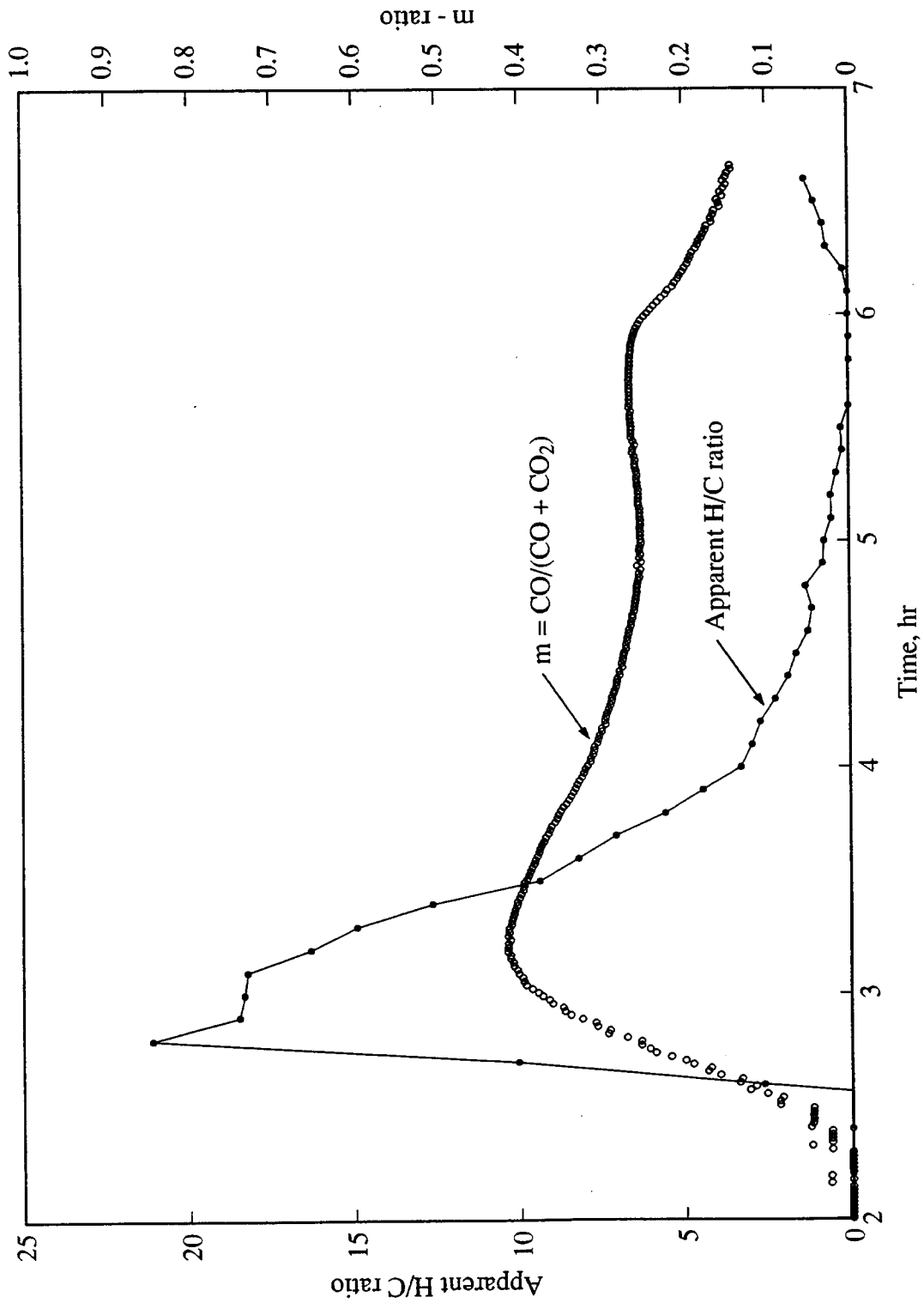


Figure 6.14: Apparent H/C and m-Ratios Versus Time (Run VEN6)

6. KINETIC EXPERIMENTAL RESULTS

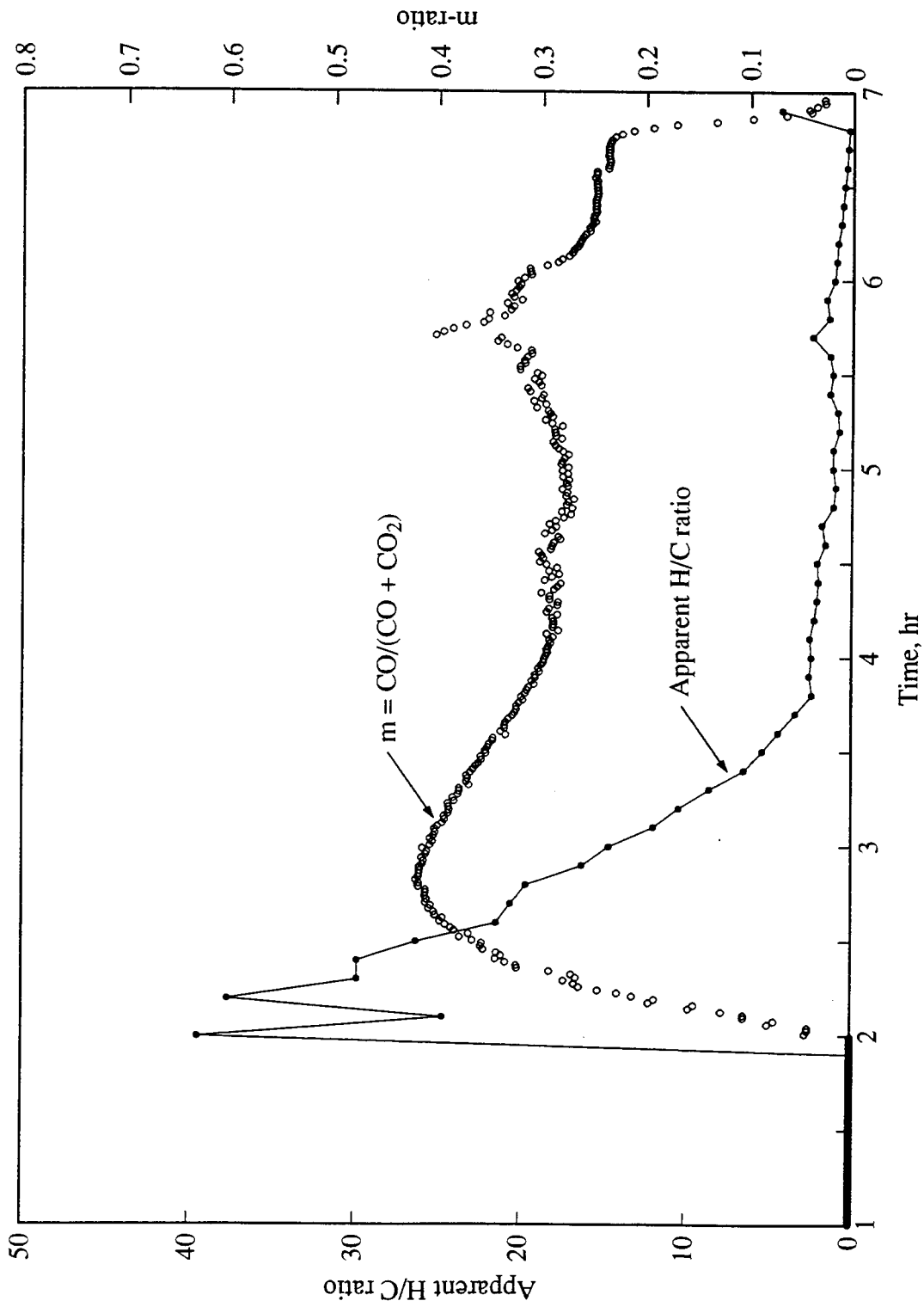


Figure 6.15: Apparent H/C and m-Ratios Versus Time (Run VEN15)

6. KINETIC EXPERIMENTAL RESULTS

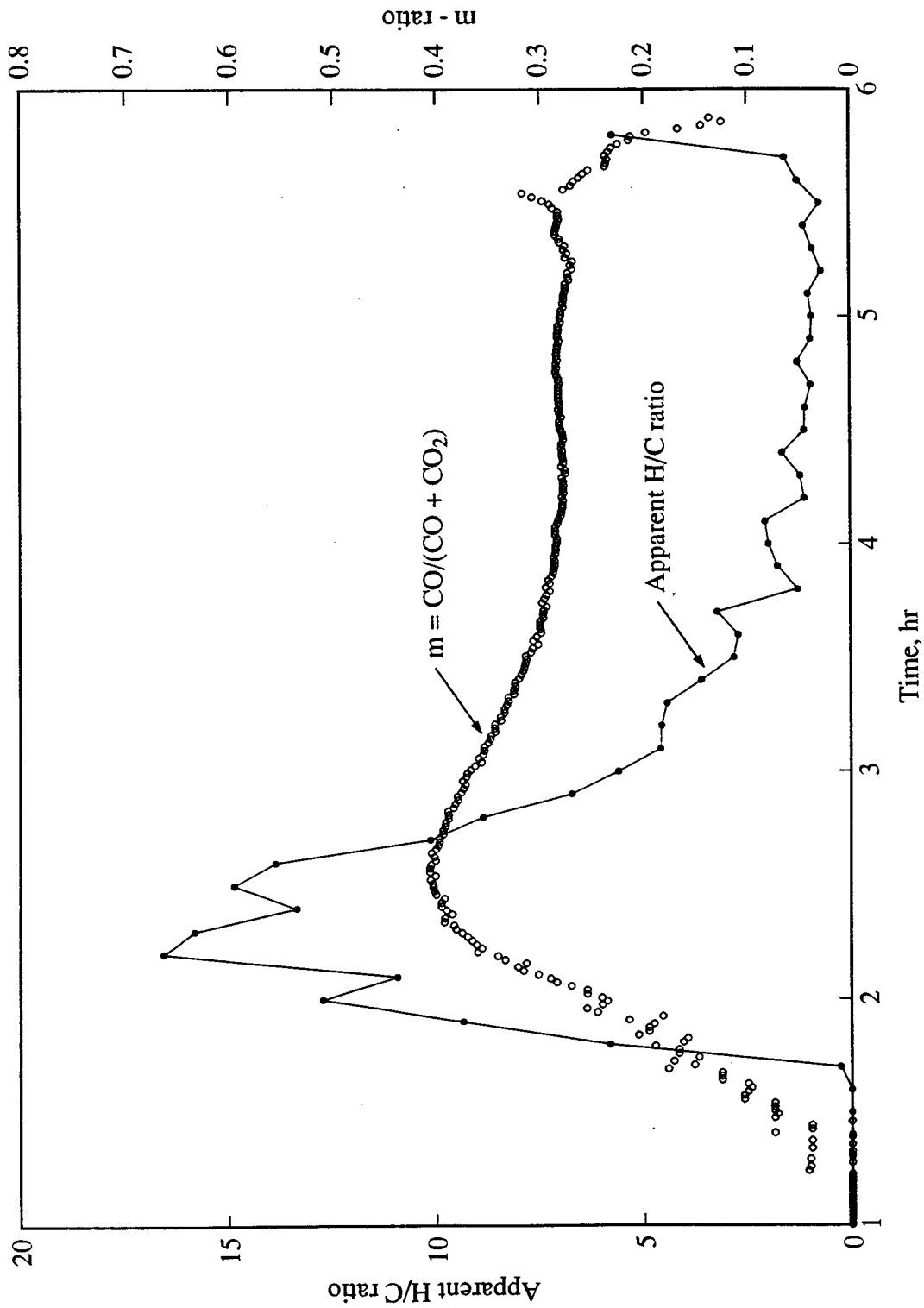


Figure 6.16: Apparent H/C and m-Ratios Versus Time (Run VEN23)

6. KINETIC EXPERIMENTAL RESULTS

6.2 An Oxygenated Fuel for HTO

During LTO, oxygenated hydrocarbon products such as ketones, aldehydes, alcohols and peroxides are formed (Burger and Sahuquet 1972). Therefore these oxygenated products form part of the fuel that is oxidized during HTO in kinetic tube experiments. The oxygen contained in these reaction products should be included in the calculation of H/C and m -ratios.

The following analyses and experiments indicate that the fuel during HTO is an oxygenated hydrocarbon. This is an important finding of this study.

1. Taking into consideration oxygen in the LTO products consumed during HTO reactions, the apparent hydrogen-carbon ratio, x , was computed on a total-gas-volume basis. That is, following Eq. 2.7:

$$x = 4 \frac{[0.2682 \int q_o N_2 dt - (\int q_o O_{2p} dt + \int q_o CO_2 dt + 0.5 \int q_o CO dt)]}{(\int q_o CO_2 dt + \int q_o CO dt)} \quad (6.2)$$

where the gas efflux rate, q_o , is a function of time, and the integration limits are from the start of LTO to the end of HTO.

Apparent H/C ratios based on Eq. 6.2 were compared with those obtained from combustion tube runs. For direct comparison, identical samples were used in each set of kinetic and combustion tube experiments (Table 6.5). This was achieved by preparing samples sufficient for both experiments. Kinetic experiment samples were placed in a deep-freezer for subsequent runs. In addition, the same air injection pressure (100 psig) was used in both types of experiments.

The combustion zone temperature in Run VEN14 was 350°C. This temperature condition was approximated in the corresponding kinetic tube experiment (Run VEN19) by increasing the temperature of the kinetic tube to a

6. KINETIC EXPERIMENTAL RESULTS

Table 6.5: Kinetic and Combustion Tube Experimental Sets

Crude oil	Mixture	Run No.	
		Combustion	Kinetic
Cold Lake bitumen	crude + 20-30 mesh sand + clay	CL13	CL14
Hamaca	crude + 20-30 mesh sand + clay	VEN5	VEN6
Hamaca	crude + 20-30 mesh sand	VEN14	VEN19
Hamaca	crude + 20-30 mesh sand + 170-270 mesh sand	VEN21	VEN23

maximum of 350°C, then decreasing temperature to 180°C while air was injected (Figs. 6.17 and 6.18).

Figures 6.19 - 6.26 present apparent H/C ratios based on total-gas-volume calculations. Results for the kinetic and combustion tube experimental sets are compared in Table 6.6. Apparent H/C values for each set of kinetic and combustion tube experiments were in good agreement. Further, apparent H/C values were similar to those of the original crudes as determined by elemental analysis. The exception was the set of runs, Nos. VEN14 (Fig. 5.12) and VEN19 (Fig. 6.25), where the apparent H/C ratios were high as a result of low-temperature oxidation.

6. KINETIC EXPERIMENTAL RESULTS

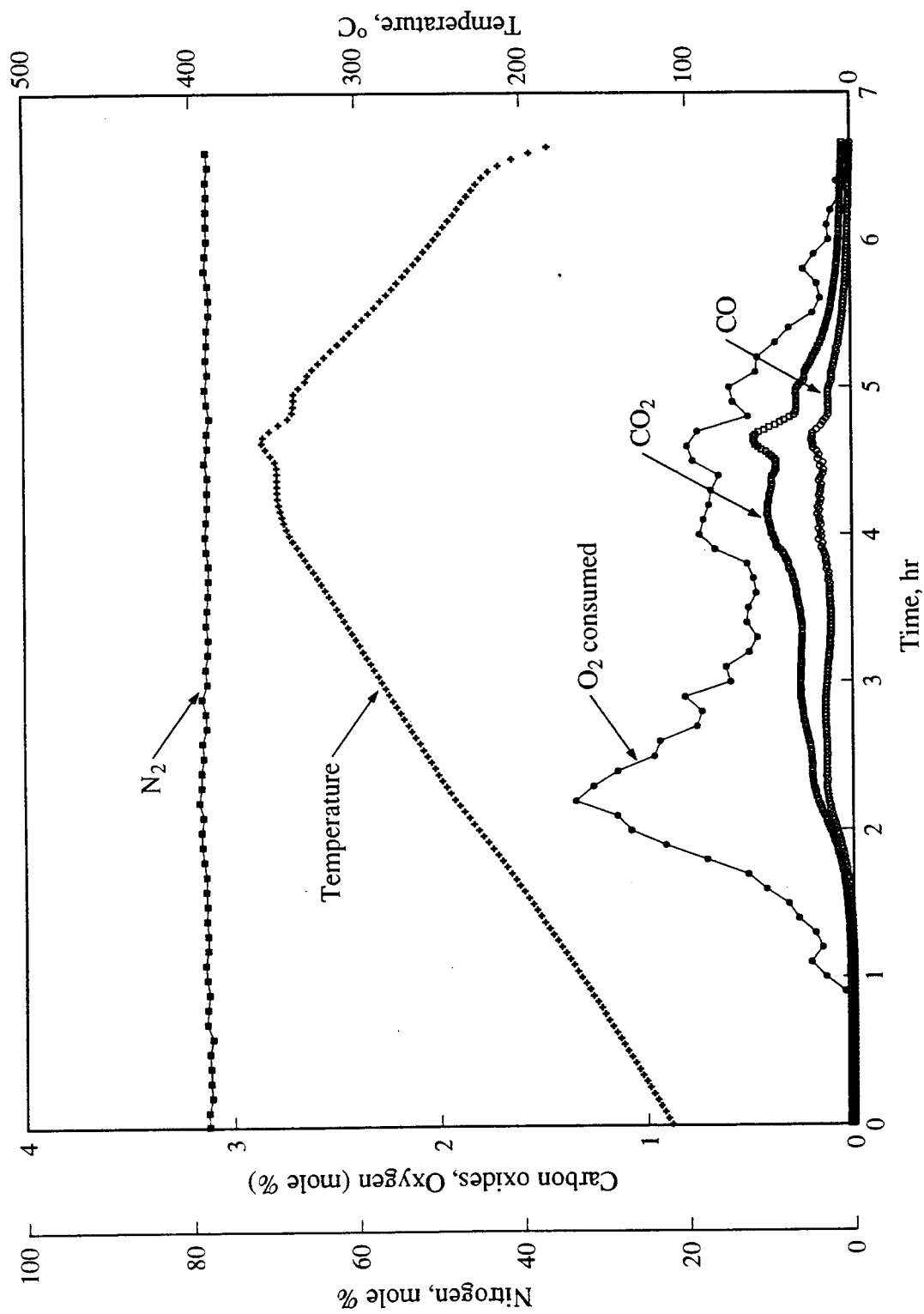


Figure 6.17: Produced Gas Composition and Temperature Versus Time (Run VEN19)

6. KINETIC EXPERIMENTAL RESULTS

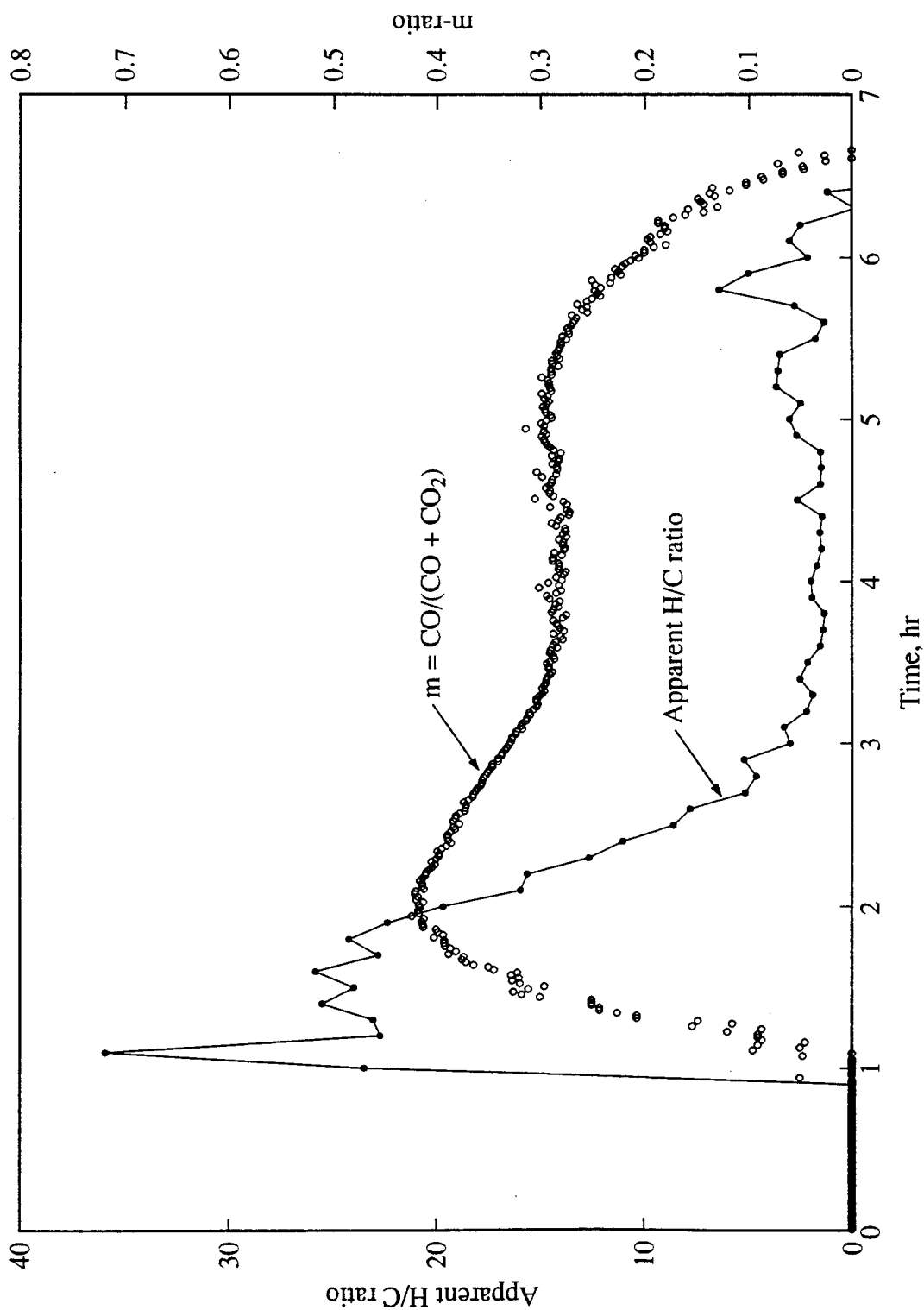


Figure 6.18: Apparent H/C and m-Ratios Versus Time (Run VEN19)

6. KINETIC EXPERIMENTAL RESULTS

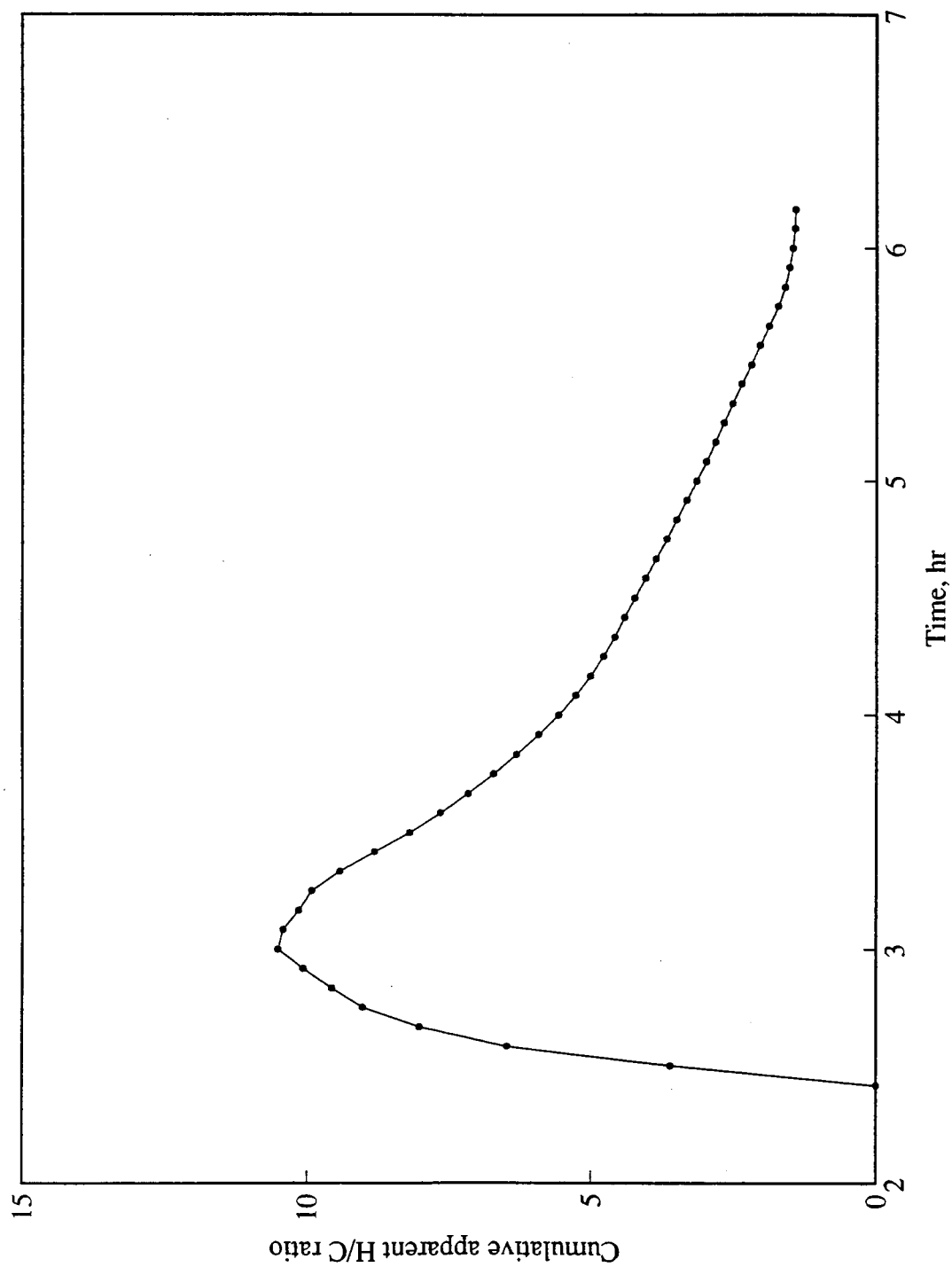


Figure 6.19: Cumulative Apparent H/C Ratio Versus Time (Run CL2)

6. KINETIC EXPERIMENTAL RESULTS

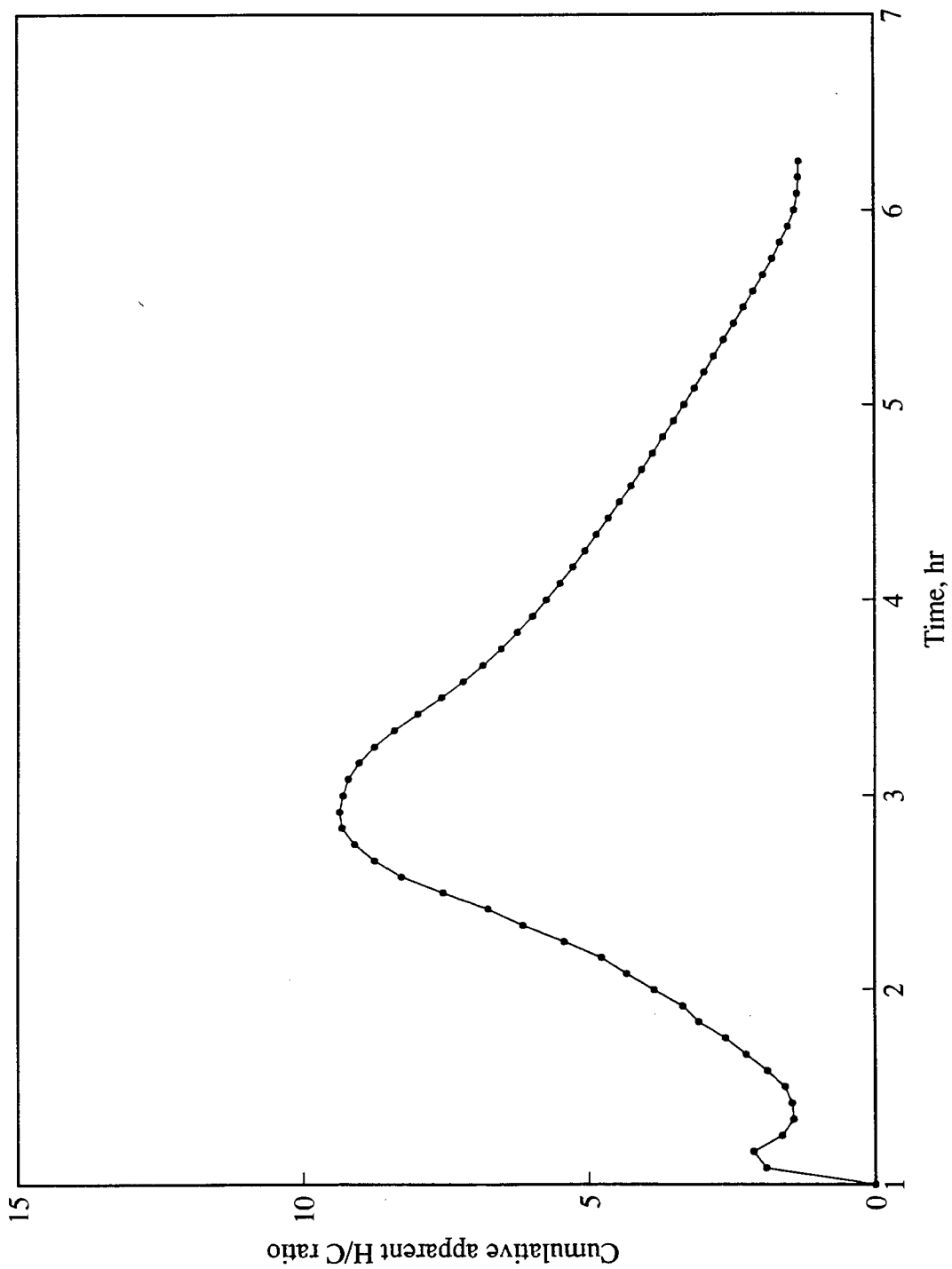


Figure 6.20: Cumulative Apparent H/C Ratio Versus Time (Run CL5)

6. KINETIC EXPERIMENTAL RESULTS

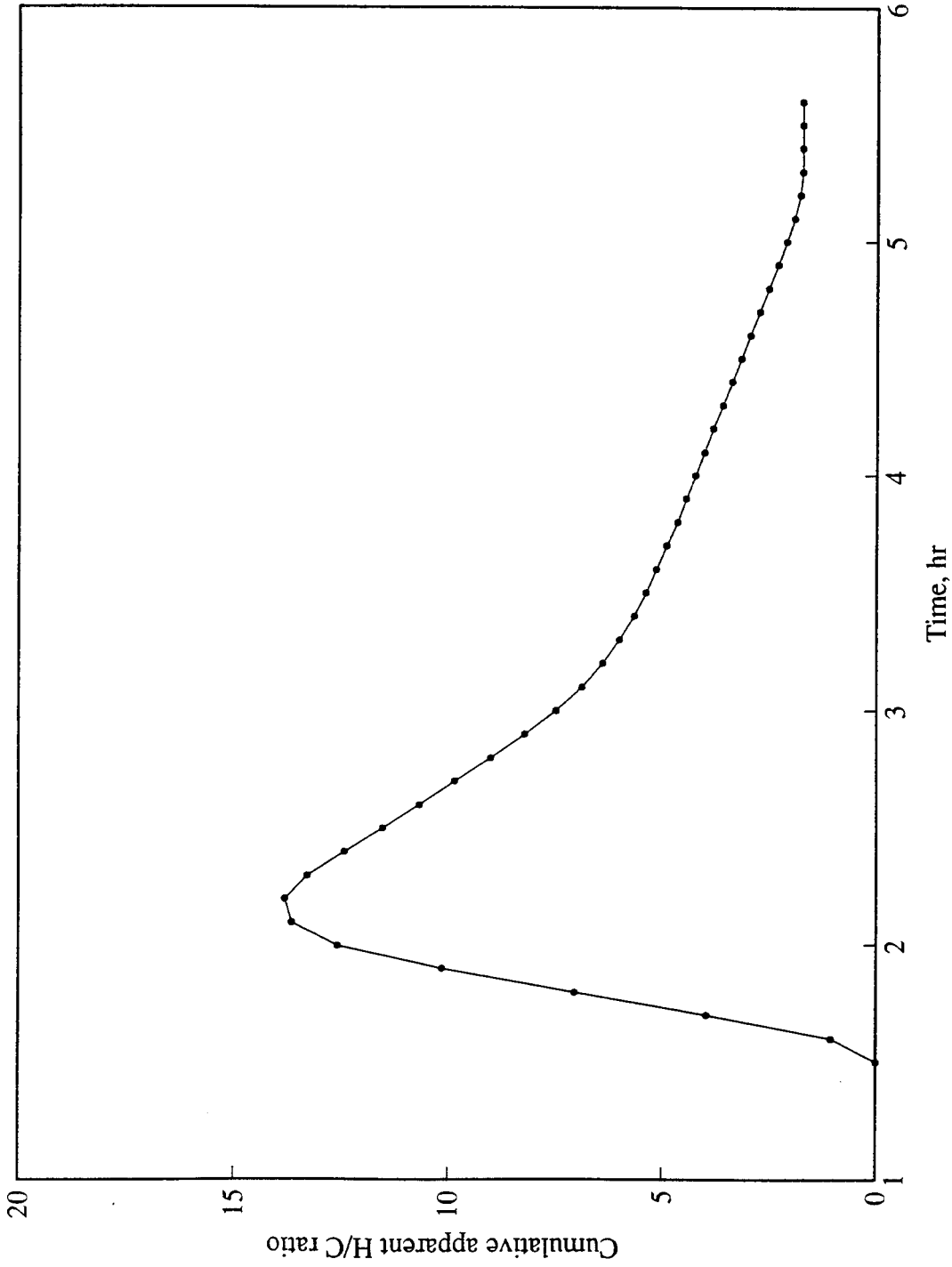


Figure 6.21: Cumulative Apparent H/C Ratio Versus Time (Run CL14)

6. KINETIC EXPERIMENTAL RESULTS

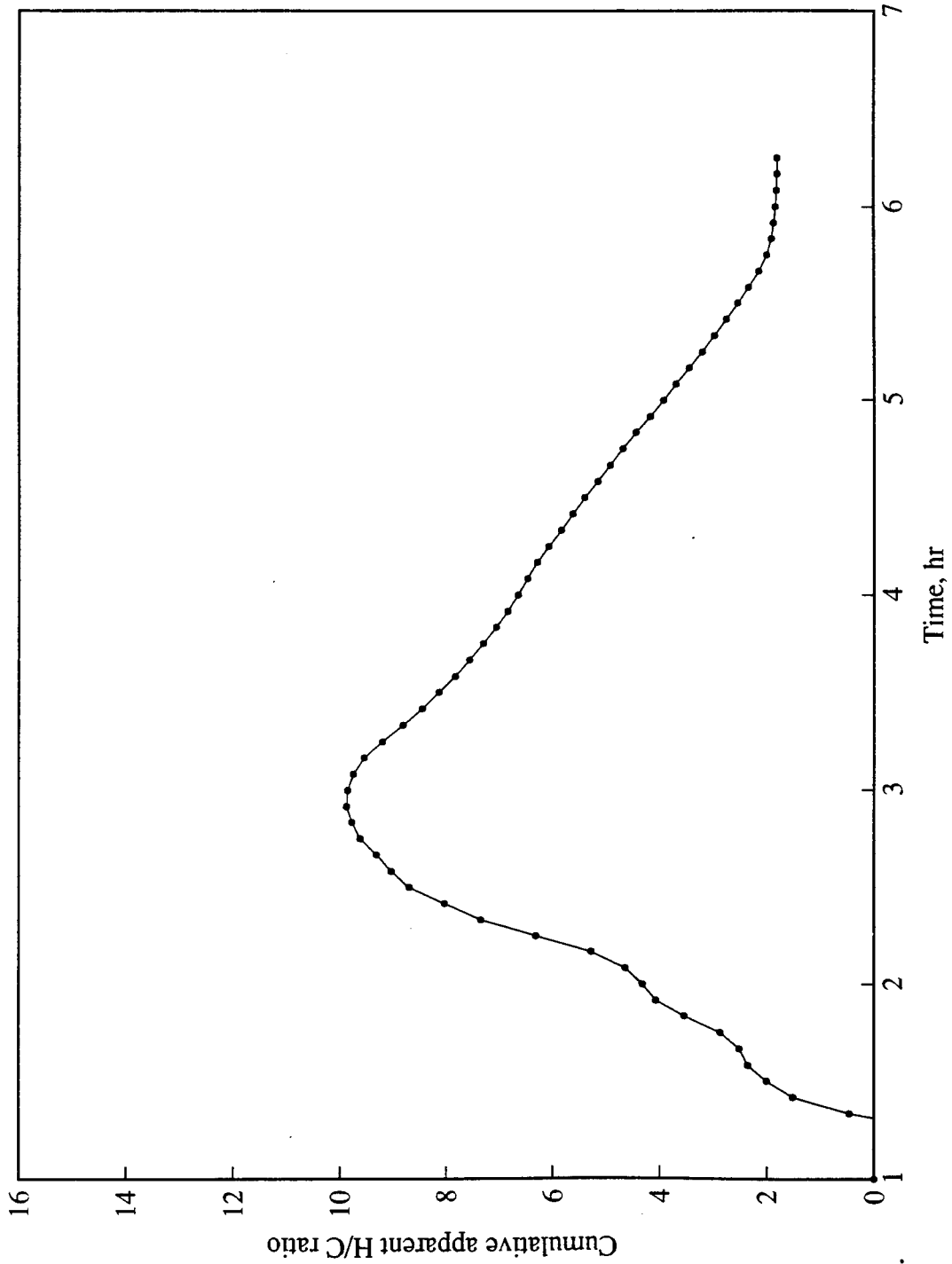


Figure 6.22: Cumulative Apparent H/C Ratio Versus Time (Run HBO2)

6. KINETIC EXPERIMENTAL RESULTS

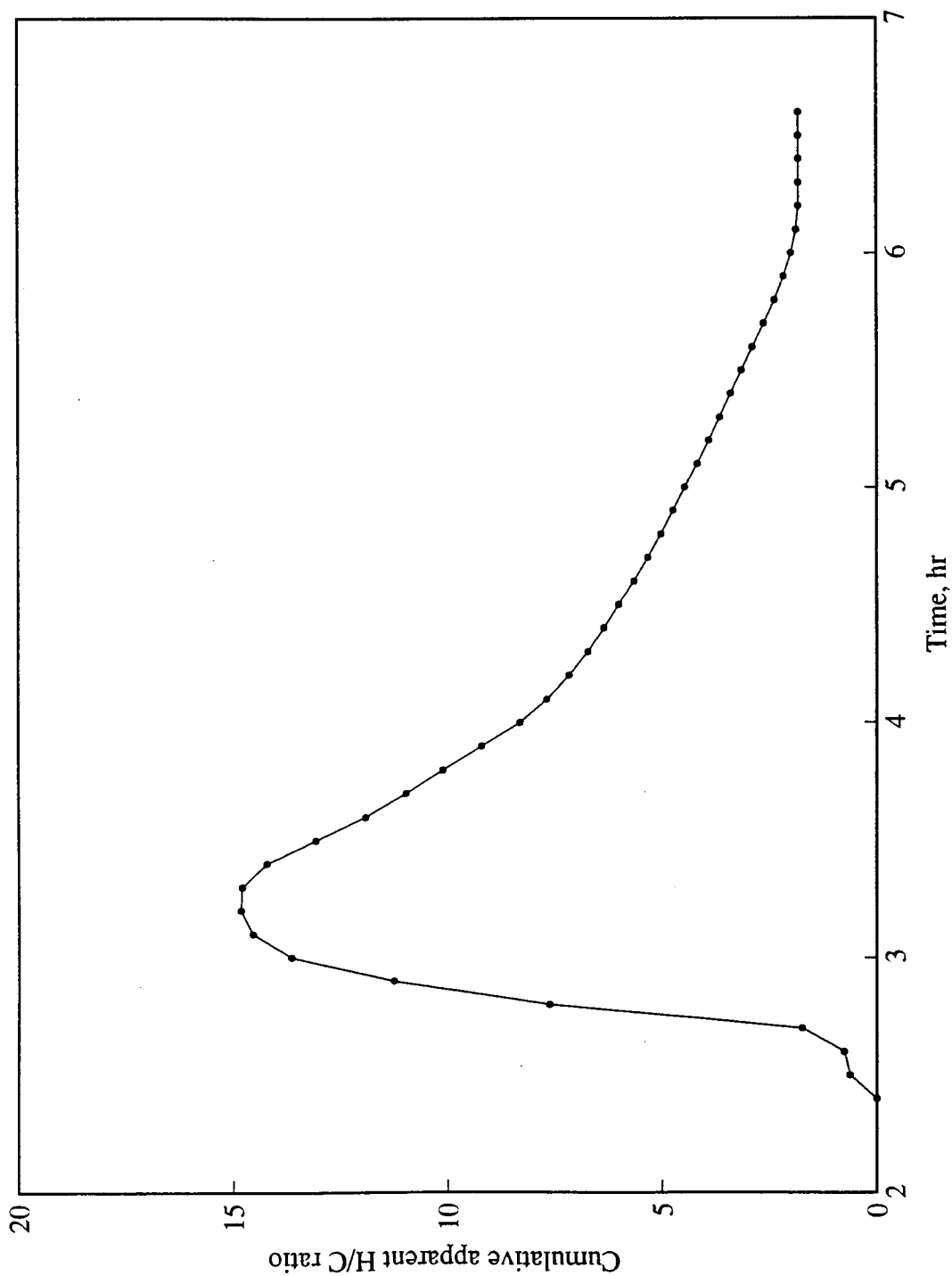


Figure 6.23: Cumulative Apparent H/C Ratio Versus Time (Run VEN6)

6. KINETIC EXPERIMENTAL RESULTS

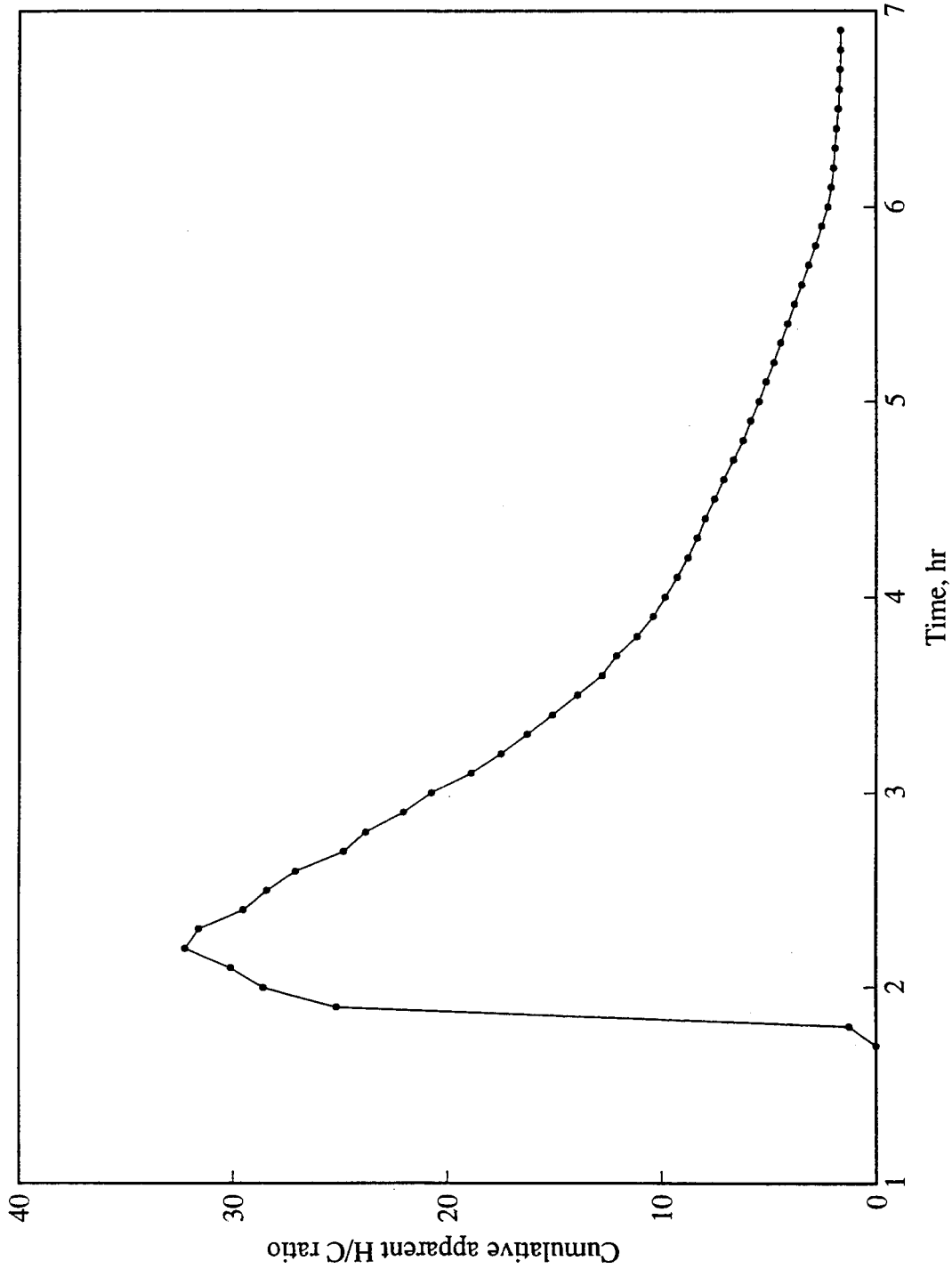


Figure 6.24: Cumulative Apparent H/C Ratio Versus Time (Run VEN15)

6. KINETIC EXPERIMENTAL RESULTS

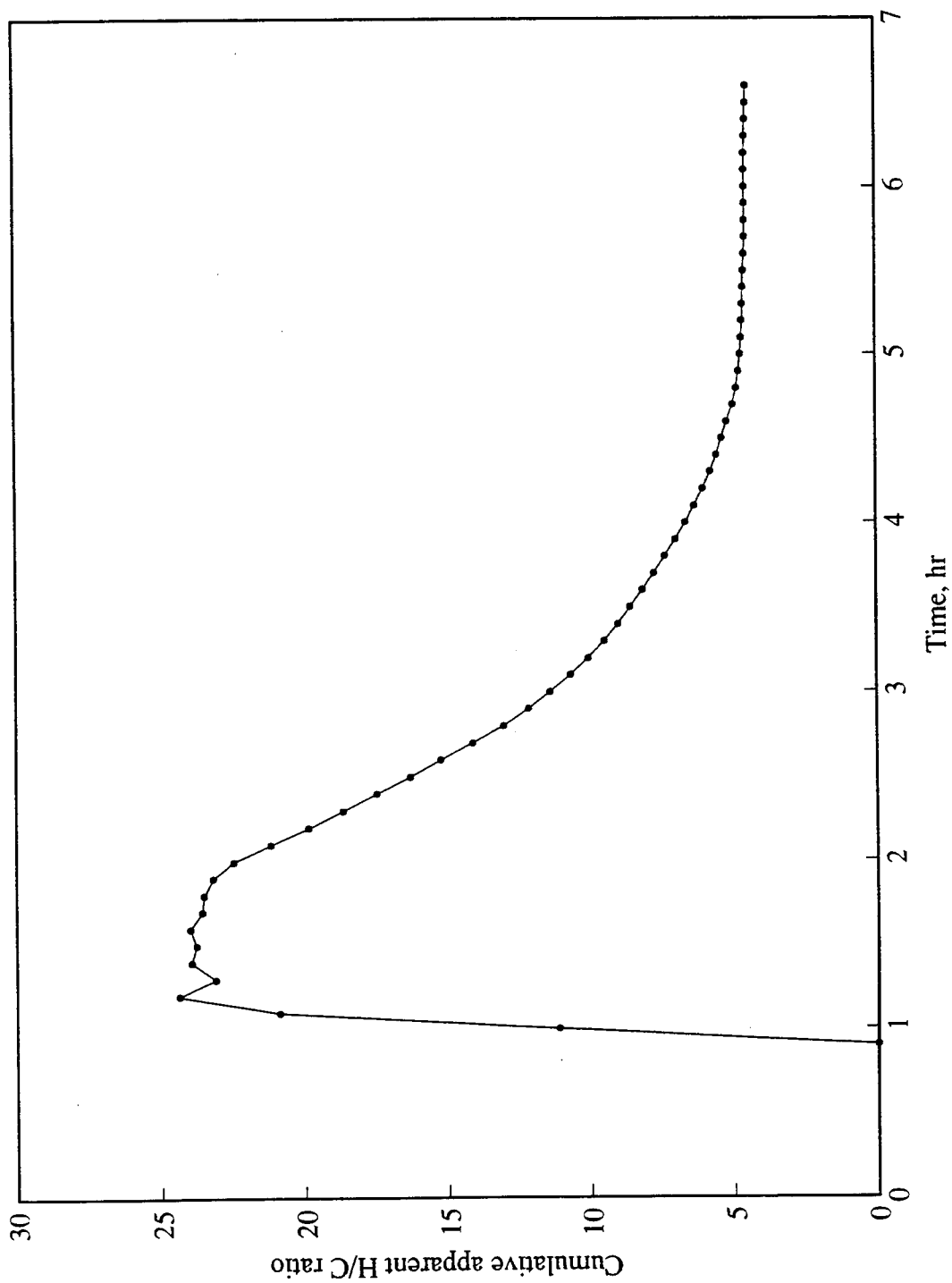


Figure 6.25: Cumulative Apparent H/C Ratio Versus Time (Run VEN19)

6. KINETIC EXPERIMENTAL RESULTS

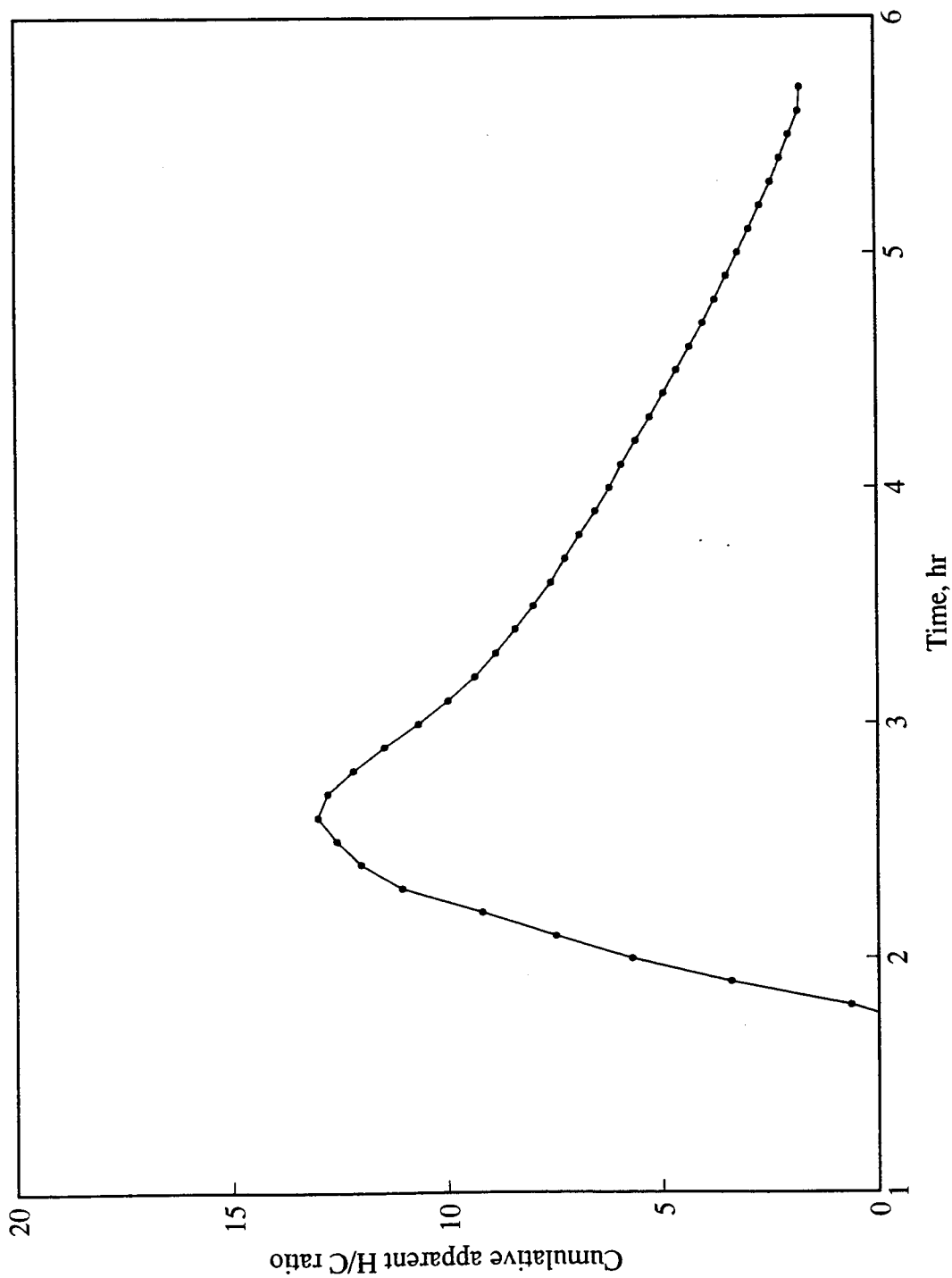


Figure 6.26: Cumulative Apparent H/C Ratio Versus Time (Run VEN23)

6. KINETIC EXPERIMENTAL RESULTS

Table 6.6: Apparent H/C Ratios for Kinetic and Combustion Tube Experiments

Run No.	Sample matrix [†]	Kinetic experiments		Combustion tube expts.	Elemental analysis
		Old method*	New method**		
Cold Lake bitumen:					
Original crude	-	-	-	-	1.53
CL2	-	0.71	1.41	-	-
CL5	-	0.49	1.32	-	-
CL13, CL14	clay	0.00	1.74	1.62	-
Huntington Beach oil:					
Original crude	-	-	-	-	1.65
HBO2	-	0.37	1.77	-	-
Hamaca crude oil:					
Original crude	-	-	-	-	1.50
VEN5, VEN6	clay	0.21	1.81	1.63	-
VEN15	-	1.02	1.65	-	-
VEN14, VEN19	-	1.51	4.47	4.35	-
VEN21, VEN23	170-270 mesh sand	1.04	1.75	1.77	-

* At HTO using Eq. 2.7.

** At HTO using Eq. 6.2.

† In addition to 20-30 mesh sand.

6. KINETIC EXPERIMENTAL RESULTS

2. The measured amount of oxygen consumed is:

$$O_{2c}(measured) = 0.2682N_2 - O_{2p} \quad (6.3)$$

If oxygen is consumed to form CO_2 , CO and water, then from stoichiometry (Eq. 2.4), the apparent amount of oxygen consumed is:

$$O_{2c}(apparent) = \frac{x}{4} (CO_2 + CO) + CO_2 + \frac{CO}{2} \quad (6.4)$$

Let:

$$\Delta O_{2c} = O_{2c}(measured) - O_{2c}(apparent) \quad (6.5)$$

The cumulative difference, $\int \Delta O_{2c} dt$, may be calculated as shown in Figs. 6.27 - 6.34. The cumulative difference increases in the LTO period due to oxygenation of the fuel, but is essentially zero at the end of HTO. This indicates that most of the oxygen from the oxygenated products takes part in the HTO reactions.

3. To verify that the fuel in kinetic tube experiments is oxygenated, an experiment (Run VEN7) was performed in which air was injected until approximately the end of LTO ($310^\circ C$). Thereafter, nitrogen was injected. The results are shown in Fig. 6.35. Carbon oxides were produced during HTO even when no oxygen was injected. The average CO_2 and CO molar concentrations during that period were 0.1% and 0.05% respectively. This experiment clearly demonstrated that oxygen from the oxygenated fuel took part in the HTO reactions. The cumulative difference between measured and apparent amount of oxygen consumed is shown in Fig. 6.36. At the end of the run, the cumulative difference is not zero. This result indicates that the oxygenated fuel was not totally consumed. Carbon oxides were still being produced at the end of the run. After the run, the sand mix was examined and found to be black in color, indicating that residual hydrocarbons on the sand mix had not been burned completely.

6. KINETIC EXPERIMENTAL RESULTS

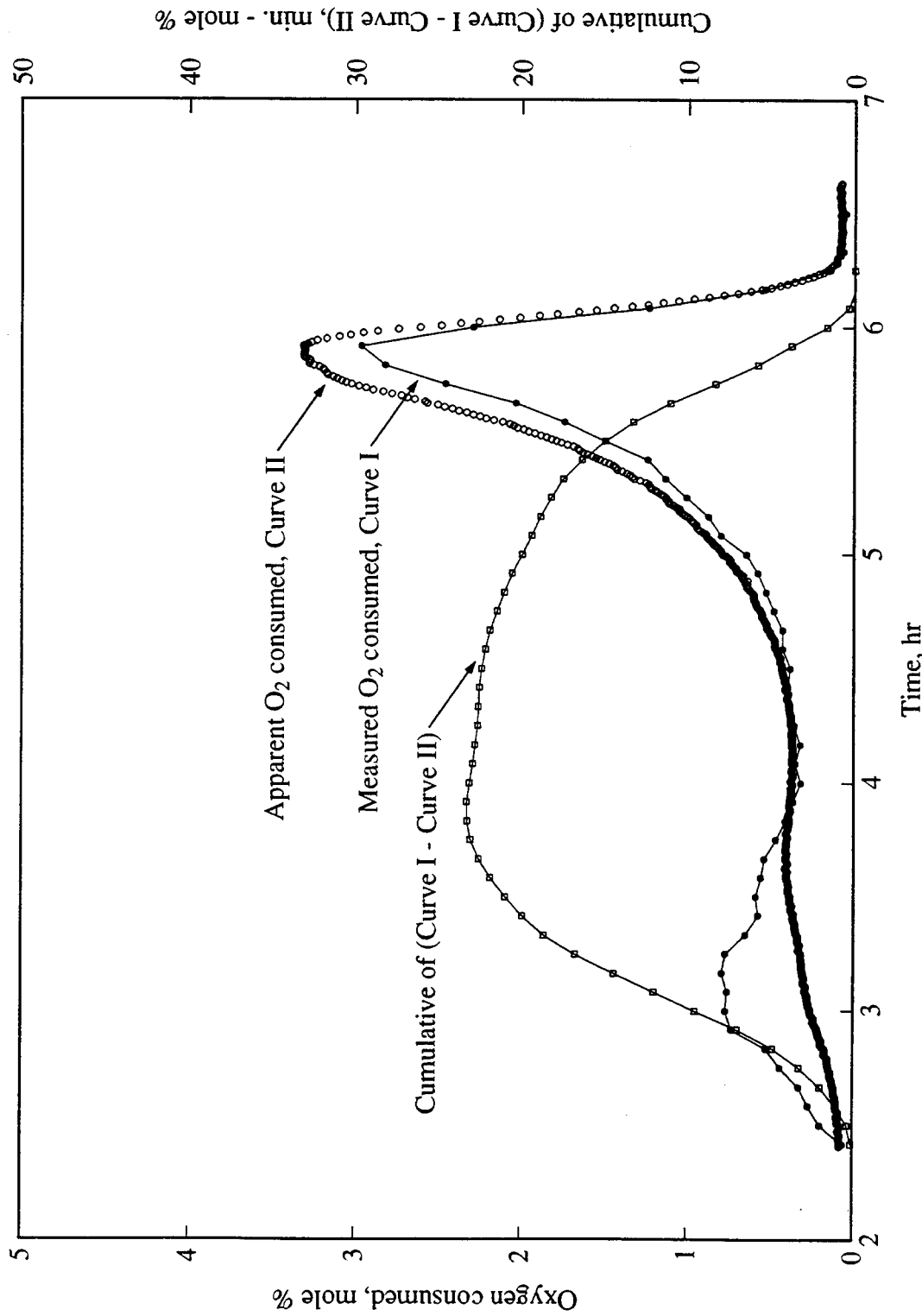


Figure 6.27: Oxygen Consumed Versus Time (Run CL2)

6. KINETIC EXPERIMENTAL RESULTS

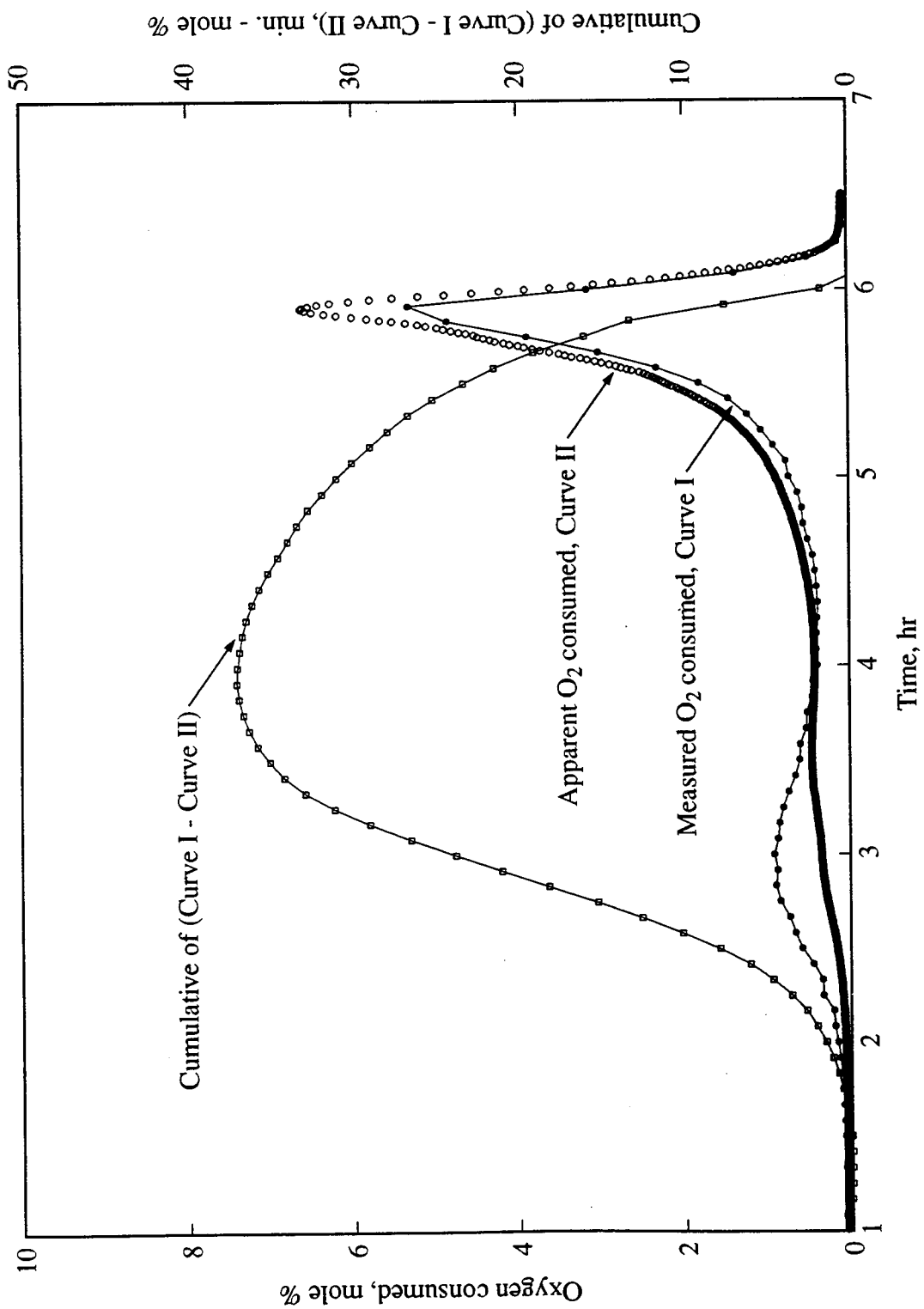


Figure 6.28: Oxygen Consumed Versus Time (Run CL5)

6. KINETIC EXPERIMENTAL RESULTS

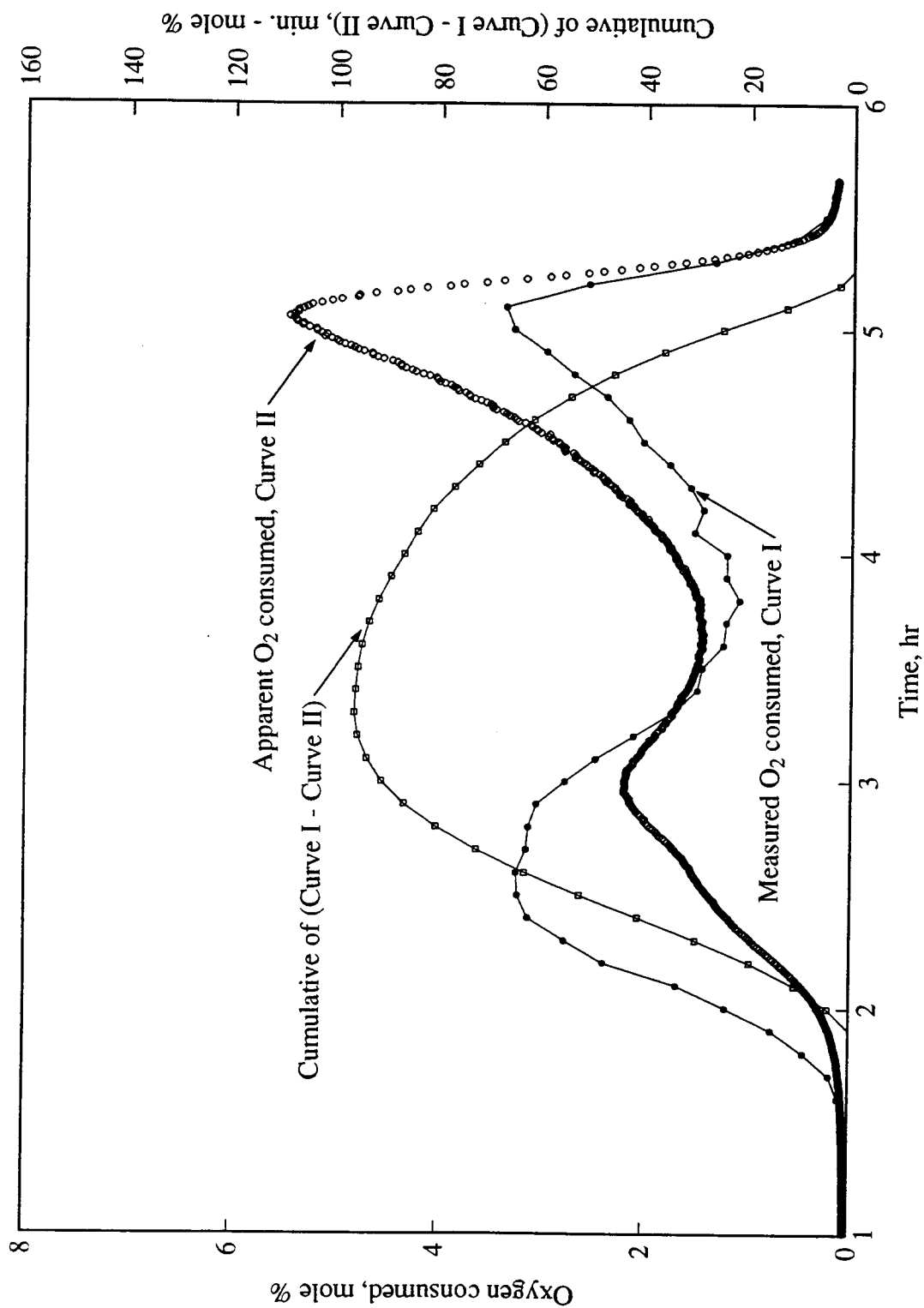


Figure 6.29: Oxygen Consumed Versus Time (Run CL14)

6. KINETIC EXPERIMENTAL RESULTS

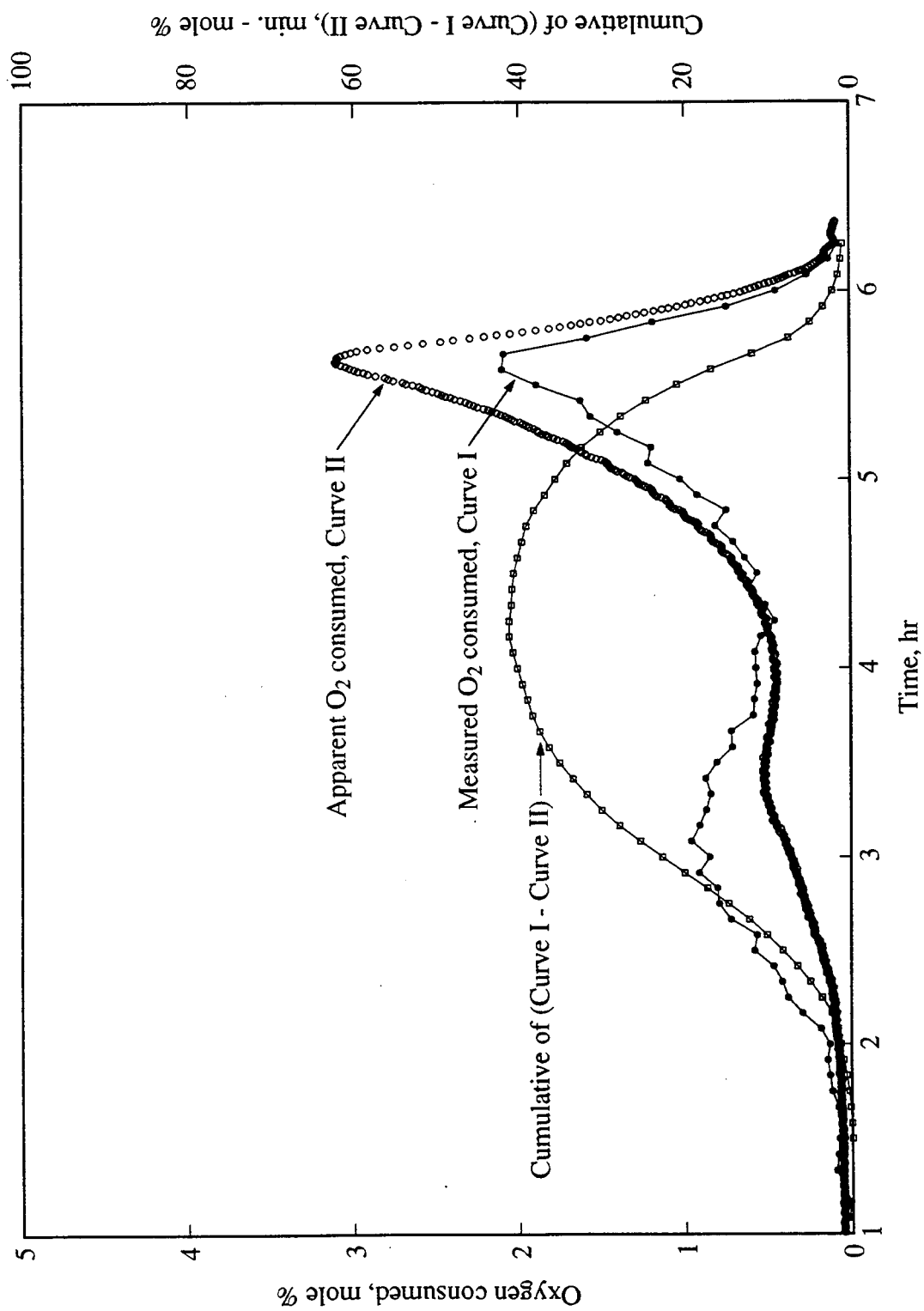


Figure 6.30: Oxygen Consumed Versus Time (Run HBO₂)

6. KINETIC EXPERIMENTAL RESULTS

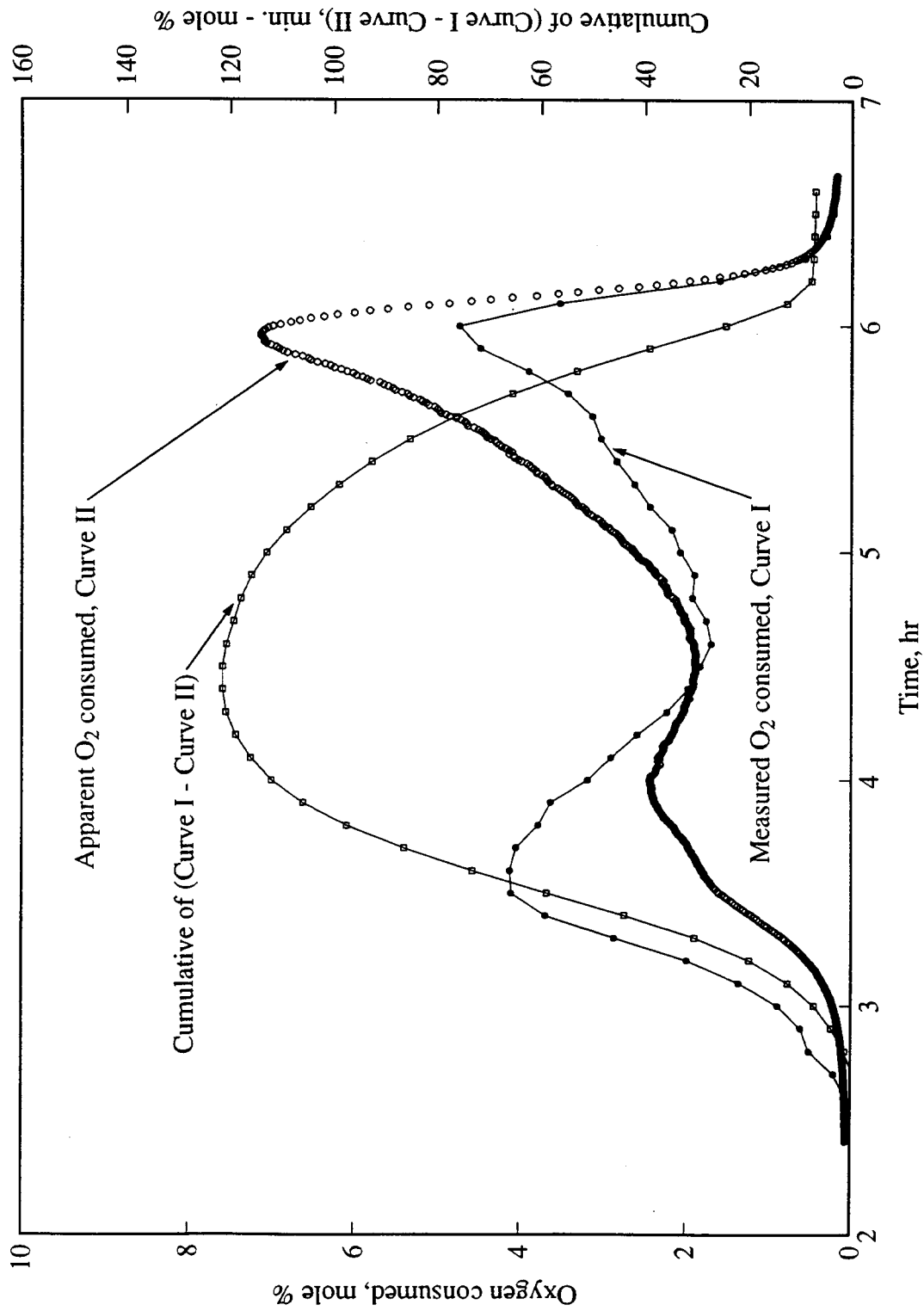


Figure 6.31: Oxygen Consumed Versus Time (Run VEN6)

6. KINETIC EXPERIMENTAL RESULTS

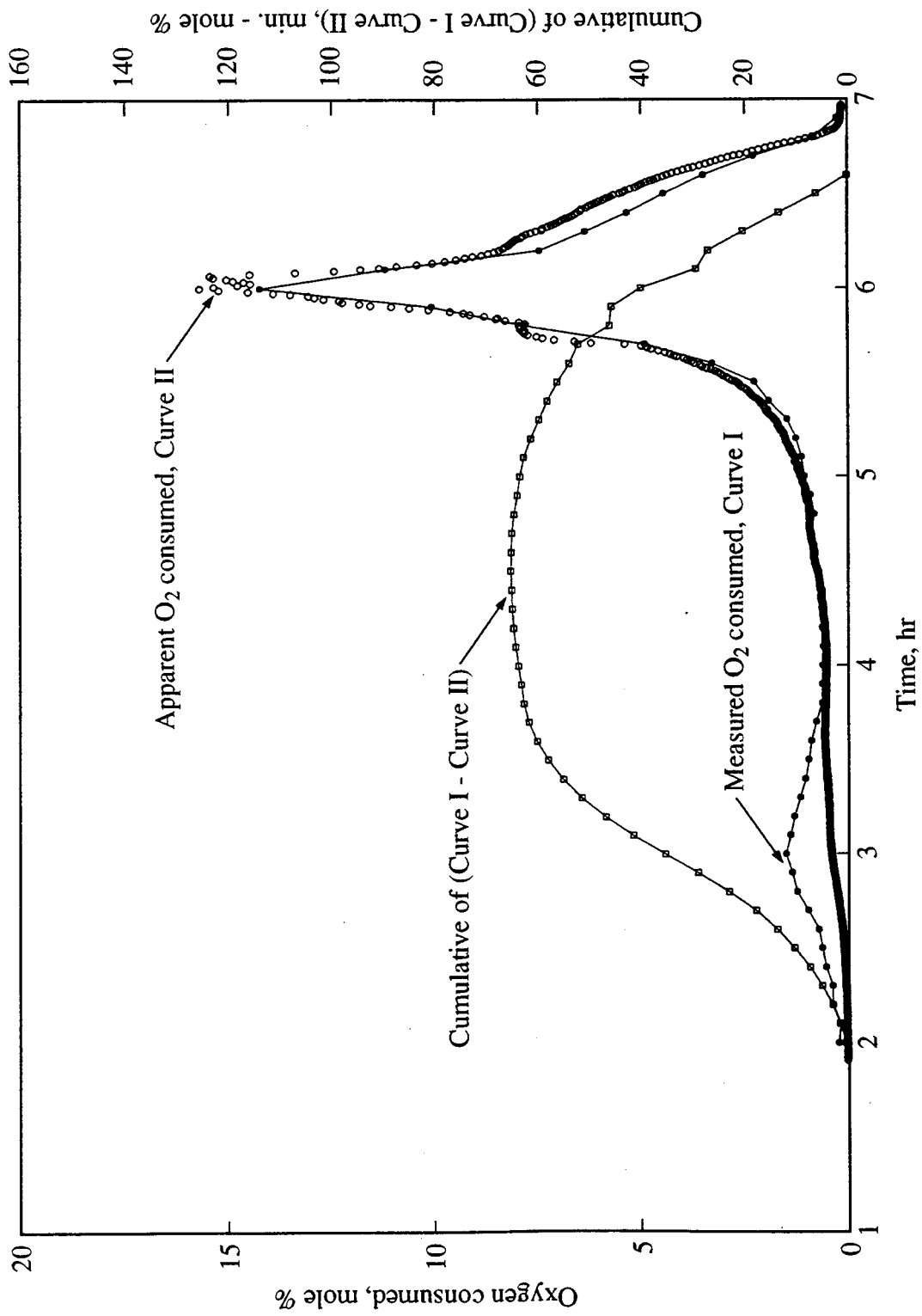


Figure 6.32: Oxygen Consumed Versus Time (Run VEN15)

6. KINETIC EXPERIMENTAL RESULTS

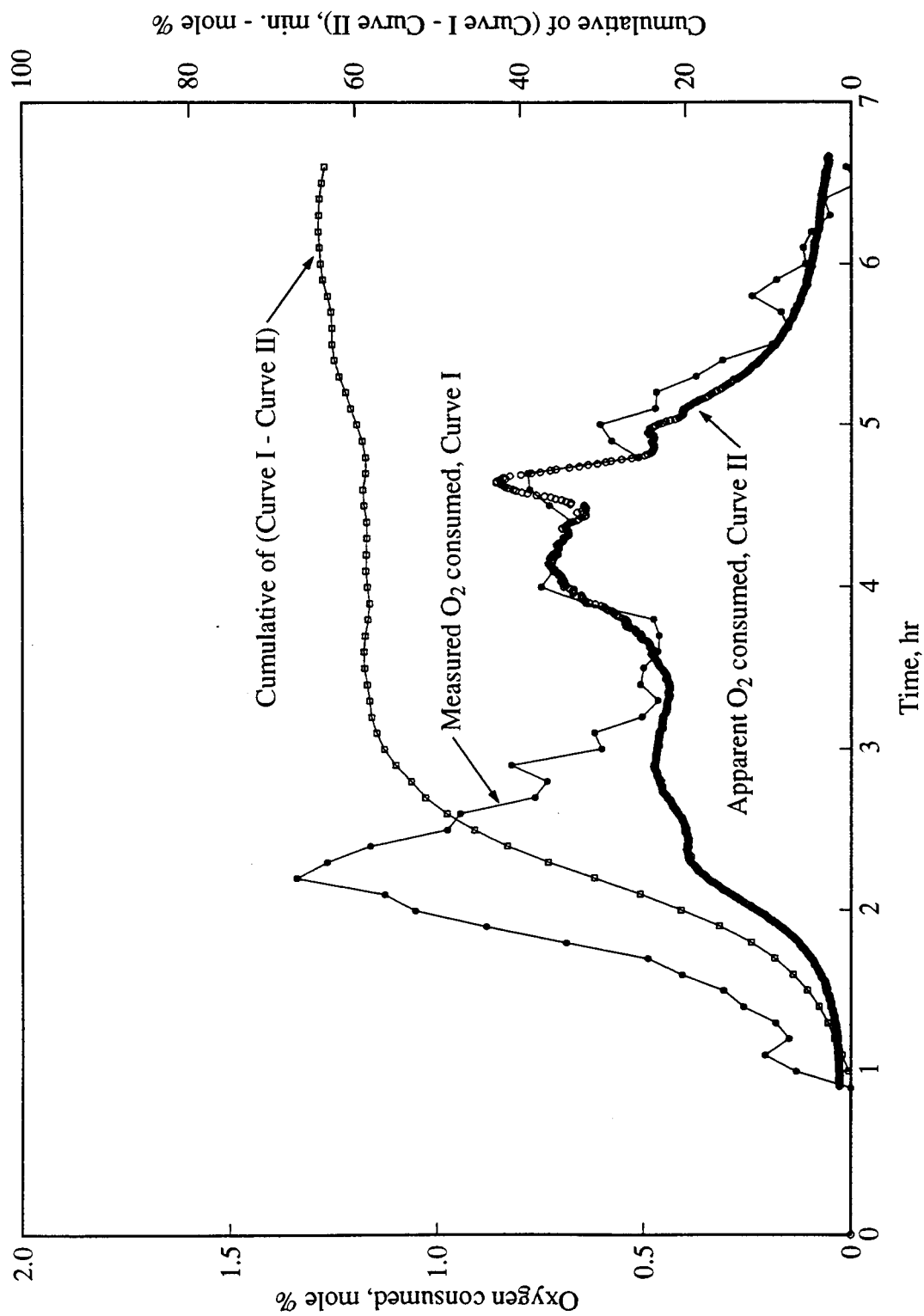


Figure 6.33: Oxygen Consumed Versus Time (Run VEN19)

6. KINETIC EXPERIMENTAL RESULTS

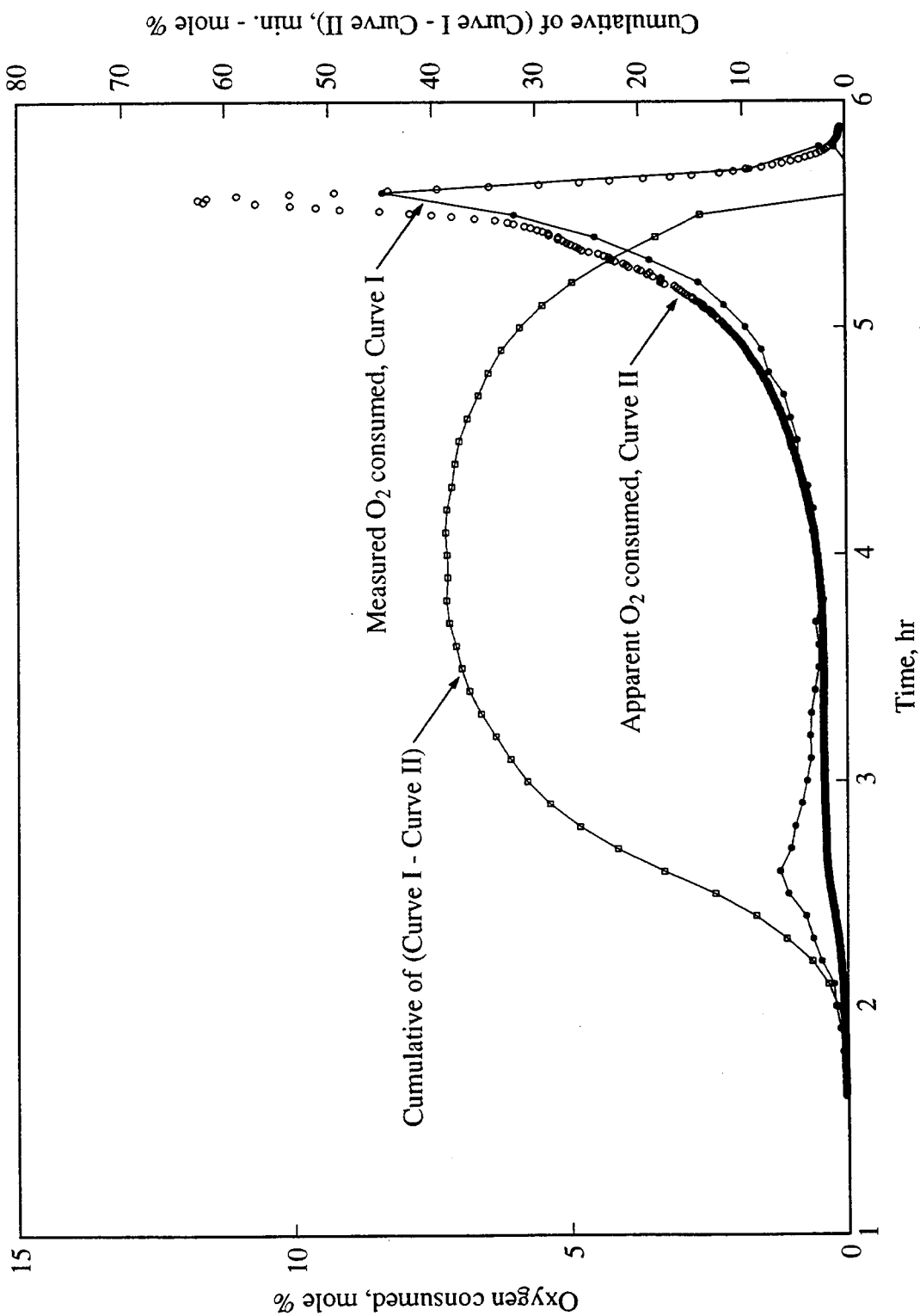


Figure 6.34: Oxygen Consumed Versus Time (Run VEN23)

6. KINETIC EXPERIMENTAL RESULTS

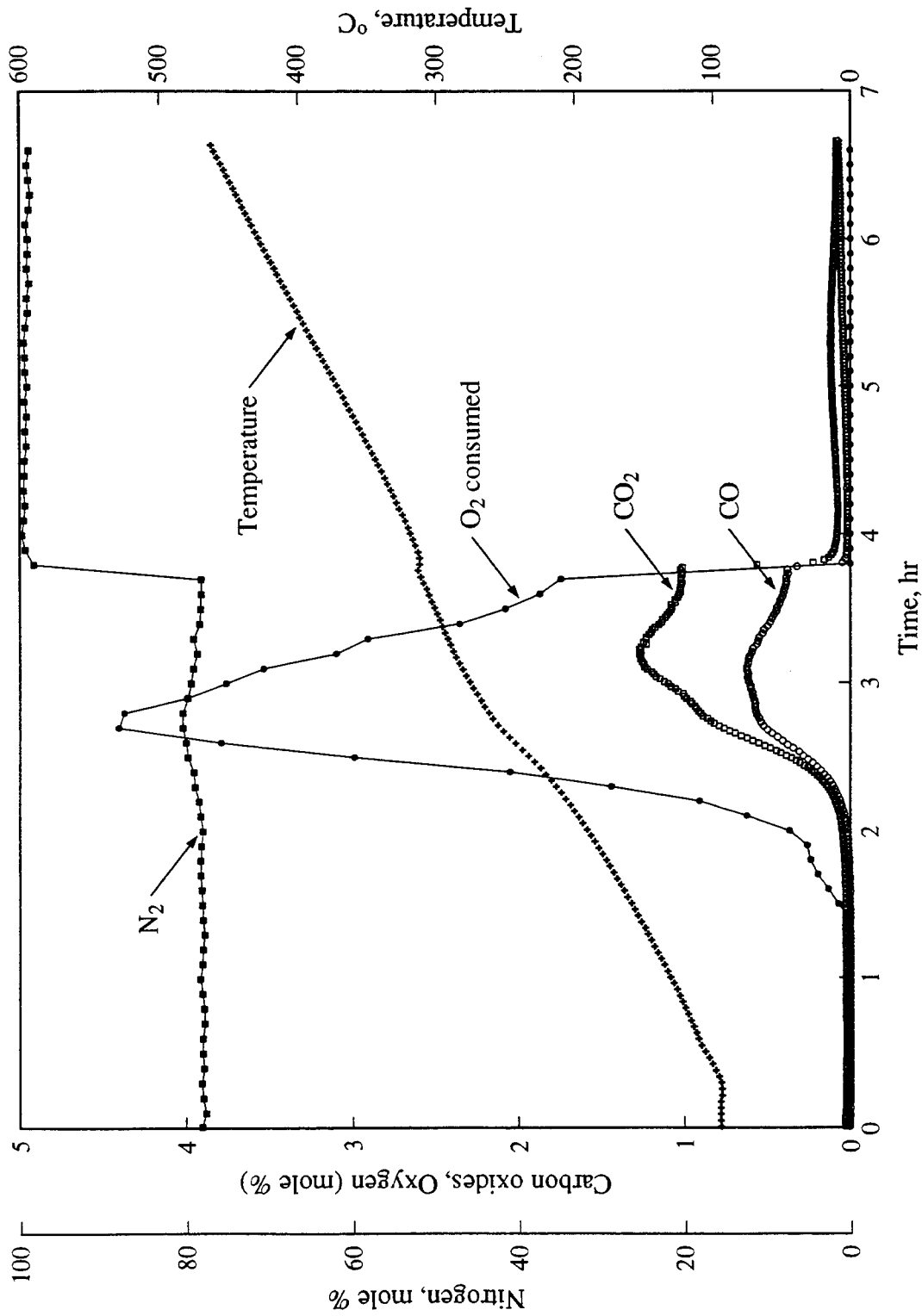


Fig. 6.35: Produced Gas Composition and Temperature Versus Time (Run VEN7)

6. KINETIC EXPERIMENTAL RESULTS

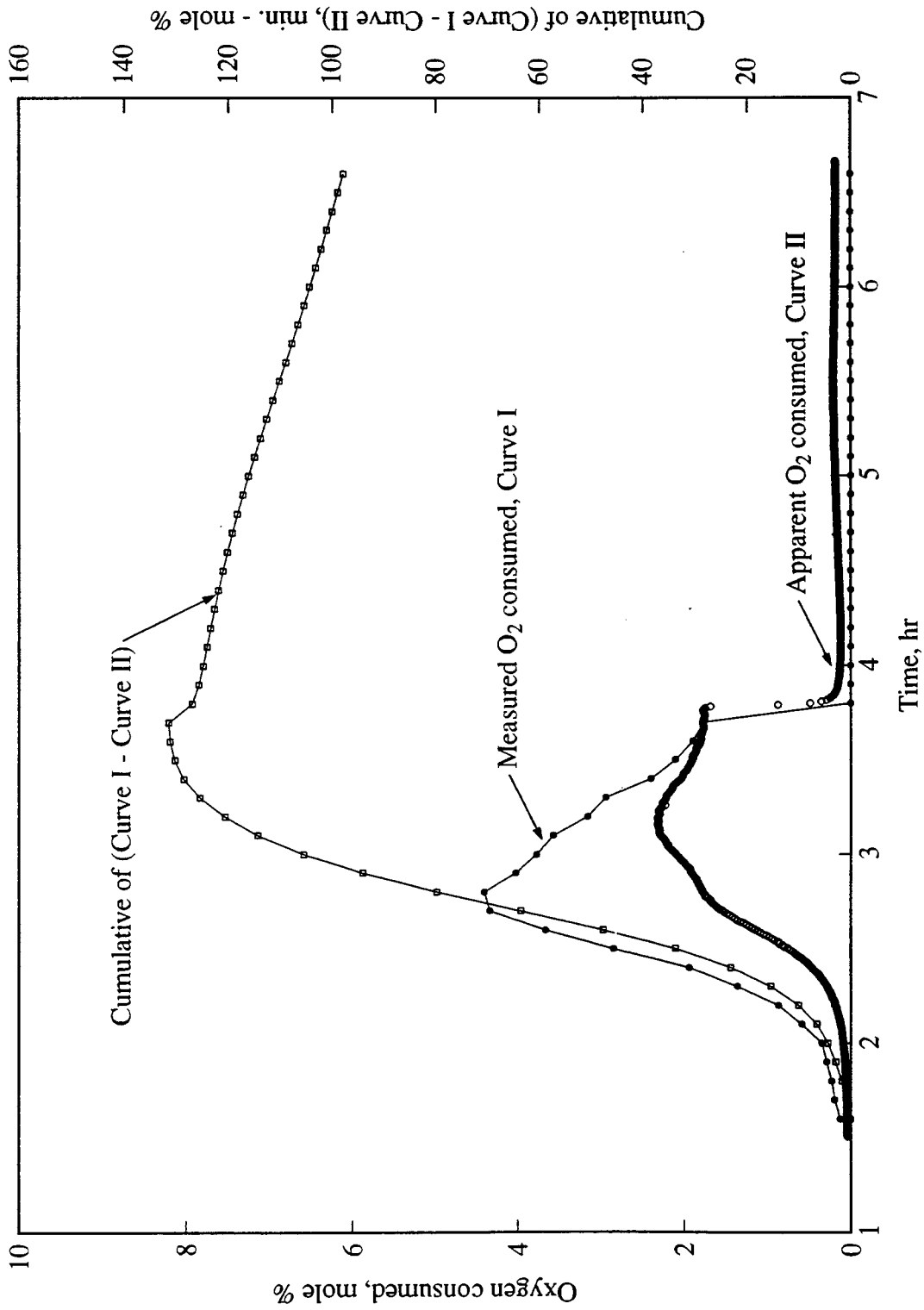


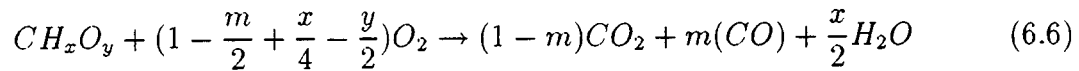
Figure 6.36: Oxygen Consumed Versus Time (Run VEN7)

6. KINETIC EXPERIMENTAL RESULTS

4. As described in Section 4.1, elemental analysis was performed on an oil sample from combustion tube Run VEN14 which was a low-temperature oxidation run. The atomic oxygen-carbon ratio of the oil sample was 0.25. This shows conclusively that oxygenated hydrocarbons are formed when crude oil is subjected to low-temperature oxidation.

6.3 Apparent O/C Ratio From Gas Analysis

Following the stoichiometric equation for fuel oxidation (Eq. 2.4), the equation for combustion of an oxygenated fuel is:



where y is the atomic O/C ratio. Based on the carbon balance, molar concentration of oxygen from the oxygenated fuel may be expressed as $(CO_2 + CO)y/2$. Taking into consideration this additional amount of oxygen, the expression for the atomic H/C ratio, x , as given in Eq. 2.7, becomes:

$$x = \frac{4 [0.2682N_2 + (CO_2 + CO)y/2 - (O_{2p} + CO_2 + CO/2)]}{(CO_2 + CO)} \quad (6.7)$$

Equation 6.7 may be rearranged to give:

$$y = \frac{2(1 - m)}{CO_2} \left[CO_2 + CO \left(\frac{1}{2} + \frac{x}{4m} \right) - O_{2c} \right] \quad (6.8)$$

where $O_{2c} = 0.2682N_2 - O_{2p}$. The atomic O/C ratio may be determined from gas analysis data if the atomic H/C ratio is known.

Using Eq. 6.8 and atomic H/C ratios calculated on a total-gas-volume basis (as described in Section 6.2), atomic O/C ratios were determined. The results are shown in Figs. 6.37 - 6.43 and summarized in Table 6.7. Average atomic O/C ratios of the fuel ranged between 0.4 (Runs CL2 and CL5) to 0.9 (Run VEN6). The results agreed

6. KINETIC EXPERIMENTAL RESULTS

Table 6.7: Averaged Apparent H/C, O/C and m -Ratios

Run No.	H/C ratio	O/C ratio	m -ratio
CL2	1.41	0.4	0.260
CL5	1.32	0.4	0.268
CL14	1.74	0.7	0.266
HBO2	1.77	0.8	0.247
VEN6	1.81	0.9	0.246
VEN15	1.66	0.5	0.288
VEN23	1.75	0.4	0.276

with the atomic O/C ratio, 0.25, determined by elemental analysis of the oxygenated sample in combustion Run VEN14. Barta *et al.* (1989) conducted elemental analysis of the products of wet combustion of Athabasca bitumen. The products were found to have atomic O/C ratios of about 1.

Experiments were performed in which low-temperature oxidation was minimized to reduce oxidation of the fuel (Runs CL10 and VEN10). Nitrogen was injected from the start until the approximate end of LTO. Thereafter air was injected. In Run CL10, a short exothermic LTO period was observed immediately after switching to air injection (Fig. 6.44). A sharp rise in temperature and oxygen consumption was observed at the start of air injection. The results indicated an average apparent H/C ratio of about 1.5 in the HTO period (Fig. 6.45). This result suggests that the fuel contained little or no oxygen. In Run VEN10, the LTO period was also short and exothermic (Fig. 6.46). However the HTO peak was greatly diminished due to premature ignition as evident by the sharp increase in temperature. Erroneous H/C ratio results were obtained due to low values of oxygen consumption and carbon oxides.

6. KINETIC EXPERIMENTAL RESULTS

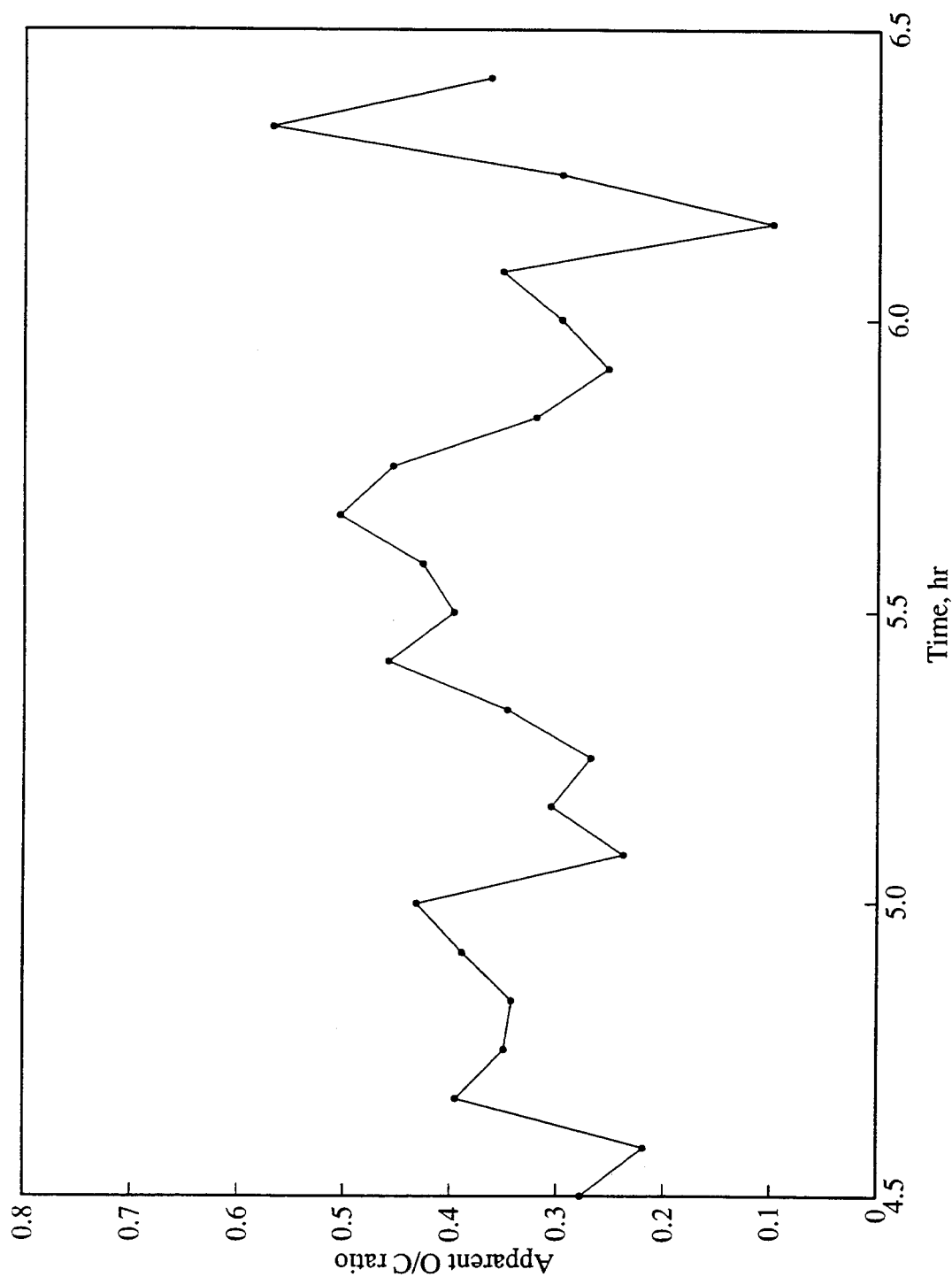


Figure 6.37: Apparent O/C Ratio Versus Time (Run CL2)

6. KINETIC EXPERIMENTAL RESULTS

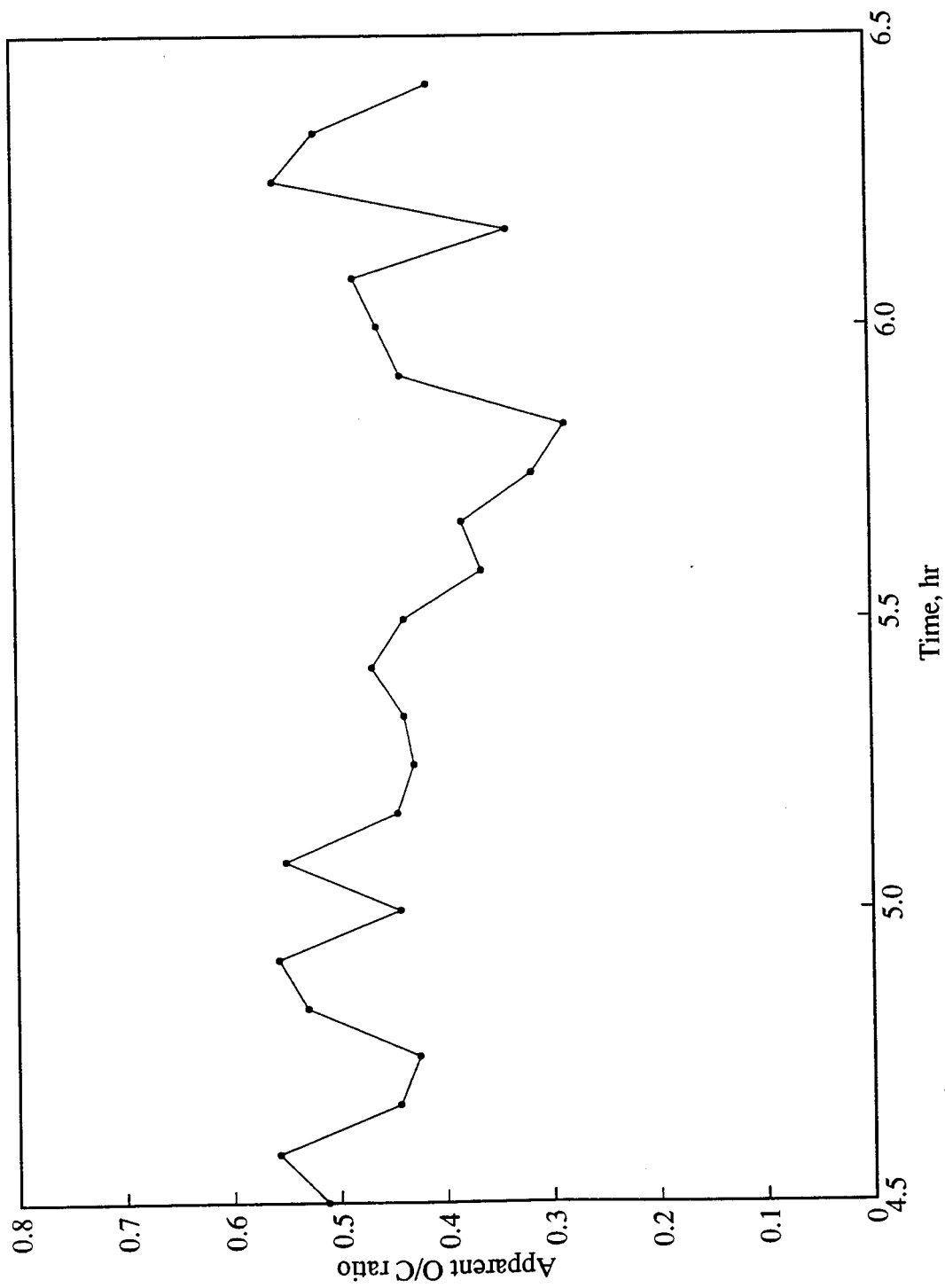


Figure 6.38: Apparent O/C Ratio Versus Time (Run CL5)

6. KINETIC EXPERIMENTAL RESULTS

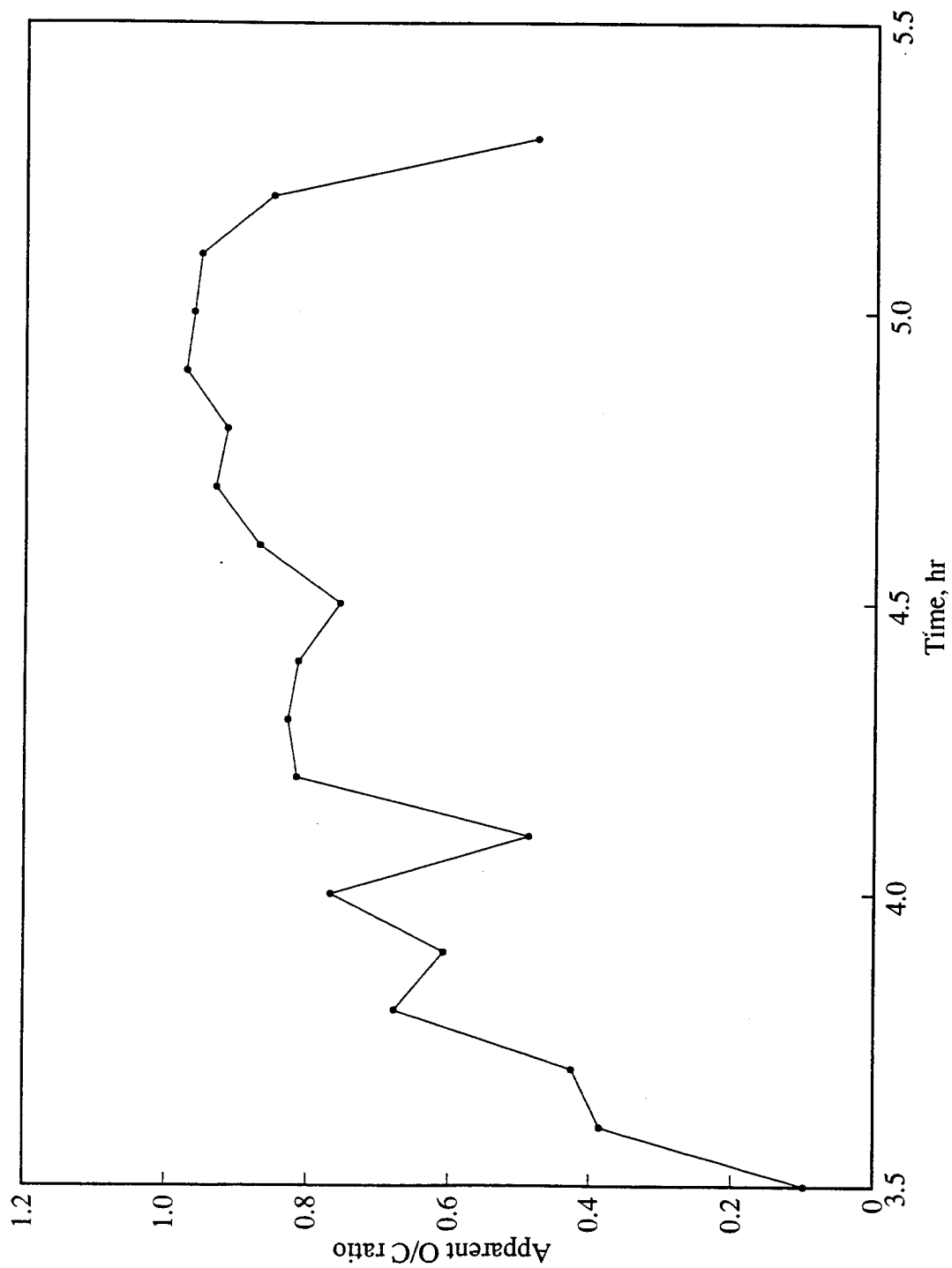


Figure 6.39: Apparent O/C Ratio Versus Time (Run CL14)

6. KINETIC EXPERIMENTAL RESULTS

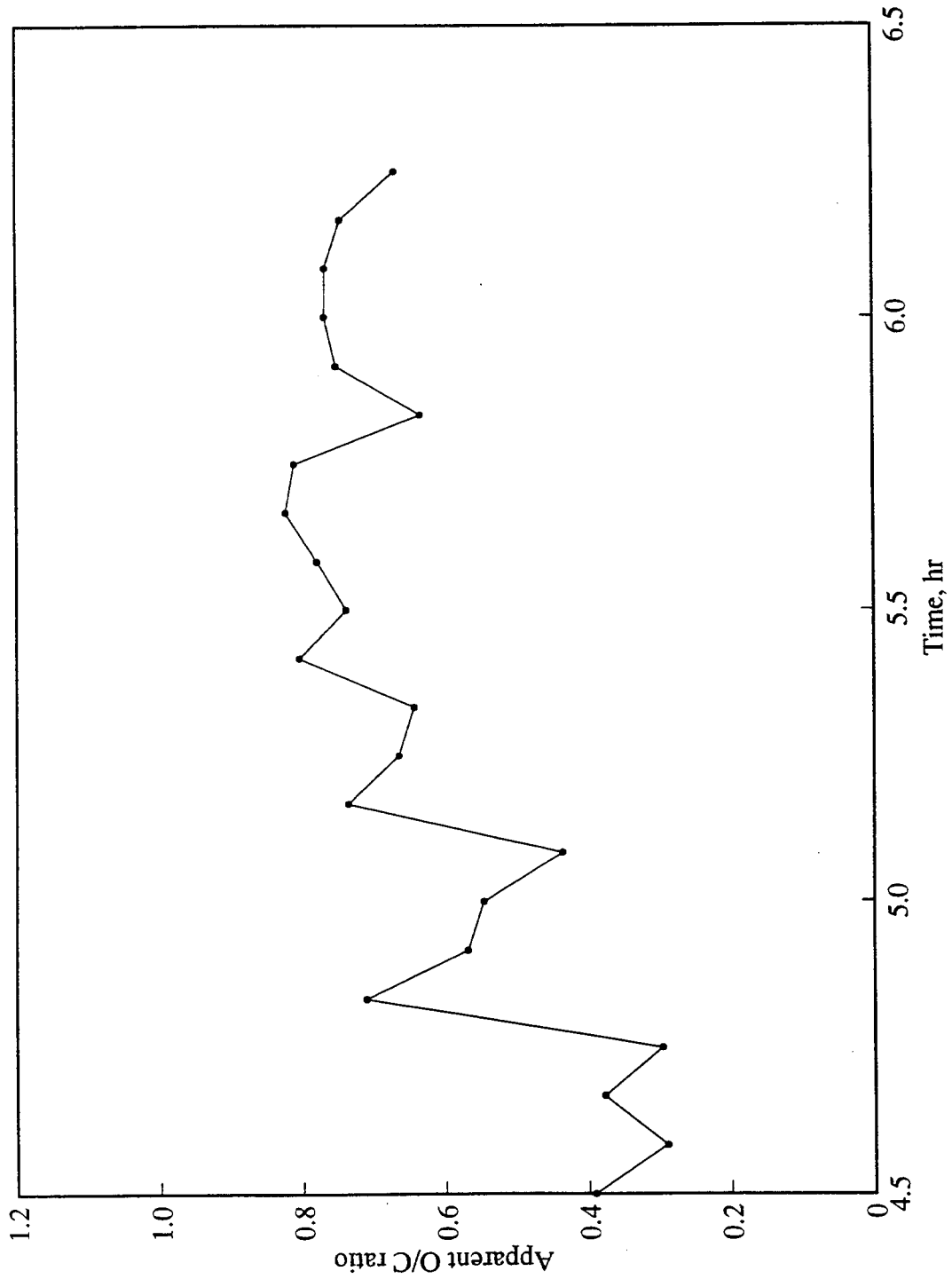


Figure 6.40: Apparent O/C Ratio Versus Time (Run HBO2)

6. KINETIC EXPERIMENTAL RESULTS

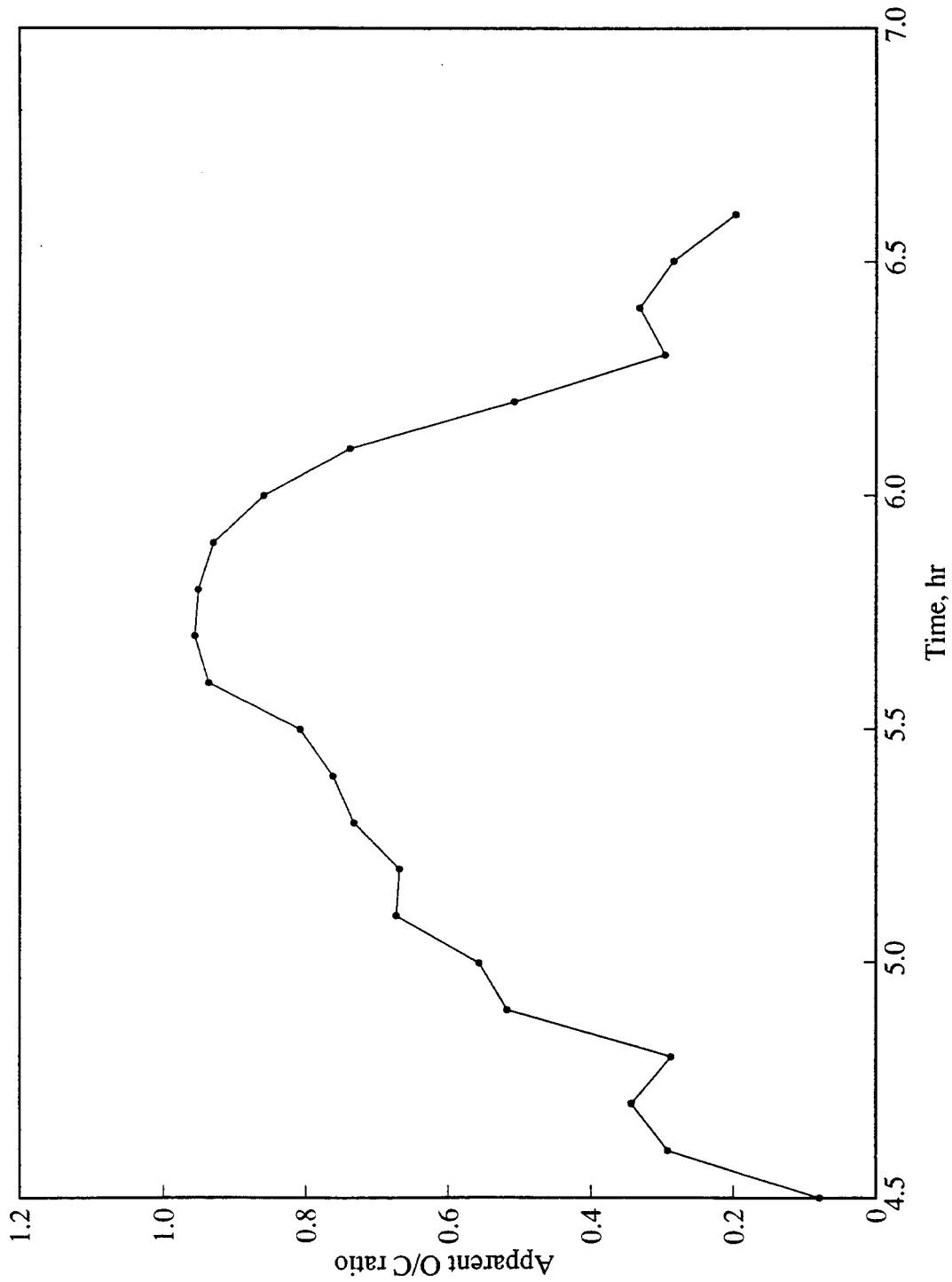


Figure 6.41: Apparent O/C Ratio Versus Time (Run VEN6)

6. KINETIC EXPERIMENTAL RESULTS

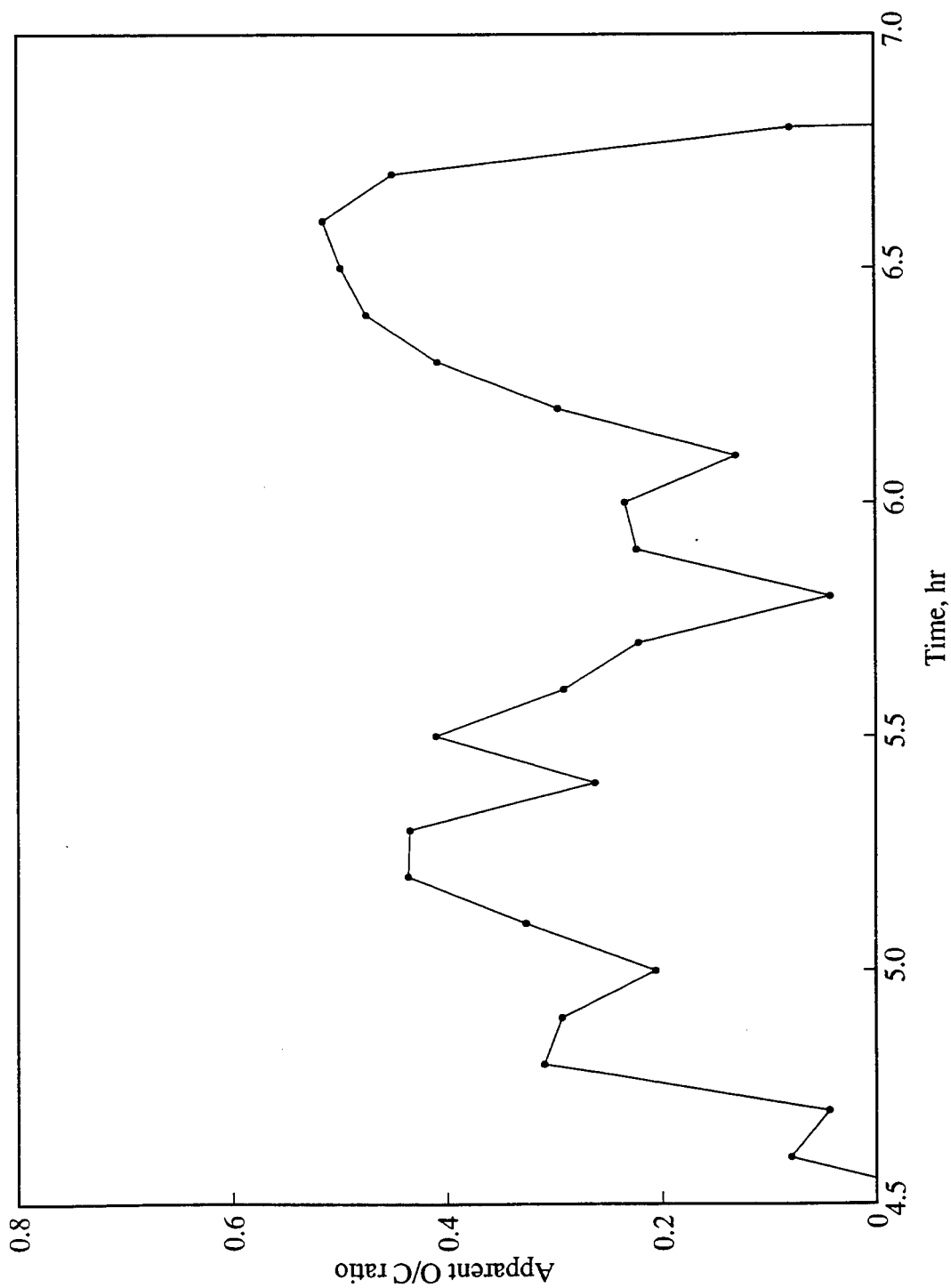


Figure 6.42: Apparent O/C Ratio Versus Time (Run VEN15)

6. KINETIC EXPERIMENTAL RESULTS

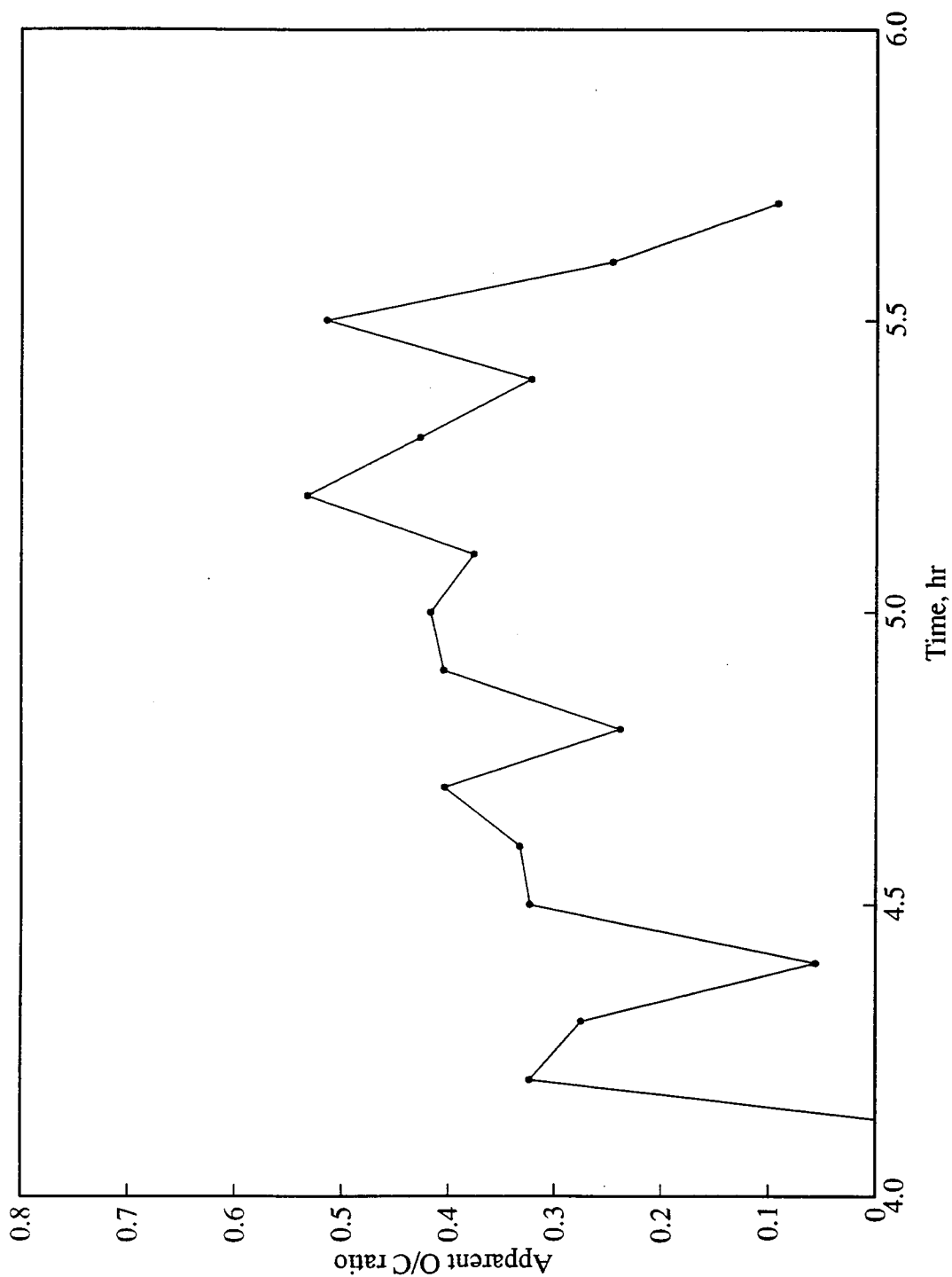


Figure 6.43: Apparent O/C Ratio Versus Time (Run VEN23)

6. KINETIC EXPERIMENTAL RESULTS

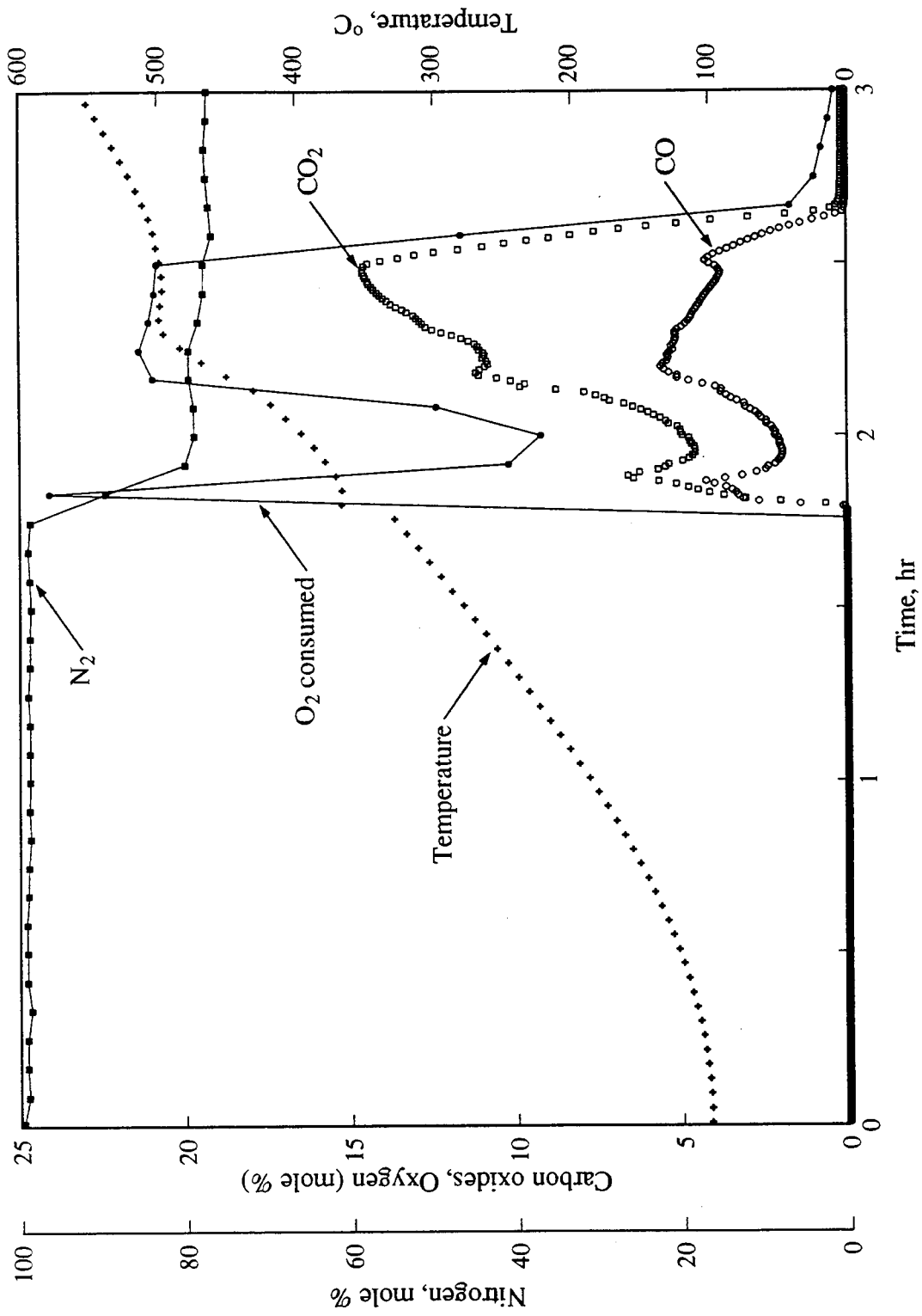


Figure 6.44: Produced Gas Composition and Temperature Versus Time (Run CL10)

6. KINETIC EXPERIMENTAL RESULTS

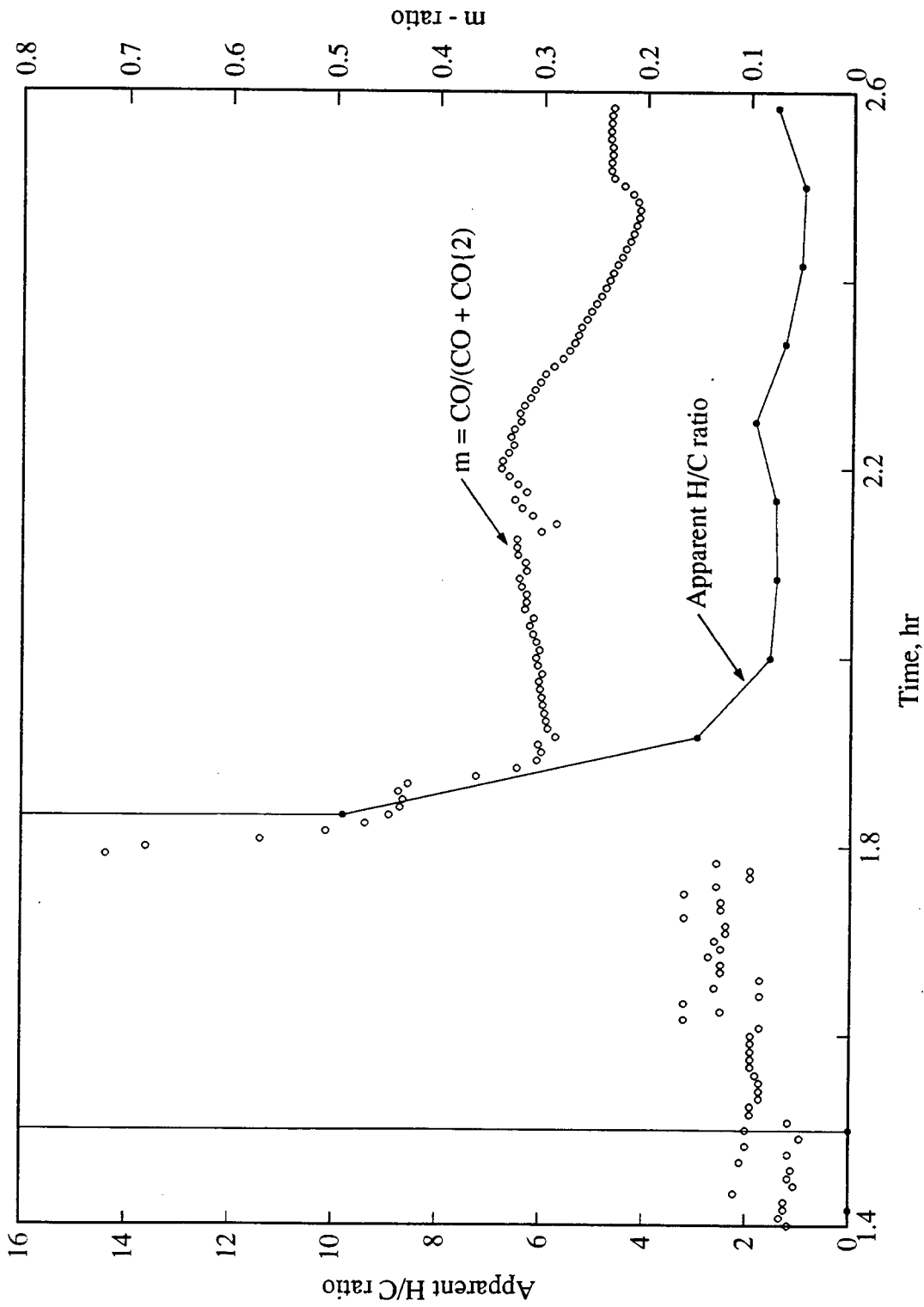


Figure 6.45: Apparent H/C and m-Ratios Versus Time (Run CL10)

6. KINETIC EXPERIMENTAL RESULTS

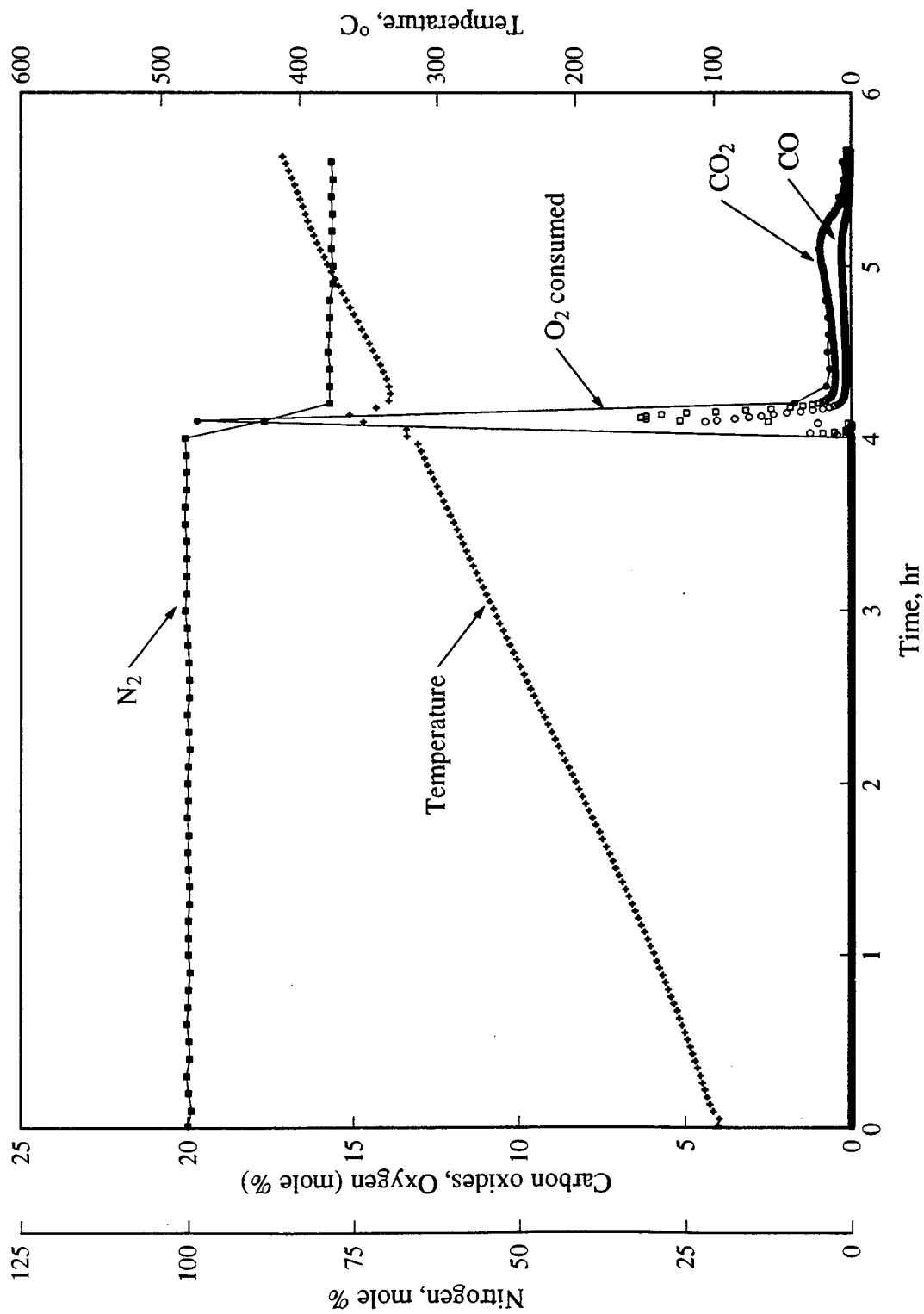


Figure 6.46: Produced Gas Composition and Temperature Versus Time (Run VEN10)

6. KINETIC EXPERIMENTAL RESULTS

6.4 Heat of Combustion of Oxygenated Fuel

For a hydrocarbon fuel (CH_x) which undergoes combustion according to the stoichiometry given by Eq. 2.4, the heat of reaction, ΔH_x (Btu/lb_m), may be estimated using Eq. 6.9 (Burger and Sahuquet 1972). It is assumed in Eq. 6.9 that the products of combustion consist of gaseous carbon dioxide and carbon monoxide and condensed water.

$$\Delta H_x = \frac{1800}{(12 + x)} (94.0 - 67.9m + 31.2x) \quad (6.9)$$

The heat of combustion for an oxygenated hydrocarbon fuel (CH_xO_y) is considerably less than that for a hydrocarbon fuel, on a per unit mass basis, because an oxygenated fuel is partially oxidized and also its mass includes oxygen. The heat of combustion of an oxygenated hydrocarbon was estimated by considering the fuel oxidation paths as shown in Fig. 6.47. In Fig. 6.47, path A is the oxidation of a hydrocarbon fuel to form carbon oxides and water. Path B represents the oxygenation of the fuel to form CH_xO_y , while Path C is the oxidation of the oxygenated fuel to form carbon oxides and water.

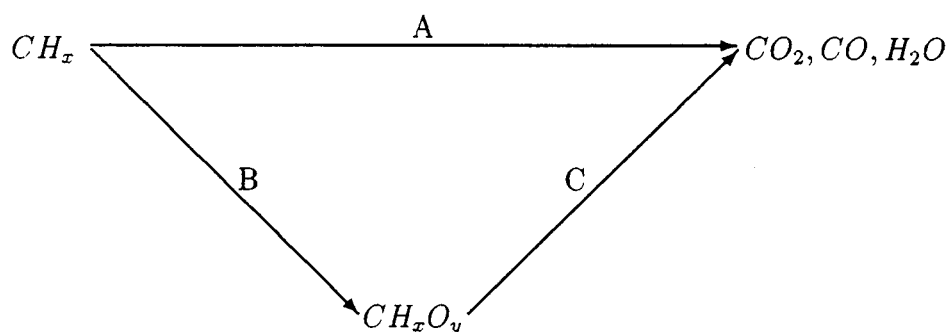


Figure 6.47: Fuel Oxidation Paths

Let ΔH_A be the heat of reaction per mole of oxygen consumed for Path A, and ΔH_B and ΔH_C the heats of reaction for Paths B and C for the same mass of fuel as in

6. KINETIC EXPERIMENTAL RESULTS

Path A. ΔH_A (KJ/mol O_2) may be calculated from Eq. 6.10 (Burger and Sahuquet 1972).

$$\Delta H_A = \frac{786.4 - 567.6m + 260.9x}{2 - m + x/2} \quad (6.10)$$

The heats of reaction (KJ/mol O_2) for the main products of hydrocarbon oxygenation (Burger and Sahuquet 1972) are as follows: carboxylic acid (430.8), aldehyde (363.1), ketone (375.7) and alcohol or phenol (306.6). The averaged heat of reaction for these oxygenated products is 369.0 KJ/mol O_2 . For one mole of oxygen consumed for Path A, the number of moles of oxygen consumed for Path B is, $(y/2)/(1 - m/2 + x/4)$. Therefore:

$$\Delta H_B = \frac{369.0y}{2(1 - m/2 + x/4)} \quad (6.11)$$

From conservation of energy:

$$\Delta H_C = \Delta H_A - \Delta H_B \quad (6.12)$$

Using Eqs. 6.10, 6.11 and 6.12:

$$\frac{\Delta H_C}{\Delta H_A} = 1 - \frac{369.0y}{786.4 - 567.6m + 260.9x} \quad (6.13)$$

Let R_{mass} denote the molar mass ratio of CH_x to CH_xO_y :

$$R_{mass} = \frac{12 + x}{12 + x + 16y} \quad (6.14)$$

The heat of reaction for an oxygenated fuel, ΔH_{xy} (Btu/lb_m of oxygenated fuel), is proportional to ΔH_x but reduced by the heat of fuel oxygenation and by the addition of oxygen to the fuel mass. That is:

$$\Delta H_{xy} = \frac{\Delta H_C}{\Delta H_A} R_{mass} \Delta H_x \quad (6.15)$$

Substituting Eqs. 6.9, 6.13 and 6.14 into Eq. 6.15:

$$\Delta H_{xy} = \frac{1800}{(12 + x + 16y)} (94.0 - 67.9m + 31.2x) \left[1 - \frac{369.0y}{(786.4 - 567.6m + 260.9x)} \right] \quad (6.16)$$

6. KINETIC EXPERIMENTAL RESULTS

Using Eq. 6.16, the heat of combustion for an oxygenated hydrocarbon fuel was computed as a function of atomic H/C, O/C and m -ratios. The results are presented in Fig. 6.48. The heat of combustion decreases significantly with increasing atomic O/C ratio, and also decreases slightly with increasing m -ratio for typical m -ratio ranges. For example, for fuel with an atomic H/C ratio of 1.5 and m -ratio of 0.3, the heat of combustion decreases from 16,000 Btu/lb_{fuel}, for an atomic O/C ratio of 0.0, down to 8,000 Btu/lb_{fuel} for an atomic O/C ratio of 0.5. If the fuel is oxygenated as a result of low-temperature oxidation, an inefficient combustion will occur. Low-temperature oxidation should be avoided in field operations. For the same reason, oxygenated gasoline used in automobiles will give considerably lower mileage per gallon than non-oxygenated gasolines.

6.5 Error Analysis

Estimates were made of the errors in apparent H/C and m -ratios determined from gas analysis. Error analyses were performed for a typical kinetic experiment (run no. CL5) and a combustion tube experiment (run no. VEN5).

Apparent H/C ratios were calculated using Eq. 2.7 which is:

$$x = 4 \frac{(0.2682N_2 - O_{2p} - CO_2 - CO/2)}{(CO_2 + CO)} \quad (6.17)$$

The error in apparent H/C ratio, Δx , may be approximated by the derivative of x in Eq. 6.17 with respect to the dependent variables:

$$\Delta x = \frac{\partial x}{\partial N_2} \Delta N_2 + \frac{\partial x}{\partial O_{2p}} \Delta O_{2p} + \frac{\partial x}{\partial CO_2} \Delta CO_2 + \frac{\partial x}{\partial CO} \Delta CO \quad (6.18)$$

ΔN_2 , ΔO_{2p} , ΔCO_2 and ΔCO represent the accuracies of the gas analysis readings.

The partial derivatives are:

$$\frac{\partial x}{\partial N_2} = \frac{1.0728}{(CO_2 + CO)} \quad (6.19)$$

6. KINETIC EXPERIMENTAL RESULTS

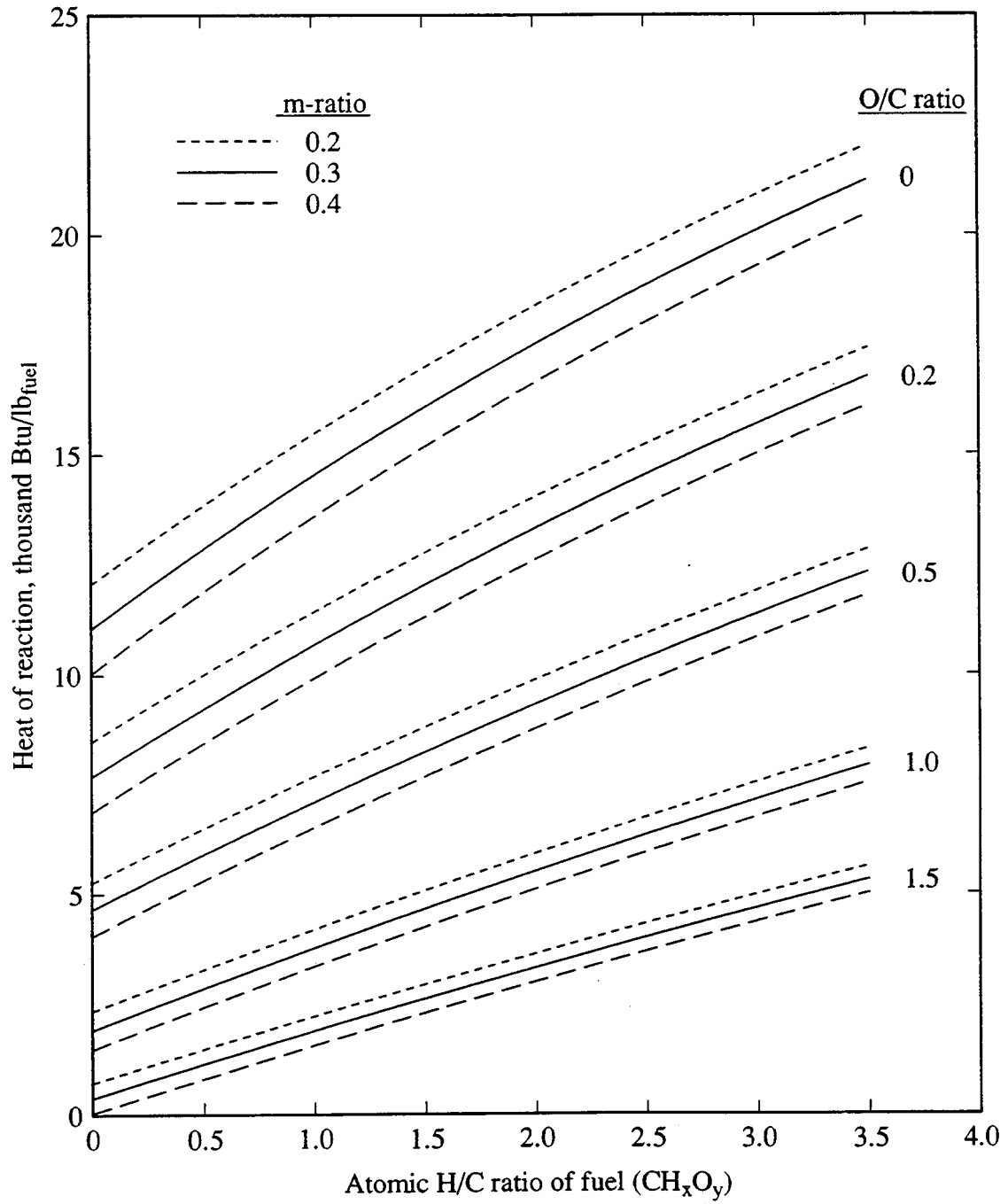


Figure 6.48: Heat of Combustion Versus Atomic H/C, O/C and *m*-Ratios

6. KINETIC EXPERIMENTAL RESULTS

$$\frac{\partial x}{\partial O_{2p}} = \frac{4}{(CO_2 + CO)} \quad (6.20)$$

$$\frac{\partial x}{\partial CO_2} = \frac{4CO_2}{(CO_2 + CO)^2} - \frac{4}{(CO_2 + CO)} \quad (6.21)$$

$$\frac{\partial x}{\partial CO} = \frac{2CO}{(CO_2 + CO)^2} - \frac{2}{(CO_2 + CO)} \quad (6.22)$$

The m -ratio is:

$$m = \frac{CO}{(CO_2 + CO)} \quad (6.23)$$

The error in m -ratio, Δm , may be approximated by:

$$\Delta m = \frac{\partial m}{\partial CO} \Delta CO + \frac{\partial m}{\partial CO_2} \Delta CO_2 \quad (6.24)$$

where:

$$\frac{\partial m}{\partial CO} = \frac{1}{(CO_2 + CO)} - \frac{CO}{(CO_2 + CO)^2} \quad (6.25)$$

$$\frac{\partial m}{\partial CO_2} = -\frac{CO}{(CO_2 + CO)^2} \quad (6.26)$$

For a conservative estimate, absolute values of the partial derivatives in Eqs. 6.20 - 6.22, 6.25 and 6.26 were used. The gas analyzers and gas chromatograph were calibrated using standard gases whose compositions were known to $\pm 0.01\%$. Since two calibrations were performed, one at the beginning and one at the end of an experiment, the accuracies of the gas analysis readings were taken to be $\pm 0.02\%$.

Error analysis results for Runs CL5 (at HTO) and VEN5 are presented in Table 6.8. Errors in apparent H/C and m -ratios are smaller in Run VEN5 than in Run CL5. This is a consequence of the difference in magnitude of the gas concentrations between combustion tube runs and kinetic tube experiments.

6. KINETIC EXPERIMENTAL RESULTS

Table 6.8: Estimated Errors in Apparent H/C and m -Ratios

Run No.	Concentration (mole %)				Δx	Δm	$x \pm \Delta x$	$m \pm \Delta m$
	CO ₂	CO	O _{2p}	N ₂				
CL5	1.77	0.69	18.4	77.94	0.06	0.008	0.49 ± 0.06	0.268 ± 0.008
VEN5	11.58	4.92	1.05	81.44	0.01	0.001	1.63 ± 0.01	0.298 ± 0.001

6.6 Previous Oxidation Reaction Model

An oxidation reaction model was presented by Fassihi (1981) and has been used by subsequent workers (De los Rios 1987, Shallcross 1989). A brief description of the model together with an example application (Figs. 6.49–6.50) follows.

In the previous model, the following assumptions were made.

1. The oxygen consumption curve can be separated into three component curves corresponding to low, medium and high temperature oxidation reactions (LTO, MTO and HTO, respectively). Each of these reactions is assumed to be the oxidation of a particular “fuel”.
2. No carbon oxides are produced during LTO.
3. The fuel during HTO is carbon.

For each reaction, the rate (equated to the oxygen consumption rate) is:

$$\frac{qO_{2c}}{AL} = A_{r_i} P_{o_2}^{m_i} C_{f_i}^{n_i} \exp(-E_i/RT) \quad (6.27)$$

where q is the volumetric flowrate, O_{2c} is the molar concentration of oxygen consumed, A and L are the cross-sectional area and length of the sand mix in the kinetic tube, A_{r_i} is the pre-Arrhenius constant, P_{o_2} is the oxygen partial pressure, C_f is the

6. KINETIC EXPERIMENTAL RESULTS

instantaneous fuel concentration, E is the activation energy, R is the universal gas constant, T is the absolute temperature, m and n are the reaction orders in respect to P_{O_2} and C_f respectively, and i is the index for either LTO, MTO or HTO.

Further, each reaction rate is proportional to the decrease in the fuel concentration, so that:

$$\frac{qO_{2c}}{AL} = -\alpha_i \frac{dC_{f_i}}{dt} \quad (6.28)$$

where α_i is a proportionality constant. Integrating Eq. 6.28 from $t = t$ to $t = \infty$ (where $C_{f_i} = 0$) yields:

$$C_f(t) = \int_t^\infty \frac{qO_{2c}}{\alpha_i AL} dt \quad (6.29)$$

From Eq. 6.27:

$$C_{f_i}^{n_i}(t) = \frac{qO_{2c}}{AL A_{r_i} P_{O_2}^{m_i} \exp(-E_i/RT)} \quad (6.30)$$

Substituting Eq. 6.30 into Eq. 6.29:

$$\frac{O_{2c}}{[\int_t^\infty O_{2c} dt]^{n_i}} = \beta_i \exp(-E_i/RT) \quad (6.31)$$

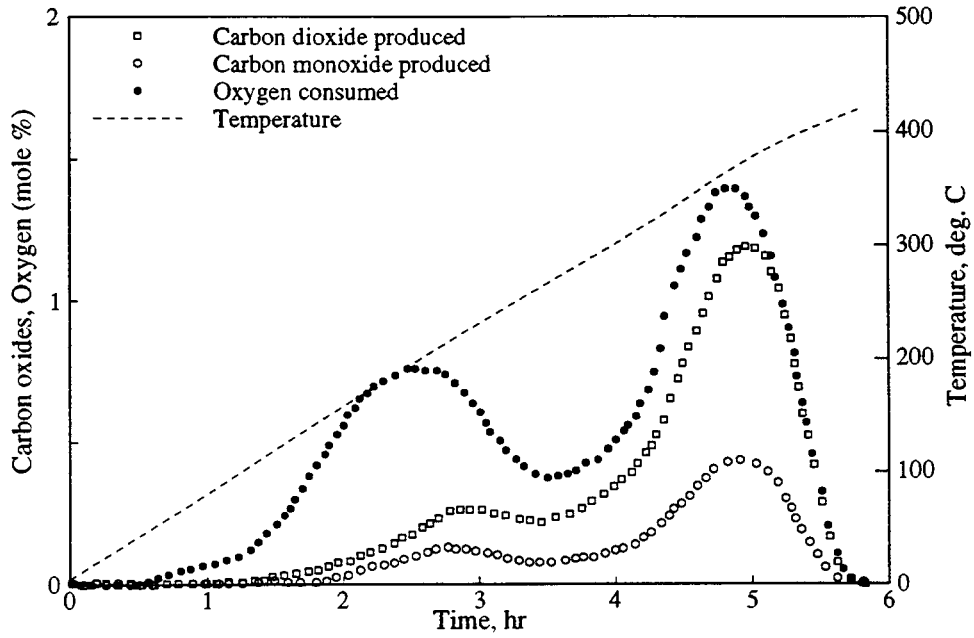
where:

$$\beta_i = \left[\frac{q}{AL} \right]^{n_i-1} \frac{A_{r_i} P_{O_2}^{m_i}}{\alpha_i^{n_i}} \quad (6.32)$$

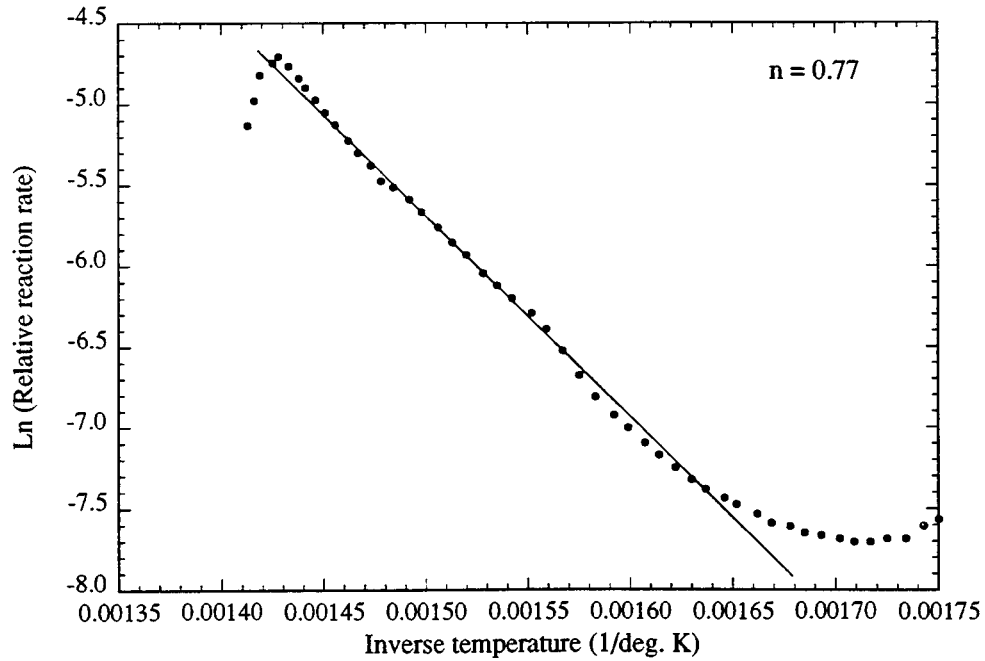
A graph of the natural logarithm of the left hand side of Eq. 6.31, termed the relative reaction rate, versus $1/T$ should yield a straight line with a slope of $-E_i/R$, and an intercept of $\ln \beta_i$. The exponent, n_i , may be obtained by trial-and-error or through a non-linear regression method. An example of such an Arrhenius graph is shown in Fig. 6.49b.

Starting with E_H and β_H obtained for HTO, Eq. 6.31 may be used to calculate an approximate oxygen consumption curve, Curve I in Fig. 6.50a. Curve I may be subtracted from the experimental data to yield Curve II, the curve for MTO and LTO oxygen consumption (Fig. 6.50a). Assuming fuel for HTO to be carbon, the oxygen consumption may be represented by the equivalent carbon dioxide and carbon

6. KINETIC EXPERIMENTAL RESULTS



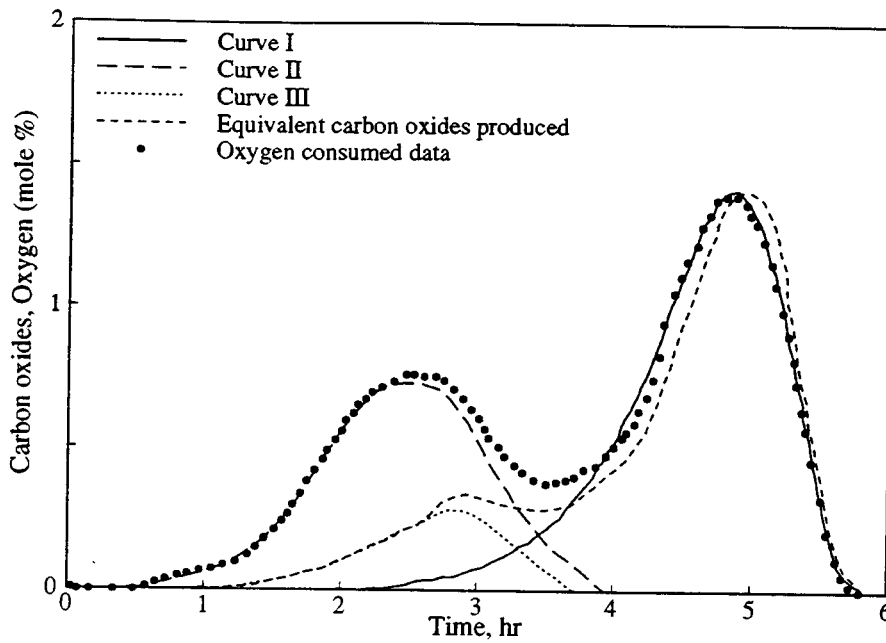
(a) Gas Composition and Temperature versus Time



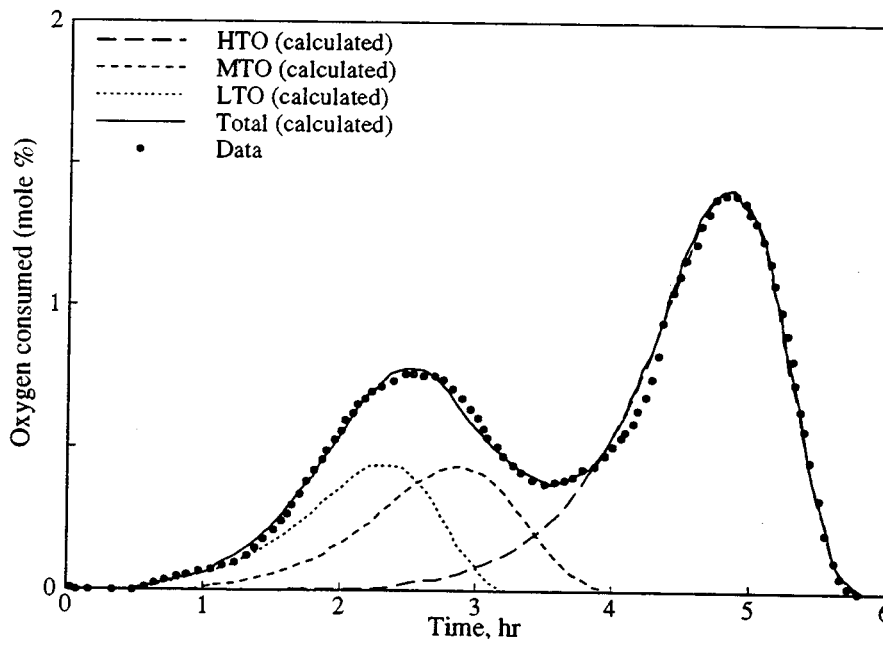
(b) Arrhenius Graph for HTO Data

Figure 6.49: Huntington Beach Oil - Analysis Based on Previous Model (*After Shallcross, 1989*)

6. KINETIC EXPERIMENTAL RESULTS



(a) Generation of MTO Curve



(b) Total Oxygen Consumption Curve

Figure 6.50: Huntington Beach Oil - Analysis Based on Previous Model (After Shallcross, 1989)

6. KINETIC EXPERIMENTAL RESULTS

monoxide concentration curve, $\delta = CO_2 + CO/2$. Curve I may be subtracted from the δ curve to yield Curve III, the curve representing LTO and MTO. The assumption that carbon oxides are not produced for LTO implies that Curve III represents the oxygen consumption for MTO only. An Arrhenius graph based on Curve III should yield E_M and β_M for MTO. Subtracting Curve III from Curve II should yield the oxygen consumption curve for LTO, from which E_L and β_L may be obtained. Superposition of Curve I, Curve III and the LTO curve should yield the total curve for the oxygen consumption of the three reactions (Fig. 6.50b).

Kinetic experimental data were analyzed using the previous oxidation reaction model. The following problems were encountered.

1. The Arrhenius graph for the HTO reaction does not yield a satisfactory straight line (Figs. 6.51 and 6.52). After reaching a maximum value, the slope of the graph becomes positive. Previous researchers appear to ignore the data points after the maximum value in the Arrhenius graph (for example, Fig. 6.49b). However these data points may represent some kinetic behaviour not considered in the previous model.
2. The assumption that carbon is the fuel for HTO is only an approximation of the combustion reaction. A kinetic tube run was performed for a sand mix containing a mixture of Cold Lake bitumen and carbon. The results (Fig. 6.53) indicate a separate carbon peak at about 450 °C, compared to about 400 °C for the HTO peak of the crude. As described in Section 6.2, fuel for HTO in kinetic tube experiments is an oxygenated hydrocarbon.
3. Kinetic experimental results indicate only two oxidation reactions, LTO followed by HTO (Section 6.1).
4. Previous researchers have found that an increase in the surface area of the porous medium increases the LTO reactions (Drici and Vossoughi 1985) which

6. KINETIC EXPERIMENTAL RESULTS

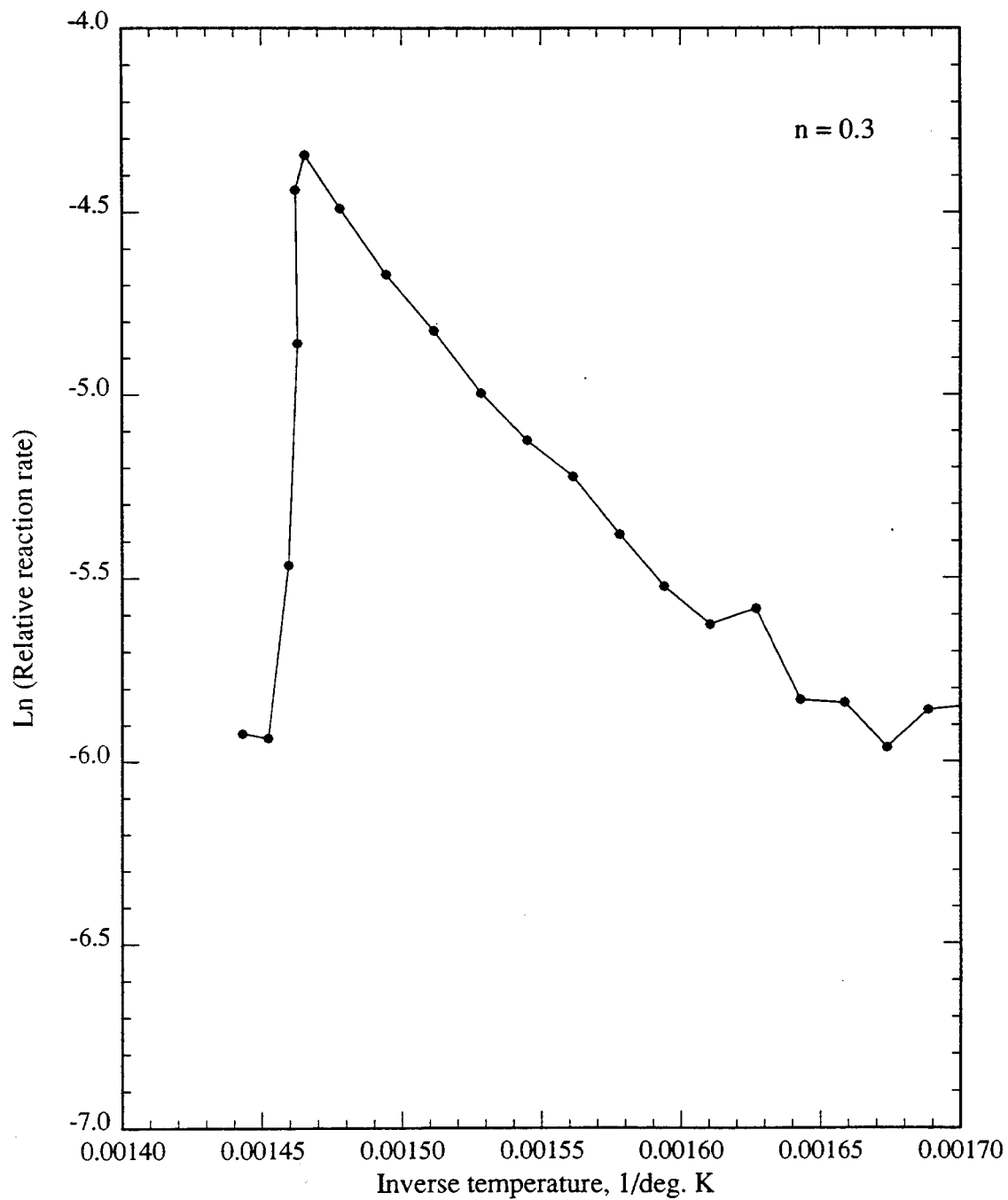


Figure 6.51: Cold Lake Bitumen (Run CL14) - Arrhenius Graph for HTO Data Based on Previous Model

6. KINETIC EXPERIMENTAL RESULTS

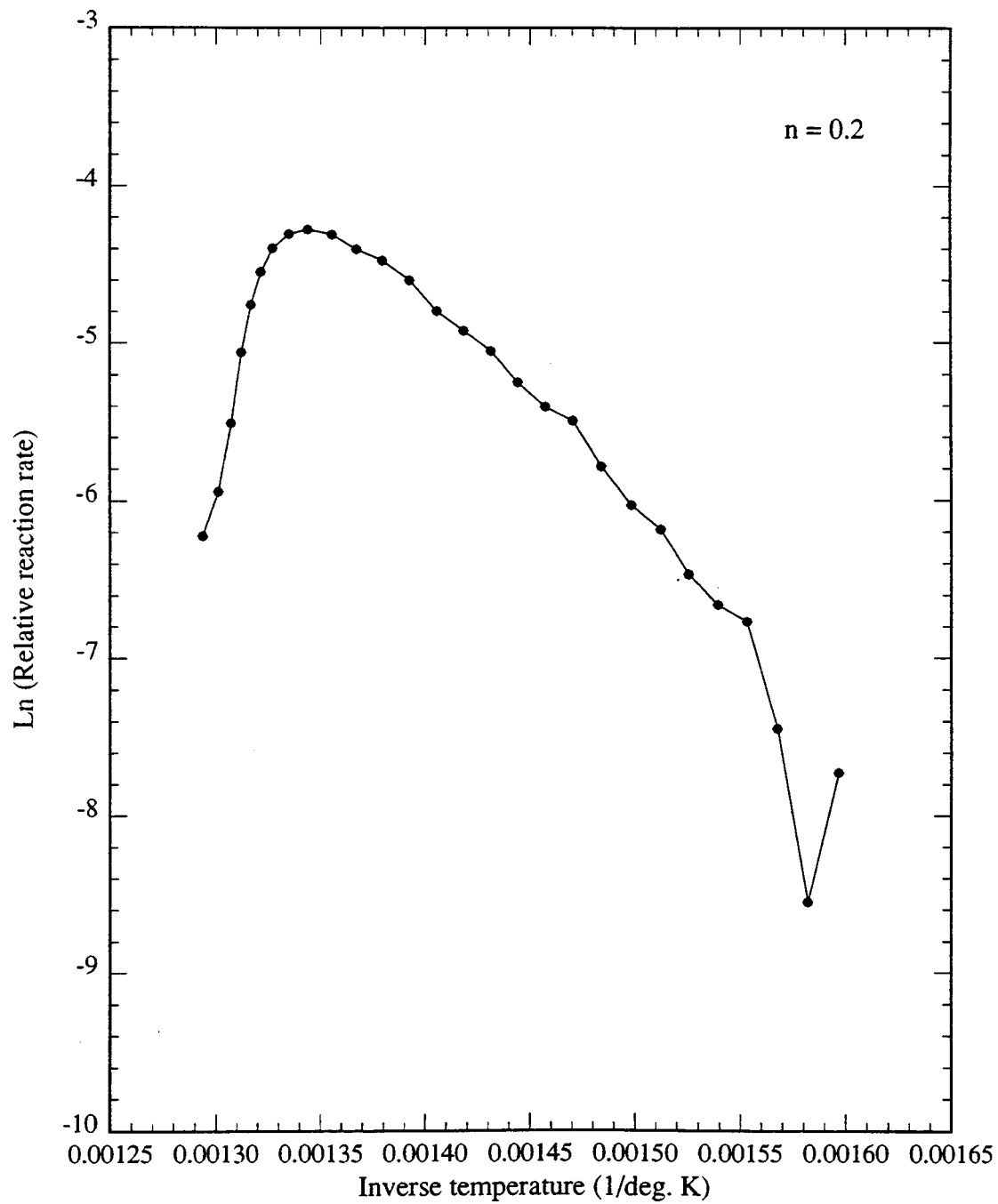


Figure 6.52: Carbon (Run C3) - Arrhenius Graph Based on Previous Model

6. KINETIC EXPERIMENTAL RESULTS

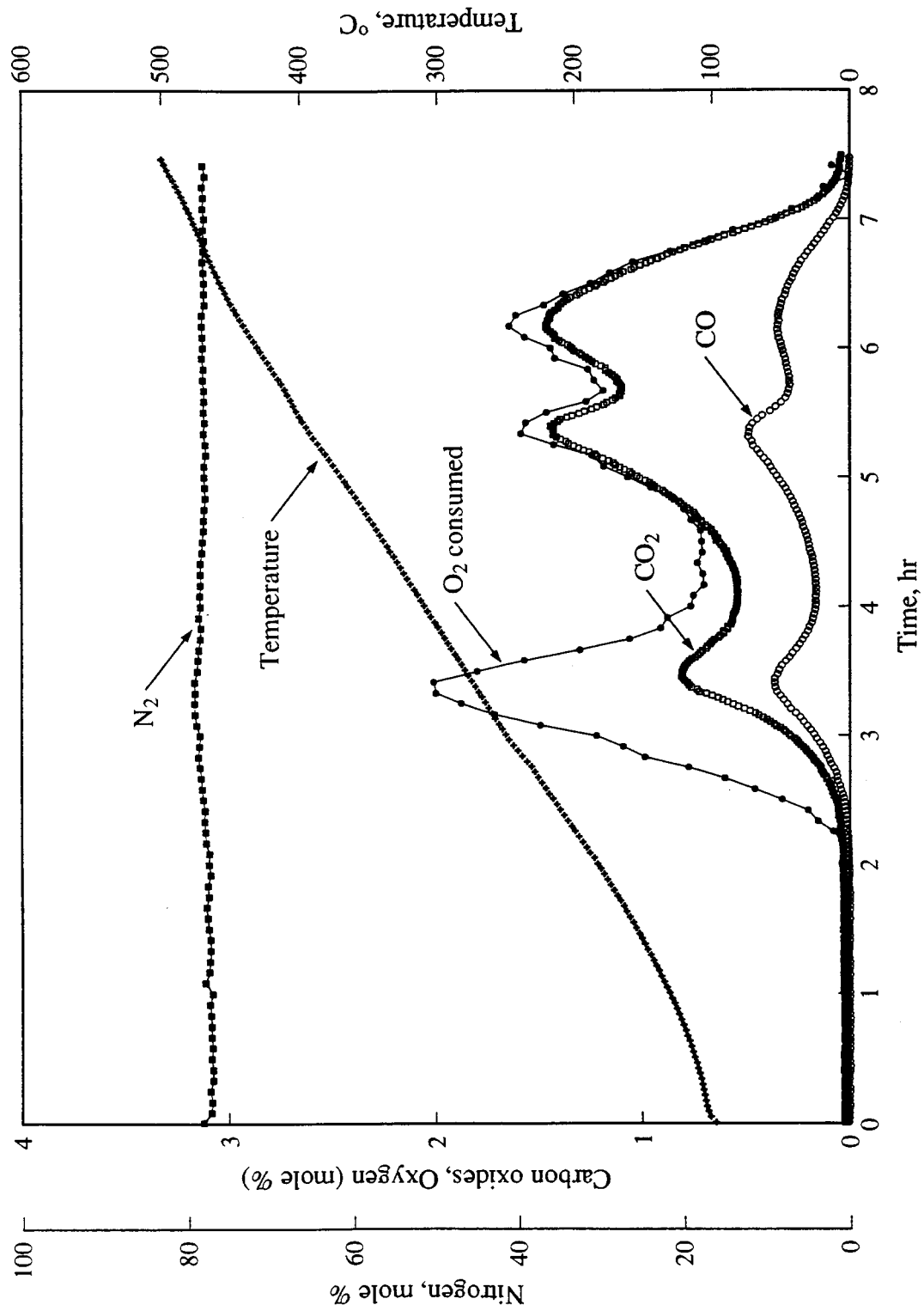


Figure 6.53: Produced Gas Composition and Temperature Versus Time (Run CLC1)

6. KINETIC EXPERIMENTAL RESULTS

result in the formation of more fuel (Shahani and Hansel 1984, Vossoughi *et al.* 1982). As described in Section 6.1, kinetic experiments indicate clay increases the amount of oxygen consumed during LTO. These results are in qualitative agreement with observations made by earlier researchers. The salient point is that a proper model should incorporate the surface area of the porous medium.

6.7 Summary of Kinetic Experimental Results

- As a result of excess oxygen during kinetic tube experiments, the fuel that reacts during HTO is an oxygenated hydrocarbon, CH_xO_y .
- Knowing the atomic H/C ratio, the atomic O/C ratio may be determined from gas composition data.
- Clay increases LTO reactions to form oxygenated fuel with large atomic O/C ratios, as indicated by results of kinetic tube Runs CL14 and VEN6. Thus in these two runs, the measured oxygen consumption during HTO is decreased due to the high oxygen content of the fuel.
- In combustion tube experiments where the apparent H/C ratio is similar to that of the original crude (e.g. Run VEN5), the atomic O/C ratio is essentially zero. Thus no LTO has occurred and the fuel is not oxygenated. These efficient burns have high combustion temperatures and virtually no or little oxygen in the produced gas stream.
- Combustion involving an oxygenated hydrocarbon fuel is an inefficient operation from the standpoint of poor usage of oxygen injected, low heat of combustion and reduced oil mobility.

6. KINETIC EXPERIMENTAL RESULTS

- Properly designed combustion tube experiments and field projects involve burning a hydrocarbon fuel which has not been oxygenated. Since kinetic tube experiments entail HTO reactions for an oxygenated fuel, the results may not pertain to combustion that occurs in a combustion tube or in field operations. Nevertheless, a new oxidation reaction model for kinetic tube experiments is presented in the next chapter.

7. New Oxidation Reaction Model

Based on experimental results described in Chapter 6, a new oxidation reaction model was formulated.

1. The oxidation of crude oil consists of two main stages: low-temperature oxidation, followed by high-temperature oxidation. The oxygen consumption curve may be separated into two, partially-overlapping curves.
2. In kinetic tube experiments, crude oil oxidation reactions occur in an oxygen abundant environment. The fuel that is oxidized during HTO is an oxygenated hydrocarbon which is characterized by a particular set of atomic H/C and O/C ratios.
3. The surface area of the porous medium, represented by the size of the sand grains and/or clay particles (i.e. reaction surface area) affects the reaction kinetics.

To assess the effect of the surface area, two models were studied: a *spherical-fuel-geometry* and a *varying-fuel-geometry* model. In the former (Fig. 7.1), the fuel is assumed to be deposited evenly around the sand grains which are assumed to be spherical in shape. As temperature increases, water and light hydrocarbons are vaporized leaving behind a residue of heavy oil fractions. Due to excess oxygen being present, the residue undergoes low-temperature oxidation to form an oxygenated fuel.

7. NEW OXIDATION REACTION MODEL

In the HTO range, the fuel undergoes oxidation to form carbon oxides and water. The mass, and therefore radius, of the fuel decreases until the fuel is completely oxidized. As discussed in Section 7.1, this model failed to match kinetic experimental data.

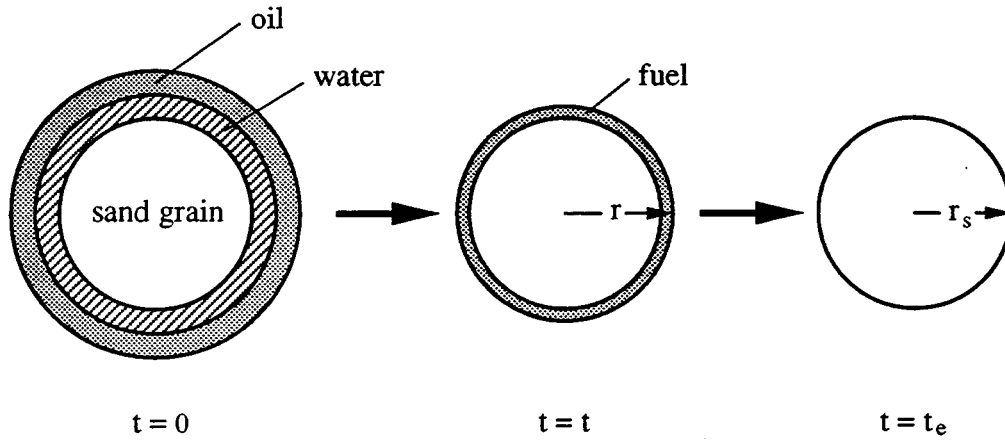


Figure 7.1: Schematic Diagram of Spherical-Fuel-Geometry Model

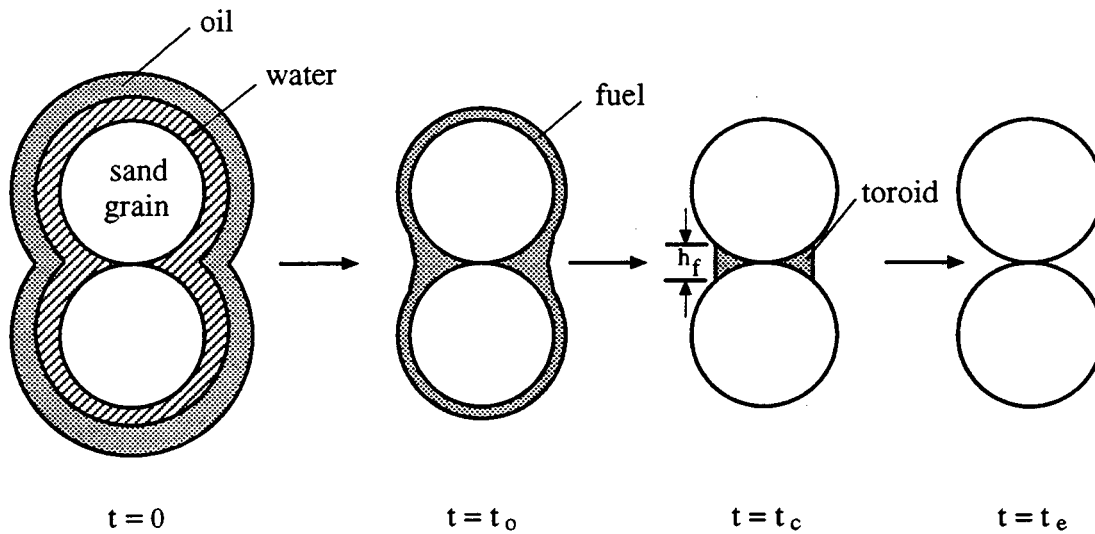


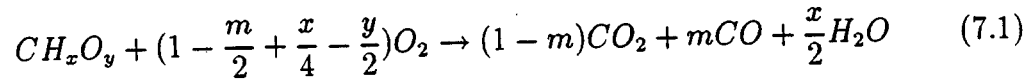
Figure 7.2: Schematic Diagram of Varying-Fuel-Geometry Model

7. NEW OXIDATION REACTION MODEL

In the varying-fuel-geometry model, the fuel has two geometries as shown in Fig. 7.2. Initially the fuel covers the entire sand grain. Due to the large surface area, fuel deposited directly on the grain surface is oxidized faster than that deposited at grain contacts. At some later time, t_c , fuel is present only at grain contacts. During this time, until fuel oxidation is complete, grain contact geometry may be approximated by a shrinking toroid.

The following features are common to both the spherical-fuel-geometry and varying-fuel-geometry models.

1. The stoichiometric equation for fuel oxidation is given by Eq. 6.6, which is:



Let CO and CO_2 be the mole percent of produced carbon monoxide and carbon dioxide, respectively, and q_o the effluent gas flow rate (liter/min). One mol of gas at standard conditions occupies 22.4138 liters. The atomic weights of carbon, oxygen and hydrogen are 12.0110, 15.9994 and 1.0000, respectively. Using the carbon balance, the number of moles of fuel oxidized per second may be expressed as $q_o(CO + CO_2)/(60 \times 22.4138)$. The molecular weight of the fuel (CH_xO_y) is equal to $12.0110 + x + 15.9994y$. Therefore, the mass of fuel consumed per second, dm_f/dt , is:

$$\frac{dm_f}{dt} = \frac{q_o(CO + CO_2)(12.0110 + x + 15.9994y)}{60 \times 22.4138} \quad (7.2)$$

2. If r_s and ρ_s are the the average radius and density of a sand grain (assumed spherical), then the mass of a sand grain is given by $4\pi r_s^3 \rho_s / 3$. The total mass of sand grains in a sand mix of length, L , and cross-sectional area, A , and porosity, ϕ , is given by $AL(1 - \phi)\rho_s$. Thus:

$$\text{No. of sand grains in the cell} = \frac{3AL(1 - \phi)}{4\pi r_s^3} \quad (7.3)$$

7. NEW OXIDATION REACTION MODEL

Table 7.1: Estimated Grain Sizes and Fuel Densities

Run No.	Average sand grain radius, r_s (cm)	Fuel density (g/cc)
C3	0.0390	2.0
C4	0.0142	2.0
CL2	0.0375	1.029
CL5	0.0375	1.029
CL14	0.0001	1.029
HBO2	0.0375	0.992
VEN6	0.0001	1.037
VEN23	0.0004	1.037

3. The average sand grain radius was based on sieve analysis (Tables 4.3 and 4.4). Mixtures of clay and sand were also used in some runs. In such cases, the average sand and clay grain radius was estimated based on mass-weighted surface area of each grain type. The average clay particle diameter was estimated to be 0.004 cm (Burger *et al.* 1985). The same method was used for mixtures containing sands of two-size distributions (e.g. 20-30 mesh and 45-70 mesh sand mixture). The estimated grain sizes of the sand mixtures used are shown in Table 7.1.
4. In Table 7.1, the fuel densities for crude oils were assumed to be similar to that of their residua at the equivalent normal boiling point of 335°C. The API versus residuum correlation (Lim 1991) was used to estimate the fuel densities. For kinetic tube runs using carbon, the fuel density was that for carbon, 2 g/cc (Chemical Rubber Co. 1982).

7. NEW OXIDATION REACTION MODEL

7.1 Spherical-Fuel-Geometry Model

In the spherical-fuel-geometry model, the fuel is deposited evenly around the sand grains which are assumed to be spherical in shape (Fig. 7.1). Let r be the radius of the fuel surface and ρ_f the fuel density at time, t .

$$\text{Mass of fuel per sand grain} = \frac{4}{3}\pi(r^3 - r_s^3)\rho_f \quad (7.4)$$

Using Eqs. 7.3 and 7.4:

$$\text{Total mass of fuel at time, } t = \frac{(r^3 - r_s^3)}{r_s^3}AL(1 - \phi)\rho_f \quad (7.5)$$

Differentiating Eq. 7.5 with respect to time and equating the result with Eq. 7.2 yields:

$$\frac{d}{dt} \left[\frac{(r^3 - r_s^3)}{r_s^3}AL(1 - \phi)\rho_f \right] = -\frac{q_o(CO + CO_2)(12.0110 + x + 15.9994y)}{60 \times 22.4138} \quad (7.6)$$

Integrating Eq. 7.6 from t to the end of fuel oxidation, t_e (where $r = r_s$) gives:

$$r^3 = r_s^3 - r_s^3 \frac{\int_t^{t_e} q_o(CO + CO_2)(12.0110 + x + 15.9994y)dt}{60 \times 22.4138AL(1 - \phi)\rho_f} \quad (7.7)$$

That is:

$$r = r_s(1 + \gamma)^{\frac{1}{3}} \quad (7.8)$$

where:

$$\gamma = \frac{\int_t^{t_e} q_o(CO + CO_2)(12.0110 + x + 15.9994y)dt}{60 \times 22.4138AL(1 - \phi)\rho_f} \quad (7.9)$$

The rate of decrease in fuel concentration is given by Eq. 6.28, which is:

$$\frac{q_i O_{2c}}{AL} = -\alpha_H \frac{dC_H}{dt} \quad (7.10)$$

where O_{2c} is the mole percent of oxygen consumed, q_i is the injected gas rate (L/min), C_H is the fuel concentration, and α_H is a proportionality constant. Since the molecular weight of oxygen is 31.9988 and if m_f is the mass of fuel at time, t , then from Eq. 7.10:

$$\frac{31.9988q_i O_{2c}}{60 \times 22.4138} = -\alpha_H \frac{dm_f}{dt} \quad (7.11)$$

7. NEW OXIDATION REACTION MODEL

The reaction rate for a particular surface area (Burger *et al.* 1985) is:

$$\frac{dm_f}{dt} = -k_o^* P_{o_2}^{m_H} \exp(-E_H/RT) \times \text{surface area} \quad (7.12)$$

where k_o^* is an equilibrium constant and E_H is the fuel activation energy at HTO.

Using Eq. 7.3 and r from Eq. 7.8:

$$\text{Fuel surface area} = 3AL(1 - \phi)(1 + \gamma)^{\frac{2}{3}}/r_s \quad (7.13)$$

Substituting Eq. 7.13 into Eq. 7.12 and equating the resulting equation with Eq. 7.11 yields:

$$\frac{31.9988q_i O_{2c}}{60 \times 22.4138} = \frac{\alpha_H}{r_s} k_o^* P_{o_2}^{m_H} \exp(-E_H/RT) \times 3AL(1 - \phi)(1 + \gamma)^{\frac{2}{3}} \quad (7.14)$$

$$\frac{q_i r_s O_{2c}}{2(1 + \gamma)^{2/3}} = \beta_H \exp(-E_H/RT) \quad (7.15)$$

where:

$$\beta_H = 63.0413\alpha_H k_o^* P_{o_2}^{m_H} AL(1 - \phi) \quad (7.16)$$

A graph of the natural logarithm of the left hand side of Eq. 7.15 versus $1/T$ for the carbon (Fig. 7.3) or crude (Fig. 7.4) HTO kinetic experimental data, however, did not yield the expected straight line fit. In Fig. 7.4, the Arrhenius graph for the spherical-fuel- geometry model has been transposed by +7 y-axis units for display purposes.

Figures 7.3 and 7.4 indicate the Arrhenius graphs to be similar in trend with those based on the previous oxidation reaction model. This is not surprising. In the previous model, the fuel surface area was assumed to be constant. In the spherical-fuel-geometry model, given the thin fuel layer, the fuel surface area is approximately constant.

Thus, the spherical-fuel-geometry model was rejected, and a model which described the fuel surface area more accurately was developed.

7. NEW OXIDATION REACTION MODEL

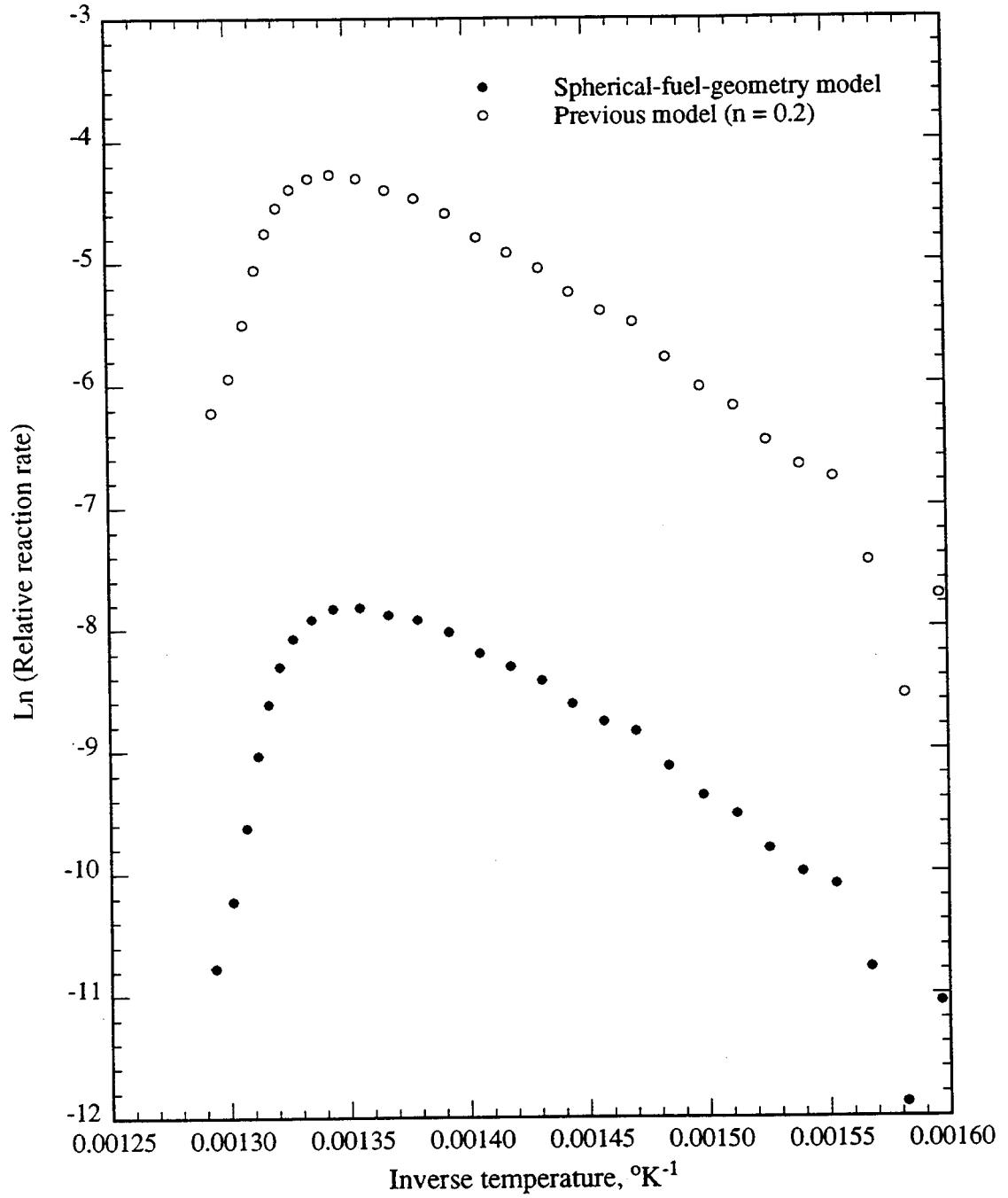


Figure 7.3: Arrhenius Graphs Based on Spherical-Fuel-Geometry and Previous Models (Carbon Run C3)

7. NEW OXIDATION REACTION MODEL

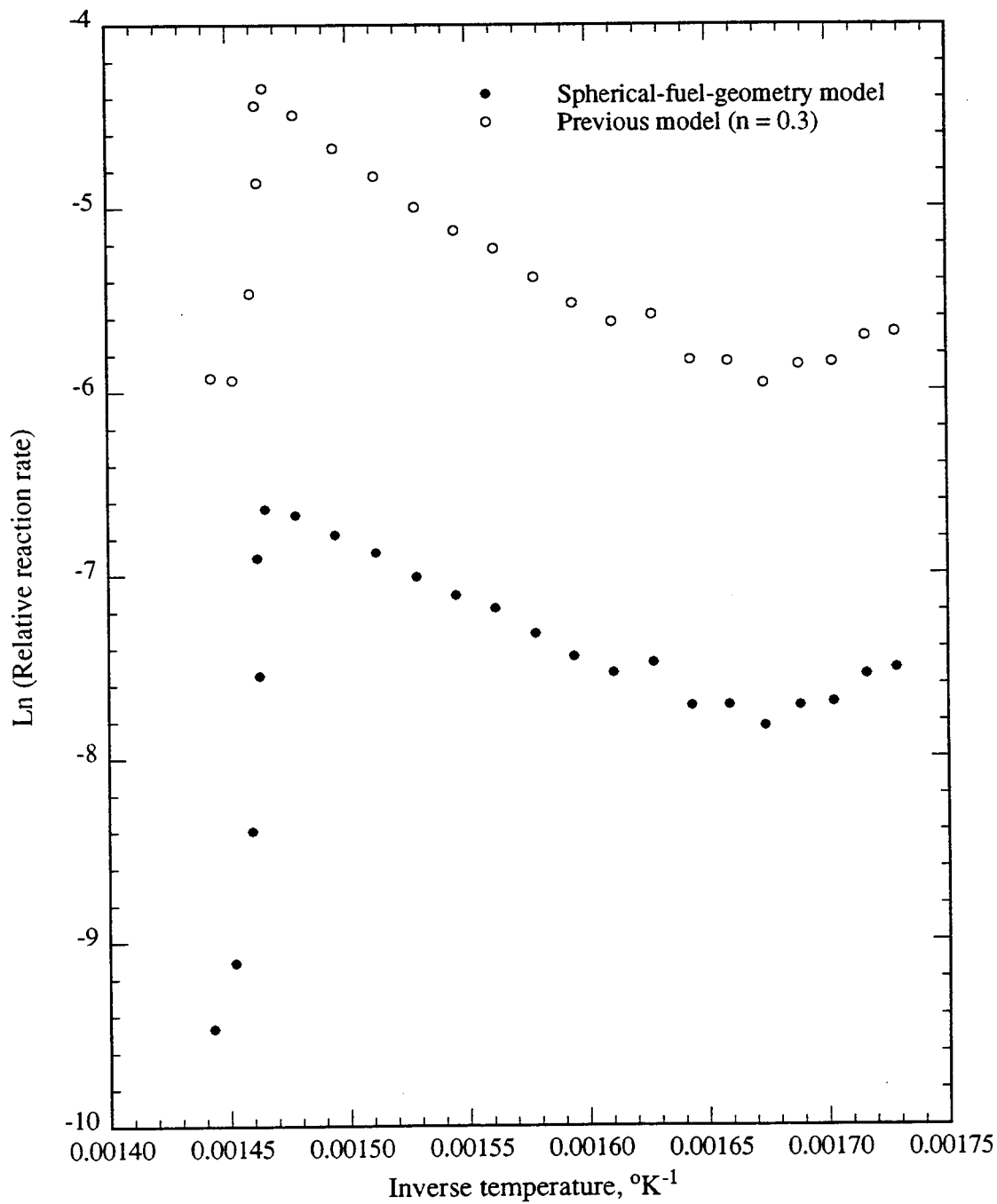


Figure 7.4: Arrhenius Graphs Based on Spherical-Fuel-Geometry and Previous Models (Cold Lake Bitumen Run CL14)

7.2 Varying-Fuel-Geometry Model

In the varying-fuel-geometry model, the fuel geometry changes with time (Fig. 7.2). Initially, the fuel is deposited over the entire sand grain surface. At some later time, t_c , fuel is present only at the grain contacts, and the fuel geometry can be approximated by a toroid.

7.2.1 Fuel in the Toroid ($t \geq t_c$)

Let h_f be the height of the toroid at time, t , where $t \geq t_c$. Sand grain cap volume from r_s to $(r_s - h_f/2)$:

$$\text{Grain cap volume} = \pi \left[\frac{r_s^2 h_f}{2} - \frac{r_s^3}{3} + \frac{1}{3} \left(r_s - \frac{h_f}{2} \right)^3 \right] \quad (7.17)$$

The perpendicular distance from a grain contact point to the toroid surface, r_1 , is:

$$r_1 = \sqrt{r_s h_f - \frac{h_f^2}{4}} \quad (7.18)$$

Using Eqs. 7.17 and 7.18, the fuel volume per grain contact, V_{grain} , is:

$$\begin{aligned} V_{grain} &= \text{half of toroid volume} \\ V_{grain} &= \pi r_1^2 \frac{h_f}{2} - \pi \left[\frac{r_s^2 h_f}{2} - \frac{r_s^3}{3} + \frac{1}{3} \left(r_s - \frac{h_f}{2} \right)^3 \right] \\ V_{grain} &\approx \pi \left[\frac{r_s h_f^2}{4} - \frac{h_f^3}{8} \right] \end{aligned} \quad (7.19)$$

neglecting h_f^3/r_s^3 and higher order terms. The average porosity of the sand mixture was assumed to be 0.37. This was based on the average porosity between a cubic packing ($\phi = 0.476$) and a rhombohedral packing ($\phi = 0.2596$)(Amyx and Bass 1962). The number of contacts per grain was taken to be six (6). Therefore:

$$\begin{aligned} \text{Fuel volume in sand mix} &= \text{fuel volume per grain contact} \\ &\quad \times \text{no. of contacts per grain} \times \text{no. of grains} \end{aligned}$$

7. NEW OXIDATION REACTION MODEL

Using Eqs. 7.3 and 7.19, the total fuel volume in the sand mix, V_{total} , is:

$$\begin{aligned} V_{total} &= \frac{9}{2} \left[\frac{h_f^2}{4r_s^2} - \frac{h_f^3}{8r_s^3} \right] AL(1 - \phi) \\ V_{total} &\approx \frac{9}{8} \frac{h_f^2}{r_s^2} AL(1 - \phi) \end{aligned} \quad (7.20)$$

In Eq. 7.20, the term $h_f^3/8r_s^3$ is small compared to $h_f^2/4r_s^2$ and can be neglected. Equation 7.20 is valid provided:

$$r_s \gg \frac{h_f}{2} \quad (7.21)$$

This condition was satisfied as discussed in Sections 7.4.1 and 7.4.2. Differentiating Eq. 7.20 and equating the result with Eq. 7.2 gives:

$$\frac{d}{dt} \left[\frac{9h_f^2}{8r_s^2} AL(1 - \phi) \rho_f \right] = - \frac{q_o(CO + CO_2)(12.0110 + x + 15.9994y)}{60 \times 22.4138} \quad (7.22)$$

Integrating Eq. 7.22 from $t = t$ (where $h_f = h_f$) to $t = t_e$ (where $h_f = 0$):

$$\frac{9h_f^2}{8r_s^2} AL(1 - \phi) = \frac{\int_t^{t_e} q_o(CO + CO_2)(12.0110 + x + 15.9994y) dt}{60 \times 22.4138} \quad (7.23)$$

That is:

$$h_f = \frac{r_s}{3} (8\gamma)^{\frac{1}{2}} \quad (7.24)$$

where γ is as defined by Eq. 7.9.

Using Eq. 7.18, fuel surface area of the toroid per grain contact, A_{grain} , is:

$$A_{grain} = \frac{\pi}{2} h_f \left(r_s h_f - \frac{h_f^2}{4} \right)^{\frac{1}{2}} \quad (7.25)$$

Total fuel surface area of the toroid in the sand mix, A_{total} , is:

$$\begin{aligned} A_{total} &= \text{fuel surface area per grain contact} \\ &\quad \times \text{no. of contacts per grain} \\ &\quad \times \text{no. of grains} \end{aligned}$$

7. NEW OXIDATION REACTION MODEL

$$\begin{aligned}
 A_{total} &= \frac{9h_f}{2r_s^3} AL(1-\phi) \left(r_s h_f - \frac{h_f^2}{4} \right)^{\frac{1}{2}} \\
 A_{total} &\approx \frac{9h_f^{\frac{3}{2}}}{2r_s^{\frac{5}{2}}} AL(1-\phi) \\
 A_{total} &= 4.1195 AL(1-\phi) \frac{\gamma^{\frac{3}{4}}}{r_s} \tag{7.26}
 \end{aligned}$$

on substituting for h_f from Eq. 7.24. Eq. 7.26 is valid provided:

$$r_s \gg \frac{h_f}{4} \tag{7.27}$$

This condition was satisfied as discussed in Sections 7.4.1 and 7.4.2. Relating the reaction rate to the fuel surface area, as was done in Eq. 7.14, yields:

$$\frac{31.9988 q_i O_{2c}}{60 \times 22.4138} = \alpha_H k_o^* \exp(-E_H/RT) \times 4.1195 AL(1-\phi) \gamma^{\frac{3}{4}} / r_s \tag{7.28}$$

That is:

$$\frac{q_i r_s O_{2c}}{\gamma^{\frac{3}{4}}} = \beta_o \exp(-E_H/RT) \tag{7.29}$$

where $\beta_o = 173.1338 AL(1-\phi) \alpha_H k_o^* P_{o_2}^{m_H}$

Equation 7.29 can be expressed in terms of β_H , as defined in Eq. 7.16, so that:

$$\frac{q_i r_s O_{2c}}{2.7464 \gamma^{\frac{3}{4}}} = \beta_H \exp(-E_H/RT) \tag{7.30}$$

7.2.2 Fuel in Non-Toroidal Part ($t < t_c$)

For $t < t_c$, the fuel surface area, S , consists of the surface area of the toroid, A_{total} , and that of the fuel deposited directly on the sand grain surface. The surface area, S , may be assumed to increase with decreasing temperature. The following exponential relationship has been postulated:

$$S = A_{total} \exp \left[a \left(\frac{1}{T} - \frac{1}{T_c} \right) \right] \tag{7.31}$$

7. NEW OXIDATION REACTION MODEL

where T_c is the temperature at time, t_c and a is a proportionality constant. Eq. 7.31 satisfies the required condition that at $t = t_c$, S is equal to the toroid surface area. Using the fuel surface area, S , as given in Eq. 7.31 in the reaction rate equation, Eq. 7.12, the following is obtained:

$$\frac{31.9988q_i O_{2c}}{60 \times 22.4138} = \alpha_H k_o^* P_{o_2}^{m_H} \exp(-E_H/RT) A_{total} \exp \left[a \left(\frac{1}{T} - \frac{1}{T_c} \right) \right] \quad (7.32)$$

Substituting for A_{total} from Eq. 7.26 into Eq. 7.32:

$$\frac{q_i r_s O_{2c}}{\gamma^{\frac{3}{4}}} = \beta \exp(-E/RT) \quad (7.33)$$

where:

$$\beta = 173.1338AL(1 - \phi)\alpha_H k_o^* P_{o_2}^{m_H} \exp(-a/T_c) \quad (7.34)$$

and:

$$E = E_H - aR \quad (7.35)$$

Equation 7.33 indicates that for $t < t_c$, a second straight line with slope, $-E/R$, and an intercept of $\ln \beta$ can be evaluated from a graph of the natural logarithm of the left hand side of Eq. 7.33 versus $1/T$. As discussed in Section 7.4.1, such a second straight line has been found, indicating that the postulate of Eq. 7.31 is acceptable. Equation 7.35 indicates the effect of a larger surface area is an apparently lower activation energy.

7.2.3 Calculation of Oxygen Consumption

The objective of the following calculations is to determine fuel height as a function of time. From Eq. 7.22:

$$\frac{9h_f}{4r_s^2} AL(1 - \phi)\rho_f \frac{dh_f}{dt} = -\frac{q_o(CO + CO_2)(12.0110 + x + 15.9994y)}{60 \times 22.4138} \quad (7.36)$$

From stoichiometry, Eq. 7.1:

$$q_o(CO + CO_2) = \frac{q_i O_{2c}}{(1 - m/2 + x/4 - y/2)} \quad (7.37)$$

7. NEW OXIDATION REACTION MODEL

From Eq. 7.30:

$$O_{2c} = \frac{2.7464\gamma^{\frac{3}{4}}}{q_i r_s} \beta_H \exp(-E_H/RT) \quad (7.38)$$

From Eq. 7.24:

$$\gamma = \frac{9h_f^2}{8r_s^2} \quad (7.39)$$

Substituting Eq. 7.39 into Eq. 7.38 yields:

$$O_{2c} = \frac{3h_f^{\frac{3}{2}}}{q_i r_s} \beta_H \exp(-E_H/RT) \quad (7.40)$$

Substituting Eqs. 7.40 and 7.37 into Eq. 7.36 yields:

$$\frac{1}{\sqrt{h_f}} \frac{dh_f}{dt} = -\kappa \exp(-E_H/RT) \quad (7.41)$$

where:

$$\kappa = \frac{9.9145 \times 10^{-4} \beta_H (12.0110 + x + 15.9994y)}{r_s^{\frac{1}{2}} (1 - m/2 + x/4 - y/2) AL(1 - \phi) \rho_f} \quad (7.42)$$

Integrating Eq. 7.41 from the start of oxidation, t_o (where $h_f = h_{f_o}$), to t (where $h_f = h_f$) yields:

$$h_f = \left[h_{f_o}^{\frac{1}{2}} - \frac{\kappa}{2} \int_{t_o}^t \exp(-E_H/RT) dt \right]^2 \quad (7.43)$$

Since $h_f = 0$ at the end of fuel oxidation, t_e :

$$h_{f_o} = \frac{\kappa}{2} \int_{t_o}^{t_e} \exp(-E_H/RT) dt \quad (7.44)$$

The integrals in Eqs. 7.43 and 7.44 were evaluated in the following manner. Assume T is linear with time between two data points at times, t_1 , and t_2 . That is:

$$T = a + bt \quad (7.45)$$

where:

$$b = \frac{T(t_1) - T(t_2)}{t_1 - t_2} \quad (7.46)$$

$$a = T(t_1) - bt_1 \quad (7.47)$$

7. NEW OXIDATION REACTION MODEL

Therefore:

$$\int_{t_1}^{t_2} \exp(-E_H/RT) dt = \int_{t_1}^{t_2} \exp\left[-\frac{E_H}{R(a+bt)}\right] dt \quad (7.48)$$

Let:

$$u = \frac{E_H}{R(a+bt)} \quad (7.49)$$

so that Eq. 7.48 becomes:

$$\begin{aligned} \int_{t_1}^{t_2} \exp(-E_H/RT) dt &= -\frac{E_H}{Rb} \int_{u_1}^{u_2} \frac{\exp(-u)}{u^2} du \\ &= -\frac{E_H}{Rb} \left\{ \left[-\frac{\exp(-u)}{u} \right]_{u_1}^{u_2} - \int_{u_1}^{u_2} \frac{\exp(-u)}{u} du \right\} \end{aligned} \quad (7.50)$$

The integral on the right hand side of Eq. 7.50 can be expressed as:

$$\int_{u_1}^{u_2} \frac{\exp(-u)}{u} du = \mathcal{E}_1(u_1) - \mathcal{E}_1(u_2) \quad (7.51)$$

$\mathcal{E}_1(u)$, the exponential integral of the first kind, is:

$$\mathcal{E}_1(u) = \int_u^\infty \frac{\exp(-u)}{u} du \quad (7.52)$$

Since $1 < u < \infty$, $\mathcal{E}_1(u)$ may be evaluated from the following expression (Abramowitz and Stegun 1972):

$$ue^u \mathcal{E}_1(u) = \frac{u^4 + a_1 u^3 + a_2 u^2 + a_3 u + a_4}{u^4 + b_1 u^3 + b_2 u^2 + b_3 u + b_4} + \delta \quad (7.53)$$

where:

$$\begin{aligned} a_1 &= 8.57333 & b_1 &= 9.57332 \\ a_2 &= 18.05902 & b_2 &= 25.63296 \\ a_3 &= 8.63476 & b_3 &= 21.09965 \\ a_4 &= 0.26777 & b_4 &= 3.95850 \end{aligned}$$

and the error term, δ , is less than 2×10^{-8} .

7. NEW OXIDATION REACTION MODEL

Substituting Eq. 7.51 into Eq. 7.50:

$$\int_{t_1}^{t_2} \exp(-E_H/RT) dt = -\frac{E_H}{Rb} \left[\frac{\exp(-u_1)}{u_1} - \frac{\exp(-u_2)}{u_2} - \mathcal{E}_1(u_1) + \mathcal{E}_1(u_2) \right] \quad (7.54)$$

Thus, the left hand integral of Eq. 7.54 can be solved, which on substitution into Eq. 7.43 yields h_f as a function of time. Having obtained h_f , the oxygen consumption curve for fuel oxidation can be computed using Eq. 7.40.

7.3 LTO Reaction Model

For LTO reactions, the fuel surface area was assumed constant and the reactions followed the Arrhenius rate law (Eq. 6.27). At $t = 0$, the concentration of oxygenated fuel, $C_L = 0$. This requires the exponential term in Eq. 6.27 to be positive. That is:

$$\frac{q_i O_{2c}}{AL} = A_r P_{o_2}^{m_L} C_L^{n_L} \exp(E_L/RT) \quad (7.55)$$

Rate of change of fuel concentration with time was based on Eq. 7.10. During LTO, the oxygenated fuel concentration increases with time. The right hand side of Eq. 7.10 is therefore positive. That is:

$$\frac{q_i O_{2c}}{AL} = \alpha_L \frac{dC_L}{dt} \quad (7.56)$$

Integrating Eq. 7.56 from $t = 0$ to $t = t$, where $C_L = 0$ at $t = 0$, results in:

$$C_L = \frac{q_i}{\alpha_L AL} \int_0^t O_{2c} dt \quad (7.57)$$

Substituting for C_L from Eq. 7.55 into Eq. 7.57 yields:

$$\frac{O_{2c}}{\left[\int_0^t O_{2c} dt \right]^{n_L}} = \beta_L \exp(E_L/RT) \quad (7.58)$$

7. NEW OXIDATION REACTION MODEL

where:

$$\beta_L = \left(\frac{q_i}{AL} \right)^{n_L-1} \frac{A_r P_{o_2}^{n_L}}{\alpha_L^{n_L}} \quad (7.59)$$

A graph of the natural logarithm of the left hand side of Eq. 7.58 should yield a straight line with a slope of E_L/R and an intercept of $\ln \beta_L$ for the correct exponent, n_L .

From the definition of derivatives and integrals, and since $O_{2c} = 0$ at $t = 0$:

$$O_{2c} = \frac{d}{dt} \left(\int_0^t O_{2c} dt \right) \quad (7.60)$$

Substituting Eq. 7.60 in Eq. 7.58:

$$\frac{d \left(\int_0^t O_{2c} dt \right)}{\left[\int_0^t O_{2c} dt \right]^n} = \beta_L \exp(E_L/RT) dt \quad (7.61)$$

Integrating Eq. 7.61 from $t = t_1$ to $t = t_2$:

$$\left[\int_0^{t_2} O_{2c} dt \right]^{1-n_L} - \left[\int_0^{t_1} O_{2c} dt \right]^{1-n_L} = (1 - n_L) \beta_L \int_{t_1}^{t_2} \exp(E_L/RT) dt \quad (7.62)$$

From Eq. 7.58:

$$\left[\int_0^t O_{2c} dt \right]^{1-n_L} = \left[\frac{O_{2c}}{\beta_L \exp(E_L/RT)} \right]^{\frac{1-n_L}{n_L}} \quad (7.63)$$

Substituting Eq. 7.63 for $t = t_1$ and $t = t_2$ in Eq. 7.62 yields:

$$\begin{aligned} O_{2c}(t_2) = \beta_L \exp(E_L/RT_2) & \left\{ \left[\frac{O_{2c}(t_1)}{\beta_L \exp(E_L/RT_1)} \right]^{\frac{1-n_L}{n_L}} \right. \\ & \left. + (1 - n) \beta_L \int_{t_1}^{t_2} \exp(E_L/RT) dt \right\}^{\frac{n_L}{1-n_L}} \end{aligned} \quad (7.64)$$

The integral in Eq. 7.64 was evaluated as follows.

Let:

$$T = a + bt$$

where:

$$b = \frac{T(t_2) - T(t_1)}{t_2 - t_1} \quad (7.65)$$

7. NEW OXIDATION REACTION MODEL

$$a = T(t_2) - bt_2 \quad (7.66)$$

Therefore:

$$\int_{t_1}^{t_2} \exp(E_L/RT) dt = \int_{t_1}^{t_2} \exp\left(\frac{E_L}{R(a+bt)}\right) dt \quad (7.67)$$

Let:

$$u = -\frac{E_L}{R(a+bt)} \quad (7.68)$$

so that:

$$\int_{t_1}^{t_2} \exp(E_L/RT) dt = \frac{E_L}{Rb} \int_{u_1}^{u_2} \frac{\exp(-u)}{u^2} du \quad (7.69)$$

The integral in Eq. 7.69 can not be evaluated using exponential integrals of the first kind since $u < 0$. Instead, the following method was used.

$$\begin{aligned} \int_{u_1}^{u_2} \frac{\exp(-u)}{u^2} du &= \int_{u_1}^{u_2} \frac{\exp(-u) \exp(u_2)}{u^2 \exp(u_2)} du \\ &= \frac{1}{\exp(u_2)} \int_{u_1}^{u_2} \frac{\exp(-u + u_2)}{u^2} du \end{aligned} \quad (7.70)$$

In the interval $u = u_1$ to $u = u_2$, the argument, $-u + u_2$, in Eq. 7.70 is small and positive. Expressing the integrand as a series expansion:

$$\begin{aligned} u^{-2} e^{-u+u_2} &= u^{-2} \left[1 + (-u + u_2)^2 + (-u + u_2)^3 + \dots \right] \\ &\approx 1 + 3u_2 - u - \frac{1}{u} (1 + 2u_2 + 3u_2^2) + \frac{1}{u^2} (1 + u_2 + u_2^2 + u_2^3) \end{aligned} \quad (7.71)$$

Integrating Eq. 7.71:

$$\begin{aligned} \int_{u_1}^{u_2} \frac{\exp(-u + u_2)}{u^2} du &= (1 + 3u_2)(u_2 - u_1) - \frac{1}{2}(u_2^2 - u_1^2) \\ &\quad - (1 + 2u_2 + 3u_2^2) \ln(u_2/u_1) \\ &\quad - (1 + u_2 + u_2^2 + u_2^3)(1/u_2 - 1/u_1) \end{aligned} \quad (7.72)$$

Substituting Eqs. 7.70 and 7.72 into Eq. 7.69 gives:

7. NEW OXIDATION REACTION MODEL

$$\int_{t_1}^{t_2} \exp(E_f/RT) dt = \frac{E_f}{Rb \exp(u_2)} [(1 + 3u_2)(u_2 - u_1) - \frac{1}{2}(u_2^2 - u_1^2) - (1 + 2u_2 + 3u_2^2) \ln(u_2/u_1) - (1 + u_2 + u_2^2 + u_2^3)(1/u_2 - 1/u_1)] \quad (7.73)$$

Using Eqs. 7.73 and 7.64, the oxygen consumption curve for an LTO reaction can be computed in a step-wise manner.

7.4 Verification of Oxidation Reaction Model

The varying-fuel-geometry model for HTO and the new LTO model constitute the new oxidation reaction model. The steps involved and the computer programs (Appendix) written to facilitate the analysis are summarized as follows.

1. Plot an Arrhenius graph for HTO using program HTO.F. Determine E_H , β_H and t_c .
2. Using program HTOFIT.F, calculate fuel height versus time, generate the oxygen consumption curve for HTO, and subtract this curve from the data to obtain the LTO oxygen consumption curve.
3. Plot an Arrhenius graph for LTO using program LTO.F. Determine E_L and β_L .
4. Using program LTOFIT.F, calculate the oxygen consumption curve for LTO, and add the calculated oxygen consumption curves for LTO and HTO to obtain the total oxygen consumption curve.

The new oxidation reaction model was tested against the results of kinetic tube experiments using carbon and crude oils. Carbon runs were made in order to minimize uncertainty with regard to fuel composition and activation energy.

7. NEW OXIDATION REACTION MODEL

7.4.1 Verification with Carbon Runs

The gas composition and temperature data for carbon Run C3 are presented in Fig. 7.5. One oxidation reaction peak at about 470°C was observed. As expected, the atomic H/C ratio for carbon was zero (Fig. 7.6). The Arrhenius graph for the oxidation reaction is shown in Fig. 7.7. Two straight-line trends were observed indicating the presence of two fuel geometries. Using the slopes and intercepts on the y-axis of the fitted straight lines, the data points were normalized to produce one straight line. From the slope of this straight line, the activation energy was determined to be 157 KJ/mol. This value agreed closely with those obtained for carbon by Massoth (1966) and Butt (1972), 150-170 KJ/mol. Figure 7.8 presents the calculated fuel height as a function of time. At the onset of oxidation, the fuel height begins to decrease sharply and is zero at the end of oxidation. In addition, $r_s > 7h_f$, satisfying the condition for approximation expressed by Eq. 7.21. The calculated oxygen consumption curve is shown in Fig 7.9. A satisfactory match was obtained with experimental data.

A repeat carbon experiment (Run C4) was made (Fig. 7.10). Based on the Arrhenius graph (Fig. 7.11), the activation energy was determined to be 159 KJ/mol. Oxygen consumption results based on the new model are shown in Fig. 7.12. A satisfactory match between the calculated oxygen consumption curve and experimental data was also obtained for this run.

7.4.2 Verification with Crude Oil Runs

The new oxidation reaction model was tested against the results of kinetic tube experiments using three crude oils: Cold Lake bitumen, Hamaca crude oil and Huntington Beach oil (Section 6.1). Analysis of Cold Lake bitumen Run CL5 is used as an example.

7. NEW OXIDATION REACTION MODEL

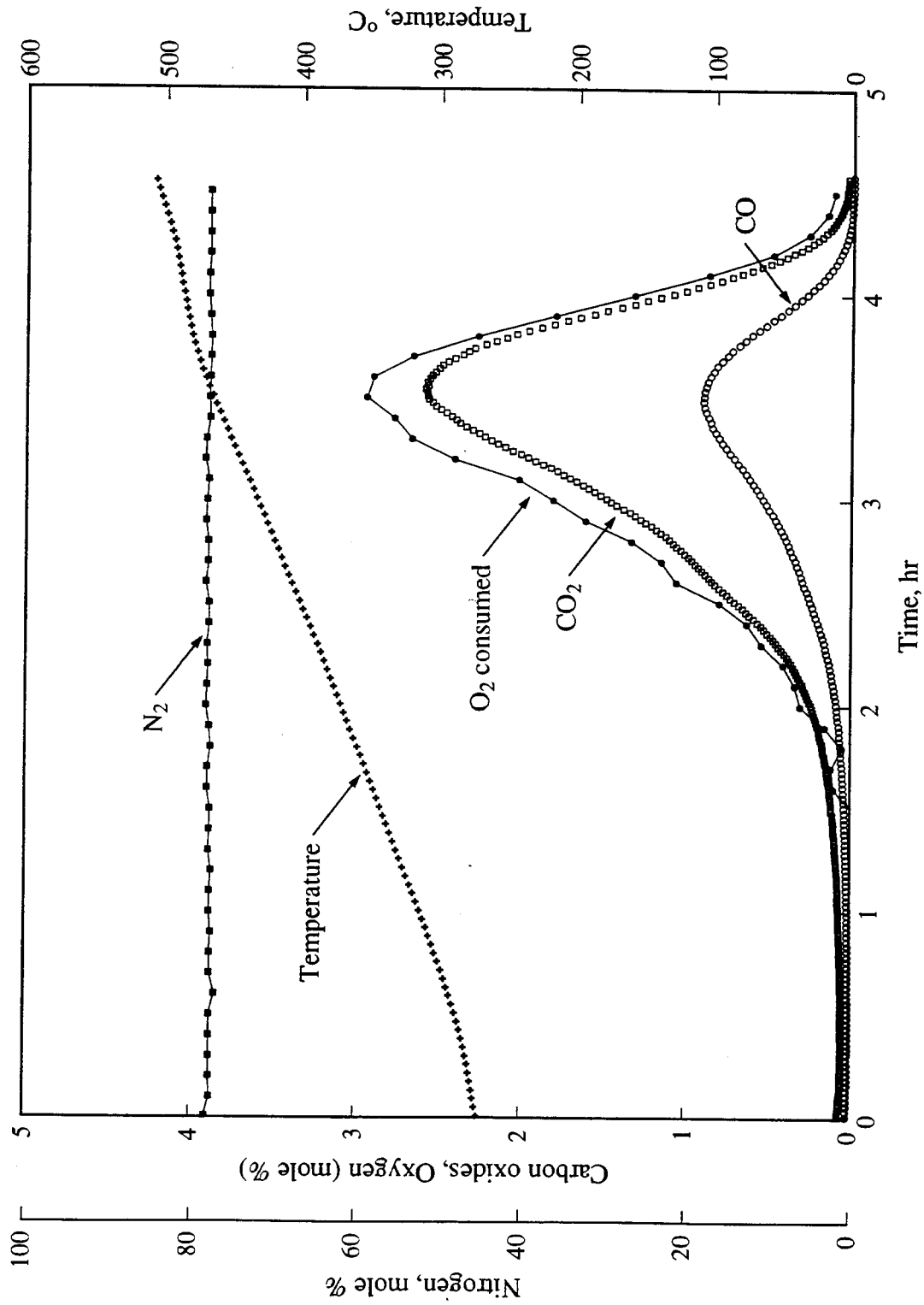


Figure 7.5: Produced Gas Composition and Temperature Versus Time (Run C3)

7. NEW OXIDATION REACTION MODEL

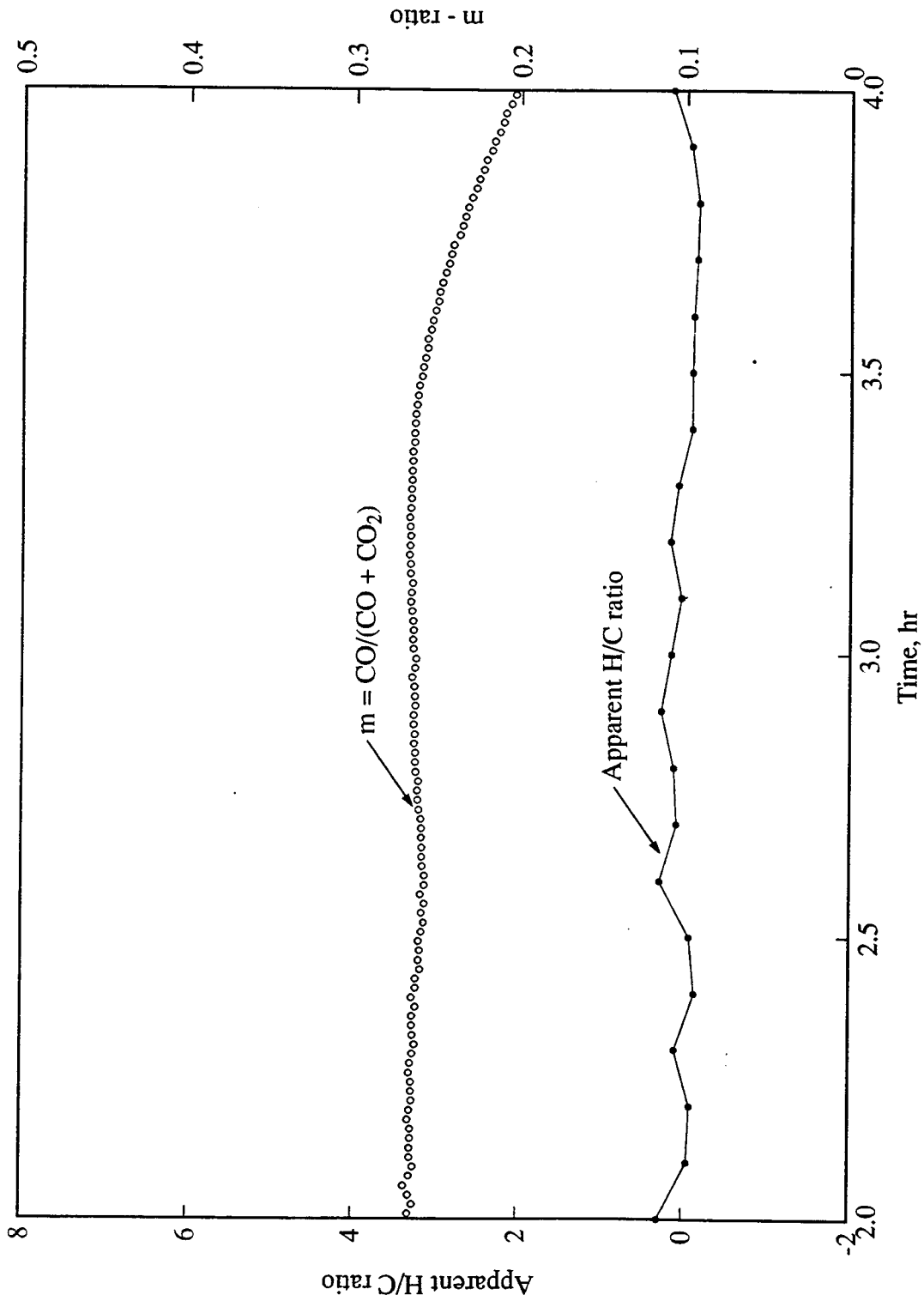


Figure 7.6: Apparent H/C and m-Ratios Versus Time (Run C3)

7. NEW OXIDATION REACTION MODEL

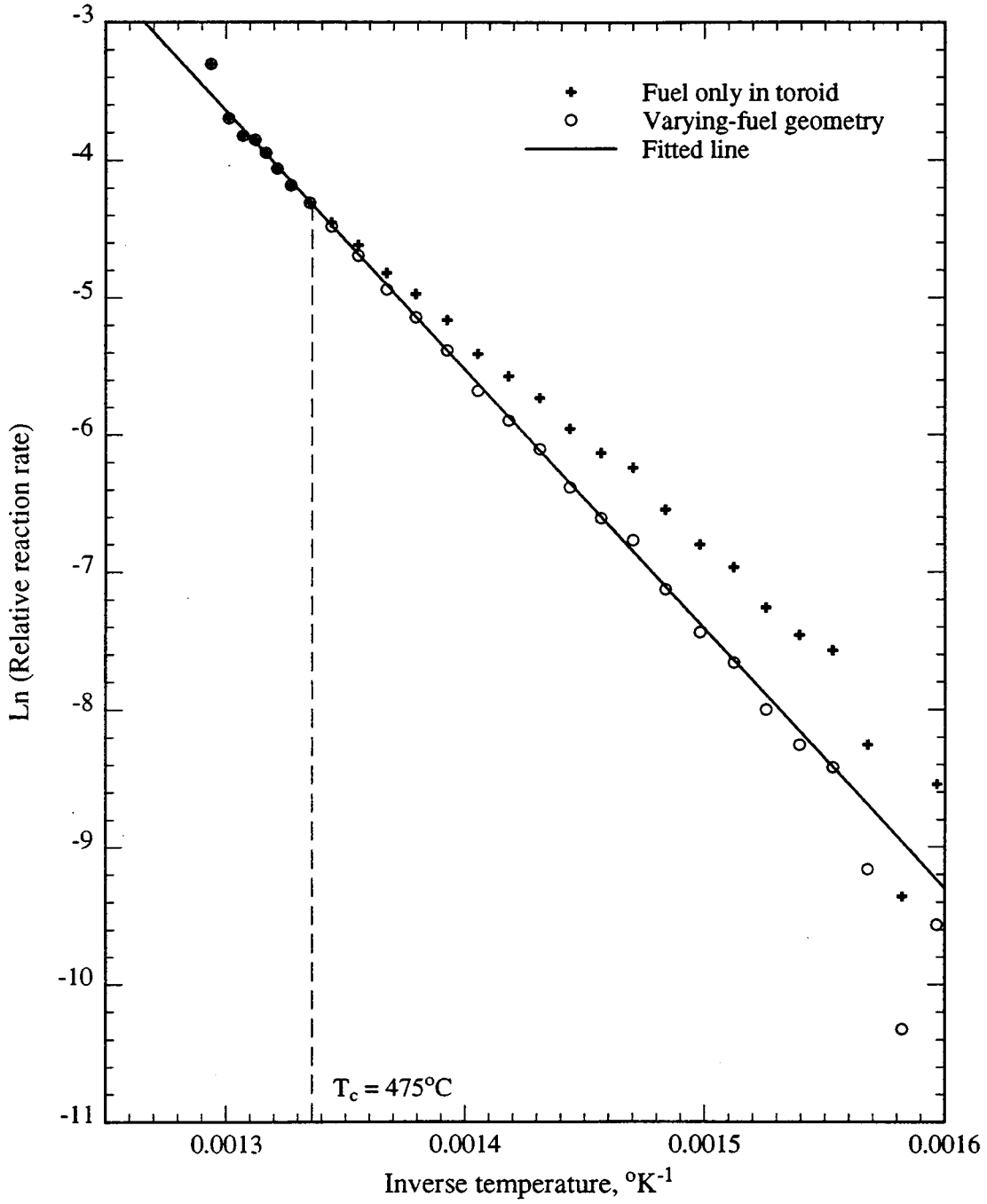


Figure 7.7: Arrhenius Graph (Run C3)

7. NEW OXIDATION REACTION MODEL

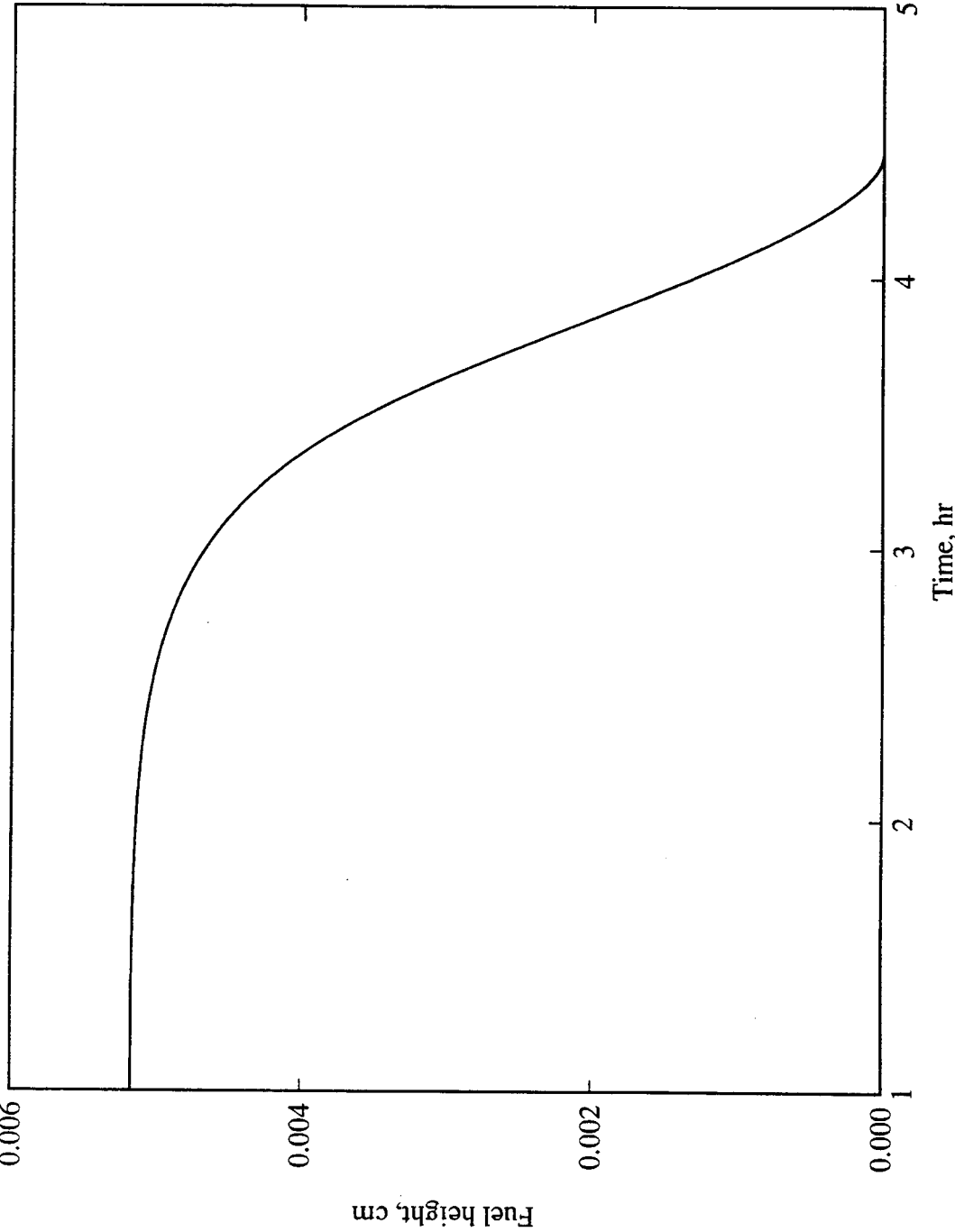


Figure 7.8: Fuel Height Versus Time (Run C3)

7. NEW OXIDATION REACTION MODEL

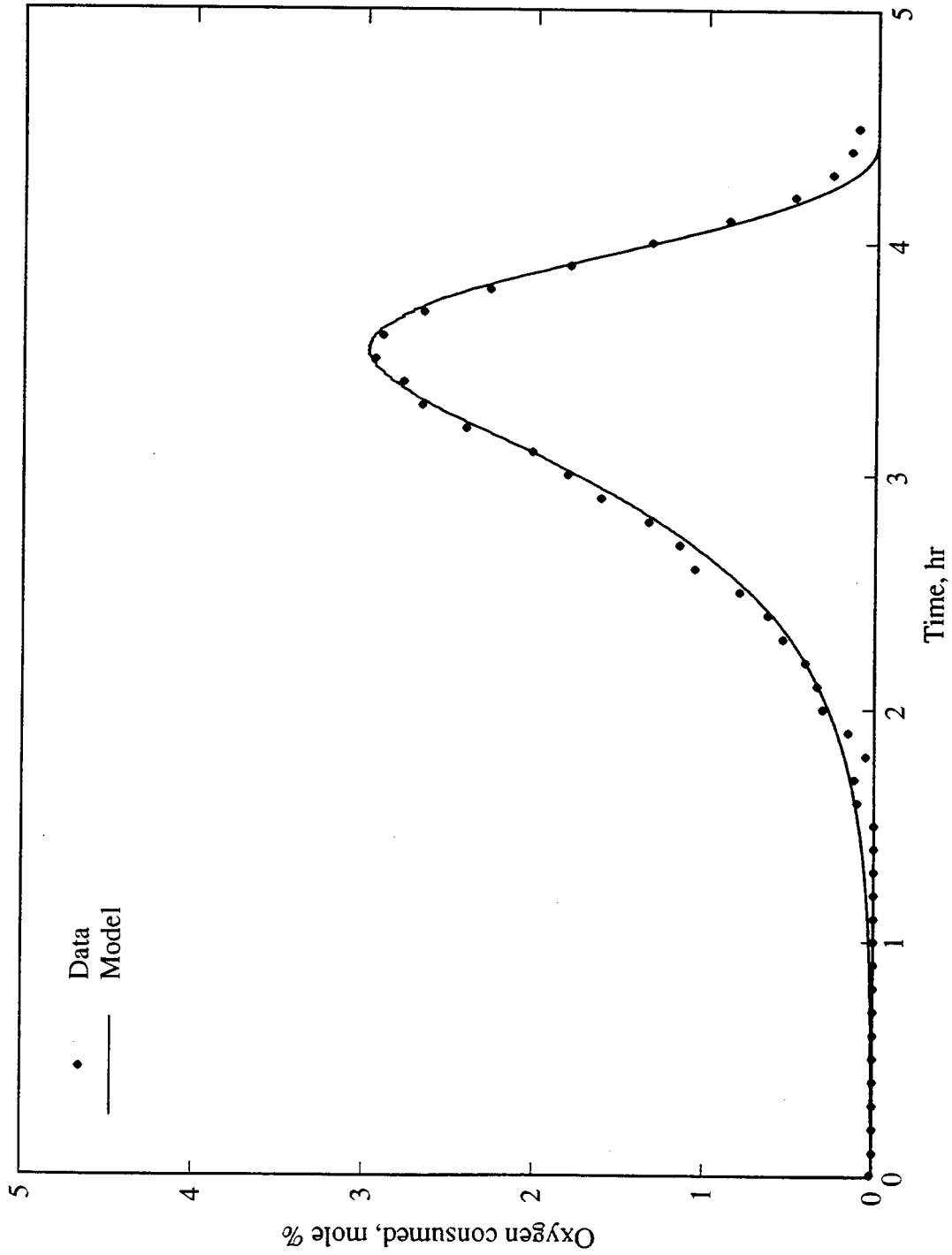


Figure 7.9: Oxygen Consumption - Model Results and Data (Run C3)

7. NEW OXIDATION REACTION MODEL

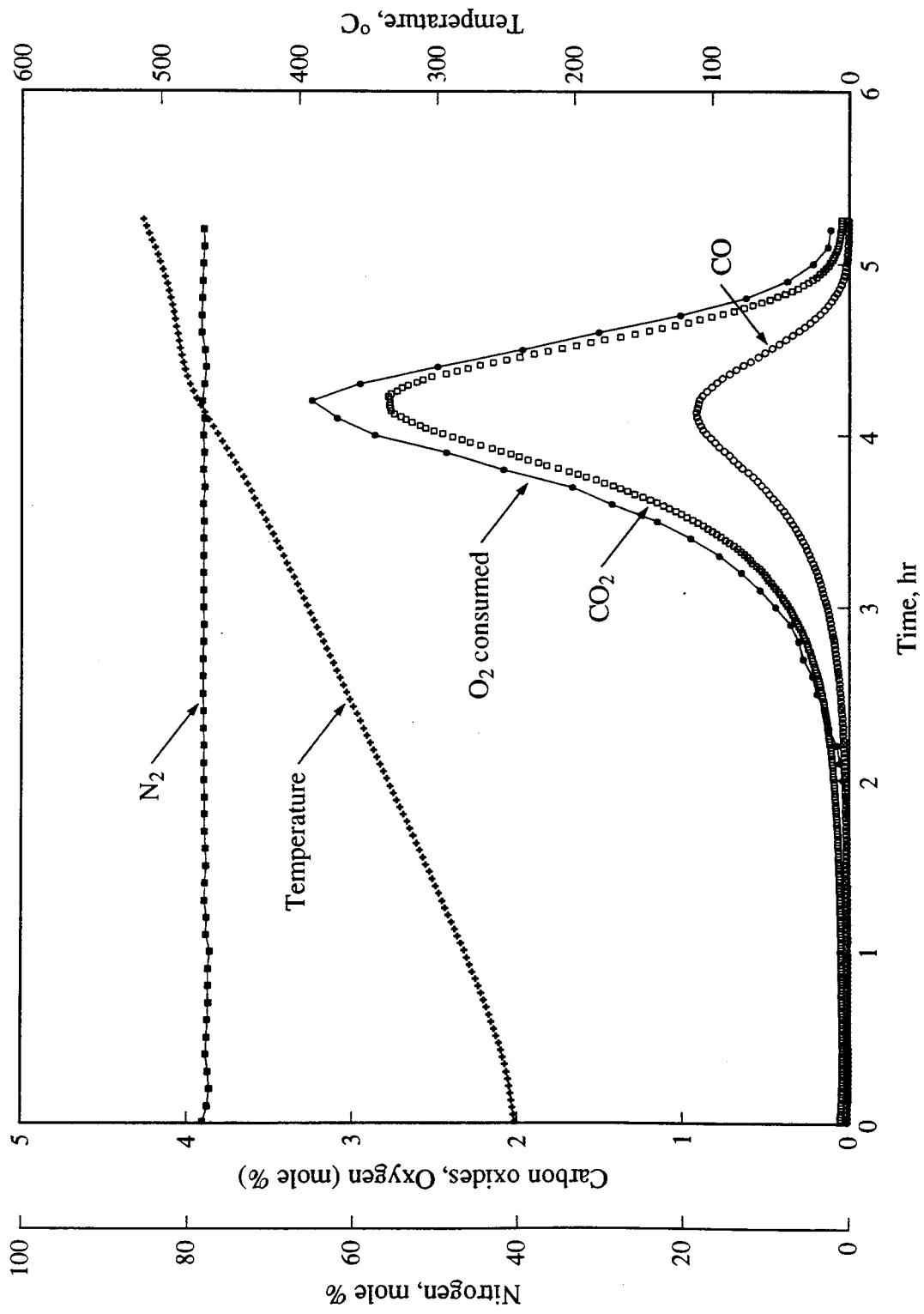


Figure 7.10: Produced Gas Composition and Temperature Versus Time (Run C4)

7. NEW OXIDATION REACTION MODEL

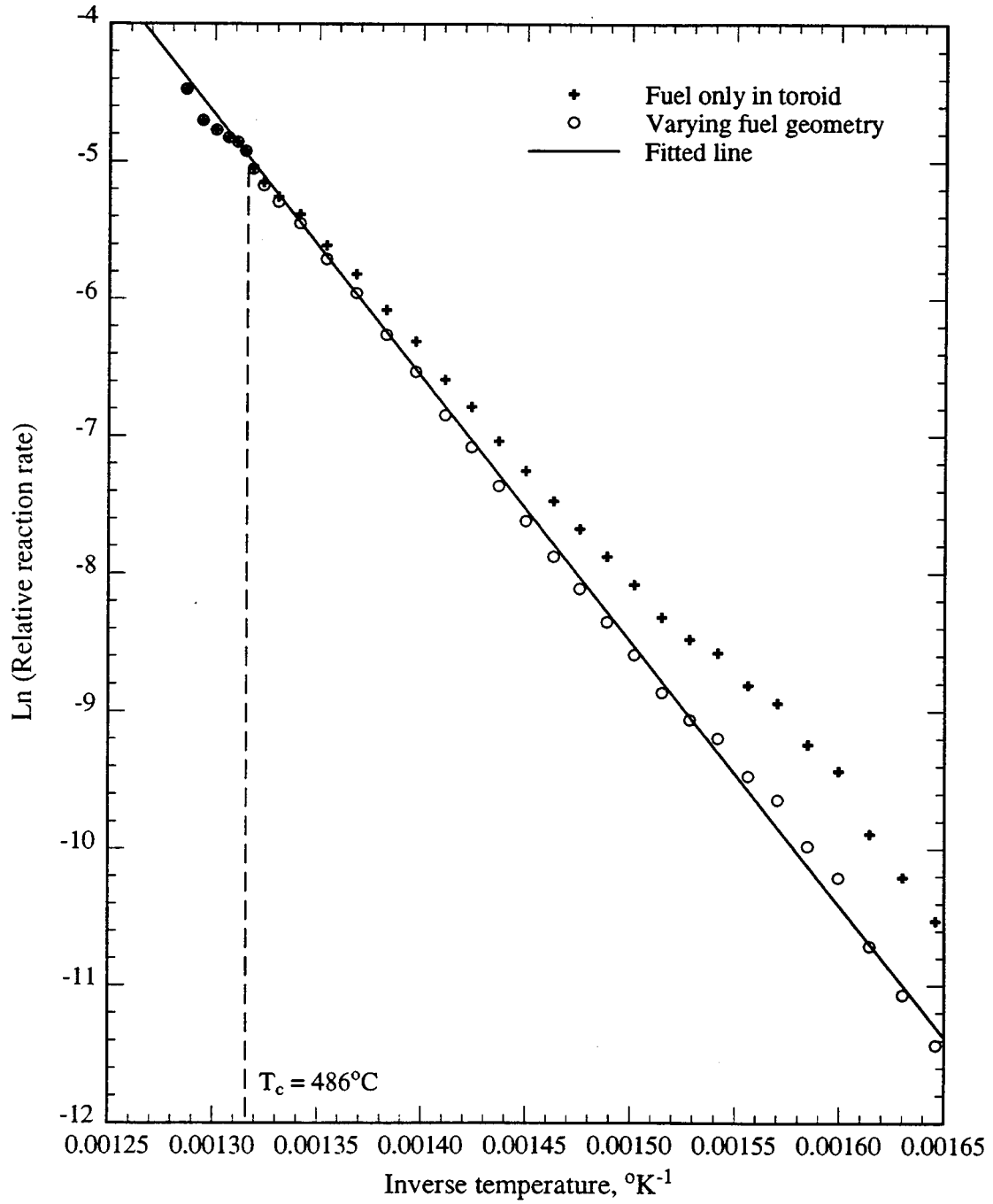


Figure 7.11: Arrhenius Graph (Run C4)

7. NEW OXIDATION REACTION MODEL

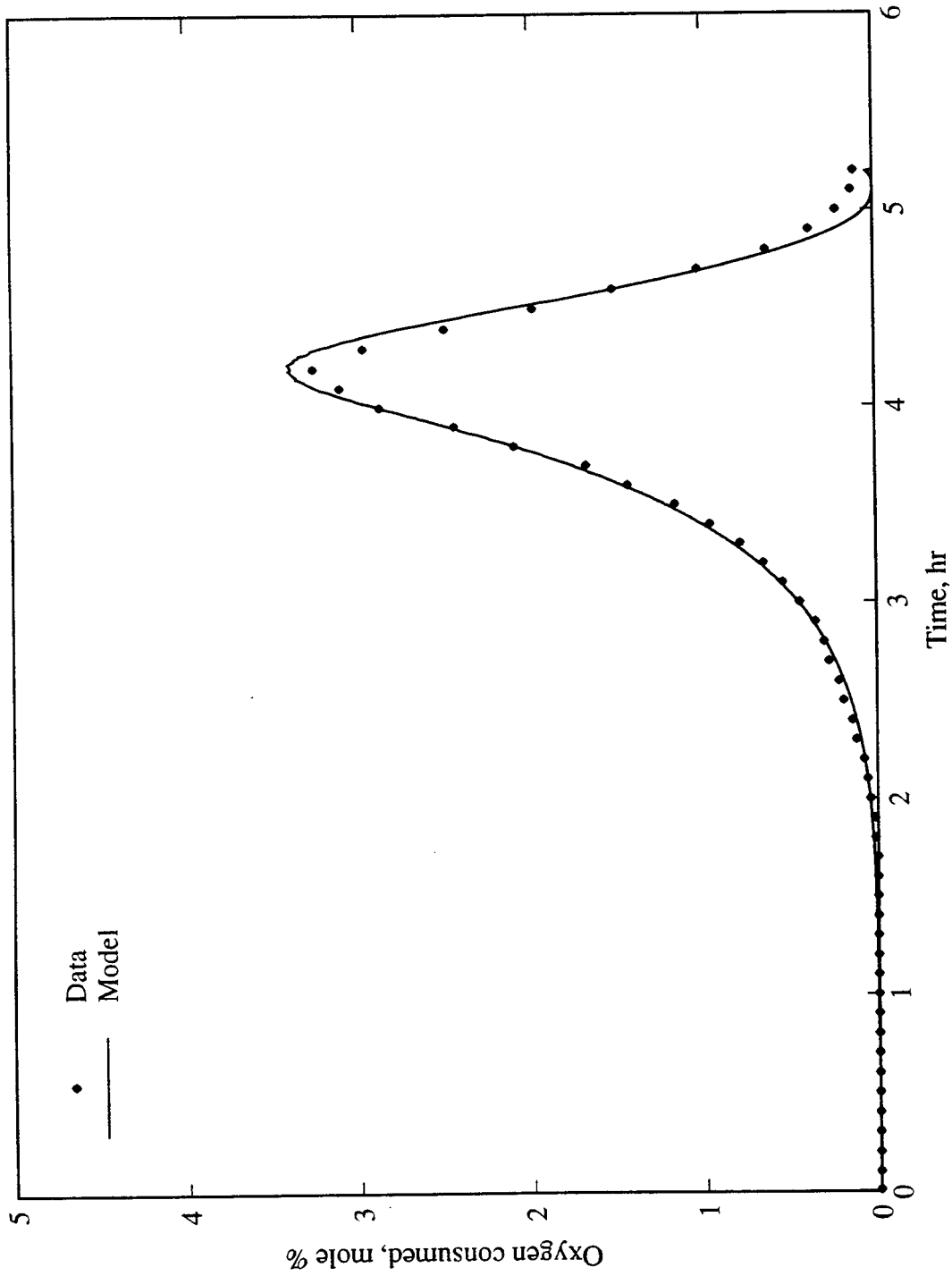


Figure 7.12: Oxygen Consumption - Model Results and Data (Run C4)

7. NEW OXIDATION REACTION MODEL

The Arrhenius graph for HTO is shown in Fig. 7.13. As in the carbon runs (Section 7.4.1), data following two straight-line trends were normalized to fall onto one straight line. The activation energy for HTO was determined from the slope of this straight line. The calculated fuel height versus time is shown in Fig. 7.14. The fuel height begins to decrease sharply near the start of HTO. The calculated oxygen consumption curve for HTO is compared with the experimental data in Fig. 7.15. The LTO data were obtained by subtracting the calculated oxygen consumption curve from the experimental data. The Arrhenius graph for LTO is shown in Fig. 7.16. The LTO data was fit to a straight line, and the activation energy was obtained from its slope. The oxygen consumption curve for LTO is plotted in Fig. 7.17, which indicates a good match between the calculated values and experimental data. Adding the calculated LTO and HTO curves, the calculated total oxygen consumption curve was obtained. This result is shown in Fig. 7.18. The calculated and experimental values were in good agreement.

HTO and LTO Arrhenius graphs and the calculated oxygen consumption curves for the other kinetic tube runs are presented in Figs. 7.19 - 7.33. Satisfactory matches between calculated values and experimental data were obtained. The kinetic parameters obtained are shown in Table 7.2. The following observations were made.

- The average activation energy for carbon oxidation, 158 KJ/mol, agreed closely with values obtained by Massoth (1966) and Butt (1972), 150–170 KJ/mol, helping to verify the varying-fuel-geometry model.
- HTO activation energy for Cold Lake bitumen, average 184 KJ/mol, was higher than that for Hamaca crude oil (averaging 146 KJ/mol) and Huntigton Beach oil (158 KJ/mol) indicating the lower reactivity of Cold Lake bitumen. This may be a reason for the less stable combustion tube Run CL13 using Cold Lake bitumen compared to tube runs using Hamaca crude oil (Chapter 5).

7. NEW OXIDATION REACTION MODEL

- For a particular crude oil, the LTO activation energy was generally lower than the HTO activation energy. LTO reaction orders ranged from 1.5 to 2.0.
- No relationship could be established between any of the kinetic parameters and the crude oil gravity.

Table 7.2: Kinetic Parameters Obtained From Experiments

Run No.	E_H (KJ/mol)	β_H (sec ⁻¹)	E_L (KJ/mol)	β_L (sec ⁻¹)	n_L
C3	157	1.2×10^9	-	-	-
C4	159	0.6×10^9	-	-	-
CL2	183	3.6×10^{11}	108	3.6×10^{-15}	1.5
CL5	149	0.7×10^9	123	1.3×10^{-17}	2.0
CL14	219	9.5×10^{11}	146	5.8×10^{-20}	2.0
HBO2	158	2.7×10^9	78	2.0×10^{-12}	1.5
VEN6	150	5.7×10^6	143	8.6×10^{-20}	2.0
VEN23	141	1.6×10^6	162	2.6×10^{-21}	2.0

7. NEW OXIDATION REACTION MODEL

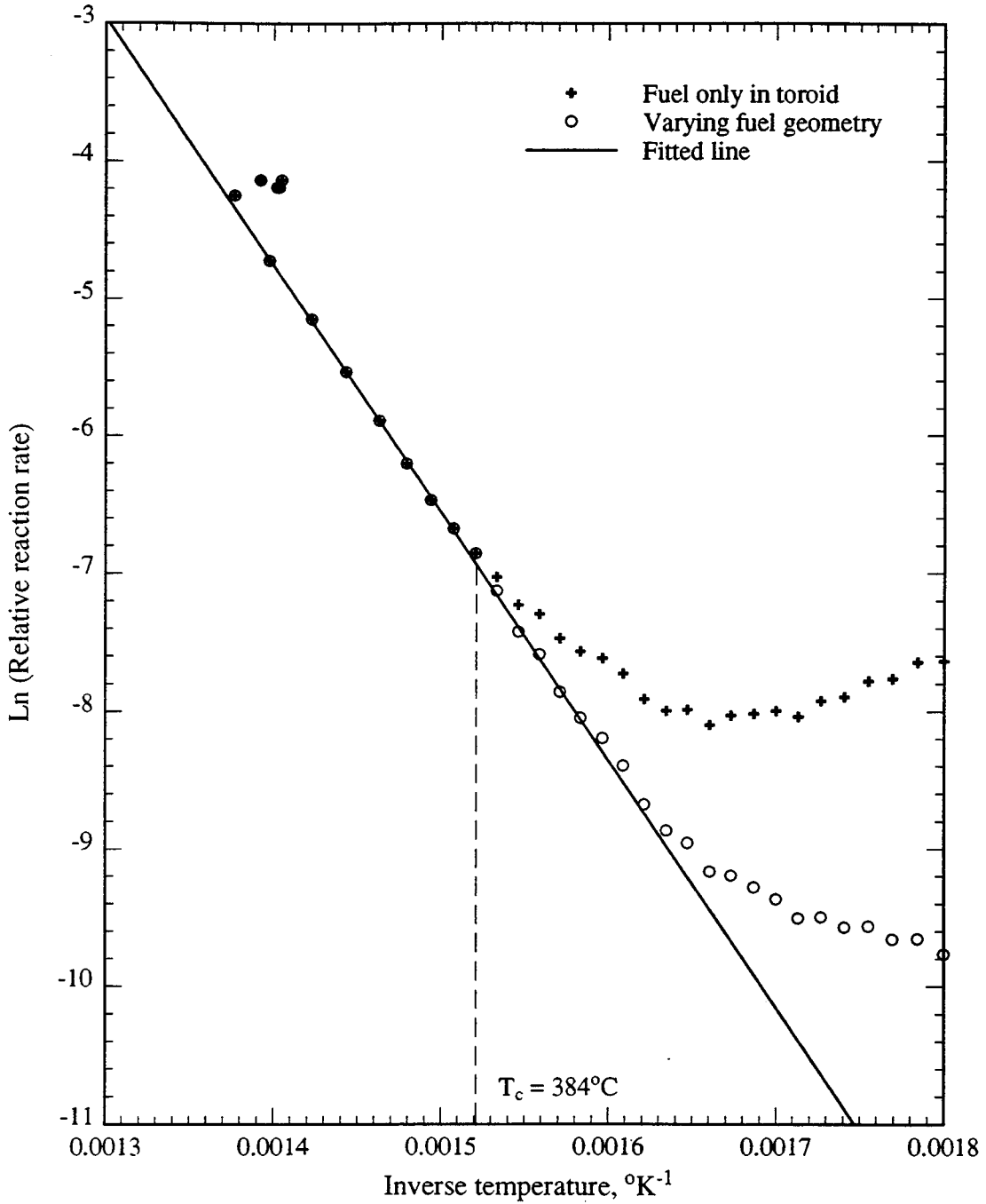


Figure 7.13: Arrhenius Graph for HTO Data (Run CL5)

7. NEW OXIDATION REACTION MODEL

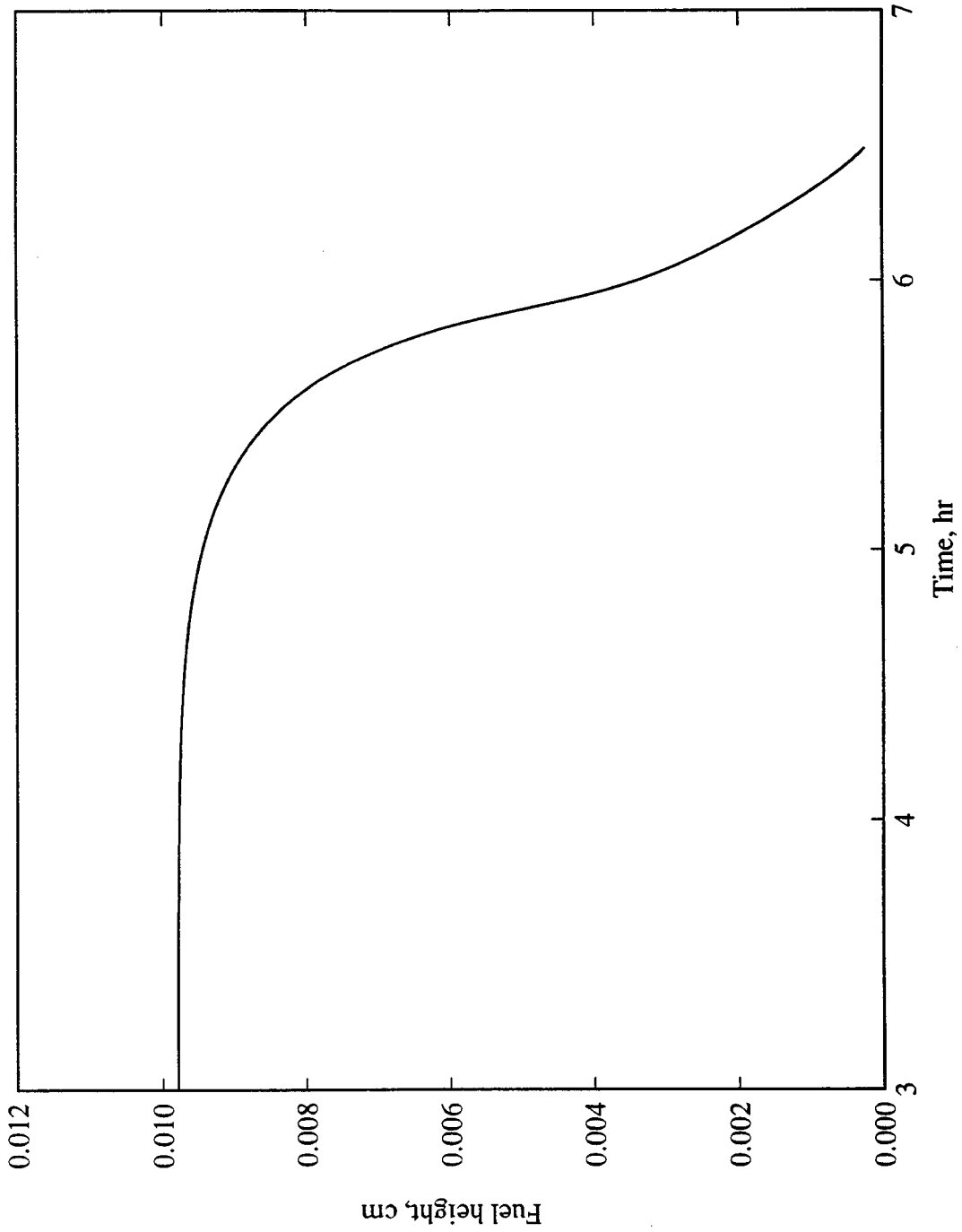


Figure 7.14: Fuel Height Versus Time (Run CL5)

7. NEW OXIDATION REACTION MODEL

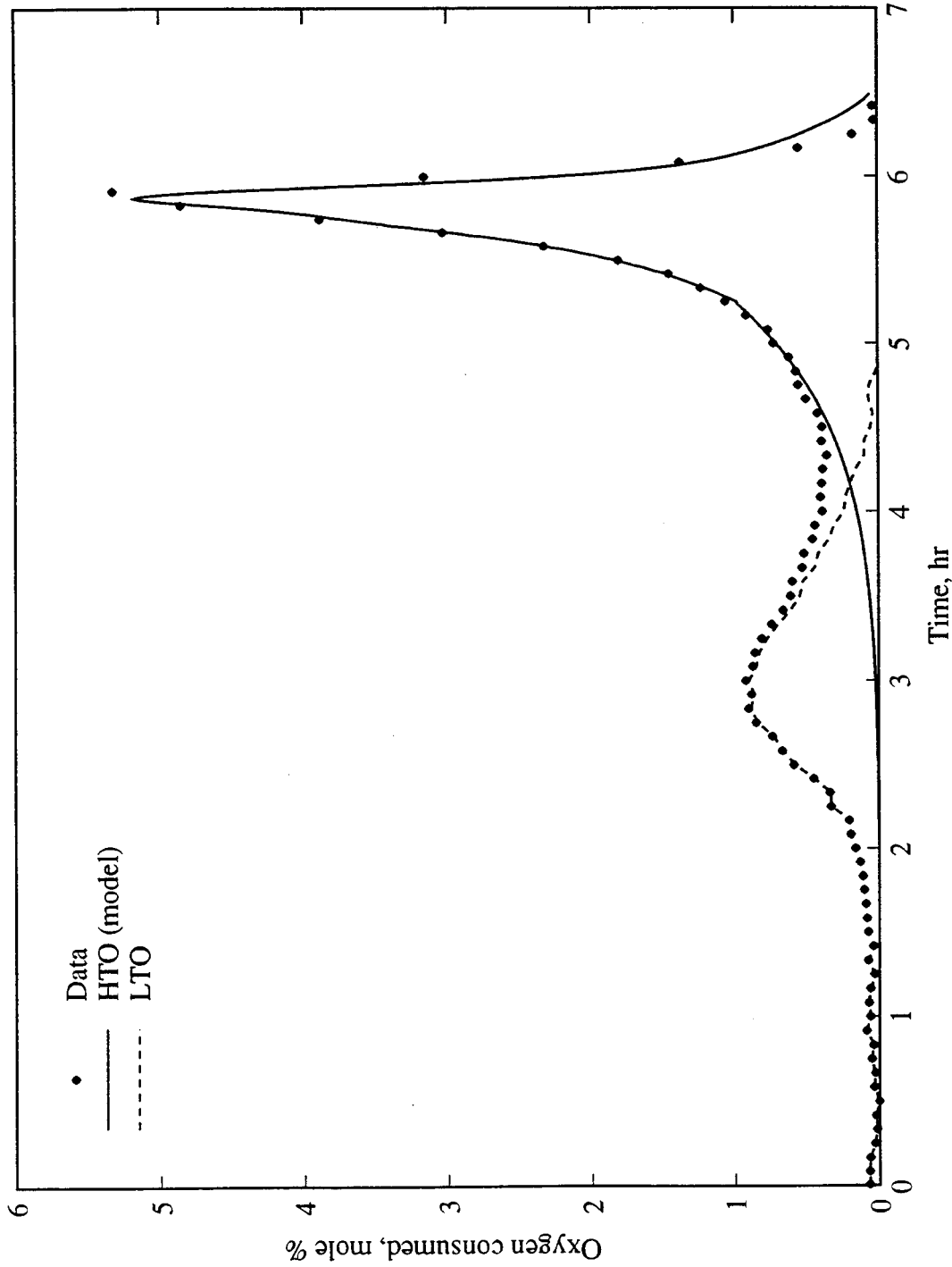


Figure 7.15: Oxygen Consumption at HTO - Model Results and Data (Run CL5)

7. NEW OXIDATION REACTION MODEL

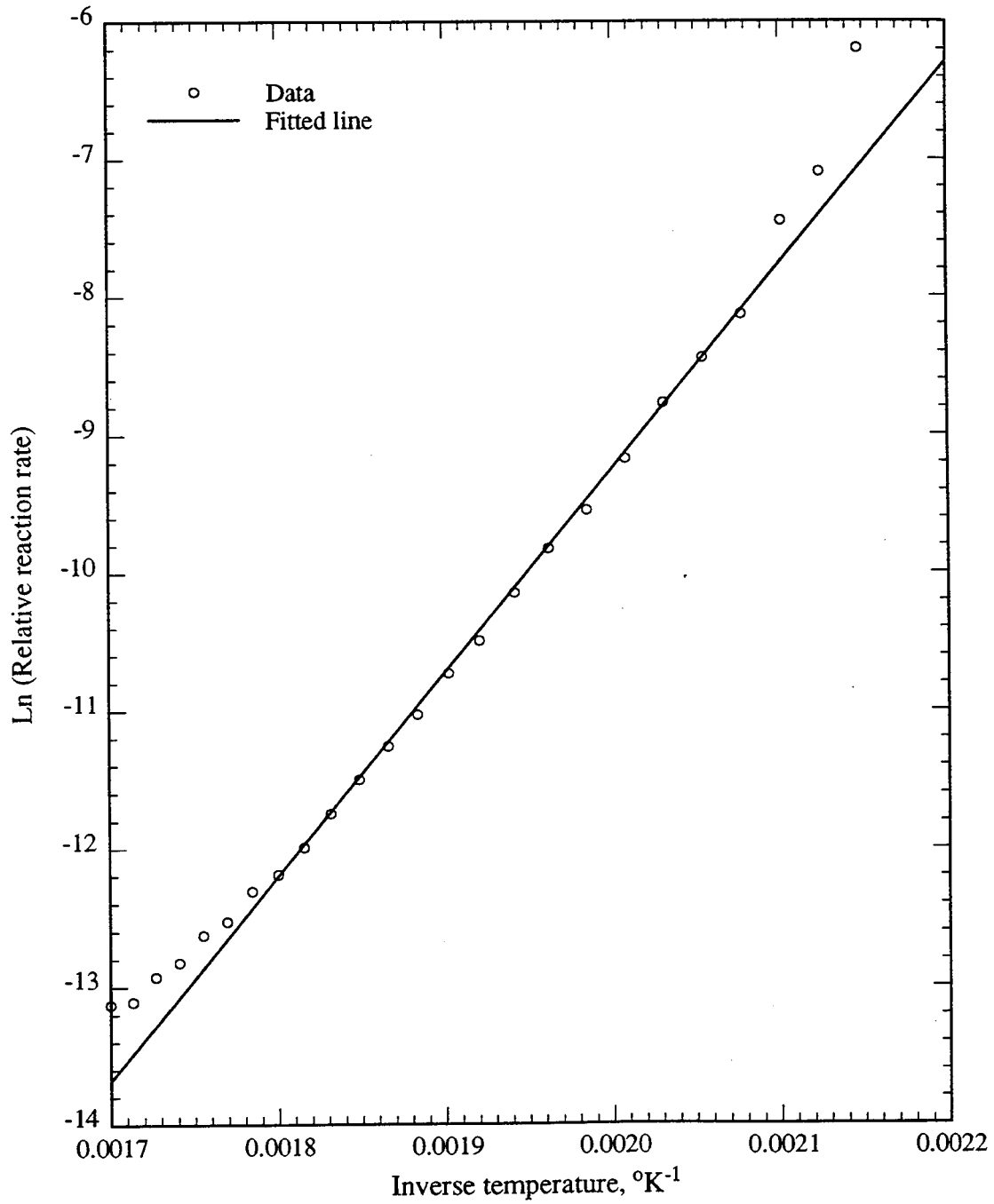


Figure 7.16: Arrhenius Graph for LTO Data (Run CL5)

7. NEW OXIDATION REACTION MODEL

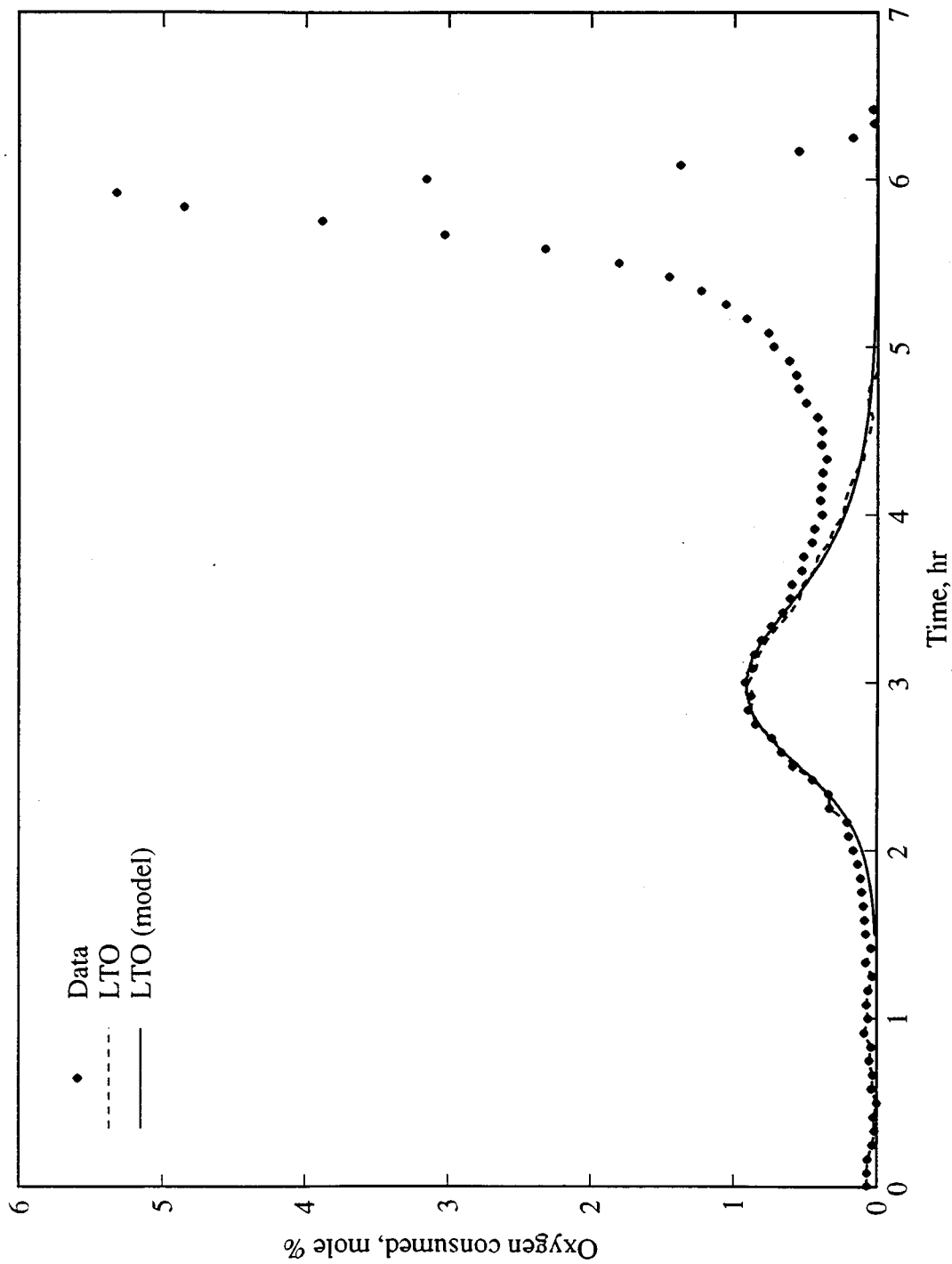


Figure 7.17: Oxygen Consumption at LTO - Model Results and Data (Run CL5)

7. NEW OXIDATION REACTION MODEL

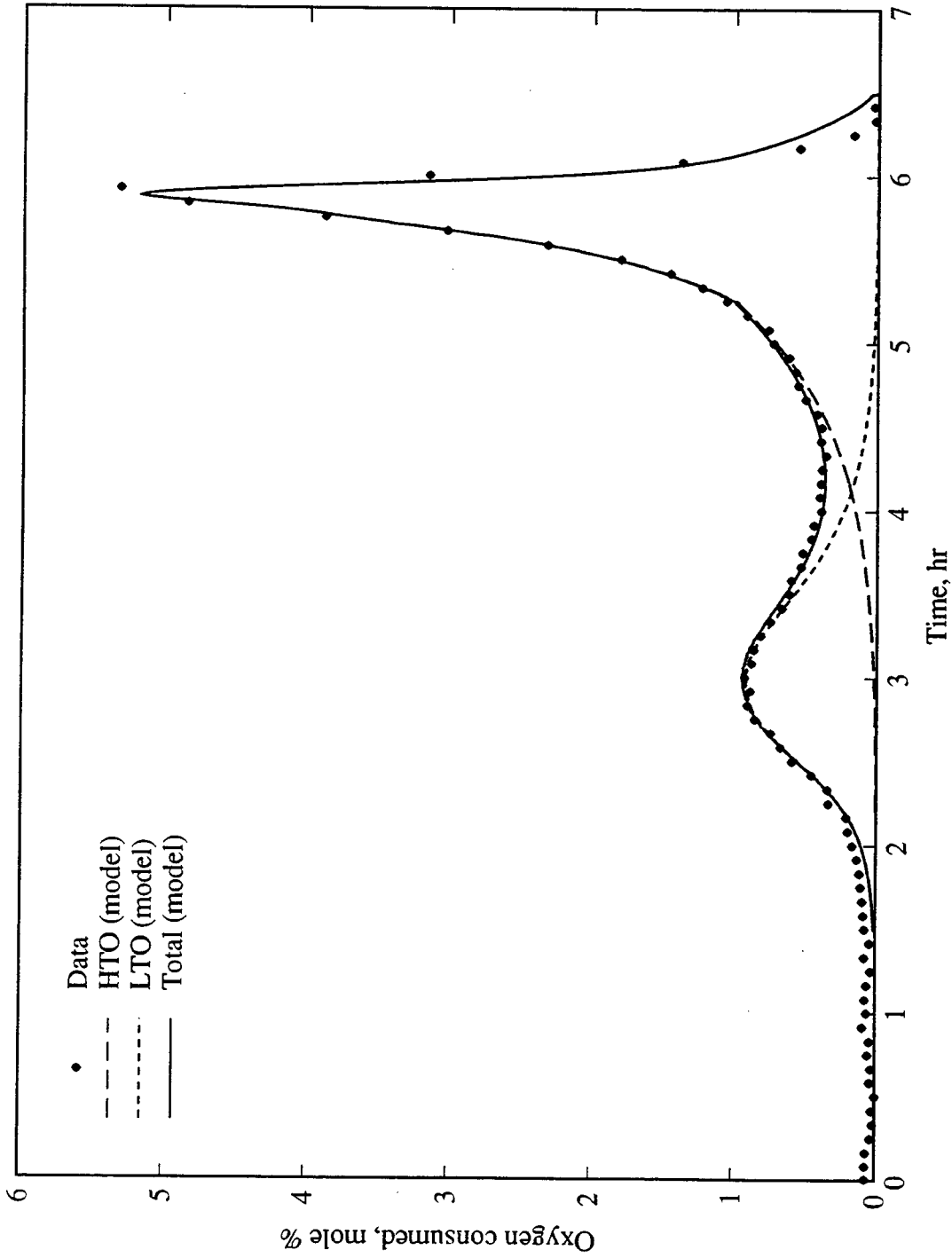


Figure 7.18: Oxygen Consumption - Model Results and Data (Run CL5)

7. NEW OXIDATION REACTION MODEL

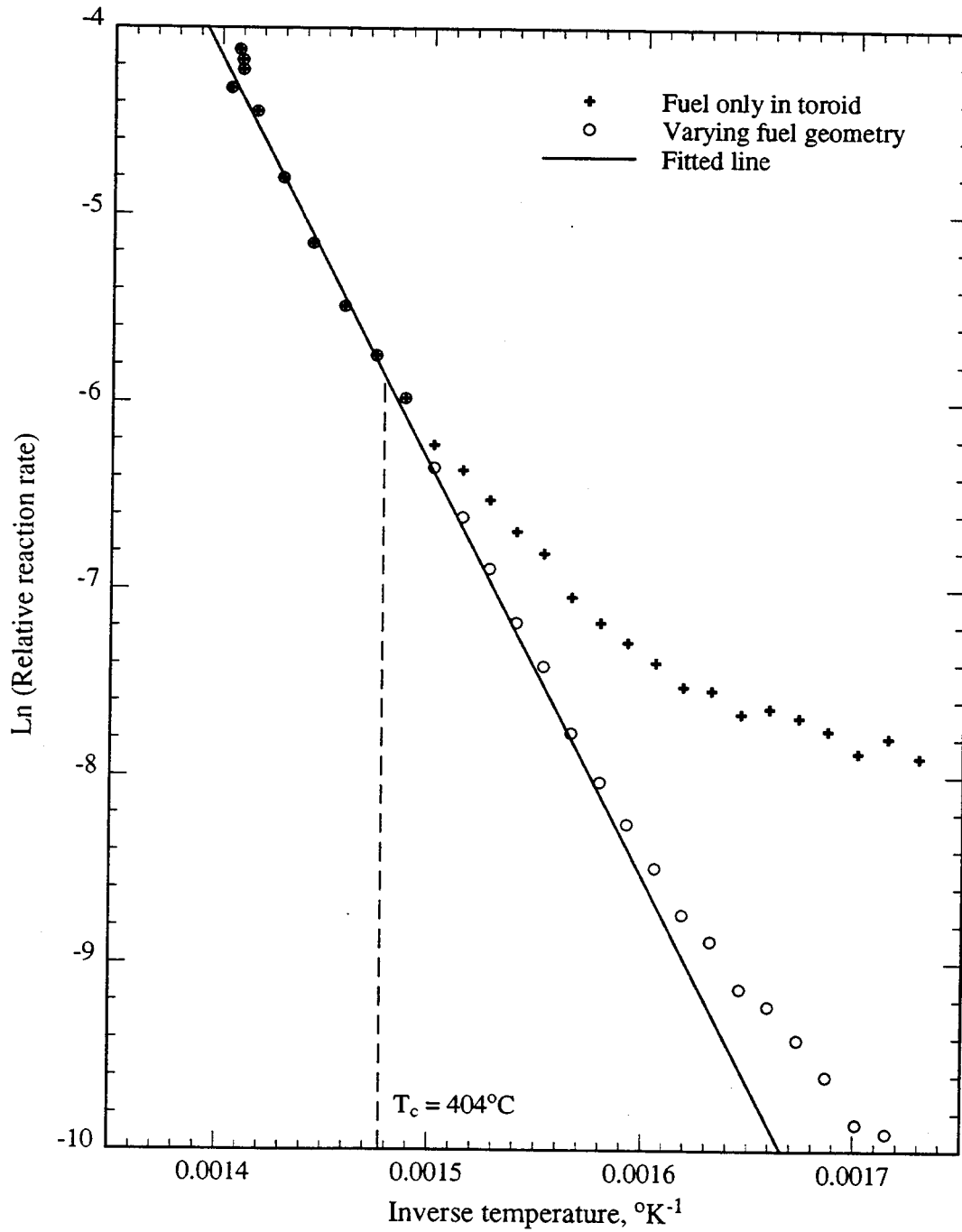


Figure 7.19: Arrhenius Graph for HTO Data (Run CL2)

7. NEW OXIDATION REACTION MODEL

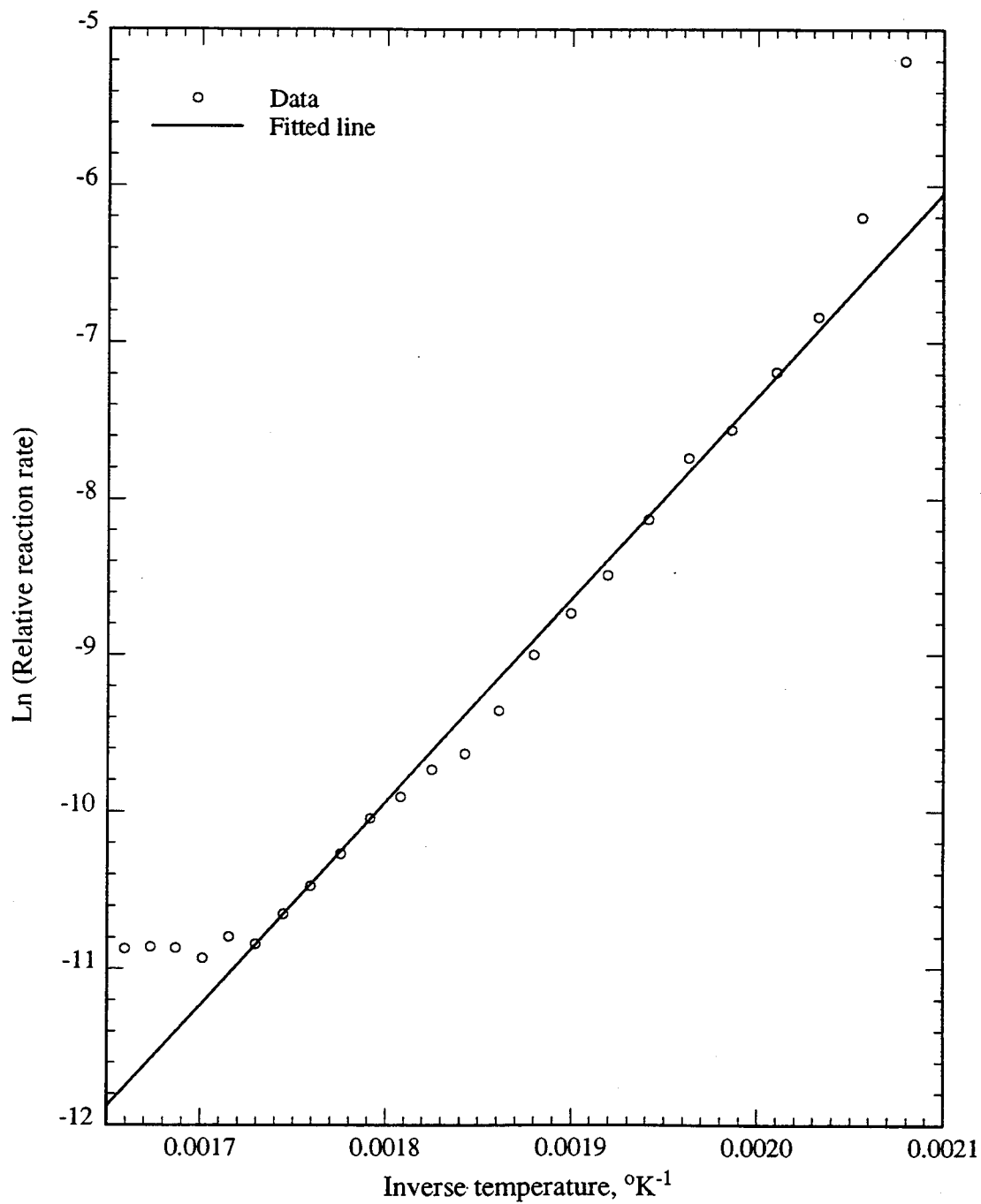


Figure 7.20: Arrhenius Graph for LTO Data (Run CL2)

7. NEW OXIDATION REACTION MODEL

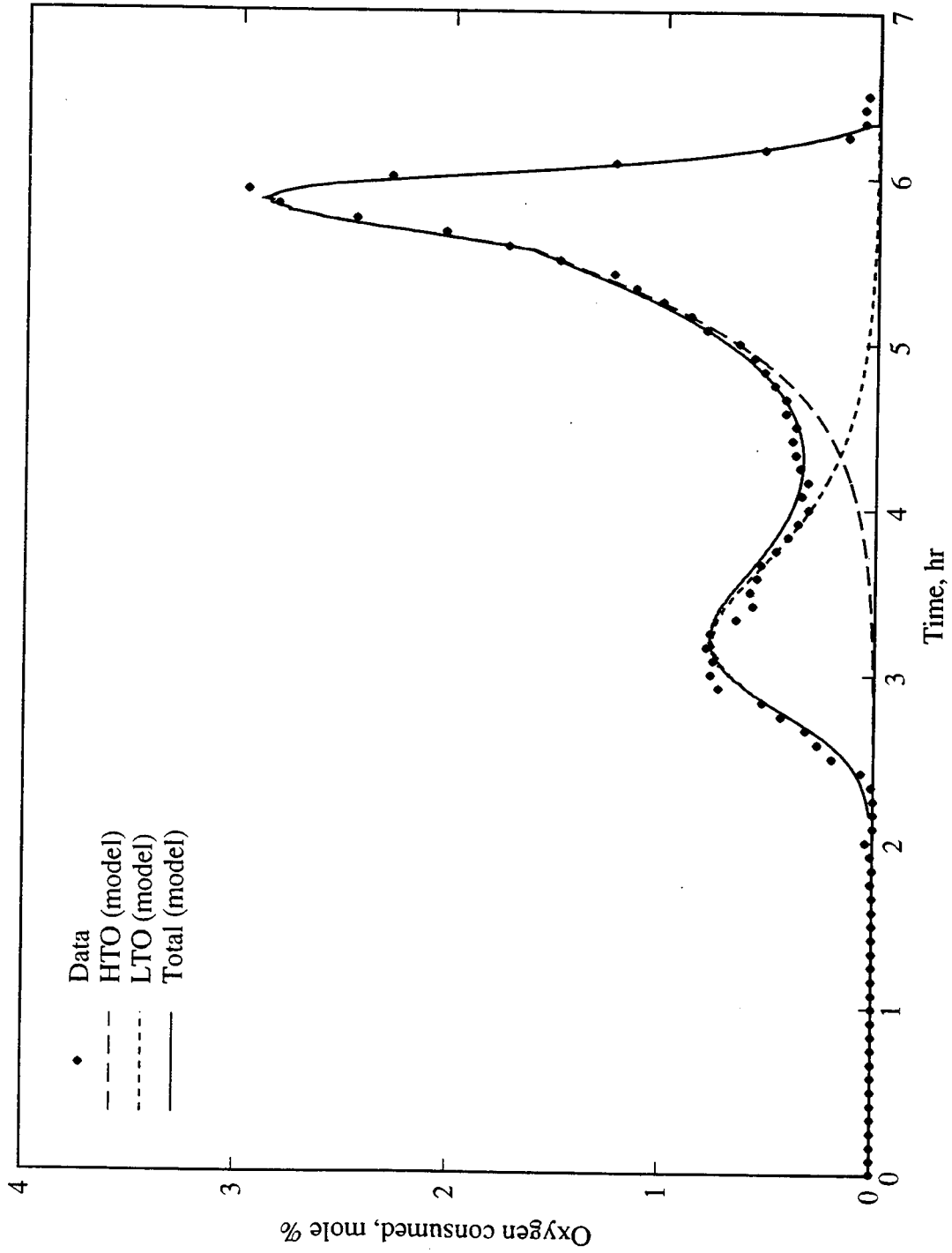


Figure 7.21: Oxygen Consumption - Model Results and Data (Run CL2)

7. NEW OXIDATION REACTION MODEL

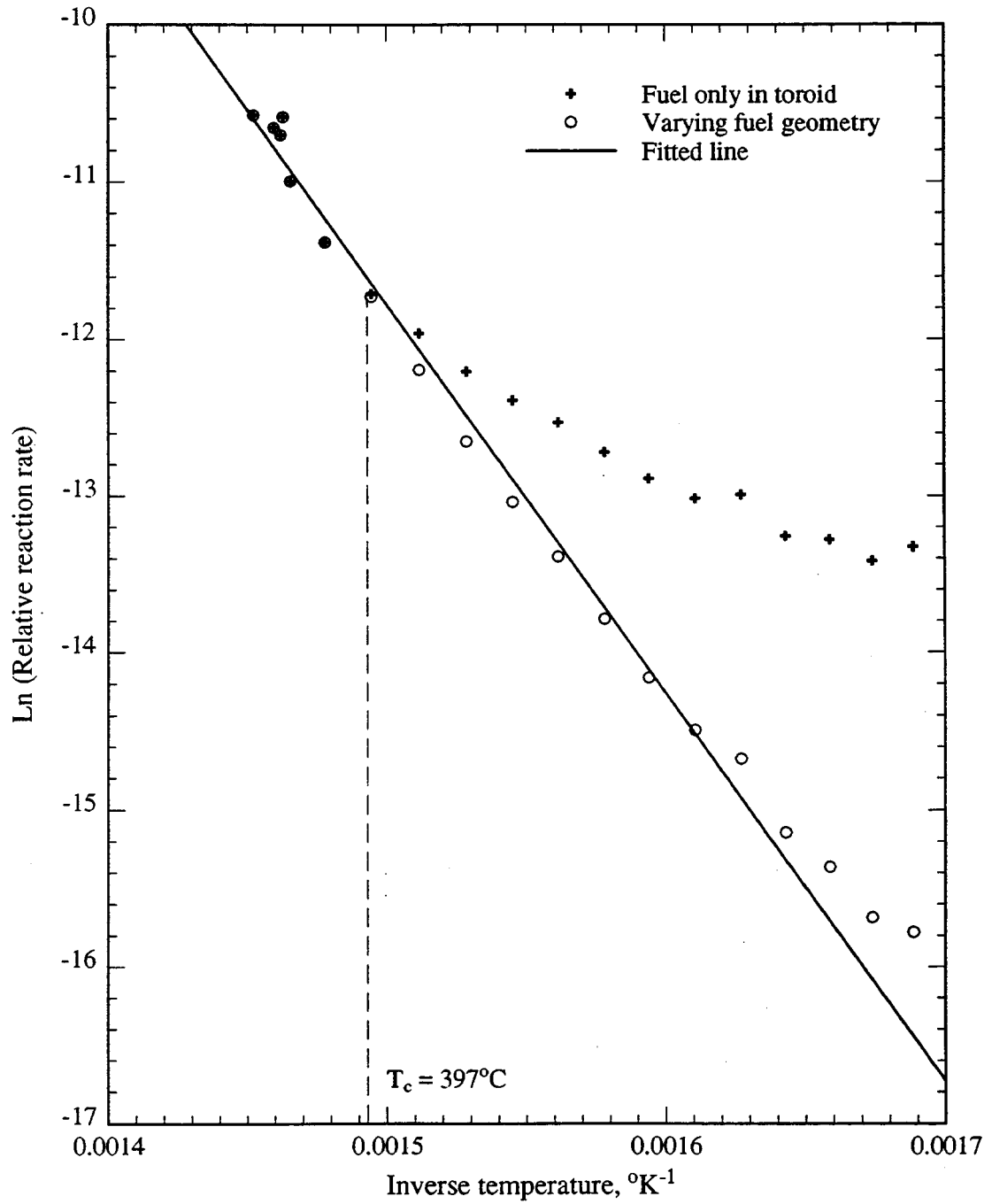


Figure 7.22: Arrhenius Graph for HTO Data (Run CL14)

7. NEW OXIDATION REACTION MODEL

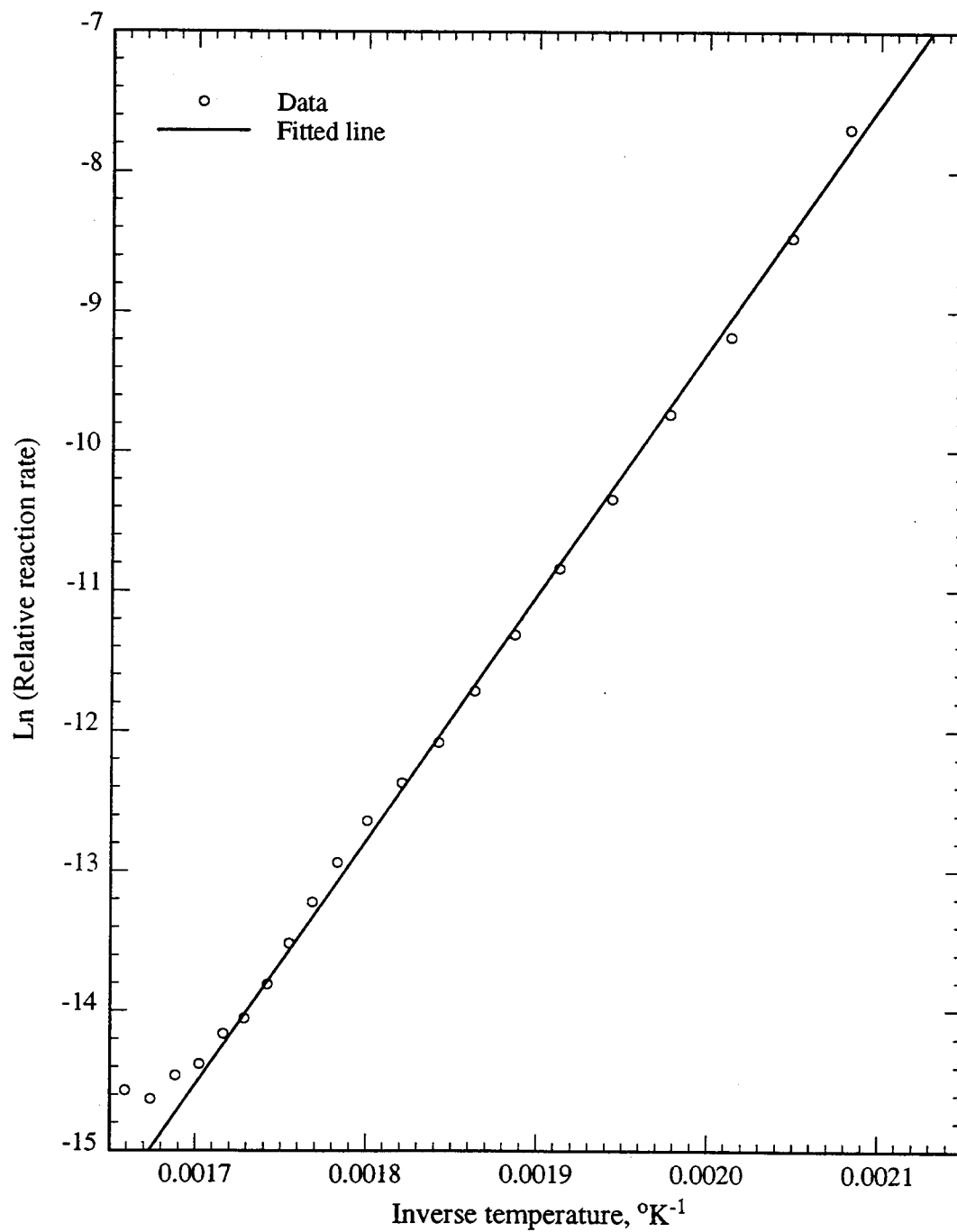


Figure 7.23: Arrhenius Graph for LTO Data (Run CL14)

7. NEW OXIDATION REACTION MODEL

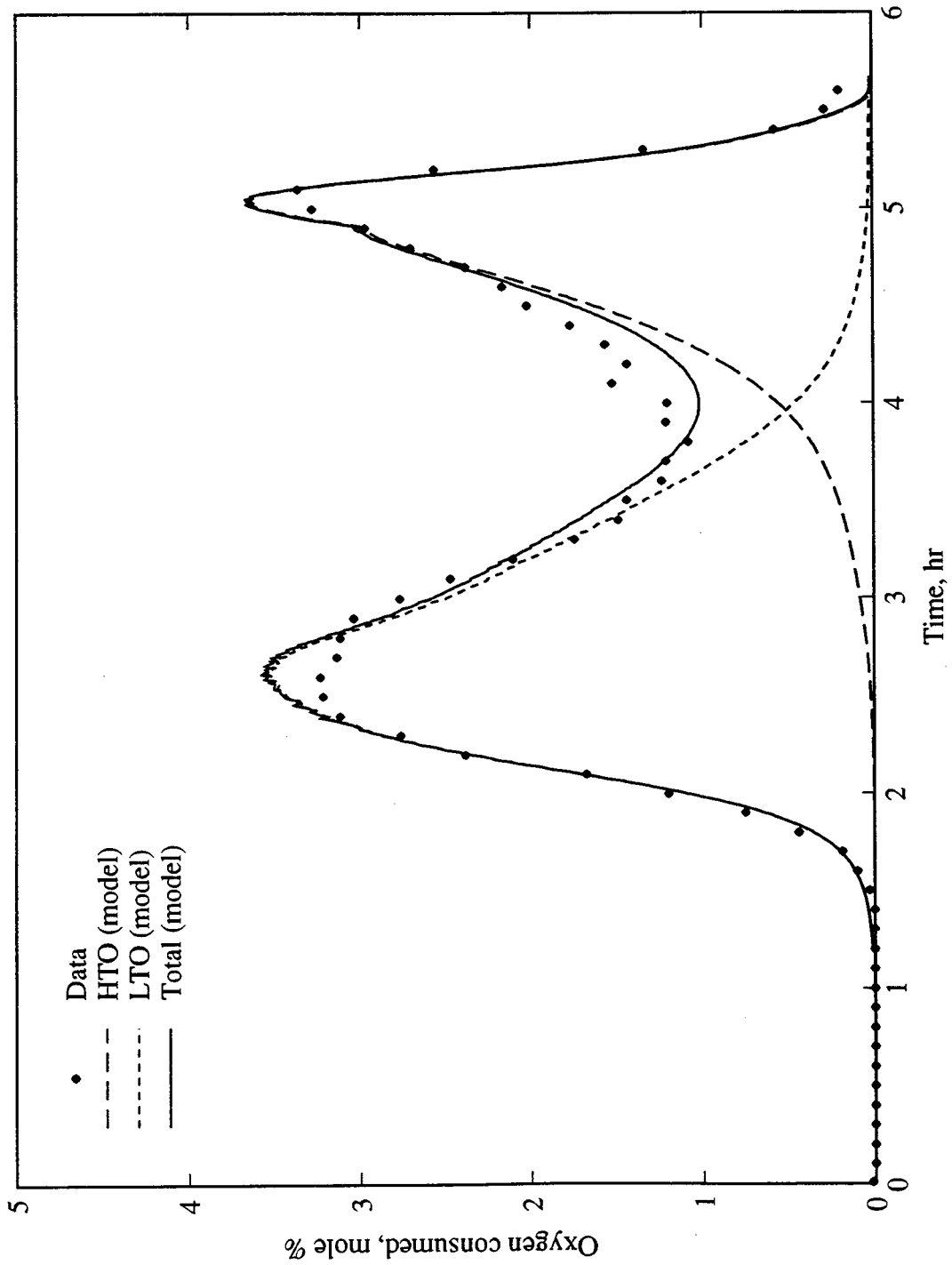


Figure 7.24: Oxygen Consumption - Model Results and Data (Run CL14)

7. NEW OXIDATION REACTION MODEL

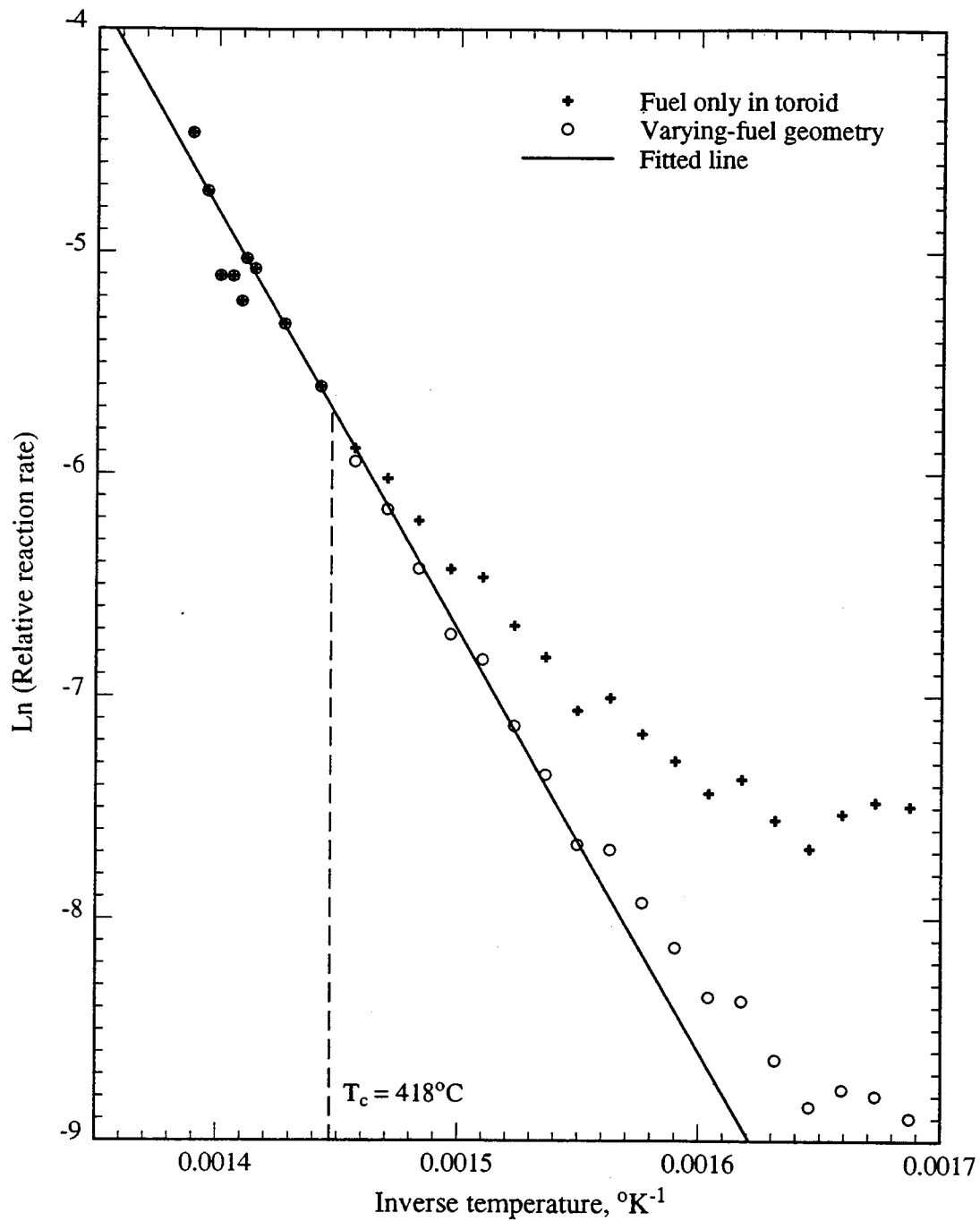


Figure 7.25: Arrhenius Graph for HTO Data (Run HBO2)

7. NEW OXIDATION REACTION MODEL

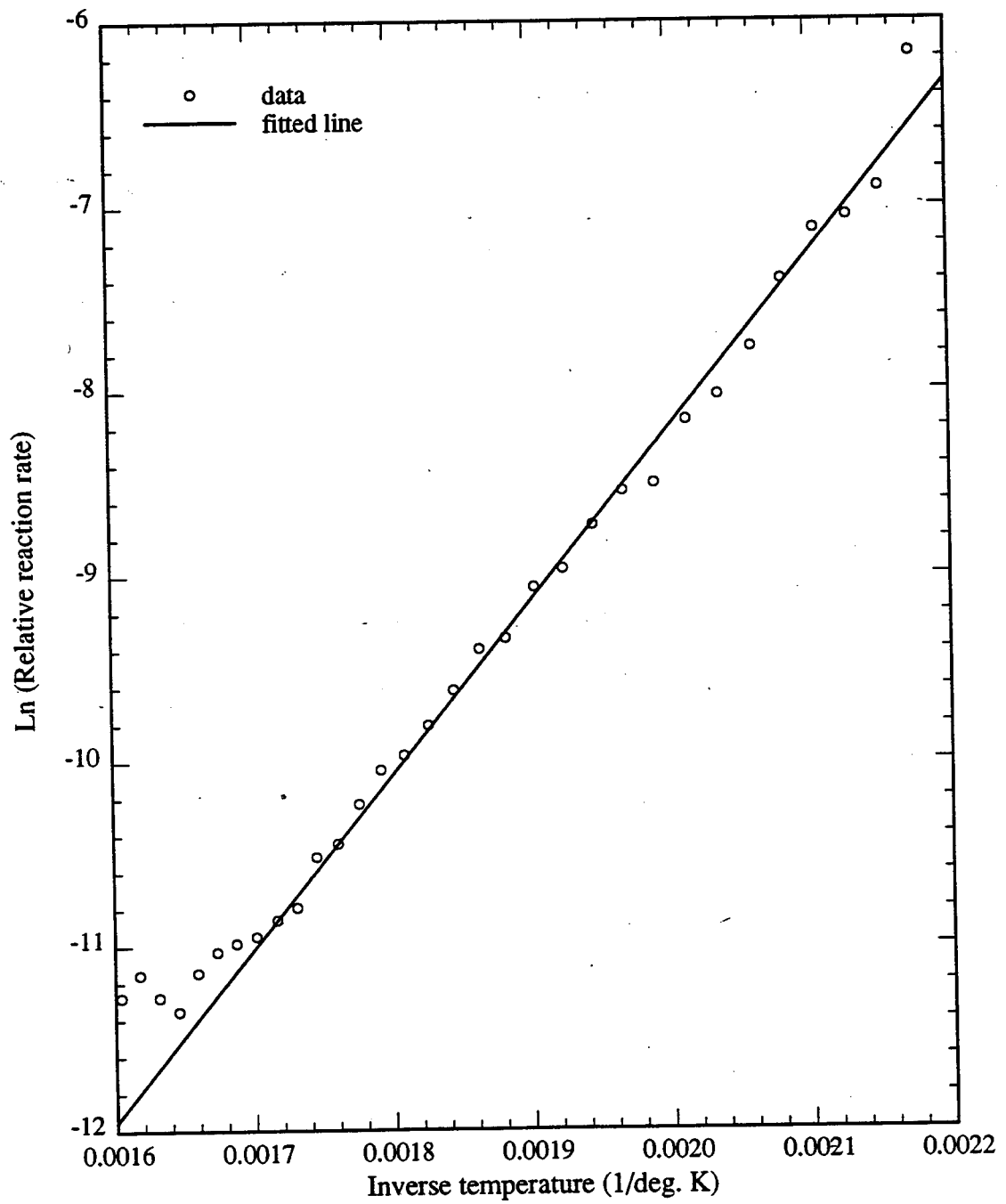


Figure 7.26: Arrhenius Graph for LTO Data (Run HBO2)

7. NEW OXIDATION REACTION MODEL

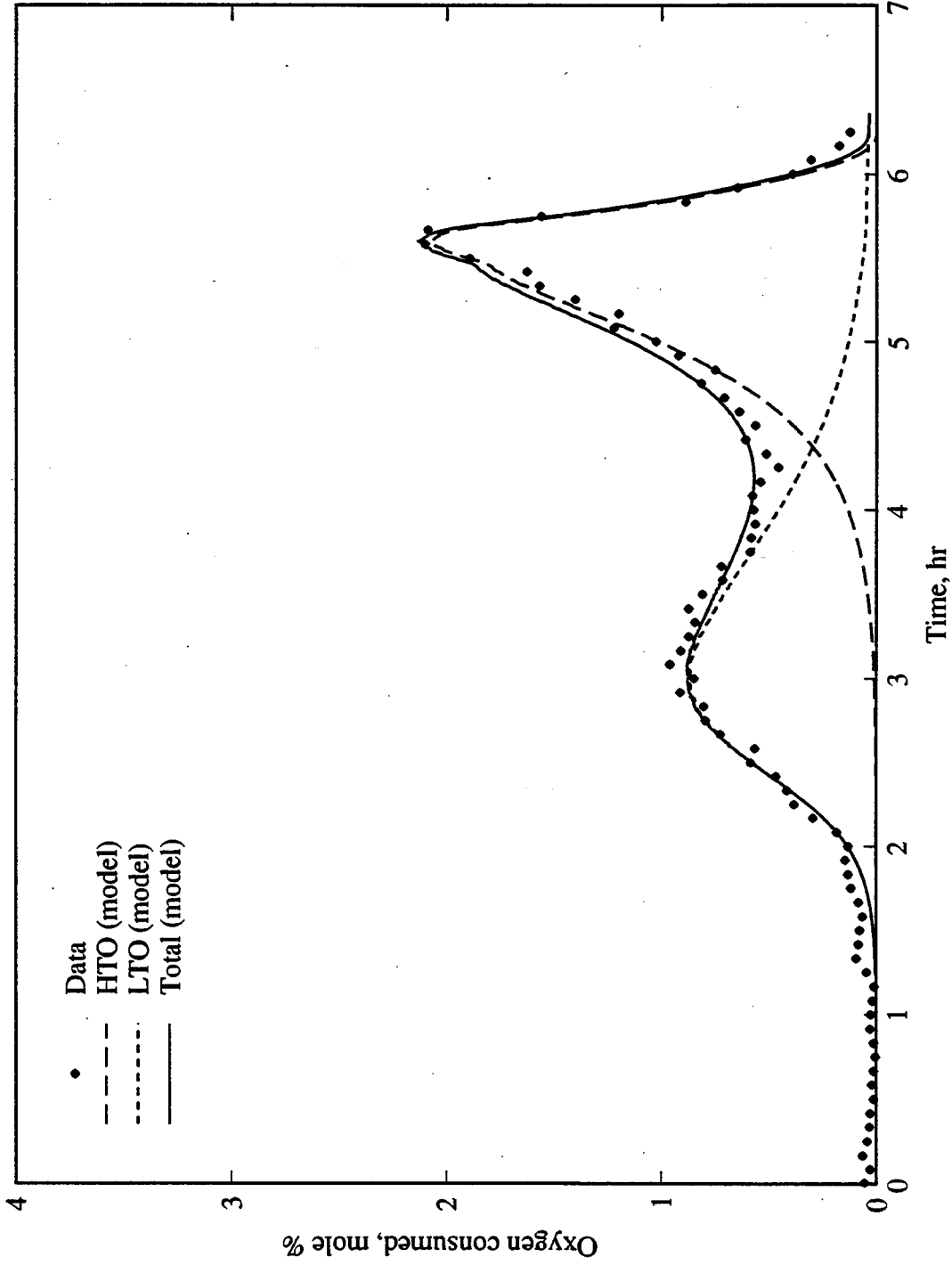


Figure 7.27: Oxygen Consumption - Model Results and Data (Run HBO2)

7. NEW OXIDATION REACTION MODEL

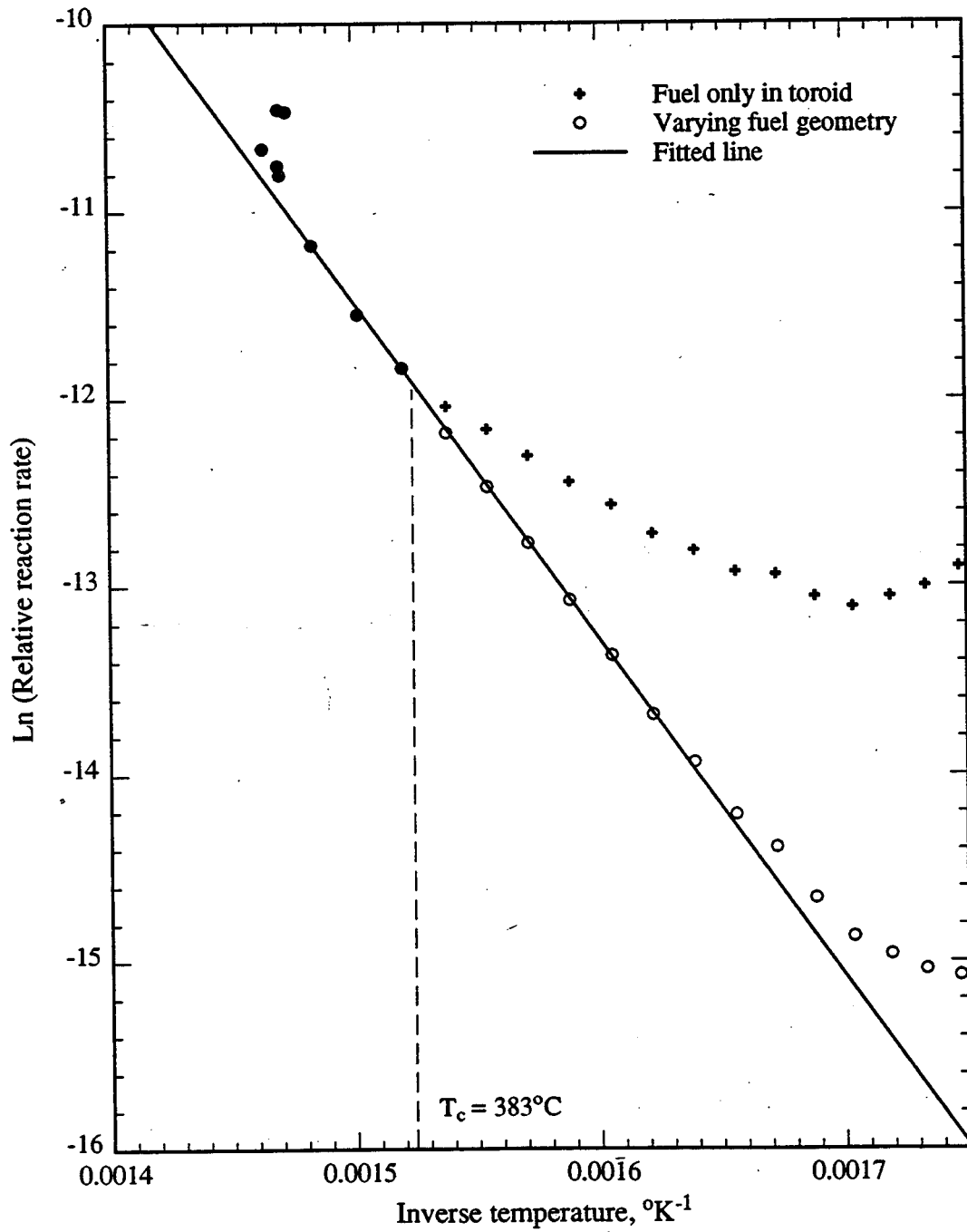


Figure 7.28: Arrhenius Graph for HTO Data (Run VEN6)

7. NEW OXIDATION REACTION MODEL

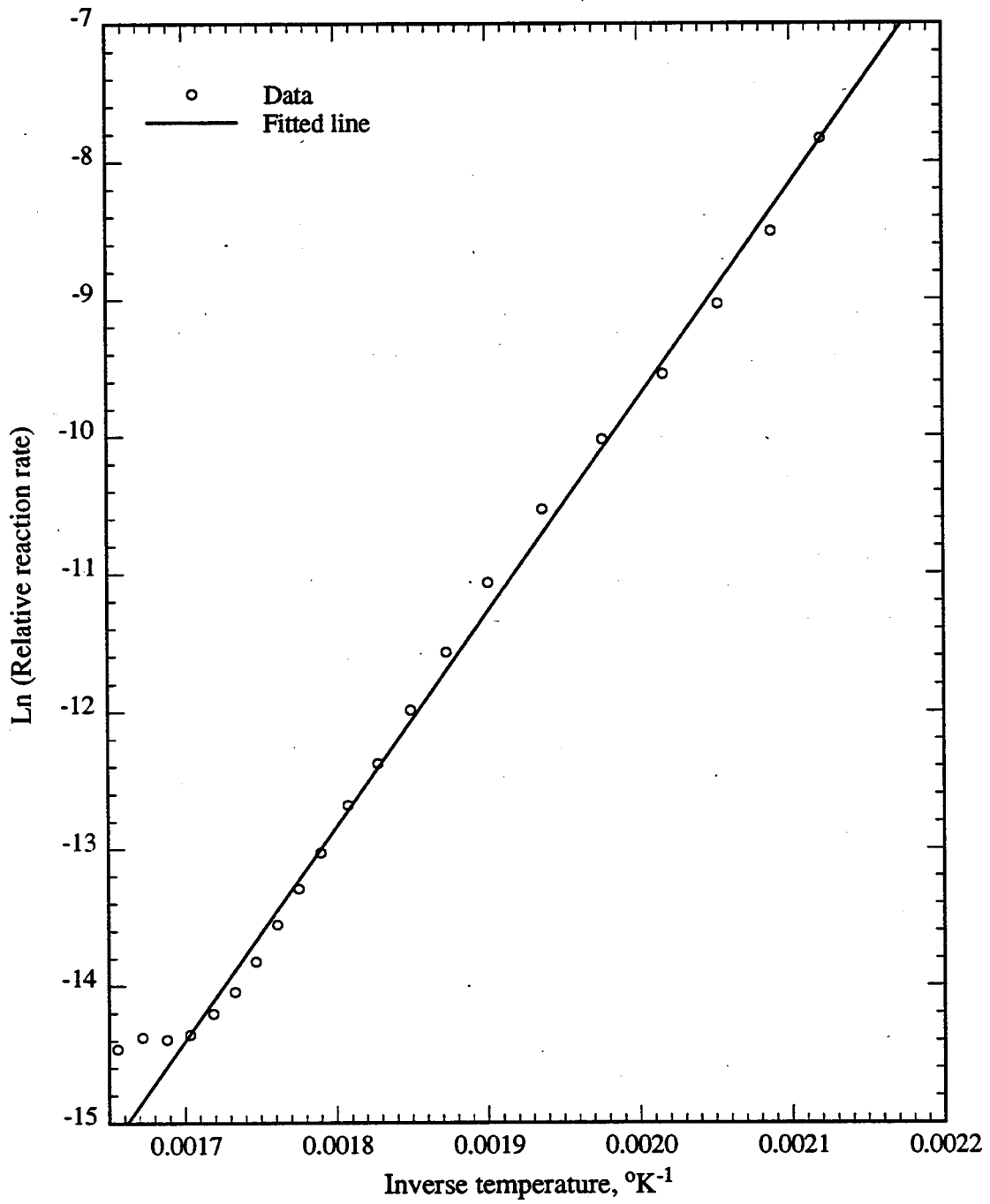


Figure 7.29: Arrhenius Graph for LTO Data (Run VEN6)

7. NEW OXIDATION REACTION MODEL

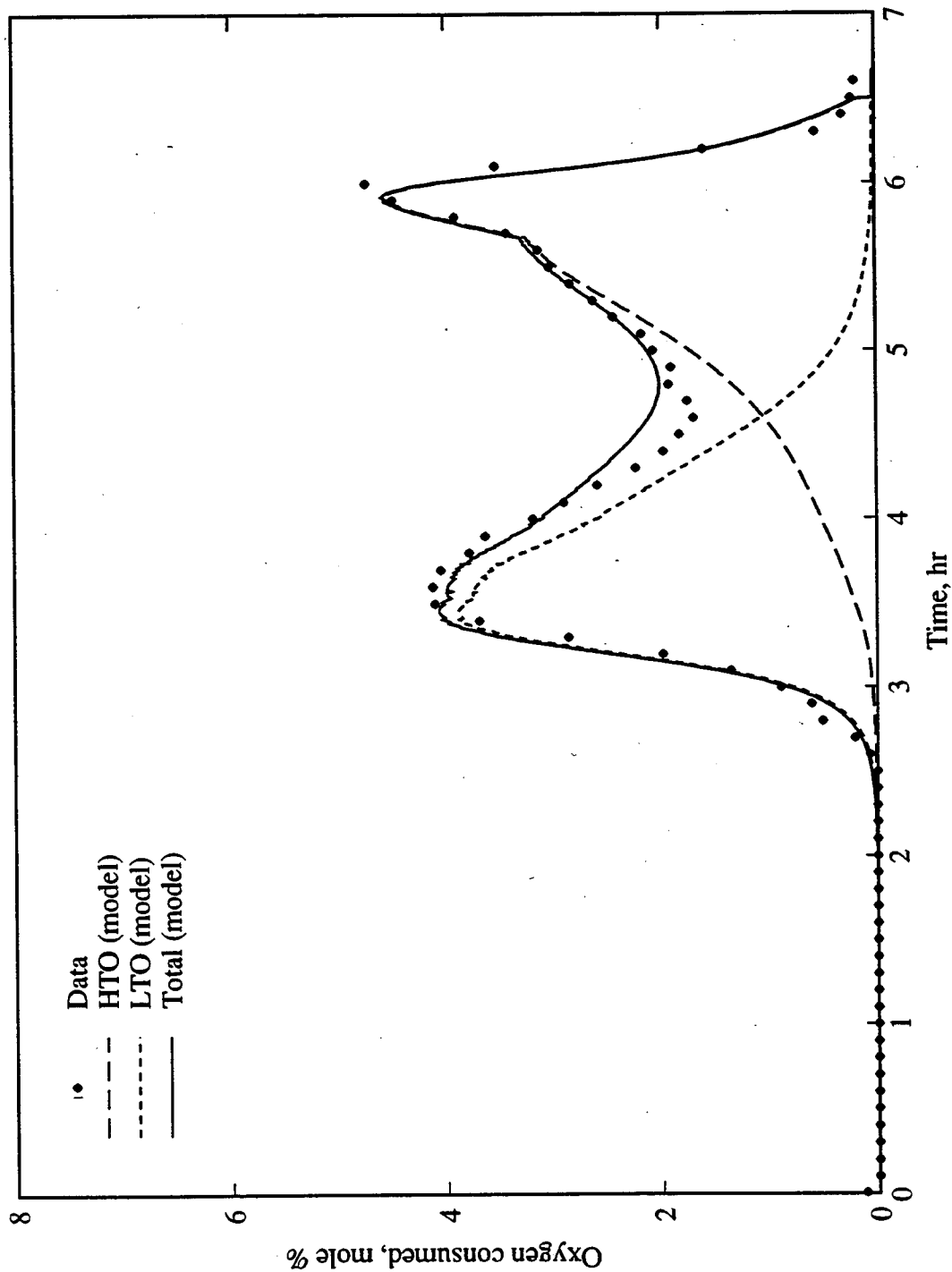


Figure 7.30: Oxygen Consumption - Model Results and Data (Run VEN6)

7. NEW OXIDATION REACTION MODEL

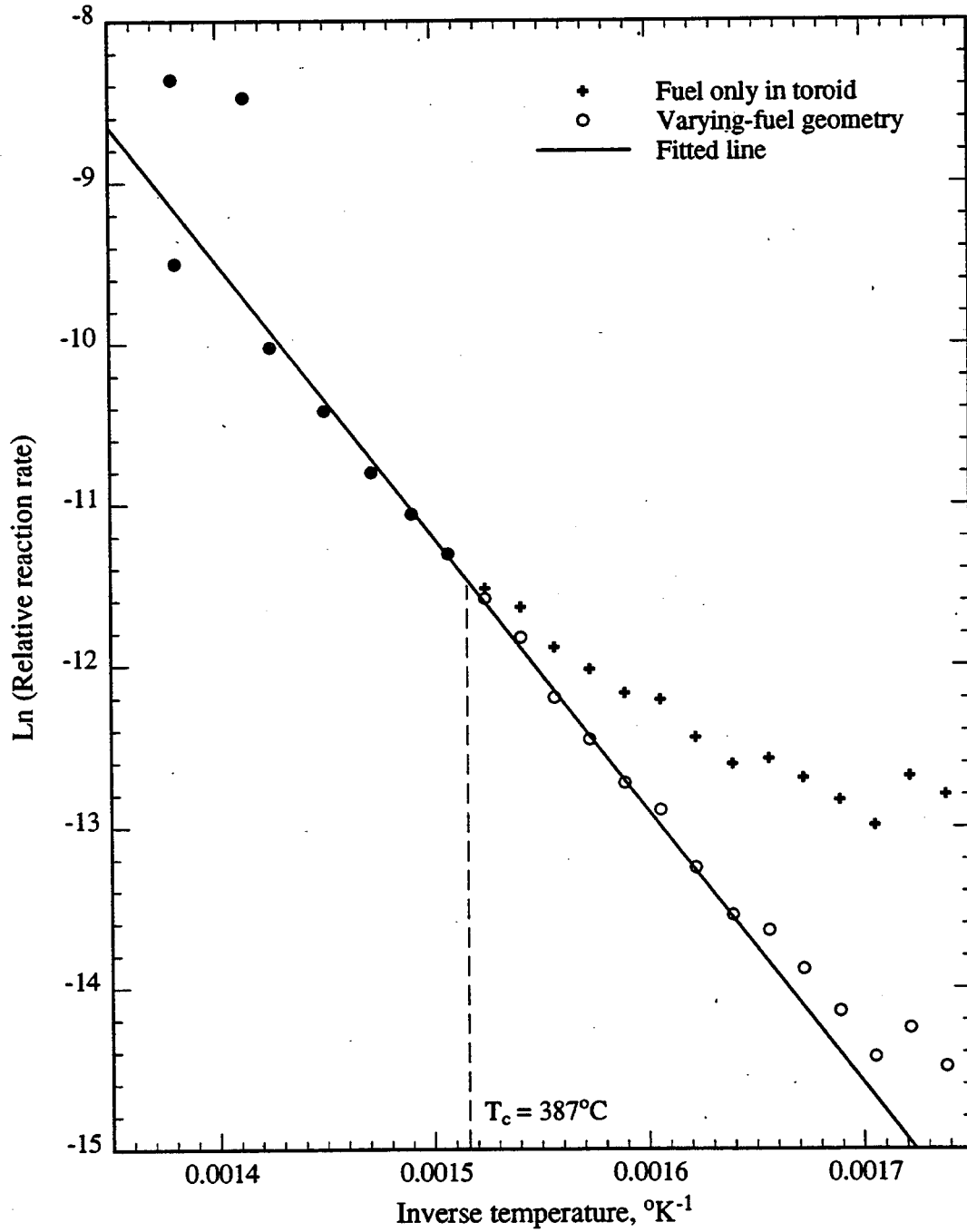


Figure 7.31: Arrhenius Graph for HTO Data (Run VEN23)

7. NEW OXIDATION REACTION MODEL

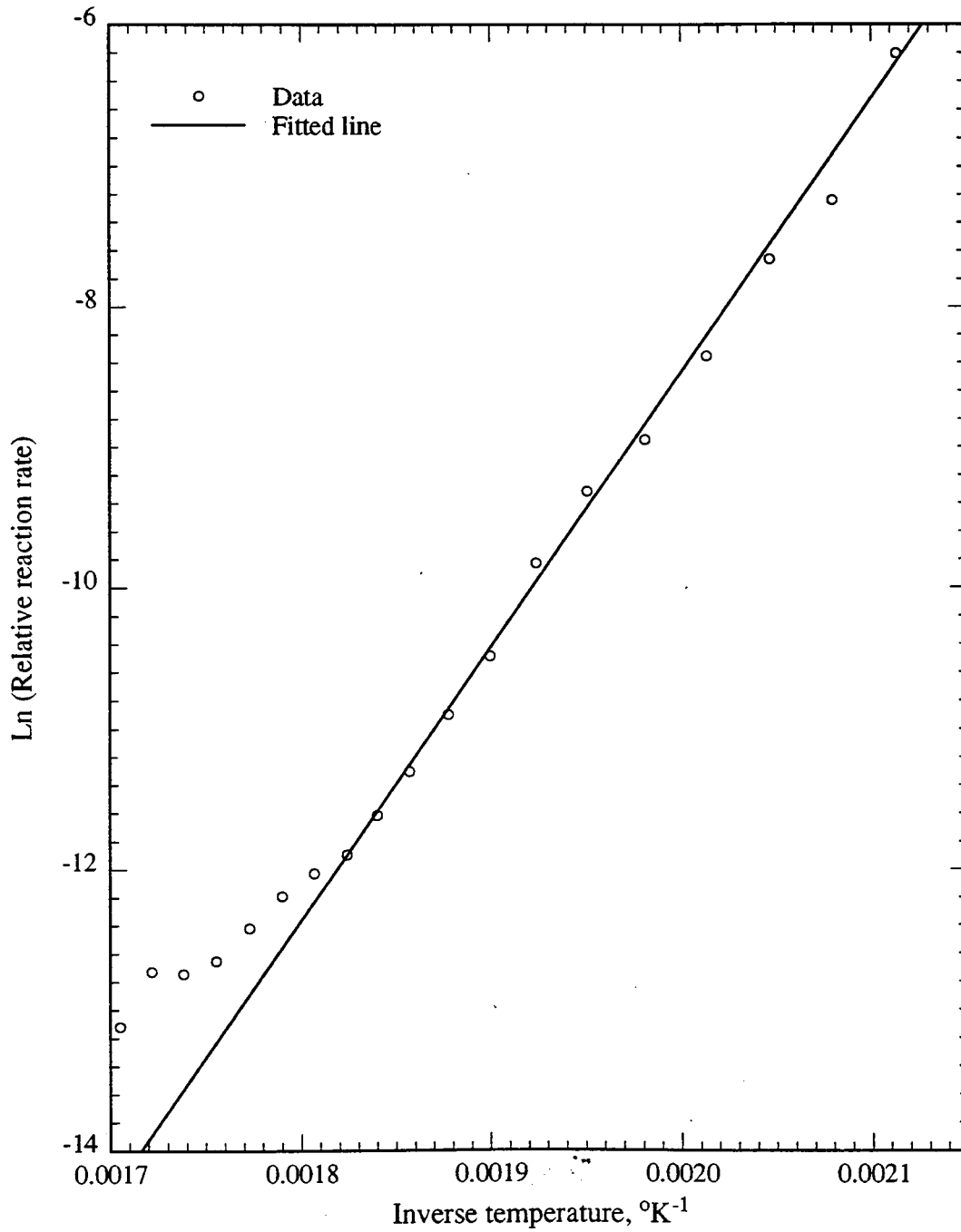


Figure 7.32: Arrhenius Graph for LTO Data (Run VEN23)

7. NEW OXIDATION REACTION MODEL

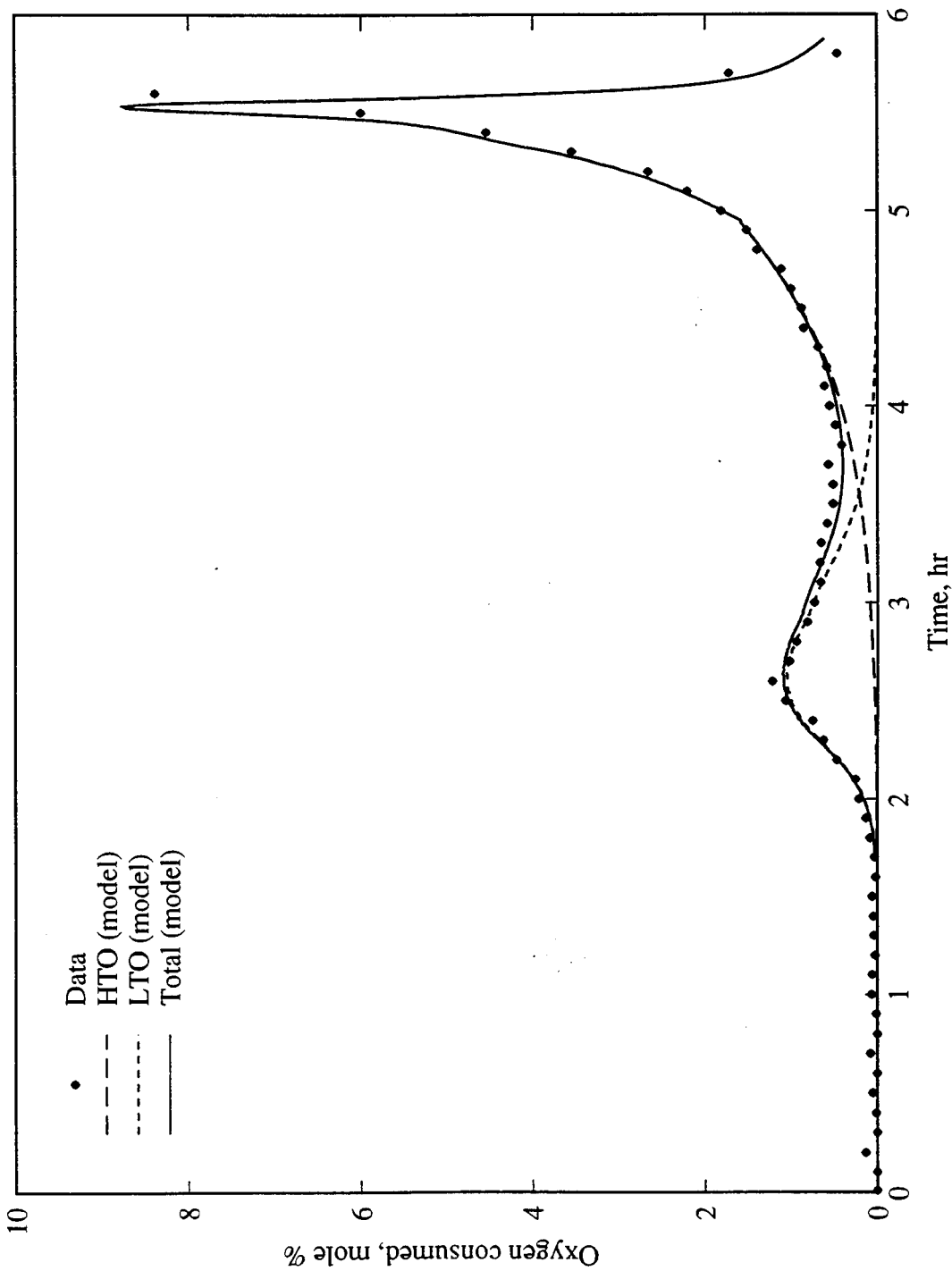


Figure 7.33: Oxygen Consumption - Model Results and Data (Run VEN23)

8. Summary, Conclusions and Recommendations

The main objectives of this study were to investigate the nature of the fuel during in-situ combustion and the factors that affect fuel deposition. The research involved carrying out a variety of experiments in a systematic manner. Kinetic and combustion tube experiments were performed using various types of crude oils and porous media. In addition, weight versus temperature experiments, differential scanning calorimetry, thermogravimetric analysis and elemental analysis were carried out. The results of this study are summarized as follows.

8.1 Summary and Conclusions

1. Major improvements were made to the kinetic and combustion tube experimental apparatus. This resulted in increased accuracy in measurements and ease of operation.
2. In combustion tube experiments, high combustion temperatures were obtained when clay or fine sands were present. These particles reduced the permeability of the sand pack and also provided a large reaction surface area. Consequently, the residual oil saturation and, hence the fuel concentration, increased, which

8. SUMMARY, CONCLUSIONS AND CONCLUSIONS

resulted in high temperature burns. Practically all of the injected oxygen was reacted at the combustion zone. Hence, hydrocarbons ahead of the combustion front did not undergo low-temperature oxidation. This resulted in atomic H/C ratios which were similar to those of the original crudes. Experimental results suggest that distillation is the main mechanism for fuel deposition.

3. In contrast, low-temperature oxidation was obtained in a combustion tube run in which the sample matrix contained only 20–30 mesh sand. Ignition was not obtained due to the low fuel concentration, and a substantial amount of oxygen moved ahead of the combustion zone. This resulted in low-temperature oxidation of the crude oil to form an oxygenated hydrocarbon fuel as inferred from elemental analysis. Low-temperature oxidation was found to be highly inefficient both from the standpoint of oxygen usage and heat generated. Further, the resulting oxygenated crude viscosity increased dramatically. It is a process to be avoided in field operations.
4. In kinetic tube experiments, oxidation reactions occur in a medium containing excess oxygen. Consequently, there is low-temperature oxidation of the crude, which results in the formation of an oxygenated hydrocarbon fuel. Fuel atomic O/C ratios in the range of 0.4 to 0.9 were found from experiments.
5. Oxygen from the oxygenated hydrocarbon fuel takes part in the HTO reactions in the kinetic tube. Oxygen present in the fuel was included in calculations of H/C and m -ratios by carrying out these calculations on a total-gas-volume basis. This new calculation method allows a direct comparison of H/C ratios obtained from kinetic and combustion tube experiments.
6. A new oxidation reaction model was developed. The new model describes the

8. SUMMARY, CONCLUSIONS AND CONCLUSIONS

physics of oxidation reactions better than the previous model. Oxygen consumption curves based on the new model agreed satisfactorily with experimental data. The main differences between the new and previous oxidation reaction models are:

New model	Previous model
(a) Two reaction stages: LTO, HTO.	(a) Three reaction stages: LTO, MTO and HTO.
(b) Fuel is an oxygenated hydrocarbon.	(b) Fuel is carbon.
(c) Varying, reaction-surface area incorporated for HTO.	(c) Reaction-surface area assumed constant.

7. The experiments performed in this study have shed new light on the complex oxidation reactions that occur during combustion of crude oil. In particular, the finding, that fuel in kinetic tube experiments is an oxygenated hydrocarbon, indicates that oxidation reactions in kinetic and combustion tube experiments differ because of the different type of fuel oxidized. A new experimental technique, or method of analysis, will be needed to obtain kinetic parameters of fuel reactions encountered in combustion tube experiments or in field operations.

8.2 Recommendations

1. Distillation is the most significant mechanism for fuel deposition. The residual oil saturation after a steam flood should be close to the fuel saturation. Steam flood experiments of oil-bearing sand packs should be run to measure residual oil saturations. Combustion tube experiments using identical oil-bearing sand packs should be run to relate fuel concentration to steam flood residual oil

8. SUMMARY, CONCLUSIONS AND CONCLUSIONS

saturation. The main objective of the study would be to find a correlation for fuel concentration. The data will also be useful for steam flood project design.

2. Numerical simulation of in-situ combustion requires kinetic parameters of the oxidation reactions. It may not be possible to obtain these parameters from kinetic tube experiments since oxygenation of the fuel may turn out to be unavoidable. A possible alternative may be to perform heat source calculations based on fuel concentration and combustion zone thickness. Factors that affect these parameters, however, are not fully quantified and need further research. The residual oil correlation study proposed above would be a step in the right direction.
3. The advantages of using horizontal wells as injectors and producers in an in-situ combustion project were not evaluated in this study. However the merits of horizontal wells appear obvious for better control of the size, shape and movement of the combustion front, and for minimizing gas breakthrough in the producers. Experimental and theoretical studies should be carried out to better understand heat and fluid flow under this scheme, and to evaluate production performance for a variety of horizontal well configurations.

Nomenclature

a	=	reaction order.
A	=	cross-sectional area of sample, cm^2 .
A_{grain}	=	fuel surface area per grain contact.
A_r	=	Arrhenius constant.
A_{total}	=	total fuel surface area in the sand mix.
b	=	reaction order.
C_f	=	fuel concentration, lb_m/ft^3 reservoir.
C_H	=	fuel concentration at HTO, g/cc .
C_L	=	fuel concentration at LTO, g/cc .
CO	=	carbon monoxide concentration in produced gas, mole %.
CO_2	=	carbon dioxide concentration in produced gas, mole %.
E	=	activation energy, KJ/mol .
E_H	=	activation energy at HTO, KJ/mol .
E_L	=	activation energy at LTO, KJ/mol .
h_f	=	height of fuel toroid, cm .
h_{f_0}	=	height of fuel toroid at time t_0 , cm .
HTO	=	high-temperature oxidation.
i	=	index for LTO, MTO and MTO.
k	=	rate constant.
k_o^*	=	equilibrium constant.

NOMENCLATURE

L	=	length of sample, cm.
LTO	=	low-temperature oxidation.
MTO	=	medium-temperature oxidation.
m -ratio	=	$CO/(CO + CO_2)$, fraction.
m_f	=	mass of fuel, g.
N_2	=	nitrogen concentration in produced gas, mole %.
n_L	=	fuel concentration exponent at LTO.
O_{2c}	=	oxygen consumed, mole %.
O_{2i}	=	oxygen concentration in injected gas, mole %.
O_{2p}	=	oxygen concentration in produced gas, mole %.
P	=	pressure in kinetics cell or combustion tube, psig.
P_{O_2}	=	oxygen partial pressure, psig.
q_i	=	injected gas rate, liter/min.
q_o	=	produced gas rate, liter/min.
r	=	radius of fuel deposited on sand grain, cm.
R	=	universal gas constant.
R_{af}	=	air-fuel ratio, scf/lbm.
R_{mass}	=	molar mass ratio, CH_x/CH_xO_y , fraction.
r_s	=	radius of sand or matrix grain, cm.
t	=	time, seconds.
T	=	temperature of sample, °K.
T_c	=	temperature of sample at time, t_c (°K).
t_c	=	start of toroid fuel geometry, min.
t_e	=	end of fuel oxidation, min.
t_o	=	start of fuel oxidation, min.
U	=	air flux at combustion front, scf/hr-ft ² .
V_F	=	combustion front velocity, ft/hr.

NOMENCLATURE

V_{grain}	=	fuel volume per grain contact.
V_{total}	=	total fuel volume in the sand mix.
x	=	atomic hydrogen-carbon ratio.
y	=	atomic oxygen-carbon ratio.
Y	=	fraction of oxygen consumed.
α_H	=	proportionality constant at HTO.
α_L	=	proportionality constant at LTO.
β_H	=	proportionality constant at HTO, s^{-1}
β_L	=	proportionality constant at LTO, s^{-1}
ΔH_A	=	heat of reaction for Path A (Section 6.4), KJ/mol O_2 .
ΔH_B	=	heat of reaction for Path B (Section 6.4), KJ/mol O_2 .
ΔH_C	=	heat of reaction for Path C (Section 6.4), KJ/mol O_2 .
ΔH_x	=	heat of reaction of fuel, CH_x , Btu/lb _{fuel} .
ΔH_{xy}	=	heat of reaction of fuel, CH_xO_y , Btu/ lb _{fuel} .
ϕ	=	porosity of sand pack, fraction.
ρ_f	=	fuel density, g/cc.
ρ_s	=	grain density, g/cc.

Bibliography

- [1] Abramowitz, M. and Stegun, I.A.: *Handbook of Mathematical Functions*, Dover Publications Inc., New York City (1972).
- [2] Adegbesan, K.O.: *Kinetics Study of Low Temperature Oxidation of Athabasca Bitumen*, PhD dissertation, The University of Calgary, Alberta, Canada (1982).
- [3] Agca, C. and Yortsos, Y.C.: "Steady-State Analysis of In-Situ Combustion," paper SPE 13624 presented at the 1985 California Regional Meeting, Bakersfield, CA, March 27-29.
- [4] Alexander, J.D., Martin, W.L., and Dew, J.N.: "Factors Affecting Fuel Availability and Composition During In-Situ Combustion," *J. Pet. Tech.* (Oct. 1962) 1154-1164.
- [5] Amyx, J.W. and Bass, D.M.: "Properties of Reservoir Rocks," *Petroleum Production Handbook*, published by Soc. of Pet. Eng., Volume II (1962) chapter 23.
- [6] AOSTRA: *AOSTRA, A 15 Year Portfolio of Achievement*, Alberta Oil Sands Technology and Research Authority, Edmonton, Alberta, Canada. (1990).
- [7] Babu, D.R. and Cormack, D.E.: "Effect of Low-Temperature Oxidation on the Composition of Athabasca Bitumen," *Fuel* (June 1984) **63**.

BIBLIOGRAPHY

- [8] Bae, J.H.: "Characterization of Crude Oil for Fireflooding Using Thermal Analysis Methods," *Soc. of Pet. Eng. J.* (June 1977) 211–217.
- [9] Bailey, H.R. and Larkin, B.K.: "Conduction-Convection in Underground Combustion," *Trans., AIME* (1960) **219**, 320–331.
- [10] Bardon, C. and Gabelle, C.: "Essai de Laboratoire Pour L'Etude de la Combustion In-Situ," Institute Francais du Petrole, Paris (May 1977).
- [11] Barta, L., Hakin, A.W. and Hepler, L.G.: "Kinetics and Energetics of Oxidation of Bitumen in Relation to In-Situ Combustion Process," "Oil-Field Chemistry, Enhanced Recovery and Production Stimulation" book published by American Chemical Society (1989) chapter 23.
- [12] Beckers, H.L. and Harmsen, G.J.: "The Effect of Water Injection on Sustained Combustion in a Porous Medium," *Soc. of Pet. Eng. J.* (June 1970) 145–163.
- [13] Belgrave, J.D.M., Moore, R.G., Ursenbach, M.G., and Bennion, D.W.: "A Comprehensive Approach to In-Situ Combustion Modelling," paper SPE 20250 presented at the 1990 SPE/DOE Symposium on Enhanced Oil Recovery, Tulsa, OK, April 22–25.
- [14] Benham, A.L. and Poettmann, F.H.: "The Thermal Recovery Process—An Analysis of Laboratory Combustion Data," *Trans., AIME* (1958) **213**, 406–408.
- [15] Berry, H.J.: *An Experimental Investigation of Forward Combustion Oil Recovery*, PhD dissertation, Texas A & M University, College Station, TX (May 1968).
- [16] Berry, V.J. Jr. and Parrish, D.R.: "A Theoretical Analysis of Heat Flow in Reverse Combustion," *Trans., AIME* (1960) **219**, 124–131.

BIBLIOGRAPHY

- [17] Boduszynski, M.M.: *Chemistry of Asphaltenes*, American Chemical Society, Washington, D.C. (1981).
- [18] Boduszynski, M.M.: "Composition of Heavy Petroleum. 1. Molecular Weight, Hydrogen Deficiency, and Heteroatom Concentration as a Function of Atmospheric Equivalent Boiling Point up to 1400°F (760°C)," *Energy & Fuels* (1987) **1**.
- [19] Boduszynski, M.M.: "Composition of Heavy Petroleum. 2. Molecular Characterization," *Energy & Fuels* (1988) **2**.
- [20] Bousaid, I.S. and Ramey, H.J. Jr.: "Oxidation of Crude Oil in Porous Media," *Soc. of Pet. Eng. J.* (June 1968) 137-148.
- [21] Brigham, W.E., Satman, A. and Soliman, M.Y.: "Recovery Correlations for In-Situ Combustion Field Projects and Application to Combustion Pilots," *J. Pet. Tech.* (Dec. 1980) 2132-38.
- [22] Broome, J.H., Bohannon, J.M. and Stewart, W.C.: "The 1984 National Petroleum Council EOR Study: Overview," paper SPE 13239 presented at the 1984 SPE Annual Technical Conference and Exhibition, Houston, Texas, Sept.
- [23] Burger, J., Sourieau, P. and Combarous, M.: *Thermal Methods of Recovery*, Institut Francais du Petrole Publications, Paris, France (1985).
- [24] Burger, J.G.: "Spontaneous Ignition in Oil Reservoirs," *Soc. of Pet. Eng. J.* (April 1976) 73-81.
- [25] Burger, J.G. and Sahuquet, B.C.: "Chemical Aspects of In-Situ Combustion - Heat of Combustion and Kinetics," *Soc. of Pet. Eng. J.* (Oct. 1972) 410-422.
- [26] Burgher, J.G. and Sahuquet, B.C.: "Laboratory Research on Wet Combustion," *J. Pet. Tech.* (Oct. 1973) 1137-1146.

BIBLIOGRAPHY

- [27] Butt, J.B.: *Catalyst Deactivation*, American Chemical Society (1972).
- [28] Carberry, J.J.: *Chemical and Catalytic Reaction Engineering*, McGraw-Hill Book Company, New York, N.Y. (1976).
- [29] Chemical Rubber Company: *Handbook of Chemistry and Physics*, CRC Press, Inc., Boca Raton, Florida (1982).
- [30] Chu, C.: "Two-Dimensional Analysis of a Radial Heat Wave," *J. Pet. Tech.* (Oct. 1963) 1137-1144.
- [31] Chu, C.: "A Study of Fireflood Field Projects," *J. Pet. Tech.* (Feb. 1977) 171-79.
- [32] Chu, C.: "State-of-the-Art Review of FireFlood Field Projects," *J. Pet. Tech.* (Jan. 1982) 19-36.
- [33] Coats, K.H.: "In-Situ Combustion Model," *Soc. of Pet. Eng. J.* (Dec. 1980) 533-554.
- [34] Crawford, P.B.: "Water Technology-Underground Combustion of Hydrocarbons," *Producers' Monthly* (June 1968) p. 15.
- [35] Crawford, P.B. and Cunningham, W.A.: "Carbon Formation in Catalytic Cracking," *Petroleum Refiner* (Jan 1956) Vol. 35, No.1, pp. 169-173.
- [36] Crookston, R.B., Culham, W.E. and Chen, W.H.: "A Numerical Simulation Model for Thermal Recovery Processes," *Soc. of Pet. Eng. J.* (Feb. 1979) 37-58.
- [37] Dabbous, M.K. and Fulton, P.F.: "Low-Temperature Oxidation Reaction Kinetics and Effects on the In-Situ Combustion Process," *Soc. of Pet. Eng. J.* (June 1974) 253-262.

BIBLIOGRAPHY

- [38] De los Rios, C.F.: "The Effect of Metallic Additives on the Kinetics of Oil Oxidation Reactions in In-Situ Combustion," Engineer's Degree Dissertation, Stanford University (1987).
- [39] Dietz, D.N.: "Wet Underground Combustion, State of the Art," *J. Pet. Tech.* (May 1970) 605-617.
- [40] Dietz, D.N. and Weijdema, J.: "Wet and Partially Quenched Combustion," *J. Pet. Tech.* (April 1963) 411-415.
- [41] Dietz, D.N. and Weijdema, J.: "Reverse Combustion Seldom Feasible," *Prod. Monthly* (May 1968) 10.
- [42] Drici, O. and Vossoughi, S.: "Study of the Surface Area Effect on Crude Oil Combustion by Thermal Analysis Techniques," *J. Pet. Tech.* (April 1985) **37**, 731-735.
- [43] Farouq Ali, S.M.: "A Current Appraisal of In-Situ Combustion Field Tests," *J. Pet. Tech.* (April 1972) 477-86.
- [44] Fassihi, M.R.: *Analysis of Fuel Oxidation in In-situ Combustion Oil Recovery*, PhD dissertation, Stanford University, Stanford, CA (May 1981).
- [45] Fassihi, M.R., Meyers, K.O. and Basile, P.F.: "Low-Temperature Oxidation of Viscous Crude Oils," *Soc. of Pet. Eng. J.* (Nov. 1990) 609-616.
- [46] Gates, G.F. and Ramey, H.J. Jr.: "Field Results of South Belridge Thermal Recovery Experiment," *Trans., AIME* (1958) **213**, 236-244.
- [47] Gates, G.F. and Ramey, H.J. Jr.: "A Method of Engineering In-Situ Combustion Oil-Recovery Projects," *J. Pet. Tech.* (Feb. 1980) 285-94.

BIBLIOGRAPHY

- [48] Gottfried, B.S.: "Some Theoretical Aspects of Underground Combustion in Segregated Oil Reservoirs," *Soc. of Pet. Eng. J.* (Sept. 1966) 281-291.
- [49] Grant, B.F. and Szasz, S.E.: "Development of an Underground Heat Wave for Oil Recovery," *J. Pet. Tech.* (May 1954) 22-23.
- [50] Greaves, M., Dudley, J.W.O. and Field, R.W.: "Real Time Mass and Energy Balance for Combustion Tube Experiments," *IN SITU* (Sept. 1989) **13**, 14, 92-96.
- [51] Gunn, R.D. and Krantz, W.B.: "Reverse Combustion Instabilities in Tar Sands and Coal," *Soc. of Pet. Eng. J.* (Aug. 1980) 267-277.
- [52] Hayashitani, M.: *Thermal Cracking of Athabasca Bitumen*, PhD dissertation, The University of Calgary, Alberta, Canada (1978).
- [53] Holt, R.J.: "In-situ combustion with metallic additives," M.S. Report, Stanford University, California (June 1992).
- [54] Hougen, O.A., Watson, K.M. and Ragatz, R.A.: *Chemical Process Principles - Part I*, John Wiley and Sons, New York (1954).
- [55] Howard, F.A.: "Method of Operating Oil Wells," U.S. Patent No. 1,473,348 (filed Aug. 9, 1920; issued Nov. 6, 1923).
- [56] Hvizdos, L.J., Howard, J.V. and Roberts, G.W.: "Enhanced Oil Recovery via Oxygen-Enriched In-Situ Combustion: Test Results From the Forest Hill Field in Texas," paper SPE 11218 presented at the 1982 SPE Annual Technical Conference and Exhibition, New Orleans, LA, Sept. 26-29.
- [57] Johnson, H.R. and Burwell, E.L.: "Carbon Deposition for Thermal Recovery of Petroleum-A Statistical Approach to Research," *Producers' Monthly* (July 1968) p. 8-15.

BIBLIOGRAPHY

- [58] Johnson, L.A., Fahy, L.J., Romanowski, L.J., Barbour, R.V., and Thomas, K.P.: "An Echoing In-Situ Combustion Oil Recovery Project in a Utah Tar Sand," *J. Pet. Tech.* (Feb. 1980) 295-305.
- [59] Kuhn, C.S. and Koch, R.L.: "In-Situ Combustion (Newest Method of Increasing Oil Recovery)," *Oil and Gas J.* (Aug. 1953) **52**, 14, 92-96.
- [60] Lewis, W.K., Gilliland, E.R. and Paxton, R.R.: "Low-Temperature Oxidation of Carbon," *Ind. & Eng. Chem.* (June 1954) 1327-1331.
- [61] Lim, K.T.: "Steam Distillation Effect and Oil Quality Change During Steam Injection," M.S. Report, Stanford University, California (June 1991).
- [62] Madgwick, G.G., Amberg, C.H. and Peterson, W.S.: "The Pyrolysis of a Heavy Crude in a Fluidized Bed," *The Can. J. of Chem. Eng.* (April 1959) 65-70.
- [63] Martin, W.L., Alexander, J.D. and Dew, J.N.: "Process Variables of In-Situ Combustion," *Trans., AIME* (1958) **213**, 28-35.
- [64] Massoth, F.E.: *Oxidation of Coked Silica-alumina Catalyst*, American Chemical Society (1966).
- [65] Millour, J.P., Moore, R.G., Bennion, D.W., Ursenbach, M.G., and Gie, D.N.: "A Simple Implicit Model for Thermal Cracking of Crude Oils," paper SPE 14226 presented at the 1985 SPE Annual Technical Conference and Exhibition, Las Vegas, NV, Sept. 22-25.
- [66] Moss, J.T., White, P.D. and McNeil, J.S. Jr.: "In-Situ Combustion Process - Results of a Five-Well Field Experiment in Southern Oklahoma," *J. Pet. Tech.* (April 1959) 55-64.
- [67] Nelson, T.W. and McNeil, J.S. Jr.: "How to Engineer an In-Situ Combustion Project," *Oil and Gas J.* (June 1961) 58-65.

BIBLIOGRAPHY

- [68] Parrish, D.R. and Craig, F.F.: "Laboratory Study of a Combination of Forward Combustion and Waterflooding – The COFCAW Process," *J. Pet. Tech.* (June 1969) 753–761.
- [69] Penberthy, W.L. Jr.: *An Investigation of the Fundamentals of Combustion Oil Recovery*, PhD dissertation, Texas A & M University, College Station, TX (May 1967).
- [70] Penberthy, W.L. Jr. and Ramey, H.J. Jr.: "Design and Operation of Laboratory Combustion Tubes," *Soc. of Pet. Eng. J.* (June 1966) 183–198.
- [71] Poettmann, F.H., Schilson, R.E. and Surkalo, H.: "Philosophy and Technology of In-Situ Combustion in Light Oil Reservoirs," *Proc. of the Seventh World Pet. Cong.*, Mexico City (1967) III, 487.
- [72] Ramey, H.J. Jr.: "Transient Heat Conduction During Radial Movement of a Cylindrical Heat Source – Applications to the Thermal Recovery Process," *Trans., AIME* (1959) **216**, 115–122.
- [73] Ramey, H.J. Jr.: "In-Situ Combustion," *Proceedings of the 8th World Petroleum Congress*, Moscow (1971) 253–262.
- [74] Ramey, H.J. Jr., Stamp, V.W., Pebdani, F.N. and Mallinson, J.E.: "Case History of South Belridge, California, In-Situ Combustion Oil Recovery," paper SPE 24200 presented at the 1992 SPE/DOE Eight Symposium on Enhanced Oil Recovery, Tulsa, Oklahoma, April 21–24.
- [75] Shahani, G.H. and Hansel, J.G.: "Oxygen Fireflooding: Combustion Tube Tests with Light, Medium and Heavy Crude Oils," paper SPE 12726 presented at the 1984 SPE/DOE Symposium on Enhanced Oil Recovery, Tulsa, Oklahoma, April.

BIBLIOGRAPHY

- [76] Shallcross, D.C.: "Modifying In-Situ Combustion Performance by the Use of Water-Soluble Additives," paper SPE 19485 presented at the 1989 Asia-Pacific Conference, Sydney, Australia, Sept. 13-15.
- [77] Sheinman, A. B., Malofeev, G. E., and Sergeev, A. I.: "The Effect of Heat on the Underground Formations for the Recovery of Crude Oil - Thermal Recovery Methods of Oil Production," *Nedra, Moscow* (1969).
- [78] Showalter, W.E.: "Combustion Drive Tests," *Soc. of Pet. Eng. J.* (March 1963) 53-58.
- [79] Smith, J.M.: *Chemical Engineering Kinetics*, McGraw-Hill Book Company, New York, N.Y. (1970).
- [80] Tadema, H.J: "Mechanism of Oil Production by Underground Combustion," Proceedings of the 5th World Petroleum Congress (1959) section II, paper 22, 279-287.
- [81] Tadema, H.J. and Weijdem, J.: "Spontaneous Ignition in Oil Sands," *Oil and Gas J.* (Dec. 1970) 77-80.
- [82] Thomas, G.W.: "A Study of Forward Combustion in a Radial System Bounded by Permeable Media," *J. Pet. Tech.* (Oct. 1963) 1145-1149.
- [83] Thomas, G.W., Buthod, A.P. and Allag, O.: "An Experimental Study of the Kinetics of Dry, Forward Combustion- Final Report," Report No. BETC-1820-1, distributed by Dept. of Energy (Feb. 1979).
- [84] Vogel, L.C. and Krueger, R.F.: "An Analog Computer for Studying Heat Transfer During a Thermal Recovery Process," *Trans., AIME* (1955) **204**, 208.

BIBLIOGRAPHY

- [85] Vossoughi, S., Willhite, G.P., Kritikos, W.P., Guvenir, I.M., and El Shoubary, Y.: "Automation of an In-Situ Combustion Tube and Study of the Effect of Clay on the In-Situ Combustion Process," *Soc. of Pet. Eng. J.* (Aug. 1982) 493-502.
- [86] Weijdem, J.: "Studies on the Oxidation Kinetics of Liquid Hydrocarbons in Porous Media With Regard to Subterranean Combustion," *Erdöl & Kohle. Erdgas Petrochem.* (Sept. 1968) 520-526.
- [87] Weisz, P.B. and Goodwin, R.D.: "Combustion of Carbonaceous Deposits within Porous Catalyst Particles, II, Intrinsic Burning Rate," *J. of Catalysis* (June 1966) 227-236.
- [88] Wilson, L.A., Qygal, R.J., Reed, D.W., Gergins, R.L. and Henderson, J.H.: "Fluid Dynamics During an Underground Combustion Process," *Trans., AIME* (1958) **213**, 146-154.
- [89] Wilson, L.A., Reed, R.L., Reed, D.W., Clay, R.R. and Harrison, N.H.: "Some Effects of Pressure on Forward and Reverse Combustion," *Soc. of Pet. Eng. J.* (Sept. 1963) 127-137.
- [90] Wolcott, E.R.: "Method of Increasing the Yield of Oil Wells," U.S. Patent No. 1,457,479 (filed Jan. 12, 1920: issued June 5, 1923).
- [91] Wu, C.H. and Fulton, P.F.: "Experimental Simulation of the Zones Preceding the Combustion Front of an In-Situ Combustion Process," *Soc. of Pet. Eng. J.* (March 1971) 38-46.
- [92] Youngren, G.K.: "Development and Application of an In-Situ Combustion Reservoir Simulator," *Soc. of Pet. Eng. J.* (Feb. 1980) 39-51.

Appendix: Computer Programs

Nine main computer programs, used for experimental data recording and analysis and for other calculations, are listed in this appendix. KIN.BAS and COMB.BAS were written in QuickBASIC5, while the other programs were written in FORTRAN 77. The main functions of the computer programs are summarized as follows. Detailed descriptions are given at the beginning of each computer program.

Program	Main Functions
1. KIN.BAS	Record and display data, and control instruments during kinetic tube experiment and calibration.
2. COMB.BAS	Record and display data, and control instruments during combustion tube experiment and calibration.
3. GASCAL.F	Calibrate produced gas composition readings based on standard gas calibration data.
4. HTO.F	Compute parameters for Arrhenius graph of HTO data.
5. HTOFIT.F	Compute fuel versus height, model HTO consumption curve, and LTO data.
6. LTO.F	Compute parameters for Arrhenius graph of LTO data.
7. LTOFIT.F	Compute model LTO and Total oxygen consumption curves.
8. UOP.F	Compute polynomial fit for H/C - API oil gravity - UOP K-factor correlation (Lim 1991).
9. HEAT.F	Compute heat of combustion for oxygenated fuel.

APPENDIX: COMPUTER PROGRAMS

1. Program KIN.BAS

```
' PROGRAM KIN.BAS
'
' BY DAULAT MAMORA, STANFORD UNIVERSITY, SEPTEMBER 1990.
'
' A. PROGRAM FOR KINETICS EXPERIMENTS.
'
' B. TO ACCESS PROGRAM, TYPE FOLLOWING AT C:\LIB>
'    QB KIN.BAS /L QB4HPIB.QLB
'
' C. COMPILE AND RUN PROGRAM PER QUICKBASICS PROCEDURE.
'
' D. PROGRAM CARRIES OUT FOLLOWING FUNCTIONS:
'
'    1. CONTROLS POSITION OF GAS AUTO-SAMPLER.
'
'    2. RECORDS READINGS OF CO2, CO AND O2 ANALYZERS, GAS INJECTION RATE,
'       GAS PRODUCTION RATE, PRESSURE AND TEMPERATURE AT 30-SEC INTERVALS.
'
'    3. READS GC READINGS, COMPUTES N2 CONCENTRATION AT 6-MIN INTERVALS.
'
'    4. DISPLAYS ON SCREEN:
'       WINDOW 1: CO2, CO, O2 AND N2 CONCENTRATIONS VERSUS TIME.
'       WINDOW 2: GC TRACE OF N2 PEAK.
'       WINDOW 3: TEMPERATURE VERSUS TIME.
'       TOP OF SCREEN: VALUES OF ALL READINGS.
'
'
' DECLARE SUB GCANALYSIS ()
' DECLARE SUB GC ()
'
'
' OPTION BASE 1
' DEFINIT A-Z
' DIM S1!(1), S2!(1), S3!(1), S4!(1), S5!(1), S6!(1), S7!(1), S8!(1)
' DIM TSEC!(3500), AS4!(3500)
' COMMON SHARED N2!, GO2!, O2X!, NONGCP!, TIMEP!
' COMMON SHARED S1!(), S2!(), S3!(), S4!(), S5!(), S6!(), S7!(), S8!()
' COMMON SHARED AS4!(), TSEC!(), TGC2!
' COMMON SHARED DEV AS LONG, ISC AS LONG
' COMMON SHARED IM AS INTEGER, I AS INTEGER, M AS INTEGER, KPEAK AS INTEGER
```

APPENDIX: COMPUTER PROGRAMS

```
COMMON SHARED MAXI AS INTEGER, MAXGC AS INTEGER, ACTUAL AS INTEGER
,
COMMON PCIB.BASERR, PCIB.ERR, PCIB.ERR$, PCIB.NAME$, PCIB.GLBERR
COMMON FALSE AS INTEGER, TRUE AS INTEGER, NOERR AS INTEGER
COMMON EUNKNOW AS SINGLE, ESEL AS SINGLE, ERANGE AS SINGLE
COMMON ETIME AS SINGLE, ECTRL AS SINGLE, EPASS AS SINGLE
COMMON ENUM AS SINGLE, EADDR AS SINGLE
,
ESTABLISH ERROR VARIABLES "ON ERROR" BRANCHING
,
PCIB.ERR = 0
PCIB.ERR$ = STRING$(64, 32)
PCIB.NAME$ = STRING$(16, 32)
PCIB.GLBERR = 0
CALL DEFERR(PCIB.ERR, PCIB.ERR$, PCIB.NAME$, PCIB.GLBERR)
PCIB.BASERR = 255
ON ERROR GOTO 99
GOTO MNEMONICS
,
ERROR HANDLING ROUTINE
,
ERRORHANDLER:
99 IF ERR = PCIB.BASERR THEN GOTO LIBERROR
PRINT "BASIC ERROR # "; ERR; "OCCURRED"
PRINT "ERROR: "; PCIB.ERR$
STOP
,
LIBERROR:
TMPERR = PCIB.ERR
IF TMPERR = 0 THEN TMPERR = PCIB.GLBERR
PRINT "HP-IB ERROR #"; TMPERR; "DETECTED"
PRINT "ERROR:"; PCIB.ERR$
STOP
,
MNEMONICS:
FALSE = 0
TRUE = NOT FALSE
NOERR = 0
EUNKNOW = 100001!
ESEL = 100002!
ERANGE = 100003!
```

APPENDIX: COMPUTER PROGRAMS

```
ETIME = 100004!
ECTRL = 100005!
EPASS = 100006!
ENUM = 100007!
EADDR = 100008!
,
,
END PROGRAM SET-UP
,
,
OPEN "KIN.DAT" FOR APPEND AS #1
,
,
HP 3497A : CHANNEL ALLOCATION
,
,
SLOT #2: DIGITAL
,
0 AUTO. GAS SAMPLER VALVE
,
1 HP GC AUTO. TEMPERATURE PROGRAM
,
,
SLOT #3:
,
61 CO2 ANALYSER, RANGE 0 - 5 %
,
62 CO ANALYSER, RANGE 0 - 2 %
,
63 O2 ANALYSER, RANGE 0 - 25 %
,
64 GAS CHROMATOGRAPH
,
65 MASS INFLOW CONTROLLER
,
66 MASS OUTFLOW
,
67 PRESSURE (INLET)
,
68 TEMPERATURE( DEG. C.)
,
69 NOT USED
,
,
INITIALISATION
,
,
ISC = 7
DEV = 709
ACTUAL = 0
MAXI = 1
MAXGC = 1
I = 1
II = 1
KK = 1
DLJ! = 3!
DINJ! = 6!
TGCP!T! = 0!
INGC = 1
```

APPENDIX: COMPUTER PROGRAMS

```
KPEAK = 1
,
,
MAXIMUM INSTRUMENT RANGES AND PRESSURE CALIBRATIONS
,
CO2RANGE! = 5!
CORANGE! = 2!
O2RANGE! = 25!
IPCALIB! = 20!      '20 PSI/DCV FOR INLET PRESSURE TRANSDUCER
,
,
SPECIFY GC TIME INTERVALS(MIN) TO BE RECORDED
,
TGC1! = 1.4
TGC2! = 1.4
TGC3! = 3!
,
,
SCREEN PLOT PARAMETERS
,
TIMEP! = 10!      'X-AXIS TIME SCALE (HRS)
NONGCP! = 25!     'NON-GC GAS% SCALE
TEMPR! = 800!    'MAX. TEMPERATURE SCALE
,
,
SYSTEM INITIALISATION
,
TIMES$ = "00:00:00"
CLS
CALL IORESET(ISC)
TIMEOUT = 5!
CALL IOTIMEOUT(ISC, TIMEOUT)
CALL IOCLEAR(ISC)
CALL IOREMOTE(ISC)
,
,
CODES$ = "SIS01VA1VD5VF1VSO"
LENGTH = LEN(CODES$)
CALL IOOUTPUTS(DEV, CODES$, LENGTH)
CODES$ = "D01,0"
LENGTH = LEN(CODES$)
CALL IOOUTPUTS(DEV, CODES$, LENGTH)
,
,
SCREEN 9
WIDTH 80, 43
VIEW PRINT 1 TO 43
```

APPENDIX: COMPUTER PROGRAMS

```

LOCATE 43, 3
PRINT "O      Time (hr)          10 0          Time (hr)          10"
LOCATE 15, 42
PRINT "O          GC (mV)          1"
LOCATE 41, 2
PRINT "O"
LOCATE 11, 1
PRINT "20"
LOCATE 26, 1
PRINT "10"
LOCATE 41, 41
PRINT "O"
LOCATE 19, 41
PRINT "8"
LOCATE 30, 41
PRINT "4"
LOCATE 2, 2
PRINT " min.  CO2 CO  O2  SLPW I/PSI DEG.C O/PSI #2"

LINE (639, 349)-(0, 0), 15, B
LINE (637, 24)-(2, 2), 15, B
LINE (17, 26)-(311, 326), 15, B
LINE (329, 26)-(631, 111), 12, B
LINE (329, 144)-(631, 326), 15, B
VIEW (18, 27)-(310, 325), 12 'VIEWPORT #1
VIEW (330, 27)-(630, 110), 15 'VIEWPORT #2
VIEW (330, 145)-(630, 325), 1 'VIEWPORT #3

VIEW (18, 27)-(310, 325)
WINDOW (0!, #ONGCP!)-(TIMEP!, 0!)
  XPO! = .75 * TIMEP!
  DELX! = TIMEP! / 80!
  YPO1! = .945 * #ONGCP!
  DELY! = .03 * #ONGCP!
  FOR I = 1 TO 10
    XP! = XPO! + (1 - I) * DELX!
    CIRCLE (XP!, YPO1!), .006, 14
    YPO2! = YPO1! - DELY!
    CIRCLE (XP!, YPO2!), .006, 0
    YPO3! = YPO1! - 2 * DELY!
    CIRCLE (XP!, YPO3!), .006, 15

```

APPENDIX: COMPUTER PROGRAMS

```
YP04! = YP01! - 3 * DELY!  
CIRCLE (XP!, YP04!), .006, 1  
NEXT 1  
LOCATE 6, 31  
PRINT "CO2 %"  
LOCATE 7, 31  
PRINT "CO %"  
LOCATE 8, 31  
PRINT "O2 %"  
LOCATE 9, 31  
PRINT "W2 x4%"  
VIEW (330, 145)-(630, 325)  
WINDOW (0!, .8)-(TIMEP!, 0!)  
LOCATE 18, 42  
PRINT "Temp.(100 C)"  
  
TIMER ON  
CODES$ = "AC61VR2VN1"  
LENGTH = LEN(CODES$)  
CALL IOOUTPUTS(DEV, CODES$, LENGTH)  
CALL IOENTERA(DEV, SEG S1!(1), MAXI, ACTUAL)  
S1!(1) = S1!(1) * CO2RANGE!  
  
CODES$ = "AC62VR2"  
LENGTH = LEN(CODES$)  
CALL IOOUTPUTS(DEV, CODES$, LENGTH)  
CALL IOENTERA(DEV, SEG S2!(1), MAXI, ACTUAL)  
S2!(1) = S2!(1) * CORANGE!  
  
CODES$ = "AC63VR2"  
LENGTH = LEN(CODES$)  
CALL IOOUTPUTS(DEV, CODES$, LENGTH)  
CALL IOENTERA(DEV, SEG S3!(1), MAXI, LENGTH)  
S3!(1) = S3!(1) * O2RANGE!  
  
TMIN! = TIMER / 60  
LOCATE 3, 2  
PRINT USING "###.# ##.# ##.# ##.#"; TMIN!; S1!(1); S2!(1); S3!(1)  
O2X! = S3!(1)  
  
SET INITIAL VALUES OF W2! AS FOLLOWS ASSUMING "NORMAL" AIR
```

APPENDIX: COMPUTER PROGRAMS

```
,
      N2! = 78.084
      G02! = S3!(1)
,
,
      EVENT TRAPPING TO SELECT RANGE OF CO2 AND CO ANALYZERS
,
      LOCATE 3, 57
      PRINT "CO2/CO RANGE= 3"
      ON KEY(11) GOSUB RANGE1
      KEY(11) ON
      ON KEY(14) GOSUB RANGE3
      KEY(14) ON
1500 TINJ! = II * DINJ!
      TLOAD! = TINJ! - DLJ!
      IF TMIN! >= TGC3! THEN
          CALL GCANALYSIS
          GOTO 4000
      END IF
      IF TMIN! < TLOAD! GOTO 1800
      IF (TMIN! >= TLOAD!) AND (KK = II) THEN
          CODES$ = "DC1,0"
          LENGTH = LEN(CODES$)
          CALL IOOUTPUTS(DEV, CODES$, LENGTH)
          KK = KK + 1
          GOTO 1800
      ELSEIF (TMIN! >= TINJ!) AND (KK > II) THEN
          O2X! = S3!(1)
          CODES$ = "D01,0"
          LENGTH = LEN(CODES$)
          CALL IOOUTPUTS(DEV, CODES$, LENGTH)
          II = II + 1
      END IF
,
1800 LOCATE 2, 72
      PRINT TIMES$
,
      IF TMIN! < TGC1! THEN GOTO 2000
      IF (TMIN! > TGC1!) AND (TMIN! < TGC3!) THEN CALL GC
,
2000 TMIN! = TIMER / 60
      XNGC! = .5 * INGC
```

APPENDIX: COMPUTER PROGRAMS

```
YNGC! = XNGC! + .1
IF (TMIN! > XNGC!) AND (TMIN! < YNGC!) THEN GOTO WONGC ELSE
GOTO 1500
,
4000 TGC1! = TGC1! + DINJ!
TGC2! = TGC2! + DINJ!
TGC3! = TGC3! + DINJ!
I = 1
GOTO 1500
END
,
WONGC:
,
, MEASURE AND STORE NON-GC READINGS
,
TIDPLT! = TIMER / 3600!
CODES$ = "AC61VR2VM1"
LENGTH = LEN(CODES$)
CALL IOOUTPUTS(DEV, CODES$, LENGTH)
CALL IOENTERA(DEV, SEG S1!(1), MAXI, ACTUAL)
S1!(1) = S1!(1) * C02RANGE!
,
IF (TMIN! > TGC1!) AND (TMIN! < TGC3!) THEN CALL GC
,
CODES$ = "AC62VR2"
LENGTH = LEN(CODES$)
CALL IOOUTPUTS(DEV, CODES$, LENGTH)
CALL IOENTERA(DEV, SEG S2!(1), MAXI, ACTUAL)
S2!(1) = S2!(1) * C0RANGE!
,
IF (TMIN! > TGC1!) AND (TMIN! < TGC3!) THEN CALL GC
,
CODES$ = "AC63VR2"
LENGTH = LEN(CODES$)
CALL IOOUTPUTS(DEV, CODES$, LENGTH)
CALL IOENTERA(DEV, SEG S3!(1), MAXI, ACTUAL)
S3!(1) = S3!(1) * O2RANGE!
,
IF (TMIN! > TGC1!) AND (TMIN! < TGC3!) THEN CALL GC
,
CODES$ = "AC65VR5"
```

APPENDIX: COMPUTER PROGRAMS

```
LENGTH = LEN(CODES$)
CALL IOOUTPUTS(DEV, CODES$, LENGTH)
CALL IOENTERA(DEV, SEG S5!(1), MAXI, ACTUAL)
,
IF (TMIN! > TGC1!) AND (TMIN! < TGC3!) THEN CALL GC
,
CODES$ = "AC66VR5"
LENGTH = LEN(CODES$)
CALL IOOUTPUTS(DEV, CODES$, LENGTH)
CALL IOENTERA(DEV, SEG S6!(1), MAXI, ACTUAL)
,
IF (TMIN! > TGC1!) AND (TMIN! < TGC3!) THEN CALL GC
,
CODES$ = "AC67VR5"
LENGTH = LEN(CODES$)
CALL IOOUTPUTS(DEV, CODES$, LENGTH)
CALL IOENTERA(DEV, SEG S7!(1), MAXI, ACTUAL)
  S7!(1) = S7!(1) * IPCALIB!
,
IF (TMIN! > TGC1!) AND (TMIN! < TGC3!) THEN CALL GC
,
CODES$ = "AC68VR5"
LENGTH = LEN(CODES$)
CALL IOOUTPUTS(DEV, CODES$, LENGTH)
CALL IOENTERA(DEV, SEG S8!(1), MAXI, ACTUAL)
  T! = S8!(1) * 1000!
,
PLOT AND STORE NON-GC DATA
,
LOCATE 3, 2
PRINT USING "###.* **.* **.* **.* *.* **.* ****."; TMIN!; S1!(1);
S2!(1); S3!(1); S5!(1); S7!(1); T!
PRINT #1, USING "###.** **.** **.** **.* *.* **.* ****.* ****.**
***.***"; TMIN!; S1!(1); S2!(1); S3!(1); S5!(1); S6!(1); S7!(1); T!; N2!
,
VIEW (18, 27)-(310, 325)
  WINDOW (0!, NONGCP!)-(TIMEP!, 0!)
  CIRCLE (TIDPLT!, S1!(1)), .006, 14
  CIRCLE (TIDPLT!, S2!(1)), .006, 0
  CIRCLE (TIDPLT!, S3!(1)), .006, 15
VIEW (330, 145)-(630, 325)
```

APPENDIX: COMPUTER PROGRAMS

```
WINDOW (0!, TEMPR!)-(TIMEP!, 0!)
S8P! = S8!(1) * 1000!
CIRCLE (TIDPLT!, S8P!), .006, 15
SOUND 800, 1
,
INGC = INGC + 1
GOTO 1500
,
,
RANGE1:
,
CO2RANGE! = 20!
CORANGE! = 10!
LOCATE 3, 71
PRINT "1"
RETURN
,
,
RANGE3:
,
CO2RANGE! = 5!
CORANGE! = 2!
LOCATE 3, 71
PRINT "3"
RETURN
END
,
,
DEFSNG A-Z
SUB GC
DIM LENGTH AS INTEGER
CODES$ = "AC64VR5VM1"
LENGTH = LEN(CODES$)
CALL IOOUTPUTS(DEV, CODES$, LENGTH)
CALL IOENTERA(DEV, SEG S4!(1), MAXGC, ACTUAL)
AS4!(I) = S4!(1)
TSEC!(I) = TIMER
IM = I
I = I + 1
END SUB
,
```

APPENDIX: COMPUTER PROGRAMS

```
,
SUB GCANALYSIS
,
SUBROUTINE TO CALCULATE N2% FROM N2, O2 and CO GC-READINGS USING O2
AND CO ANALYZER READINGS
,
DIM J AS INTEGER, I AS INTEGER, IB1 AS INTEGER, IB2 AS INTEGER
,
KPEAK = 1
CAREA! = 0!
IB1 = .05 * (IM - 1)
IB2 = .75 * (IM - 1)
,
BLINE! = .5 * (AS4!(IB1) + AS4!(IB2))
,
COMPUTE N2 PEAK USING SIMPSON'S RULE
,
FOR J = IB1 TO IB2 STEP 2
  IF J >= IB2 THEN
    AVEH! = TSEC!(J + 1) - TSEC(J)
    DAREA! = (AS4(J + 1) + AS4!(J) - 2 * BLINE!) * .5
    DAREA! = AVEH! * DAREA!
  ELSE
    AVEH! = (TSEC!(J + 2) - TSEC!(J)) / 2
    DAREA! = AS4!(J) + AS4!(J + 2) + 4 * AS4!(J + 1) - 6 * BLINE!
    DAREA! = AVEH! * DAREA! / 3
  END IF
  CAREA! = CAREA! + DAREA!
NEXT J
,
FACGC! = 8752.657
N2! = CAREA! * FACGC!
TGC! = TSEC!(2) / 60!
VIEW (330, 27)-(630, 110)
  CLS 1
VIEW (330, 27)-(630, 110), 15
VIEW (330, 27)-(630, 110)
WINDOW (-.00002, TSEC!(IM - 1))-(.001, TSEC!(2))
FOR I = 2 TO IM - 1
  IF I = 2 THEN GOTO 4001
  LINE (AS4!(1), TSEC!(1))-(AS4!(I - 1), TSEC!(I - 1)), 1
```

APPENDIX: COMPUTER PROGRAMS

4001 NEXT 1

LINE (AS4!(IB1), TSEC!(IB1))-(AS4!(IB2), TSEC!(IB2)), 12

LOCATE 3, 51

PRINT USING "###.##"; N2!

N2X! = N2! / 4!

VIEW (18, 27)-(310, 325)

WINDOW (0!, NONGCP!)-(TIMEP!, 0!)

TGC! = TGC! / 60!

CIRCLE (TGC!, N2X!), .007, 1

END SUB

APPENDIX: COMPUTER PROGRAMS

2. Program COMBUS.BAS

```
' PROGRAM COMBUS.BAS
'
' BY DAULAT MAMORA, STANFORD UNIVERSITY, JUNE 12, 1992.
'
' A. PROGRAM FOR COMBUSTION TUBE EXPERIMENTS IN WHICH ONE MOVEABLE
' AND 9 STATIONARY THERMOCOUPLES ARE USED.
'
' B. TO ACCESS PROGRAM, TYPE FOLLOWING AT C:\LIB>
' QB COMBUS.BAS /L QB4HPIB.QLB
'
' C. COMPILE AND RUN PROGRAM PER QUICKBASICS PROCEDURE.
'
' D. PROGRAM CARRIES OUT FOLLOWING FUNCTIONS.
'
' 1. CONTROLS POSITION OF GAS AUTO-SAMPLER.
'
' 2. RECORDS READINGS OF CO2, CO AND O2 ANALYZERS, GAS INJECTION RATE,
' GAS PRODUCTION RATE AND PRESSURE AT 30-SEC INTERVALS.
'
' 3. READS GC MILLIVOLTS, COMPUTES N2 CONCENTRATION AT 6-MIN INTERVALS.
'
' 4. WITH AUTO-SAMPLER ON BACKFLUSH MODE, TEMPERATURES ARE RECORDED
' AS FOLLOWS.
' 4.1 PRESS "RIGHT ARROW" KEY. TYPE DEPTH OF MOVEABLE THERMOCOUPLE
' IN CM, TO 1 DECIMAL PLACE.
' 4.2 RECORD TIME, POSITION AND TEMPERATURE OF MOVEABLE THERMOCOUPLE
' BY PRESSING 'ENTER' KEY.
' 4.3 REPEAT STEPS 4.1 AND 4.2 FOR EACH MOVEABLE THERMOCOUPLE
' POSITION.
' 4.4 RECORD TIME, POSITIONS AND TEMPERATURES OF STATIONARY
' THERMOCOUPLES BY PRESSING "LEFT ARROW" KEY.
' 4.5 COMPLETE STEP 4.4 BEFORE AUTO-SAMPLER SWITCHES TO SAMPLING
' MODE. THAT IS, MAX. 3 MIN. TO EXECUTE STEPS 4.1 - 4.4.
'
' 5. PLOTS ON SCREEN:
' WINDOW 1: CO2, CO AND O2 CONCENTRATION VERSUS TIME.
' WINDOW 2: DEPTH OF MOVEABLE THERMOCOUPLE
' WINDOW 3: TEMPERATURE PROFILE.
```

APPENDIX: COMPUTER PROGRAMS

```
'      WINDOW 4: GC TRACE OF W2 PEAK.
'      WINDOW 5: TEMPERATURE PROFILE OF MOVEABLE THERMOCOUPLE.
'
DECLARE SUB GCANALYSIS ()
DECLARE SUB GC ()
DECLARE SUB TEMP ()
'
'
OPTION BASE 1
DEFINT A-Z
DIM S1!(1), S2!(1), S3!(1), S4!(1), S5!(1), S6!(1), S9!(1), S8!(1),
    RCOLD!(1)
DIM TSEC!(3500), AS4!(3500), TCLOC!(20), TCTEMP!(20), TCL1!(20), TCT1!(20)
DIM MTCLOC!(20), MTEMP!(20)
COMMON SHARED W2!, GO2!, O2X!, WONGCP!, TIMEP!, TUBLEN!, TEMPR!, TIP$
COMMON SHARED S1!(), S2!(), S3!(), S4!(), S6!(), S9!(), S8!(), RCOLD!()
COMMON SHARED AS4!(), TSEC!(), TGC2!, TCLOC!(), TCTEMP!(), TCL1!(), TCT1!()
COMMON SHARED DEV AS LONG, ISC AS LONG, KPEAK AS INTEGER, TREC AS INTEGER
COMMON SHARED IM AS INTEGER, I AS INTEGER, M AS INTEGER, K AS INTEGER
COMMON SHARED MAXI AS INTEGER, MAXGC AS INTEGER, ACTUAL AS INTEGER
COMMON SHARED MTCLOC!(), MTEMP!(), ITC AS INTEGER, ITCMAX AS INTEGER
'
COMMON PCIB.BASERR, PCIB.ERR, PCIB.ERR$, PCIB.NAME$, PCIB.GLBERR
COMMON FALSE AS INTEGER, TRUE AS INTEGER, NOERR AS INTEGER
COMMON EUNKNOWN AS SINGLE, ESEL AS SINGLE, ERANGE AS SINGLE
COMMON ETIME AS SINGLE, ECTRL AS SINGLE, EPASS AS SINGLE
COMMON ENUM AS SINGLE, EADDR AS SINGLE
'
' ESTABLISH ERROR VARIABLES "ON ERROR" BRANCHING
'
PCIB.ERR = 0
PCIB.ERR$ = STRING$(64, 32)
PCIB.NAME$ = STRING$(16, 32)
PCIB.GLBERR = 0
CALL DEFERR(PCIB.ERR, PCIB.ERR$, PCIB.NAME$, PCIB.GLBERR)
PCIB.BASERR = 255
ON ERROR GOTO 99
GOTO MNEMONICS
'
' ERROR HANDLING ROUTINE
'
```

APPENDIX: COMPUTER PROGRAMS

```
ERRORHANDLER:
99 IF ERR = PCIB.BASERR THEN GOTO LIBERROR
   PRINT "BASIC ERROR # "; ERR; "OCCURRED"
   PRINT "ERROR: "; PCIB.ERR$
   STOP
,
LIBERROR:
TMPERR = PCIB.ERR
IF TMPERR = 0 THEN TMPERR = PCIB.GLBERR
PRINT "HP-IB ERROR #"; TMPERR; "DETECTED"
PRINT "ERROR:"; PCIB.ERR$
STOP
,
MNEMONICS:
FALSE = 0
TRUE = NOT FALSE
NOERR = 0
EUNKNOWN = 100001!
ESEL = 100002!
ERANGE = 100003!
ETIME = 100004!
ECTRL = 100005!
EPASS = 100006!
ENUM = 100007!
EADDR = 100008!
,
,
END PROGRAM SET-UP
,
OPEN "COMBUS.DAT" FOR APPEND AS #1
OPEN "TEMP.DAT" FOR APPEND AS #2
,
,
HP 3497A : CHANNEL ALLOCATION
,
,
SLOT #0:
    8-16 STATIONARY THERMOCOUPLES
,
,
SLOT #1: DIGITAL
    0    AUTO. GAS SAMPLER VALVE
    1    HP GC AUTO. TEMPERATURE PROGRAM
,
,
SLOT #3:
```

APPENDIX: COMPUTER PROGRAMS

```
,      60  NOT USED
,      61  CO2 ANALYZER
,      62  CO ANALYZER
,      63  O2 ANALYZER
,      64  GAS CHROMATOGRAPH
,      65  MASS FLOW CONTROLLER (GAS INJECTION RATE)
,      66  MASS FLOWMETER (GAS PRODUCTION RATE)
,      67  NOT USED
,      68  MOVEABLE THERMOCOUPLE TEMPERATURE
,      69  INLET PRESSURE TRANSDUCER
,
,
,      INITIALISATION OF VALUES
,
,
ISC = 7
DEV = 709
ACTUAL = 0
MAXI = 1
MAXGC = 1
I = 1
II = 1
KK = 1
DLJ! = 3!
DINJ! = 6!
TGCPLT! = 0!
INGC = 1
KPEAK = 1
ITC = 0
TREC = 0
,
,      DEPTHS OF FIXED PROBE THERMOCOUPLES FROM TOP OF FLANGE (CM)
,
,
TCLOC!(9) = 96.8
TCLOC!(10) = 86.8
TCLOC!(11) = 76.8
TCLOC!(12) = 66.8
TCLOC!(13) = 56.8
LOC!(14) = 46.8
TCLOC!(15) = 36.8
TCLOC!(16) = 26.8
TCLOC!(17) = 3!
```

APPENDIX: COMPUTER PROGRAMS

```
,  
,  
    MAXIMUM INSTRUMENT RANGES/ PRESSURE CALIBRATIONS  
,  
  
    CO2RANGE! = 20!  
    CORANGE! = 10!  
    O2RANGE! = 25!  
    IPCALIB! = 20!      '20 PSI/DCV FOR INLET PRESSURE TRANSDUCER  
,  
  
    SPECIFY GC TIME INTERVALS(MIN) TO BE RECORDED  
,  
  
    TGC1! = 1.5  
    TGC2! = 1.5  
    TGC3! = 3!  
,  
  
    SCREEN PLOT PARAMETERS  
,  
  
    TIMEP! = 10!      'X- AXIS TIME SCALE (HRS)  
    NONGCP! = 25!     'NON -GC GAS% SCALE  
    TUBLEN! = 100!   'TUBE LENGTH AXIS SCALE (METERS)  
    TEMPR! = 700!    'TEMPERATURE RANGE (DEG. C)  
,  
  
    SYSTEM INITIALISATION  
,  
  
    TIME$ = "00:00:00"  
    CLS  
    CALL IORESET(ISC)  
    TIMEOUT = 5!  
    CALL IOTIMEOUT(ISC, TIMEOUT)  
    CALL IOCLEAR(ISC)  
    CALL IOREMOTE(ISC)  
,  
  
    CODES$ = "SIS01VA1VD5VF1VSO"  
    LENGTH = LEN(CODES$)  
    CALL IOOUTPUTS(DEV, CODES$, LENGTH)  
    CODES$ = "D01,0"  
    LENGTH = LEN(CODES$)  
    CALL IOOUTPUTS(DEV, CODES$, LENGTH)  
,  
  
    SCREEN 9  
    WIDTH 80, 43  
    VIEW PRINT 1 TO 43
```

APPENDIX: COMPUTER PROGRAMS

```
LOCATE 2, 2
PRINT " min.  CO2 CO  O2  SLPM I/PSI DEG.C O/PSI #2"
LOCATE 26, 4
PRINT "O          Time (hr)          10"
LOCATE 15, 45
PRINT "O          GC (mV)          1"
LOCATE 42, 4
PRINT "O          Distance (cm)          100"
LOCATE 25, 3
PRINT "O"
LOCATE 17, 2
PRINT "10"
LOCATE 8, 2
PRINT "20"
LOCATE 6, 2
PRINT "%"
LOCATE 25, 41
PRINT "O"
LOCATE 8, 41
PRINT "80"
LOCATE 6, 41
PRINT "%"
LOCATE 16, 41
PRINT "#2"
LOCATE 41, 3
PRINT "O"
LOCATE 28, 1
PRINT "700"
LOCATE 34, 1
PRINT "deg"
LOCATE 35, 2
PRINT "C"
LOCATE 41, 51
PRINT "O"
LOCATE 17, 49
PRINT "700"
```

```
LINE (639, 349)-(0, 0), 15, B
LINE (637, 24)-(2, 2), 15, B
LINE (330, 140)-(393, 196), 14, B
LOCATE 19, 43
```

APPENDIX: COMPUTER PROGRAMS

```
PRINT "Mov.TC"
LOCATE 20, 43
PRINT "at (cm)"

LINE (27, 26)-(316, 196), 15, B
LINE (27, 218)-(397, 326), 15, B
LINE (352, 26)-(631, 111), 12, B
LINE (408, 131)-(631, 326), 15, B
VIEW (28, 27)-(315, 195), 12 'VIEWPORT #1
VIEW (28, 219)-(396, 325), 1 'VIEWPORT #2
VIEW (353, 27)-(630, 110), 15 'VIEWPORT #3
VIEW (409, 132)-(630, 325), 1 'VIEWPORT #4

VIEW (18, 27)-(310, 195)
WINDOW (0!, NONGCP!)-(TIMEP!, 0!)
XPO! = .9 * TIMEP!
DELX! = TIMEP! / 80!
YPO1! = .945 * NONGCP!
DELY! = .05 * NONGCP!
FOR I = 1 TO 10
  XP! = XPO! + (1 - I) * DELX!
  CIRCLE (XP!, YPO1!), .006, 14
  YPO2! = YPO1! - DELY!
  CIRCLE (XP!, YPO2!), .006, 0
  YPO3! = YPO1! - 2 * DELY!
  CIRCLE (XP!, YPO3!), .006, 15
  YPO4! = YPO1! - 3 * DELY!
  CIRCLE (XP!, YPO4!), .006, 1
NEXT I
LOCATE 5, 37
PRINT "C02"
LOCATE 6, 37
PRINT "C0"
LOCATE 7, 37
PRINT "O2"
LOCATE 8, 37
PRINT "E2"

VIEW (409, 132)-(630, 325)
LOCATE 18, 55
PRINT "Moveable Probe Profile"
```

APPENDIX: COMPUTER PROGRAMS

```
,
TIMER ON
CODES$ = "AC61VR2VH1"
LENGTH = LEN(CODES$)
CALL IOOUTPUTS(DEV, CODES$, LENGTH)
CALL IOENTERA(DEV, SEG S1!(1), MAXI, ACTUAL)
  S1!(1) = S1!(1) * CD2RANGE!
,
CODES$ = "AC62VR2"
LENGTH = LEN(CODES$)
CALL IOOUTPUTS(DEV, CODES$, LENGTH)
CALL IOENTERA(DEV, SEG S2!(1), MAXI, ACTUAL)
  S2!(1) = S2!(1) * CD2RANGE!
,
CODES$ = "AC63VR2"
LENGTH = LEN(CODES$)
CALL IOOUTPUTS(DEV, CODES$, LENGTH)
CALL IOENTERA(DEV, SEG S3!(1), MAXI, LENGTH)
  S3!(1) = S3!(1) * O2RANGE!
,
TMIN! = TIMER / 60
LOCATE 3, 2
PRINT USING "###.# ##.# ##.# ##.#"; TMIN!; S1!(1); S2!(1); S3!(1)
O2X! = S3!(1)
,
,
SET INITIAL VALUES OF H2! AND G02! AS FOLLOWS ASSUMING STANDARD AIR
,
H2! = 100! - S3!(1) - .03
G02! = S3!(1)
,
,
EVENT TRAPPING TO SELECT RANGE OF CO2 AND CO ANALYZERS
,
LOCATE 3, 57
PRINT "CO2/CO RANGE= 1"
ON KEY(11) GOSUB RANGE1
KEY(11) ON
ON KEY(14) GOSUB RANGE3
KEY(14) ON
,
,
EVENT TRAPPING TO ENTER MOVEABLE (SINGLE) THERMOCOUPLE DISTANCE
AND DISTANCE
```

APPENDIX: COMPUTER PROGRAMS

```
,
ON KEY(13) GOSUB TIPLOC
KEY(13) ON
,
,
EVENT TRAPPING TO STORE TIME, DISTANCE AND TEMPERATURES
OF ALL THERMOCOUPLES
,
ON KEY(12) GOSUB TEMPREC
KEY(12) ON
,
1500 TINJ! = II * DINJ!
TLOAD! = TINJ! - DLJ!
IF TMIN! >= TGC3! THEN
CALL GCANALYSIS
GOTO 4000
END IF
IF TMIN! < TLOAD! GOTO 1800
IF (TMIN! >= TLOAD!) AND (KK = II) THEN
CODES$ = "DC1,0"
LENGTH = LEN(CODES$)
CALL IOOUTPUTS(DEV, CODES$, LENGTH)
KK = KK + 1
GOTO 1800
ELSEIF (TMIN! >= TINJ!) AND (KK > II) THEN
O2X! = S3!(1)
CODES$ = "D01,0"
LENGTH = LEN(CODES$)
CALL IOOUTPUTS(DEV, CODES$, LENGTH)
II = II + 1
END IF
,
1800 LOCATE 2, 72
PRINT TIME$
,
IF TMIN! < TGC1! THEN GOTO 2000
IF (TMIN! > TGC1!) AND (TMIN! < TGC3!) THEN CALL GC
,
2000 TMIN! = TIMER / 60
XNGC! = .5 * INGC
YNGC! = XNGC! + .1
IF (TMIN! > XNGC!) AND (TMIN! < YNGC!) THEN GOTO WONGC ELSE
```

APPENDIX: COMPUTER PROGRAMS

```
GOTO 1500
,
4000 TGC1! = TGC1! + DINJ!
      TGC2! = TGC2! + DINJ!
      TGC3! = TGC3! + DINJ!
      I = 1
      GOTO 1500
      END
,
,
NONGC:
,
, MEASURE AND STORE NON-GC READINGS
,
      TIDPLT! = TIMER / 3600!
      CODES$ = "AC61VR2VH1"
      LENGTH = LEN(CODES$)
      CALL IOOUTPUTS(DEV, CODES$, LENGTH)
      CALL IOENTERA(DEV, SEG S1!(1), MAXI, ACTUAL)
      S1!(1) = S1!(1) * C02RANGE!
,
      IF (TMIN! > TGC1!) AND (TMIN! < TGC3!) THEN CALL GC
,
      CODES$ = "AC62VR2"
      LENGTH = LEN(CODES$)
      CALL IOOUTPUTS(DEV, CODES$, LENGTH)
      CALL IOENTERA(DEV, SEG S2!(1), MAXI, ACTUAL)
      S2!(1) = S2!(1) * C0RANGE!
,
      IF (TMIN! > TGC1!) AND (TMIN! < TGC3!) THEN CALL GC
,
      CODES$ = "AC63VR2"
      LENGTH = LEN(CODES$)
      CALL IOOUTPUTS(DEV, CODES$, LENGTH)
      CALL IOENTERA(DEV, SEG S3!(1), MAXI, ACTUAL)
      S3!(1) = S3!(1) * 02RANGE!
,
      IF (TMIN! > TGC1!) AND (TMIN! < TGC3!) THEN CALL GC
,
      CODES$ = "AC65VR5"
      LENGTH = LEN(CODES$)
```

APPENDIX: COMPUTER PROGRAMS

```
CALL IOOUTPUTS(DEV, CODES$, LENGTH)
CALL IOENTERA(DEV, SEG S5!(1), MAXI, ACTUAL)
,
IF (TMIN! > TGC1!) AND (TMIN! < TGC3!) THEN CALL GC
,
CODES$ = "AC66VR5"
LENGTH = LEN(CODES$)
CALL IOOUTPUTS(DEV, CODES$, LENGTH)
CALL IOENTERA(DEV, SEG S6!(1), MAXI, ACTUAL)
,
IF (TMIN! > TGC1!) AND (TMIN! < TGC3!) THEN CALL GC
,
CODES$ = "AC69VR5"
LENGTH = LEN(CODES$)
CALL IOOUTPUTS(DEV, CODES$, LENGTH)
CALL IOENTERA(DEV, SEG S9!(1), MAXI, ACTUAL)
  S9!(1) = S9!(1) * IPCALIB!
,
IF (TMIN! > TGC1!) AND (TMIN! < TGC3!) THEN CALL GC
,
PLOT AND STORE NON-GC DATA
,
LOCATE 3, 2
PRINT USING "###.* **.* **.* **.* *.* **.* ****. "; TMIN!; S1!(1);
S2!(1); S3!(1); S5!(1); S9!(1); MTEMP!(1)
PRINT #1, USING "###.* **.* **.* **.* **.* *.* **.* ****.* ****.*
***.***"; TMIN!; S1!(1); S2!(1); S3!(1); S5!(1); S6!(1); S9!(1);
MTEMP!(1); N2!
,
VIEW (28, 27)-(315, 195)
  WINDOW (0!, NONGCP!)-(TIMEP!, 0!)
  CIRCLE (TIDPLT!, S1!(1)), .006, 14
  CIRCLE (TIDPLT!, S2!(1)), .006, 0
  CIRCLE (TIDPLT!, S3!(1)), .006, 15
SOUND 600, 1
,
INGC = INGC + 1
GOTO 1500
,
RANGE1:
```

APPENDIX: COMPUTER PROGRAMS

```
CO2RANGE! = 20!
```

```
CORANGE! = 10!
```

```
LOCATE 3, 71
```

```
PRINT "1"
```

```
RETURN
```

```
RANGE3:
```

```
CO2RANGE! = 5!
```

```
CORANGE! = 2!
```

```
LOCATE 3, 71
```

```
PRINT "3"
```

```
RETURN
```

```
TIPLOC:
```

```
RECORD DEPTH, TEMPERATURE OF MOVEABLE THERMOCOUPLE
```

```
IF NEW SET OF TEMPERATURES, DELETE PREVIOUS TEMPERATURE PLOT
```

```
IF (ITC = 0) THEN
```

```
VIEW (409, 132)-(630, 325)
```

```
PX1! = TCL1!(1) - 10!
```

```
PX2! = TCL1!(1) + 10!
```

```
WINDOW (PX1!, TEMPR!)-(PX2!, 0!)
```

```
FOR I = 1 TO ITCMAX
```

```
  CIRCLE (TCL1!(I), TCT1!(I)), .006, 1
```

```
  NEXT I
```

```
END IF
```

```
RECORD DEPTH AND TEMPERATURE
```

```
ITC = ITC + 1
```

```
LOCATE 23, 43
```

```
INPUT ":", TIP$
```

```
MTCLOC!(ITC) = VAL(TIP$)
```

```
CODES$ = "AC68VR5"
```

```
LENGTH = LEN(CODES$)
```

APPENDIX: COMPUTER PROGRAMS

```
CALL IOOUTPUTS(DEV, CODES$, LENGTH)
CALL IOENTERA(DEV, SEG S8!(1), MAXI, ACTUAL)
MTEMP!(ITC) = S8!(1) * 1000!
TCL1!(ITC) = MTCLOC!(ITC)
TCT1!(ITC) = MTEMP!(ITC)
,
,
PLOT TEMPERATURE PROFILE
,
IF (ITC = 1) THEN
  PX1! = TCL1!(1) - 10!
  PX2! = TCL1!(1) + 10!
  LOCATE 42, 52
  PRINT USING "##.*"          ##.*"; PX1!; PX2!
END IF
,
,
VIEW (409, 132)-(630, 325)
WINDOW (PX1!, TEMPR!)-(PX2!, 0!)
CIRCLE (TCL1!(ITC), TCT1!(ITC)), .006, 15
RETURN
,
,
TEMPREC:
,
,
STORE TIME,DEPTH AND TEMPERATURE ON HARD DISK
,
CALL TEMP
ITCMAX = ITC
ITC = 0
RETURN
END
,
,
DEFSNG A-Z
SUB GC
DIM LENGTH AS INTEGER
CODES$ = "AC64VR5VM1"
LENGTH = LEN(CODES$)
CALL IOOUTPUTS(DEV, CODES$, LENGTH)
CALL IOENTERA(DEV, SEG S4!(1), MAXGC, ACTUAL)
AS4!(I) = S4!(1)
TSEC!(I) = TIMER
```

APPENDIX: COMPUTER PROGRAMS

```
IM = I
I = I + 1
END SUB
,
,
SUB GCANALYSIS
DIM J AS INTEGER, I AS INTEGER, IB1 AS INTEGER, IB2 AS INTEGER
,
,
SUBROUTINE TO CALCULATE N2% FROM GC-READINGS
,
KPEAK = 1
CAREA! = 0!
IB1 = .07 * (IM - 1)
IB2 = .7 * (IM - 1)
BLINE! = .5 * (AS4!(IB1) + AS4!(IB2))
,
,
COMPUTE N2 PEAK USING SIMPSON'S RULE
,
FOR J = IB1 TO IB2 STEP 2
  IF J >= IB2 THEN
    AVEH! = TSEC!(J + 1) - TSEC(J)
    DAREA! = (AS4!(J + 1) + AS4!(J) - 2 * BLINE!) * .5
    DAREA! = AVEH! * DAREA!
  ELSE
    AVEH! = (TSEC!(J + 2) - TSEC!(J)) / 2
    DAREA! = AS4!(J) + AS4!(J + 2) + 4 * AS4!(J + 1) - 6 * BLINE!
    DAREA! = AVEH! * DAREA! / 3
  END IF
  CAREA! = CAREA! + DAREA!
NEXT J
,
FACGC! = 8837.21
N2! = CAREA! * FACGC!
,
TGC! = TSEC!(2) / 60!
VIEW (353, 27)-(630, 110)
CLS 1
VIEW (353, 27)-(630, 110), 15
VIEW (353, 27)-(630, 110)
WINDOW (-.00002, TSEC!(IM - 1))-(.001, TSEC!(2))
FOR I = 2 TO IM - 1
```

APPENDIX: COMPUTER PROGRAMS

```
IF 1 = 2 THEN GOTO 4001
LINE (AS4!(1), TSEC!(1))-(AS4!(1 - 1), TSEC!(1 - 1)), 1
4001 NEXT 1
,
LINE (AS4!(IB1), TSEC!(IB1))-(AS4!(IB2), TSEC!(IB2)), 12
LOCATE 3, 51
PRINT USING "###.##"; N2!
N2X! = N2! / 4!
VIEW (18, 27)-(310, 204)
WINDOW (0!, HONGCP!)-(TIMEP!, 0!)
TGC! = TGC! / 60!
CIRCLE (TGC!, N2X!), .007, 1
END SUB

SUB TEMP
DIM LENGTH AS INTEGER
DIM V2!(1)
,
R0# = -.00000075004344#
R1# = .0000505321995#
R2# = 2.348050017D-08
P0# = -.3595568424#
P1# = 19750.87948#
P2# = -175116.5425#
P3# = 18212965.58#
P4# = -2831128435#
P5# = 271508383300#
P6# = -13801412100000#
P7# = 379243843260000#
P8# = -5371925517000000#
P9# = 3.0840255439D+16
,
,
READ COLD JUNCTION CHANNEL #19
,
CODES$ = "AC19VR5VW1"
LENGTH = LEN(CODES$)
CALL IOOUTPUTS(DEV, CODES$, LENGTH)
CALL IOENTERA(DEV, SEG RCOLD!(1), MAXI, ACTUAL)
TCOLD# = RCOLD!(1) * 10!
V1! = R0# + TCOLD# * (R1# + TCOLD# * R2#)
,
```

APPENDIX: COMPUTER PROGRAMS

```
, READ THERMOCOUPLE EMF AT CHANNELS 8 TO 16
,
CODES$ = "AF8AL15ASVR5VM1"
LENGTH = LEN(CODES$)
FOR I = 9 TO 17
  CALL IOOUTPUTS(DEV, CODES$, LENGTH)
  CALL IOENTERA(DEV, SEG V2!(1), MAXI, ACTUAL)
  V! = V1! + V2!(1)
  P79# = P7# + V! * (P8# + V! * P9#)
  P56# = P5# + V! * (P6# + V! * P79#)
  P34# = P3# + V! * (P4# + V! * P56#)
  P12# = P1# + V! * (P2# + V! * P34#)
  T1# = P0# + V! * P12#
  TTEMP!(I) = INT(T1# * 100! + .5) / 100!
NEXT I
,
, STORE TIME, DEPTH AND TEMPERATURE FOR ALL THERMOCOUPLES
,
TR! = TIMER / 60!
FOR I = 1 TO ITC
  PRINT #2, USING "###.###    ###.##    ####.####"; TR!; MTCLOC!(I);
  MTEMP!(I)
NEXT I
FOR I = 9 TO 17
  PRINT #2, USING "###.###    ###.##    ####.####"; TR!; TCLOC!(I);
  TTEMP!(I)
NEXT I
,
, PLOT PROFILE OF ALL TEMPERATURES
,
VIEW (28, 219)-(396, 325)
WINDOW (0!, TEMPR!)-(TUBLEN!, 0!)
FOR I = 9 TO 17
  CIRCLE (TCLOC!(I), TTEMP!(I)), .006, 15
NEXT I
FOR I = 1 TO ITC
  CIRCLE (MTCLOC!(I), MTEMP!(I)), .006, 15
NEXT I
,
END SUB
```

APPENDIX: COMPUTER PROGRAMS

3. Program GASCAL.F

```
C PROGRAM GASCAL.F
C
C BY DAULAT MAMORA, STANFORD UNIVERSITY, OCTOBER 1990.
C
C
C PROGRAM EXECUTES THE FOLLOWING:
C
C 1) COMPUTATION OF CALIBRATED CO2 AND CO ANALYZER READINGS
C    USING POLYNOMIALS OF ORDER 5 AND O2 ANALYZER READINGS
C    USING A LINEAR FIT, AT START AND END OF EXPERIMENT.
C
C 2) COMPUTATION OF CALIBRATED NITROGEN READINGS, USING TIME
C    WEIGHTED CALIBRATION POINTS AT START AND END OF EXPERIMENT.
C
C 3) COMPUTES OXYGEN CONSUMED.
C
C 4) CREATES GAS COMPOSITION AND TEMPERATURE PLOT DATA FILE.
C
C 5) CREATES OXYGEN CONCENTRATION, GAS INJECTION AND PRODUCTION
C    RATE, AND PRESSURE PLOT DATA FILE.
C
C
C    IMPLICIT DOUBLE PRECISION (A-H,O-Z)
C    DOUBLE PRECISION T(1000),RCO2(1000),RCO(1000),RO2(1000),
C    +QI(1000),QO(1000),P(1000),TEMP(1000),XN2(1000),XN2C(1000),
C    +CO2(1000),CO(1000),O2(1000)
C    COMMON T,RCO2,RCO,RO2,QI,QO,P,TEMP,XN2,XN2C,CO2,CO,O2
C    DOUBLE PRECISION O2P(10),O2B(10),O2E(10),CO2P(10),CO2B(10),
C    +CO2E(10),COP(10),COB(10),COE(10),CO2PLT(110),COPLT(110),
C    +O2PLT(110)
C
C    OPEN (UNIT=1,STATUS='OLD',FILE='c3.dat')
C    OPEN (UNIT=2,STATUS='OLD',FILE='c3.cor')
C    OPEN (UNIT=3,STATUS='OLD',FILE='c3.co2')
C    OPEN (UNIT=4,STATUS='OLD',FILE='c3.co')
C    OPEN (UNIT=7,STATUS='OLD',FILE='c3.o2')
C    OPEN (UNIT=8,STATUS='OLD',FILE='c3p1.dat')
C    OPEN (UNIT=9,STATUS='OLD',FILE='c3.ins')
```

APPENDIX: COMPUTER PROGRAMS

```
C
C DEFAULT MAXIMUM ANALYZER RANGES
C
  CO2RGE=5.
  CORGE=2.
  O2RGE=25.
  NDATA=550
  TSPAN=NDATA*.5
  TR1B=0.
  IN2=1
C
C PLOTTING PARAMETERS FOR FITS
C
  DEL=0.01
  NPT=101
C
C TEMPERATURE AND NITROGEN PLOT SCALE FACTORS
C
  SCALEN2=100./5.
  SCALET=600./5.
  SCALEP=150./2.
  SCALEO2=25./2.
C
C READ RAW EXPERIMENTAL DATA
C
  DO 1 I=1,NDATA
    READ(1,500) T(I),RCO2(I),RCO(I),RO2(I),QI(I),QO(I),
+ P(I),TEMP(I),XN2(I)
1  CONTINUE
500  FORMAT(F6.2,3F7.3,2F6.3,F7.1,F9.3,F7.3)
C
C
C CARBON DIOXIDE
C
C CALIBRATION DATA
C
  ICO2=5
  CO2P(1)=.0
  CO2P(2)=.033
  CO2P(3)=1.11
  CO2P(4)=2.53
```

APPENDIX: COMPUTER PROGRAMS

```
      C02P(5)=4.46
C
      C02B(1)=.0023
      C02B(2)=.0159
      C02B(3)=.2972
      C02B(4)=.5826
      C02B(5)=.9288
C
      C02E(1)=.0049
      C02E(2)=.0161
      C02E(3)=.2980
      C02E(4)=.5840
      C02E(5)=.9336
C
      CALL CALFIT (C02P,C02B,IC02,AC02,BC02,CC02,DC02,EC02,FC02)
      AB=AC02
      BB=BC02
      CB=CC02
      DB=DC02
      EB=EC02
      FB=FC02
      CALL CALFIT (C02P,C02E,IC02,AC02,BC02,CC02,DC02,EC02,FC02)
      AE=AC02
      BE=BC02
      CE=CC02
      DE=DC02
      EE=EC02
      FE=FC02
C
      WRITE(8,990) NDATA
C
      DO 350 I=1,NDATA
      RC02V= RC02(I)/C02RGE
      C021= (AB +BB*RC02V +CB*(RC02V**2.) +DB*(RC02V**3.)
+         +EB*(RC02V**4.) +FB*(RC02V**5.))*(TSPAN-T(I))
      C022= (AE +BE*RC02V +CE*(RC02V**2.) +DE*(RC02V**3.)
+         +EE*(RC02V**4.) +FE*(RC02V**5.))*T(I)
      C02(I)=(C021+C022)/TSPAN
      WRITE(8,999) T(I)/60., C02(I)
350  CONTINUE
C
```

APPENDIX: COMPUTER PROGRAMS

```
C CREATE PLOT DATA FILE
C
  WRITE(3,101) IC02
  DO 351 I=1,IC02
351  WRITE(3,102) C02B(I),C02P(I)
      WRITE(3,101) IC02
      DO 352 I=1,IC02
352  WRITE(3,102) C02E(I),C02P(I)
      WRITE(3,103) NPT
      DO 353 I=1,NPT
          C02V= (I-1)*DEL
          C02PLT(I)=AB+BB*C02V+CB*(C02V**2.)+DB*(C02V**3.)
+           +EB*(C02V**4.) +FB*(C02V**5.)
353  WRITE(3,102) C02V,C02PLT(I)
      WRITE(3,103) NPT
      DO 354 I=1,NPT
          C02V= (I-1)*DEL
          C02PLT(I)=AE+BE*C02V+CE*(C02V**2.)+DE*(C02V**3.)
+           +EE*(C02V**4.) +FE*(C02V**5.)
354  WRITE(3,102) C02V,C02PLT(I)
C
C
C CARBON MONOXIDE
C
C CALIBRATION DATA
C
  IC0=4
  COP(1)=.0
  COP(2)=.50
  COP(3)=1.04
  COP(4)=1.84
C
  COB(1)=.0028
  COB(2)=.3000
  COB(3)=.5907
  COB(4)=.9384
C
  COE(1)=.0005
  COE(2)=.2985
  COE(3)=.5863
  COE(4)=.9348
```

APPENDIX: COMPUTER PROGRAMS

```
C
CALL CALFIT (COP,COB,ICO,ACO,BCO,CCO,DCO,ECO,FCO)
  AB=ACO
  BB=BCO
  CB=CCO
  DB=DCO
  EB=ECO
  FB=FCO
CALL CALFIT (COP,COE,ICO,ACO,BCO,CCO,DCO,ECO,FCO)
  AE=ACO
  BE=BCO
  CE=CCO
  DE=DCO
  EE=ECO
  FE=FCO
C
WRITE(8,990) NDATA
C
DO 450 I=1,NDATA
  RCOV= RCO(I)/CORGE
  CO1= (AB +BB*RCOV +CB*(RCOV**2.) +DB*(RCOV**3.)
+      +EB*(RCOV**4.) +FB*(RCOV**5.))*TSPAN-T(I)
  CO2X= (AE +BE*RCOV +CE*(RCOV**2.) +DE*(RCOV**3.)
+      +EE*(RCOV**4.) +FE*(RCOV**5.))*T(I)
  CO(I)=(CO1+CO2X)/TSPAN
  IF (CO(I).LE.0.) CO(I)=0.
  WRITE(8,999) T(I)/60., CO(I)
450 CONTINUE
C
C CREATE PLOT DATA FILE
C
WRITE(4,101) ICO
DO 451 I=1,ICO
451 WRITE(4,102) COB(I),COP(I)
  WRITE(4,101) ICO
DO 452 I=1,ICO
452 WRITE(4,102) COE(I),COP(I)
  WRITE(4,103) NPT
DO 453 I=1,NPT
  COV= (I-1)*DEL
  COPLT(I)=AB+BB*COV+CB*(COV**2.)+DB*(COV**3.)
```

APPENDIX: COMPUTER PROGRAMS

```
      +          +EB*(COV**4.) +FB*(COV**5.)
453  WRITE(4,102) COV,COPLT(I)
      WRITE(4,103) NPT
      DO 454 I=1,NPT
          COV= (I-1)*DEL
          COPLT(I)=AE+BE*COV+CE*(COV**2.)+DE*(COV**3.)
      +          +EE*(COV**4.) +FE*(COV**5.)
454  WRITE(4,102) COV,COPLT(I)
C
C
C OXYGEN
C
C CALIBRATION DATA
C
      I02=6
      O2P(1)=0.0
      O2P(2)=0.99
      O2P(3)=2.57
      O2P(4)=10.5
      O2P(5)=18.29
      O2P(6)=20.95
C
      O2B(1)=.0000
      O2B(2)=.0407
      O2B(3)=.1033
      O2B(4)=.4179
      O2B(5)=.7355
      O2B(6)=.8405
C
      O2E(1)=.0000
      O2E(2)=.0415
      O2E(3)=.1047
      O2E(4)=.4218
      O2E(5)=.7444
      O2E(6)=.8418
C
      CALL LINEARFIT (O2P,O2B,I02,A02,B02)
          AB=A02
          BB=B02
      CALL LINEARFIT (O2P,O2E,I02,A02,B02)
          AE=A02
```

APPENDIX: COMPUTER PROGRAMS

```
      BE=B02
C
      DO 250 I=1,NDATA
          R02V= R02(I)/O2RGE
          O21= (AB +BB*R02V)*(TSPAN-T(I))
          O22= (AE +BE*R02V)*T(I)
          O2(I)=(O21+O22)/TSPAN
250  CONTINUE
C
C CREATE PLOT DATA FILE
C
      WRITE(7,101) I02
      DO 251 I=1,I02
251  WRITE(7,102) O2B(I),O2P(I)
      WRITE(7,101) I02
      DO 252 I=1,I02
252  WRITE(7,102) O2E(I),O2P(I)
      WRITE(7,103) NPT
      DO 253 I=1,NPT
          O2V= (I-1)*DEL
          O2PLT(I)=AB+BB*O2V
253  WRITE(7,102) O2V,O2PLT(I)
      WRITE(7,103) NPT
      DO 254 I=1,NPT
          O2V= (I-1)*DEL
          O2PLT(I)=AE+BE*O2V
254  WRITE(7,102) O2V,O2PLT(I)
C
C
C NITROGEN
C
C CALIBRATION DATA
C
      XN2S= 78.084
      XN2B= 78.84
C      XN2B= 78.34
      XN2E= 78.56
      FACB= XN2S/XN2B
      FACE= XN2S/XN2E
      XN2C(1)=XN2S
      DO 200 I=12,NDATA,12
```

APPENDIX: COMPUTER PROGRAMS

```

      XN2C(I)=XN2(I+7)*((I-1)*FACE +(NDATA-I)*FACB)/(NDATA-1)
      IF(XN2C(I).LE.0.) GOTO 200
      IN2=IN2 +1
200  CONTINUE
      C
      WRITE(8,990) IN2
      C
      DO 220 I=1,NDATA
      IF(XN2C(I).LE.0.) GOTO 220
      WRITE(8,999) T(I)/60., XN2C(I)/SCALEW2
220  CONTINUE
      C
      WRITE(8,990) IN2
      C
      C COMPUTE OXYGEN CONSUMED
      C
      DO 650 I=1,NDATA
      IF(XN2C(I).LE.0.) GOTO 650
      IF(T(I).LT.TR1B) THEN
        O2C=0.
      ELSE
        O2C=0.2682*XN2C(I) -O2(I)
      ENDIF
      WRITE(8,999) T(I)/60., O2C
650  CONTINUE
      C
      WRITE(8,990) NDATA
      C
      DO 300 I=1,NDATA
      WRITE(2,500) T(I),CO2(I),CO(I),O2(I),QI(I),QO(I),P(I),
+          TEMP(I),XN2C(I)
      WRITE(8,999) T(I)/60., TEMP(I)/SCALET
300  CONTINUE
      C
      C
      WRITE(9,103) NDATA
      DO 400 I=1,NDATA
400  WRITE(9,999) T(I)/60.,O2(I)/SCALEO2
      C
      WRITE(9,103) NDATA
      DO 401 I=1,NDATA

```

APPENDIX: COMPUTER PROGRAMS

```
401 WRITE(9,999) T(I)/60.,QI(I)
C
      WRITE(9,103) NDATA
      DO 402 I=1,NDATA
402 WRITE(9,999) T(I)/60.,QO(I)
C
      WRITE(9,103) NDATA
      DO 403 I=1,NDATA
403 WRITE(9,999) T(I)/60.,P(I)/SCALEP
C
101 FORMAT(I1)
102 FORMAT(2F10.5)
103 FORMAT(I3)
990 FORMAT(I5)
999 FORMAT(F15.10,5X,F15.10)
C
1000 CLOSE(1)
      STOP
      END
C
C
C SUBROUTINE CALFIT
C
C SUBROUTINE COMPUTES CONSTANTS IN 5TH ORDER POLYNOMIAL EQUATION THAT
C LEAST-SQUARES FIT THE GAS CALIBRATION DATA
C
      SUBROUTINE CALFIT (Y,X,N,A,B,C,D,E,F)
      IMPLICIT DOUBLE PRECISION (A-H,O-Z)
      DOUBLE PRECISION Y(N),X(N)
C
      X1=0.
      X2=0.
      X3=0.
      X4=0.
      X5=0.
      X6=0.
      X7=0.
      X8=0.
      X9=0.
      X10=0.
      Y1=0.
```

APPENDIX: COMPUTER PROGRAMS

```
X1Y1=0.
X2Y1=0.
X3Y1=0.
X4Y1=0.
X5Y1=0.
C
DO 10 I=1,N
  X1=X1 +X(I)
  X2=X2 +X(I)**2.
  X3=X3 +X(I)**3.
  X4=X4 +X(I)**4.
  X5=X5 +X(I)**5.
  X6=X6 +X(I)**6.
  X7=X7 +X(I)**7.
  X8=X8 +X(I)**8.
  X9=X9 +X(I)**9.
  X10=X10 +X(I)**10.
  Y1=Y1 +Y(I)
  X1Y1=X1Y1 +X(I)*Y(I)
  X2Y1=X2Y1 +(X(I)**2.) *Y(I)
  X3Y1=X3Y1 +(X(I)**3.) *Y(I)
  X4Y1=X4Y1 +(X(I)**4.) *Y(I)
  X5Y1=X5Y1 +(X(I)**5.) *Y(I)
10 CONTINUE
C
XL1=X1/N
XL2=X2/N
XL3=X3/N
XL4=X4/N
XL5=X5/N
C
R22=X2 -XL1*X1
XM1=(X3 -XL2*X1)/R22
XM2=(X4 -XL3*X1)/R22
XM3=(X5 -XL4*X1)/R22
XM4=(X6 -XL5*X1)/R22
C
R23=X3 -XL1*X2
R33=X4 -XL2*X2 -XM1*R23
XN1=(X5 -XL3*X2 -XM2*R23)/R33
XN2=(X6 -XL4*X2 -XM3*R23)/R33
```

APPENDIX: COMPUTER PROGRAMS

```
      XW3=(X7 -XL5*X2 -XM4*R23)/R33
C
      R24=X4 -XL1*X3
      R34=X5 -XL2*X3 -XM1*R24
      R44=X6 -XL3*X3 -XM2*R24 -XW1*R34
      XP1=(X7 -XL4*X3 -XM3*R24 -XW2*R34)/R44
      XP2=(X8 -XL5*X3 -XM3*R24 -XW3*R34)/R44
C
      R25=X5 -XL1*X4
      R45=X7 -XL3*X4 -XM2*R25 -XW1*R34
      R55=X8 -XL4*X4 -XM3*R25 -XW2*R34 -XP1*R45
      XQ1=(X9 -XL5*X4 -XM4*R25 -XW3*R34 -XP2*R45)/R55
C
      R26=X6 -XL1*X5
      R27=X1Y1 -XL1*Y1
C
      R35=X6 -XL2*X4 -XM1*R25
      R36=X7 -XL2*X5 -XM1*R26
      R37=X2Y1 -XL2*Y1 -XM1*R27
C
      R46=X8 -XL3*X5 -XM2*R26 -XW1*R36
      R47=X3Y1 -XL3*Y1 -XM2*R27 -XW1*R37
      R56=X9 -XL4*X5 -XM3*R26 -XW2*R36 -XP1*R46
      R66=X10 -XL5*X5 -XM4*R26 -XW3*R36 -XP2*R46 -XQ1*R56
C
      R57=X4Y1 -XL4*Y1 -XM3*R27 -XW2*R37 -XP1*R47
      R66=X10 -XL5*X5 -XM4*R26 -XW3*R36 -XP2*R46 -XQ1*R56
      R67=X5Y1 -XL5*Y1 -XM4*R27 -XW3*R37 -XQ1*R57
C
C SOLVE VECTOR OF UNKNOWNS
C
      F=R67/R66
      E=(R57 -R56*F)/R55
      D=(R47 -R45*E -R46*F)/R44
      C=(R37 -R34*D -R35*E -R36*F)/R33
      B=(R27 -R23*C -R24*D -R25*E -R26*F)/R22
      A=(Y1 -X1*B -X2*C -X3*D -X4*E -X5*F)/W
C
      RETURN
      END
C
```

APPENDIX: COMPUTER PROGRAMS

```
C
C SUBROUTINE LINEARFIT
C
C SUBROUTINE COMPUTES CONSTANTS IN STRAIGHT LINE FIT OF O2 ANALYZER
C CALIBRATION DATA
C
  SUBROUTINE LINEARFIT (Y,X,N,A,B)
  IMPLICIT DOUBLE PRECISION (A-H,O-Z)
  DOUBLE PRECISION Y(N),X(N)
C
  SUMXY=0.
  SUMX=0.
  SUMY=0.
  SUMX2=0.
C
  DO 10 I=1,N
    SUMXY= SUMXY +X(I)*Y(I)
    SUMX=SUMX +X(I)
    SUMY=SUMY +Y(I)
    SUMX2=SUMX2 +X(I)**2.
10  CONTINUE
C
  BN= SUMXY -SUMX*SUMY/N
  BD= SUMX2 -(SUMX**2.)/N
  B=BN/BD
C
  A= (SUMY -B*SUMX)/N
  RETURN
  END
```

APPENDIX: COMPUTER PROGRAMS

4. Program HTO.F

```
C PROGRAM HTO.F
C
C BY DAULAT MAMORA, STANFORD UNIVERSITY, UPDATED SEPTEMBER 1992.
C
C
C PROGRAM CALCULATES VALUES FOR:
C
C 1. ARRHENIUS PLOT (HTO): FUEL IN TOROID ONLY
C
C 2. ARRHENIUS PLOT (HTO): VARYING-FUEL-GEOMETRY MODEL
C
C
C      IMPLICIT DOUBLE PRECISION (A-H,O-Z)
C      DOUBLE PRECISION T(1000),O2(1000),TEMP(1000),O2C(1000),CO2(1000)
C      DOUBLE PRECISION CO(1000),XN2(1000),QI(1000),QO(1000)
C
C
C      OPEN (UNIT=1,STATUS='OLD',FILE='ven23.cor')
C      OPEN (UNIT=2,STATUS='OLD',FILE='ven23hto.arr')
C
C
C NOMENCLATURE
C
C 1. EXPERIMENTAL DATA
C
C T      TIME
C O2     OXYGEN PRODUCED, MOLE PERCENT
C O2C    OXYGEN CONSUMED, MOLE PERCENT
C CO2    CARBON DIOXIDE PRODUCED, MOLE PERCENT
C CO     CARBON MONOXIDE PRODUCED, MOLE PERCENT
C XN2    NITROGEN PRODUCED, MOLE PERCENT
C TEMP   TEMPERATURE, DEG. C
C QI     INJECTED GAS RATE, SLPM
C QO     PRODUCED GAS RATE, SLPM
C BHTO   TIME AT BEGINNING OF HTO, MIN
C ENTO   TIME AT END OF HTO, MIN
C EKIN   TIME AT END OF RUN, MIN
C RHOF   FUEL DENSITY, G/CC
```

APPENDIX: COMPUTER PROGRAMS

```
C ACELL  CROSS-SECTIONAL AREA OF KINETICS CELL, CM
C HCELL  HEIGHT OF MIX IN KINETICS CELL, CM
C PHI    POROSITY OF MIX, FRACTION
C RS     SAND GRAIN RADIUS, CM
C
C 2.  ARRHENIUS PLOT PARAMETERS
C
C IARR   = 0 (FUEL IN TOROID ONLY)
C IARR   = 1 (VARYING FUEL GEOMETRY MODEL)
C EE     HTO ACTIVATION ENERGY, J/MOL
C BETA   LN(BETA) IS Y-AXIS INTERCEPT IN HTO ARRHENIUS PLOT, 1/S
C SBETA  LN(SBETA) IS Y-AXIS INTERCEPT IN HTO ARRHENIUS PLOT,
C        FOR T>TC, 1/S
C
C 3.  PARAMETERS IN MODEL PREDICTION
C
C HC     ATOMIC HYDROGEN-CARBON RATIO
C Y      ATOMIC OXYGEN-CARBON RATIO
C XM     M-RATIO
C TC     TIME AFTER WHICH FUEL ASSUMES TOROIDAL SHAPE, MIN
C GAMMA  FUEL RADIUS=RS*(1+GAMMA)**(1/3)
C HF     HEIGHT OF SURFACE OF FUEL TOROID, CM
C HFO    INITIAL HEIGHT OF SURFACE OF FUEL TOROID, CM
C R      UNIVERSAL GAS CONSTANT
C
C
C
C TIME DATA
C
C      BHTO=180.
C      EHTO=348.
C      EKIN=353.
C      TC=297.
C
C      NEHTO=EHTO*2.
C      NBHTO=BHTO*2.
C
C      NDATA=EKIN*2.
C
C      NTC=TC*2.
C
C      O2CLAST=1.E-6
C
C KINETICS CELL/SAMPLE DATA
C
```

APPENDIX: COMPUTER PROGRAMS

```
O2S=20.95
RHOF=1.0366
ACELL=5.5798
HCELL=3.5
PHI=0.37
GOD=RHOF*ACELL*HCELL*(1.-PHI)
G1D=GOD*60.*22.41383
RS=.000408

C
C KINETICS/STOICHIOMETRIC PARAMETERS
C
HC=1.73
XM=0.286
Y=0.4
EE=141.1671E3
BETA=1577.1390E3
SBETA=-9375.0
R=8.31441
EER=EE/R
XKC1=9.9145129E-4
XKCN=XKC1*BETA*(12.011+HC+15.9994*Y)
XKCD=SQRT(RS)*(1.-XM/2.+HC/4.-Y/2.)*GOD
XKC=XKCN/XKCD

C
C SPECIFICATIONS/INITIALISATION
C
IHC=0
IARR=1

C
C
C READ EXPERIMENTAL DATA
C
READ(1,31) (T(I),CO2(I),CO(I),O2(I),QI(I),QO(I),TEMP(I),
+XM2(I),I=1,NDATA)
31 FORMAT(F6.2,3F7.3,2F6.3,7X,F9.3,F7.3)

C
C
C COMPUTE O2 CONSUMED. CONVERT GAS READINGS TO FRACTIONS,
C TEMP. FROM DEG. C TO DEG. K, TIME FROM MIN. TO SEC.
C
DO 30 I=1,NDATA
```

APPENDIX: COMPUTER PROGRAMS

```

        IF(XN2(I).LE.0) THEN
            O2C(I)=0.
            GOTO 32
        ENDIF
        IF((I.GE.NBHTO).AND.(I.LE.NEHTO)) IHC=IHC+1
        O2C(I)=(.2682*XN2(I) -O2(I))/100.
        IF(O2C(I).LE.0.) O2C(I)=0.
32      CO2(I)=CO2(I)/100.
        IF(CO2(I).LE.0.0) CO2(I)=0.
        CO(I)=CO(I)/100.
        IF(CO(I).LE.0.0) CO(I)=0.
        TEMP(I)=TEMP(I)+273.15
        T(I)= T(I) *60.
30      CONTINUE
C
C
        WRITE(2,653) IHC-1
        DO 751 I=NEHTO-1,NBHTO,-1
            IF(I.EQ.(NEHTO-1)) THEN
                O2C(I)=O2CLAST
                CO2(I)=0.
                CO(I)=0.
            ENDIF
            CPLT=0.
            IF(XN2(I).LE.0.) GOTO 751
C
C COMPUTE GAMMA
C
        DO 752 J=I,NEHTO-1
            CPLT1=(CO2(J)+CO(J))*Q0(J)
            CPLT2=(CO2(J+1)+CO(J+1))*Q0(J+1)
            CPLT3=(CPLT1+CPLT2)/2.
            CPLT=CPLT+(CPLT3*(12.011+HC+15.9994*Y))*(T(J+1)-T(J))
752      CONTINUE
        GAMMA=CPLT/G1D
C
C
C FUEL IN TOROID ONLY
C
        DENOM1=GAMMA**0.75
        DENOM=2.746356*DENOM1

```

APPENDIX: COMPUTER PROGRAMS

```
RC=O2C(I)*QI(I)*RS/DENOM
RC=DLOG(RC)
WRITE(2,853) 1./TEMP(I),RC
751 CONTINUE
C
IF(IARR.EQ.0) GOTO 1000
C
C VARYING-FUEL-GEOMETRY MODEL
C
600 WRITE(2,653) IHC-1
DO 851 I=NEHTO-1,MBHTO,-1
IF((O2C(I).LE.O.).OR.(O2C(I).EQ.O2CLAST)) GOTO 851
CPLT=0.
C
C COMPUTE GAMMA
C
DO 852 J=I,WEHTO-1
CPLT1=(CO2(J)+CO(J))*QO(J)
CPLT2=(CO2(J+1)+CO(J+1))*QO(J+1)
CPLT3=(CPLT1+CPLT2)/2.
CPLT=CPLT+(CPLT3*(12.011+HC+15.9994*Y))*(T(J+1)-T(J))
852 CONTINUE
GAMMA=CPLT/G1D
C
C COMPUTE RELATIVE REACTION RATE T>=TC
C
DENOM1=GAMMA**0.75
DENOM=2.746356*DENOM1
RC=O2C(I)*QI(I)*RS/DENOM
RC=DLOG(RC)
IF(I.LT.NTC) GOTO 222
WRITE(2,853) 1./TEMP(I),RC
GOTO 851
C
C COMPUTE RELATIVE REACTION RATE, T<TC
C
222 RG=(1./TEMP(I) -1./TEMP(NTC))*(EER+SBETA)
RT=RC-RG
WRITE(2,853) 1./TEMP(I),RT
C
851 CONTINUE
```

APPENDIX: COMPUTER PROGRAMS

C

653 FORMAT(I3)

853 FORMAT(E15.8,5X,E15.8)

1000 CONTINUE

STOP

END

APPENDIX: COMPUTER PROGRAMS

5. Program HTOFIT.F

```
C PROGRAM HTOFIT.F
C
C BY DAULAT MAMORA, STANFORD UNIVERSITY, UPDATED SEPTEMBER 1992.
C
C
C PROGRAM CALCULATES:
C
C 1) FUEL HEIGHT VERSUS TIME
C
C 2) HTO OXYGEN CONSUMED CURVE
C
C 3) LTO OXYGEN CONSUMED 'DATA'
C
C
C
C      IMPLICIT DOUBLE PRECISION (A-H,O-Z)
C      DOUBLE PRECISION O2(1000),O2C(1000),
C      +CO2(1000),CO(1000),QI(1000),QO(1000),CURVE1(1000),
C      +CURVE2(1000),XN2(1000)
C      COMMON T(1000),TEMP(1000)
C
C
C      OPEN (UNIT=1,STATUS='OLD',FILE='c15.cor')
C      OPEN (UNIT=2,STATUS='OLD',FILE='c15.hf')
C      OPEN (UNIT=3,STATUS='OLD',FILE='c15hto.cuv')
C      OPEN (UNIT=4,STATUS='OLD',FILE='c15.lto')
C      OPEN (UNIT=7,STATUS='OLD',FILE='c15hto.cal')
C
C
C NOMENCLATURE
C
C 1. EXPERIMENTAL DATA
C
C T      TIME
C O2     OXYGEN PRODUCED, MOLE PERCENT
C O2C    OXYGEN CONSUMED, MOLE PERCENT
C CO2    CARBON DIOXIDE PRODUCED, MOLE PERCENT
C CO     CARBON MONOXIDE PRODUCED, MOLE PERCENT
```

APPENDIX: COMPUTER PROGRAMS

```
C XN2  NITROGEN PRODUCED, MOLE PERCENT
C TEMP TEMPERATURE, DEG. C
C QI   INJECTED GAS RATE, SLPM
C QO   PRODUCED GAS RATE, SLPM
C BHTO TIME AT BEGINNING OF HTO, MIN
C EHTO TIME AT END OF HTO, MIN
C EKIN TIME AT END OF RUN, MIN
C RHOF FUEL DENSITY, G/CC
C ACELL CROSS-SECTIONAL AREA OF KINETICS CELL, CM
C HCELL HEIGHT OF MIX IN KINETICS CELL, CM
C PHI  POROSITY OF MIX, FRACTION
C RS   SAND GRAIN RADIUS, CM
C
C 2. ARRHENIUS PLOT PARAMETERS
C
C EEC  HTO ACTIVATION ENERGY, J/MOL
C BETAC LN(BETAC) IS Y-AXIS INTERCEPT IN HTO ARRHENIUS PLOT, 1/S
C EECT  HTO ACTIVATION ENERGY FOR T < TC, J/MOL
C BETAT LN(BETAT) IS Y-AXIS INTERCEPT IN HTO ARRHENIUS PLOT FOR
C       T < TC, 1/S
C
C 3. PARAMETERS IN MODEL PREDICTION
C
C HC   ATOMIC HYDROGEN-CARBON RATIO
C Y    ATOMIC OXYGEN-CARBON RATIO
C XM   M-RATIO
C TC   TIME AFTER WHICH FUEL ASSUMES TOROIDAL SHAPE, MIN
C GAMMA FUEL RADIUS=RS*(1+GAMMA)**(1/3)
C HF   HEIGHT OF SURFACE OF FUEL TOROID, CM
C HFO  INITIAL HEIGHT OF SURFACE OF FUEL TOROID, CM
C R    UNIVERSAL GAS CONSTANT
C ILTO = 0 LTO OXYGEN CONSUMED 'DATA' NOT GENERATED
C ILTO = 1 LTO OXYGEN CONSUMED 'DATA' GENERATED
C
C TIME DATA
C
C       BCAL=0.5
C       BHTO=210.
C       EHTO=390.
C       EKIN=390.
C       TC=315.
```

APPENDIX: COMPUTER PROGRAMS

```
ELTO=300.
  NBCAL=BCAL*2.
  NEHTO=EHTO*2.
  NBHTO=BHTO*2.
  NDATA=EKIN*2.
  NTC=TC*2.
  NELTO=ELTO*2.

C
C CELL/SAMPLE DATA
C
  O2S=20.95
  RHOF=1.0291
  ACELL=5.5798
  HCELL=5.5
  PHI=0.37
  GOD=RHOF*ACELL*HCELL*(1.-PHI)
  G1D=GOD*60.*22.41383
  RS=.0375

C
C KINETICS/STOICHIOMETRY PARAMETERS
C
  EEC=149.2330E3
  BETAC=692.9097E6
  EET=85.8047E3
  BETAT=6.4125E3
  R=8.31441
  EERC=EEC/R
  EERT=EET/R

C
C SPECIFICATIONS, CONSTANTS
C
  HC=1.32
  XM=0.278
  Y=0.45
  XK1=9.9145129E-4
  IHC=0
  ILTO=1

C
C READ EXPERIMENTAL DATA
C
  READ(1,31) (T(I),CO2(I),CO(I),O2(I),QI(I),QO(I),TEMP(I),
```

APPENDIX: COMPUTER PROGRAMS

```
+XW2(I),I=1,NDATA)
31  FORMAT(F6.2,3F7.3,2F6.3,7X,F9.3,F7.3)
C
C COMPUTE O2 CONSUMED. CONVERT GAS READINGS TO FRACTIONS,
C TEMPERATURE FROM DEG. C TO DEG. K, TIME FROM MIN. TO SEC.
C
DO 30 I=1,NDATA
  IF(XW2(I).LE.0.) THEN
    O2C(I)=0.
    GOTO 32
  ENDIF
  IHC=IHC+1
  O2C(I)=(.2682*XW2(I)-O2(I))/100.
  IF(O2C(I).LE.0.) O2C(I)=0.
32  CO2(I)=CO2(I)/100.
  CO(I)=CO(I)/100.
  T(I)= T(I) *60.
  TEMP(I)=TEMP(I)+273.15
30  CONTINUE
C
C COMPUTE HFO, THE INITIAL FUEL HEIGHT AT TOROID
C
CPLT=0.
DO 40 J=NBHTO-1,NTC,-1
  CPLT1=(CO2(J)+CO(J))*Q0(J)
  CPLT2=(CO2(J+1)+CO(J+1))*Q0(J+1)
  CPLT3=(CPLT1+CPLT2)/2.
  CPLT=CPLT+(CPLT3*(12.011+HC+15.9994*Y))*(T(J+1)-T(J))
40  CONTINUE
GC=CPLT/G1D
AC1=RS/3.
AC2=(8.*GC)**0.5
HFC=AC1*AC2
C
EER=EERC
BETA=BETAC
XKCH=XKC1*BETA*(12.011+HC+15.9994*Y)
XKCD=SQRT(RS)*(1.-XM/2.+HC/4.-Y/2.)*GOD
XKC=XKCH/XKCD
C
CALL INTEGRAL(TEMP,T,NDATA,NBHTO,NTC,EER,GS1)
```

APPENDIX: COMPUTER PROGRAMS

```
C
      A01=XKC*GS1/2.
      A02=A01+SQRT(HFC)
      HF0=A02**2.
      WRITE(6,*)HF0
C
C COMPUTE HF AND CURVE1 (HTO OXYGEN CONSUMED CURVE)
C
      DO 70 I=NEHTO-1,NBCAL,-1
          IF(I.GE.NTC) THEN
              EER=EERC
              BETA=BETAC
          ELSE
              EER=EERT
              BETA=BETAT
          ENDIF
          C1=3.*BETA*DEXP(-EER/TEMP(I))
          C3=QI(I)*(RS**2.5)
C
C      COMPUTE HF
C
          EER=EERC
          BETA=BETAC
          CALL INTEGRAL(TEMP,T,NDATA,NBCAL,I-1,EER,GA1)
C
          XKCN=XKC1*BETA*(12.011+HC+15.9994*Y)
          XKCD=SQRT(RS)*(1.-XM/2.+HC/4.-Y/2.)*GOD
          XKC=XKCN/XKCD
          X3=GA1*XKC/2.
          X4=SQRT(HF0)
          HF=(X4-X3)**2.
          IF(I.EQ.NTC) HFC=HF
          WRITE(2,75) T(I)/3600.,HF
C
C      COMPUTE CURVE1
C
          CURVE1(I)=(HF**1.5)*C1/C3
C
70    CONTINUE
C
      WRITE(3,73)IHC
```

APPENDIX: COMPUTER PROGRAMS

C

```
EU2H=U2**4. +A1*(U2**3.) +A2*(U2**2.) +A3*U2 +A4
EU2D=U2**4. +B1*(U2**3.) +B2*(U2**2.) +B3*U2 +B4
EU2X=U2*DEXP(U2)
EU2=EU2H/(EU2D*EU2X)
```

C

```
SUME1=-EE/TG
SUME2=DEXP(-U1)/U1
SUME3=DEXP(-U2)/U2
SS= SS+ SUME1*(SUME2 -SUME3 -EU1 +EU2)
```

50

```
CONTINUE
RETURN
END
```

APPENDIX: COMPUTER PROGRAMS

```
C
C
C SUBROUTINE INTEGRAL
C
C APPROXIMATE SOLUTION TO EXPONENTIAL INTEGRAL OF THE FIRST KIND
C
C
C SUBROUTINE INTEGRAL (TEMP,T,NDATA,K1,K2,EE,SS)
C
C IMPLICIT DOUBLE PRECISION (A-H,O-Z)
C DOUBLE PRECISION TEMP(NDATA),T(NDATA)
C
C
C
C A1=8.57333
C A2=18.05902
C A3=8.63476
C A4=0.26777
C B1=9.57332
C B2=25.63296
C B3=21.09965
C B4=3.95850
C SS=0.
C
C DO 50 J=K1,K2
C IF(TEMP(J+1).NE.TEMP(J)) THEN
C TG=(TEMP(J+1)-TEMP(J))/(T(J+1)-T(J))
C TGPREV=TG
C TC=TEMP(J+1)-T(J)*TG
C TCPREV=TC
C ELSE
C TG=TGPREV
C TC=TCPREV
C ENDIF
C
C U1=EE/(TC +TG*T(J))
C U2=EE/(TC +TG*T(J+1))
C
C EU1N=U1**4. +A1*(U1**3.) +A2*(U1**2.) +A3*U1 +A4
C EU1D=U1**4. +B1*(U1**3.) +B2*(U1**2.) +B3*U1 +B4
C EU1X=U1*DEXP(U1)
C EU1=EU1N/(EU1D*EU1X)
```

APPENDIX: COMPUTER PROGRAMS

```
      DO 80 I=1,NDATA
          IF(XN2(I).LE.0.) GOTO 80
          WRITE(3,75) T(I)/3600.,02C(I)*100.
80     CONTINUE
C
      NP=NDATA-NBCAL
      WRITE(3,73) NP
      DO 77 I=NBCAL,NDATA-1
77     WRITE(3,75) T(I)/3600.,CURVE1(I)*100.
C
          IF(ILTO.EQ.0) GOTO 1000
C
C COMPUTE CURVE2 (LTO OXYGEN CONSUMED 'DATA')
C
      WRITE(3,73)IHC
      DO 85 I=1,NDATA
          IF(XN2(I).LE.0.) GOTO 85
          IF(I.GE.NEHTO) THEN
              CURVE2(I)=0.
              GOTO 88
          ENDIF
          CURVE2(I)=02C(I)-CURVE1(I)
88     IF(CURVE2(I).LT.0.) CURVE2(I)=0.
          IF(I.GE.NELTO) CURVE2(I)=0.
          WRITE(3,75) T(I)/3600.,CURVE2(I)*100.
          TT=TEMP(I)-273.15
          WRITE(4,76) T(I)/60.,02C(I),CURVE2(I),TT
85     CONTINUE
C
C WRITE TO FILE CALCULATED HTO CURVE1 AND TEMPERATURE
C
      DO 89 I=1,NDATA
          TT=TEMP(I)-273.15
89     WRITE(7,74) T(I)/60.,CURVE1(I),TT
C
73     FORMAT(I3)
74     FORMAT(F15.8,5X,E15.8,5X,E15.8)
75     FORMAT(F15.8,5X,E15.8)
76     FORMAT(F8.3,3X,E15.8,3X,E15.8,3X,E15.8)
1000  STOP
      END
```

APPENDIX: COMPUTER PROGRAMS

6. Program LTO.F

```
C PROGRAM LTO.F
C
C BY DAULAT MAMORA, STANFORD UNIVERSITY, UPDATED SEPTEMBER 1992.
C
C
C PROGRAM COMPUTES VALUES FOR LTO ARRHENIUS PLOT
C
      IMPLICIT DOUBLE PRECISION (A-H,O-Z)
      DOUBLE PRECISION T(1000),TEMP(1000),O2C(1000)
C
      OPEN (UNIT=1,STATUS='OLD',FILE='c15.lto')
      OPEN (UNIT=2,STATUS='OLD',FILE='c15lto.arr')
C
C TIME DATA
C
      NDATA=78
      BLTO=120.
      ELTO=300.
C
C LTO EXPONENT, XN
C
      XN=2.0
C
      READ(1,31) (T(I),O2C(I),TEMP(I),I=1,NDATA)
31  FORMAT(F8.3,3X,E15.8,21X,E15.8)
C
      DO 30 I=1,NDATA
          TEMP(I)=TEMP(I)+273.15
          T(I)= T(I) *60.
30  CONTINUE
C
C COMPUTE RELATIVE REACTION RATE
C
41  FORMAT(15)
      DO 51 I=1,NDATA
          TMIN=T(I)/60.
          IF((TMIN.LT.BLTO).OR.(TMIN.GT.ELTO)) GOTO 51
          O2PLT=0.
```

APPENDIX: COMPUTER PROGRAMS

```
C
DO 52 J=I,1,-1
  TMIN=T(J)/60.
  IF((TMIN.LT.BLTO).OR.(TMIN.GT.ELTO)) GOTO 52
  IF(O2C(J-1).LT.0.) O2C(J-1)=0.
  IF(O2C(J).LT.0.) O2C(J)=0.
  O2PLT=O2PLT +(O2C(J) +O2C(J-1))*(T(J) -T(J-1))/2.
52 CONTINUE
C
  IF (O2PLT.LE.0.) GOTO 51
  Y= O2C(I)/O2PLT**XN
  Y=DLOG(Y)
  WRITE(2,53) 1./TEMP(I),Y
51 CONTINUE
C
53 FORMAT(E15.7,5X,E15.7)
1000 CONTINUE
STOP
END
```

APPENDIX: COMPUTER PROGRAMS

7. Program LTOFIT.F

```
C PROGRAM LTOFIT.F
C
C BY DAULAT MAMORA, STANFORD UNIVERSITY, UPDATED SEPTEMBER 1992.
C
C
C PROGRAM CALCULATES:
C
C 1) LTO OXYGEN CONSUMED CURVE
C
C 2) TOTAL OXYGEN CONSUMED CURVE
C
C
C      IMPLICIT DOUBLE PRECISION (A-H,O-Z)
C      DOUBLE PRECISION T(1000),O2CON(1000),CURVE1(1000),CURVE2(1000),
C      +CURVE3(1000),TEMP(1000),TX(1000)
C
C
C      OPEN (UNIT=1,STATUS='OLD',FILE='c15hto.cal')
C      OPEN (UNIT=2,STATUS='OLD',FILE='c15.lto')
C      OPEN (UNIT=3,STATUS='OLD',FILE='c15lto.cuv')
C      OPEN (UNIT=4,STATUS='OLD',FILE='c15.tot')
C
C
C TIME DATA
C
C      NHTO=780
C      NLTO=78
C      BLTO=90.
C      ELTO=300.
C      NBLTO=BLTO*2.
C
C KINETICS PARAMETERS
C
C      XE=2.0
C      EE=123.1172E3
C      BETA=1.3061E-17
C
C CONSTANTS/SPECIFICATIONS
C
```

APPENDIX: COMPUTER PROGRAMS

```
R=8.31441
EER=EE/R
C3S=0.13926E-3

C
C READ DATA FILES
C
  READ(1,21) (T(I),CURVE1(I),TEMP(I),I=1,NHTO)
  READ(2,22) (TX(I),O2CON(I),CURVE2(I),I=1,NLTO)

C
C COMPUTE TIME IN SECONDS, TEMPERATURE IN DEG.K
C
  DO 30 I=1,NHTO
    T(I)= T(I)*60.
    TEMP(I)=TEMP(I)+273.15
30  CONTINUE

C
C WRITE TO FILE OXYGEN CONSUMED DATA
C
  WRITE(3,101)NLTO
  DO 211 I=1,NLTO
211  WRITE(3,201) TX(I)/60.,O2CON(I)*100.

C
C WRITE TO FILE LTO CURVE 'DATA', CURVE2
C
  WRITE(3,101)NLTO
  DO 200 I=1,NLTO
200  WRITE(3,201) TX(I)/60.,CURVE2(I)*100.

C
C COMPUTE LTO OXYGEN CONSUMED, CURVE3
C
  DO 100 I=2,NHTO
    IF(I.LT.(NBLTO+1))CURVE3(I)=0.
    IF(I.EQ.(NBLTO+1)) CURVE3(NBLTO)=C3S
    O1=BETA*DEXP(EER/TEMP(I))
    O2A=BETA*DEXP(EER/TEMP(I-1))
    O2B=(1.-XN)/XN
    O2C=CURVE3(I-1)/O2A
    O2=O2C**O2B
    IF(TEMP(I).NE.TEMP(I-1)) THEN
      TG=(TEMP(I)-TEMP(I-1))/(T(I)-T(I-1))
      TGPREV=TG
```

APPENDIX: COMPUTER PROGRAMS

```

        TC=TEMP(I-1) -T(I-1)*TG
        TCPREV=TC
    ELSE
        TG=TGPREV
        TC=TCPREV
    ENDIF
    U1=-EER/(TC+TG*T(I-1))
    U2=-EER/(TC+TG*T(I))
    E2=DEXP(U2)
    O3A=EER*BETA/(TG*E2)
    O3B=(1.+3.*U2)*(U2-U1)
    O3C=(U2**2. -U1**2.)/2.
    O3D=(1.+2.*U2 +3.*(U2**2.))*DLOG(U2/U1)
    O3E=(1. +U2 +U2**2. +U2**3.)*(1./U2 -1./U1)
    O3F=O3A*(O3B-O3C-O3D-O3E)
    O3=(1.-XN)*O3F
    OX=XN/(1.-XN)
    O4=(O2+O3)**OX
    CURVE3(I)=O1*O4
100  CONTINUE
C
    WRITE(3,101)NHTO
    DO 210 I=1,NHTO
210  WRITE(3,201) T(I)/3600.,CURVE3(I)*100.
C
C COMPUTE TOTAL OXYGEN CONSUMED CURVE, = CURVE1 + CURVE3
C
    WRITE(4,101)NLTO
    DO 300 I=1,NLTO
300  WRITE(4,201) TX(I)/60.,O2CON(I)*100.
    WRITE(4,101)NHTO
    DO 310 I=1,NHTO
310  WRITE(4,201) T(I)/3600.,CURVE1(I)*100.
    WRITE(4,101)NHTO
    DO 320 I=1,NHTO
320  WRITE(4,201) T(I)/3600.,CURVE3(I)*100.
    WRITE(4,101)NHTO
    DO 340 I=1,NHTO
        O2T=CURVE3(I)+CURVE1(I)
340  WRITE(4,201) T(I)/3600.,O2T*100.
C

```

APPENDIX: COMPUTER PROGRAMS

```
101  FORMAT(I5)
21   FORMAT(F15.8,5X,E15.8,5X,E15.8)
22   FORMAT(F8.3,3X,E15.8,3X,E15.8,18X)
201  FORMAT(F10.6,5X,F15.8)
      STOP
      END
```

APPENDIX: COMPUTER PROGRAMS

8. Program UOP.F

```
C PROGRAM UOP.F
C
C BY DAULAT D. MAMORA, STANFORD UNIVERSITY, 1993
C
C PROGRAM CREATES H/C VERSUS API CURVE WITH UOP K-FACTOR AS
C CORRELATING PARAMETER. OIL API GRAVITY, ATOMIC H/C RATIO AND
C UOP K-FACTOR DATA ARE BASED ON HOUGEN-WATSON CORRELATION CHARTS
C (1954). A 5TH ORDER POLYNOMIAL IS FITTED THROUGH THESE DATA.
C
      IMPLICIT REAL*8 (A-H,O-Z)
      COMMON API1(20),HC1(20),API2(20),HC2(20),API3(20),
+ HC3(20),API4(20),HC4(20),API5(20),HC5(20),API6(20),HC6(20)
      DIMENSION U1(110),U2(110),U3(110),U4(110),U5(110),U6(110)
C
C
      OPEN (UNIT=1,STATUS='OLD',FILE='UOP.DAT')
C
C PLOTTING PARAMETERS
C
      DEL=0.01
      NPT=101
C
C UOP K-FACTOR = 10.0
C
      N1=8
      API1(1)=-7.0
      API1(2)=-3.8
      API1(3)=-0.5
      API1(4)=3.1
      API1(5)=7.2
      API1(6)=11.8
      API1(7)=17.2
      API1(8)=40.0
      HC1(1)=0.952
      HC1(2)=1.008
      HC1(3)=1.055
      HC1(4)=1.093
      HC1(5)=1.129
```

APPENDIX: COMPUTER PROGRAMS

```
HC1(6)=1.154
HC1(7)=1.172
HC1(8)=1.201
DELA=(API1(8)-API1(1))/NPT
C
C CREATE PLOT DATA FILE
C
CALL CALFIT (HC1,API1,N1,A,B,C,D,E,F)
C
WRITE(1,103) NPT+1
API=API1(1)-DELA
DO 21 I=1,NPT+1
  API= DELA +API
  U1(I)=A+B*API+C*(API**2.)+D*(API**3.)
+      +E*(API**4.) +F*(API**5.)
21  WRITE(1,102) API, U1(I)
C
C UOP K-FACTOR = 10.5
C
API2(1)=-0.3
API2(2)=2.9
API2(3)=6.2
API2(4)=10.0
API2(5)=14.2
API2(6)=19.2
API2(7)=25.0
API2(8)=48.6
HC2(1)=1.122
HC2(2)=1.180
HC2(3)=1.230
HC2(4)=1.274
HC2(5)=1.311
HC2(6)=1.341
HC2(7)=1.360
HC2(8)=1.393
DELA=(API2(8)-API2(1))/NPT
C
C CREATE PLOT DATA FILE
C
CALL CALFIT (HC2,API2,N1,A,B,C,D,E,F)
C
```

APPENDIX: COMPUTER PROGRAMS

```
WRITE(1,103) NPT+1
API=API2(1)-DELA
DO 22 I=1,NPT+1
  API= DELA +API
  U2(I)=A+B*API+C*(API**2.)+D*(API**3.)
+      +E*(API**4.) +F*(API**5.)
22  WRITE(1,102) API, U2(I)
C
C UOP K-FACTOR = 11.0
C
  API3(1)=5.8
  API3(2)=9.2
  API3(3)=12.9
  API3(4)=16.8
  API3(5)=21.2
  API3(6)=26.2
  API3(7)=32.8
  API3(8)=57.5
  HC3(1)=1.296
  HC3(2)=1.356
  HC3(3)=1.415
  HC3(4)=1.460
  HC3(5)=1.506
  HC3(6)=1.536
  HC3(7)=1.559
  HC3(8)=1.590
  DELA=(API3(8)-API3(1))/NPT
C
C CREATE PLOT DATA FILE
C
  CALL CALFIT (HC3,API3,N1,A,B,C,D,E,F)
C
  WRITE(1,103) NPT+1
  API=API3(1)-DELA
  DO 23 I=1,NPT+1
    API= DELA +API
    U3(I)=A+B*API+C*(API**2.)+D*(API**3.)
+      +E*(API**4.) +F*(API**5.)
23  WRITE(1,102) API, U3(I)
C
C UOP K-FACTOR = 11.5
```

APPENDIX: COMPUTER PROGRAMS

C

```
API4(1)=12.0
API4(2)=15.5
API4(3)=19.3
API4(4)=24.4
API4(5)=28.1
API4(6)=33.6
API4(7)=39.6
API4(8)=66.0
HC4(1)=1.479
HC4(2)=1.541
HC4(3)=1.605
HC4(4)=1.660
HC4(5)=1.706
HC4(6)=1.738
HC4(7)=1.761
HC4(8)=1.801
DELA=(API4(8)-API4(1))/NPT
```

C

C CREATE PLOT DATA FILE

C

```
CALL CALFIT (HC4,API4,N1,A,B,C,D,E,F)
```

C

```
WRITE(1,103) NPT+1
API=API4(1)-DELA
DO 24 I=1,NPT+1
  API= DELA +API
  U4(I)=A+B*API+C*(API**2.)+D*(API**3.)
+      +E*(API**4.) +F*(API**5.)
```

```
24  WRITE(1,102) API, U4(I)
```

C

C UOP K-FACTOR = 12.0

C

```
API5(1)=18.5
API5(2)=22.0
API5(3)=26.0
API5(4)=30.3
API5(5)=35.1
API5(6)=41.0
API5(7)=47.2
API5(8)=74.6
```

APPENDIX: COMPUTER PROGRAMS

```
HC5(1)=1.667
HC5(2)=1.730
HC5(3)=1.798
HC5(4)=1.857
HC5(5)=1.913
HC5(6)=1.945
HC5(7)=1.975
HC5(8)=2.011
DELA=(API5(8)-API5(1))/NPT
C
C CREATE PLOT DATA FILE
C
CALL CALFIT (HC5,API5,N1,A,B,C,D,E,F)
C
WRITE(1,103) NPT+1
API=API5(1)-DELA
DO 25 I=1,NPT+1
  API= DELA +API
  US(I)=A+B*API+C*(API**2.)+D*(API**3.)
+      +E*(API**4.) +F*(API**5.)
25  WRITE(1,102) API, US(I)
C
C UOP K-FACTOR = 12.5
C
API6(1)=24.8
API6(2)=28.5
API6(3)=32.5
API6(4)=37.0
API6(5)=42.1
API6(6)=47.8
API6(7)=54.5
API6(8)=83.0
HC6(1)=1.857
HC6(2)=1.921
HC6(3)=1.994
HC6(4)=2.060
HC6(5)=2.126
HC6(6)=2.159
HC6(7)=2.193
HC6(8)=2.226
DELA=(API6(8)-API6(1))/NPT
```

APPENDIX: COMPUTER PROGRAMS

```
C
C CREATE PLOT DATA FILE
C
      CALL CALFIT (HCG,API6,N1,A,B,C,D,E,F)
C
      WRITE(1,103) NPT+1
      API=API6(1)-DELA
      DO 26 I=1,NPT+1
        API= DELA +API
        U6(I)=A+B*API+C*(API**2.)+D*(API**3.)
+          +E*(API**4.) +F*(API**5.)
26      WRITE(1,102) API, U6(I)
C
102     FORMAT(2F10.5)
103     FORMAT(I3)
990     FORMAT(I5)
999     FORMAT(F15.10,5X,F15.10)
C
1000    CLOSE(1)
      STOP
      END
C
C
C SUBROUTINE CALFIT
C
C SUBROUTINE COMPUTES CONSTANTS IN 5TH ORDER POLYNOMIAL EQUATION
C THAT LEAST-SQUARES FIT THE DATA
C
      SUBROUTINE CALFIT (Y,X,N,A,B,C,D,E,F)
      IMPLICIT REAL*8 (A-H,O-Z)
      DIMENSION Y(N),X(N)
C
      R11=N
      X1=0.
      X2=0.
      X3=0.
      X4=0.
      X5=0.
      X6=0.
      X7=0.
      X8=0.
```

APPENDIX: COMPUTER PROGRAMS

```
X9=0.  
X10=0.  
Y1=0.  
X1Y1=0.  
X2Y1=0.  
X3Y1=0.  
X4Y1=0.  
X5Y1=0.
```

C

```
DO 10 I=1,N  
  X1=X1 +X(I)  
  X2=X2 +X(I)**2.  
  X3=X3 +X(I)**3.  
  X4=X4 +X(I)**4.  
  X5=X5 +X(I)**5.  
  X6=X6 +X(I)**6.  
  X7=X7 +X(I)**7.  
  X8=X8 +X(I)**8.  
  X9=X9 +X(I)**9.  
  X10=X10 +X(I)**10.  
  Y1=Y1 +Y(I)  
  X1Y1=X1Y1 +X(I)*Y(I)  
  X2Y1=X2Y1 +(X(I)**2.) *Y(I)  
  X3Y1=X3Y1 +(X(I)**3.) *Y(I)  
  X4Y1=X4Y1 +(X(I)**4.) *Y(I)  
  X5Y1=X5Y1 +(X(I)**5.) *Y(I)
```

10 CONTINUE

C

```
XL1=X1/N  
XL2=X2/N  
XL3=X3/N  
XL4=X4/N  
XL5=X5/N
```

C

```
R22=X2 -XL1*X1  
XM1=(X3 -XL2*X1)/R22  
XM2=(X4 -XL3*X1)/R22  
XM3=(X5 -XL4*X1)/R22  
XM4=(X6 -XL5*X1)/R22
```

C

```
R23=X3 -XL1*X2
```

APPENDIX: COMPUTER PROGRAMS

R33=X4 -XL2*X2 -XM1*R23
XN1=(X5 -XL3*X2 -XM2*R23)/R33
XN2=(X6 -XL4*X2 -XM3*R23)/R33
XN3=(X7 -XL5*X2 -XM4*R23)/R33

C

R24=X4 -XL1*X3
R34=X5 -XL2*X3 -XM1*R24
R44=X6 -XL3*X3 -XM2*R24 -XN1*R34
XP1=(X7 -XL4*X3 -XM3*R24 -XN2*R34)/R44
XP2=(X8 -XL5*X3 -XM3*R24 -XN3*R34)/R44

C

R25=X5 -XL1*X4
R45=X7 -XL3*X4 -XM2*R25 -XN1*R34
R55=X8 -XL4*X4 -XM3*R25 -XN2*R34 -XP1*R45
XQ1=(X9 -XL5*X4 -XM4*R25 -XN3*R34 -XP2*R45)/R55

C

R26=X6 -XL1*X5
R27=X1Y1 -XL1*Y1

C

R35=X6 -XL2*X4 -XM1*R25
R36=X7 -XL2*X5 -XM1*R26
R37=X2Y1 -XL2*Y1 -XM1*R27

C

R46=X8 -XL3*X5 -XM2*R26 -XN1*R36
R47=X3Y1 -XL3*Y1 -XM2*R27 -XN1*R37
R56=X9 -XL4*X5 -XM3*R26 -XN2*R36 -XP1*R46
R66=X10 -XL5*X5 -XM4*R26 -XN3*R36 -XP2*R46 -XQ1*R56

C

R57=X4Y1 -XL4*Y1 -XM3*R27 -XN2*R37 -XP1*R47
R66=X10 -XL5*X5 -XM4*R26 -XN3*R36 -XP2*R46 -XQ1*R56
R67=X5Y1 -XL5*Y1 -XM4*R27 -XN3*R37 -XQ1*R57

C

C SOLVE VECTOR OF UNKNOWNNS

C

F=R67/R66
E=(R57 -R56*F)/R55
D=(R47 -R45*E -R46*F)/R44
C=(R37 -R34*D -R35*E -R36*F)/R33
B=(R27 -R23*C -R24*D -R25*E -R26*F)/R22
A=(Y1 -X1*B -X2*C -X3*D -X4*E -X5*F)/R11

C

APPENDIX: COMPUTER PROGRAMS

RETURN

END

APPENDIX: COMPUTER PROGRAMS

9. Program HEAT.F

```
C PROGRAM HEAT.F
C
C BY DAULAT D. MAMORA, STANFORD UNIVERSITY, JAN. 1993
C
C PROGRAM CALCULATES HEAT OF REACTION FOR OXYGENATED FUEL
C AS A FUNCTION OF X, Y AND M-RATIO.
C
C
C      IMPLICIT DOUBLE PRECISION (A-H,O-Z)
C      DOUBLE PRECISION HC(380), Y(10), XM(5)
C
C      OPEN(UNIT=1,STATUS='OLD',FILE='heat.dat')
C
C
C      DELHC=0.01
C      NHC=350
C      Y(1)=0.0
C      Y(2)=0.2
C      Y(3)=0.5
C      Y(4)=1.0
C      Y(5)=1.5
C
C      NY=5
C      XM(1)=0.2
C      XM(2)=0.3
C      XM(3)=0.4
C      EXM=3
C
C
C      DO 4 IM=1,EXM
C          XMM=XM(IM)
C          DO 5 I=1,NY
C              WRITE(1,15) NHC+1
C              DO 10 J=1,NHC+1
C                  HC(J)=0.01*(J-1)
C
C
C      C HEAT EVOLVED VIA PATH A PER MOL O2
C
C
C          A1=786.4-567.6*XMM+260.9*HC(J)
C          A2=2.-XMM+HC(J)/2.
```

APPENDIX: COMPUTER PROGRAMS

```
DHA1=A1/A2

C
C HEAT EVOLVED VIA PATH B FOR SAME FUEL MASS AS IN PATH A
C
      B1=369.0*Y(I)
      B2=2.*(1.-XMM/2.+HC(J)/4.)
      DHB1=B1/B2

C
C HEAT EVOLVED VIA PATH C FOR SAME FUEL MASS AS IN PATH A
C
      DHC1=DHA1-DHB1

C
C HEAT EVOLVED VIA PATH A PER POUND MASS OF FUEL (CHx)
C
      A=1800.*(94.0-67.9*XMM+31.2*HC(J))
      B=12.+HC(J)
      DHA2=A/B

C
C HEAT EVOLVED PER POUND MASS OF OXYGENATED FUEL (CHxOy)
C
      FMASS=(12.+HC(J))/(12.+HC(J)+16.*Y(I))
      FOXY=DHC1/DHA1
      FACTOR=FMASS*FOXY
      QY=DHA2*FACTOR
      WRITE(1,20) HC(J), QY

10    CONTINUE
5     CONTINUE
4     CONTINUE
C
C
15    FORMAT(I5)
20    FORMAT(F10.7,5X,F15.5)
      STOP
      END
```

STANFORD UNIVERSITY

PETROLEUM RESEARCH INSTITUTE
School of Earth Sciences

MITCHELL BUILDING 360
STANFORD, CALIFORNIA 94305-2220
(415)723-0691, FAX:(415)725-2099

June 9, 1993

Mr. Thomas B. Reid
Project Manager, EOR Processes
U.S. Department of Energy
P.O. Box 1398
Bartlesville, OK 74005

Dear Tom:

Enclosed, please find the corrected page of "Kinetics of In-Situ Combustion" by Daulat D. Mamora, Henry J. Ramey, Jr., William E. Brigham, and Louis M. Castanier.

Sincerely,



Angharad Jones
Secretary to W.E. Brigham

TR[#]91

indicated two exothermic reaction peaks, one at about 270°C (520°F) and the other at about 400°C (750°F) (Fig. 2.1). Similar results were obtained by Berry (1968).

Thermogravimetric experiments also involve heating a crude oil and sand sample at a constant rate in the presence of flowing air. However, the change in weight of the sample is recorded against temperature. Based on TGA and DTA thermograms, Bae (1977) concluded that at least two reactions occur at different temperatures during the oxidation of crude oil.

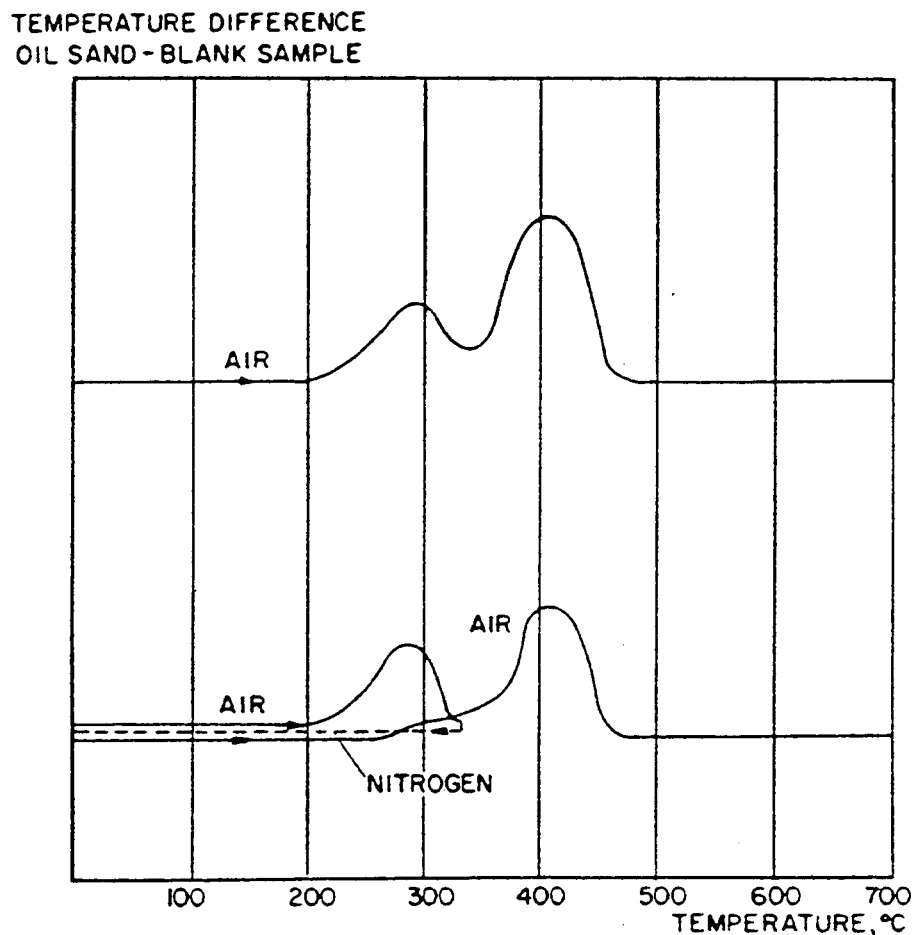


Figure 2.1: Differential Thermal Analysis of an Oil Sand (*Tadema, 1959*)

STANFORD UNIVERSITY

PETROLEUM RESEARCH INSTITUTE
School of Earth Sciences

MITCHELL BUILDING 360
STANFORD, CALIFORNIA 94305-2220
(415)723-0691, FAX:(415)725-2099

June 3, 1993

Mr. Thomas B. Reid
Project Manager, EOR Processes
Bartlesville Project Office
P. O. Box 1398
Bartlesville, OK 74005

Dear Tom:

Enclosed are two copies of the report (TR 91) entitled "Kinetics of In-Situ Combustion" by Daulat Mamora.

Sincerely,

A handwritten signature in black ink, appearing to read "Rosalee J. Benelli", with a long horizontal flourish extending to the left.

Rosalee J. Benelli

Enc.

